

**STATUS REPORTS**

to the

**PAPERMAKING**

***PROJECT ADVISORY COMMITTEE***

March 8 - 9, 2000

INSTITUTE OF PAPER SCIENCE AND TECHNOLOGY

Atlanta, Georgia

**ANNUAL PROGRAM REVIEW**

*PAPERMAKING*

March 8-9, 2000





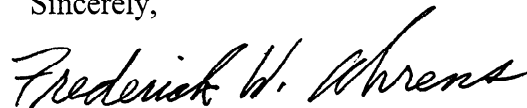
February 10, 2000

TO: MEMBERS OF THE PAPERMAKING PROJECT ADVISORY COMMITTEE

Attached for your review are the Status Reports for the projects to be discussed at the Papermaking Project Advisory Committee meeting being held at the Institute of Paper Science and Technology. The Program Review is scheduled for Wednesday, March 8, 2000, from 8:00 a.m. to 6:00 p.m. and the PAC Committee Meeting will meet on Thursday, March 9, from 8:00 a.m. to 12:30 p.m.

We look forward to seeing you at this time.

Sincerely,



Frederick W. Ahrens, Ph.D.  
Professor of Engineering & Unit Leader  
Water Removal Research

FWA/map

Attachments

**IPST Confidential Information - Not for Public Disclosure**  
(For IPST Member Company's Internal Use Only)

***Institute of Paper Science and Technology, Inc.***



**PAPERMAKING  
PROJECT ADVISORY COMMITTEE**

**IPST Liaison: Dr. David Orloff (404) 894-6649; FAX (404) 894-1496**  
**RAC Liaison: Mr. John Bergin (715) 422-2239; FAX (715) 422-2227**  
**Chairman: Dr. Jay Shands (608) 364-8501; FAX (608) 364-8600**

Dr. Dwight E. Anderson \*(2001) Vice Chairman  
Manufacturing Manager  
Weyerhaeuser Company  
WTC 2F39  
Post Office Box 2999  
Tacoma, WA 98477-2999  
(253) 924-6466  
(253) 924-6541 FAX  
andersd2@wdni.com

Mr. John Bergin \*(RAC Liaison)  
Director of Research and Development  
Consolidated Papers, Inc.  
Post Office Box 8050  
300 N. Biron Drive  
Wisconsin Rapids, WI 54495-8050  
(715) 422-2239  
(715) 422-2227 FAX  
john.bergin@conpapers.com

Mr. Jack Burke \*(1999)  
Principle Project Manager  
Radian International LLC  
1979 Lakeside Parkway  
Suite 800  
Tucker, GA 30084  
(770) 414-4522  
(770) 414-4919 FAX

Mr. Frank Cunnane \*(1999)  
Vice President, Technology  
AstenJohnson  
4399 Corporate Road  
Post Office Box 118001  
Charleston, SC 29423  
(843) 747-7800  
(843) 747-3856 FAX  
frank.cunnane@asten.com

Dr. Christopher P. Devlin \*(2001)  
Process Engineering Manager  
Inland Eastex  
A Temple-Inland Company  
Post Office Box 816  
Silsbee, TX 77656  
(409) 276-3190  
(409) 276-3419 FAX  
cdevlin@iccnet.com

Mr. Thomas M. Haller \*(2001)  
Paper Applications Supervisor  
Specialty Minerals Inc.  
9 Highland Avenue  
Bethlehem, PA 18017  
(610) 882-8756  
(610) 861-3412 FAX

Dr. Slava Babinsky \*(2001)  
Fellow  
Mead Central Research  
Eighth & Hickory Streets  
Post Office Box 1700  
Chillicothe, OH 45601-5700  
(740) 772-3056  
(740) 772-3595 FAX  
VAB@mead.com

Dr. G. Ronald Brown \*(2001)  
Director of Research  
Westvaco Corporation  
11101 Johns Hopkins Road  
Laurel, MD 20723-6006  
(301) 497-1301  
(301) 497-1275 FAX  
grbrown@westvaco.com

Dr. Partha S. Chaudhuri \*(1999)  
Senior Scientist, Papermaking  
Champion International Corporation  
Technical Center  
West Nyack Road  
West Nyack, NY 10994  
(914) 578-7123  
(914) 578-7474 FAX  
chaudp@champint.com

Mr. Richard Daniell \*(Alternate)  
R&D Laboratory Manager  
EHV Weidmann  
One Gordon Mills Way  
St. Johnsbury, VT 05819  
(802) 751-3328  
(802) 751-3373 FAX  
rdaniell@ehv.mhs.compuserve.com

Mr. R. Doug Estridge \*(Alternate)  
Staff Engineer  
BE&K Engineering Company  
2000 International Park Drive  
Post Office Box 12607  
Birmingham, AL 35202-6607  
(205) 972-6416  
(205) 972-6300 FAX  
estrledged@bek.com

Mr. Ed R. Hendrickson \*(2001)  
Research Engineer  
Potlatch Corporation  
Post Office Box 503  
Cloquet, MN 55720-0503  
(218) 879-0626  
(218) 879-2375 FAX  
erhendri@potlatchcorp.com

## **Papermaking PAC (cont.)**

Mr. Kenneth Kaufman \*(2001)  
Senior Research Manager  
Kimberly-Clark Corporation  
1400 Holcomb Bridge Road  
Building 400/2  
Roswell, GA 30076  
(770) 587-7493  
(770) 587-7709 FAX  
kkaufman@kcc.com

Dr. Alexander A. Koukoulas \*(2002)  
Manager, Papermaking Process Research  
International Paper Company  
Corporate Research Center  
1422 Long Meadow Road  
Tuxedo Park, NY 10987  
(914) 577-7275  
(914) 577-7507 FAX  
alex.koukoulas@ipaper.com

Mr. David J. Lacz \*(2001)  
Technical Associate  
Eastman Kodak Company  
Paper Support Division B-319  
1669 Lake Avenue  
Rochester, NY 14652-3622  
(716) 477-6301  
(716) 588-2680 FAX  
dlacz@kodak.com

Mr. Greg Maule \*(2001)  
Production Manager  
Consolidated Papers, Inc.  
1101 Main Street  
Niagara, WI 54151  
(715) 251-8326  
(715) 251-1540 FAX  
greg.maule@conpapers.com

Dr. Franco Palumbo \*(1997)  
Riverwood International Corporation  
Post Office Box 35800  
West Monroe, LA 71294-5800  
(318) 362-2000  
(318) 362-2441 FAX

Mr. Jeffrey R. Reese \*(2001)  
Consultant, Paper Mill  
Georgia-Pacific Corporation  
133 Peachtree Street, NE  
18th Floor  
Atlanta, GA 30303  
(404) 652-4880  
(404) 584-1466 FAX  
JRRESE@GAPAC.com

Mr. Markku Korpela \*(Alternate)  
Kymni Paper R&D  
UPM-Kymmene Fine Paper  
FIN-45700  
Kuusankoski, FINLAND  
+358-204-15-3541  
+358-204-15-2552  
markku.s.korpela@upm-kymmene.com

Dr. Charles Kramer \*(2001)  
Director  
Albany International Research Company  
Post Office Box 9114  
Mansfield, MA 02048-9114  
(508) 337-9541  
(508) 339-4996 FAX  
charlie\_kramer@albint.com

Dr. Jeffrey D. Lindsay \*(Alternate)  
Associate Research Fellow  
Kimberly-Clark Corporation  
2100 Winchester Road  
Post Office Box 999  
Neenah, WI 54957-0999  
(920) 721-3990  
(920) 721-7748 FAX

Mr. Vic Nisita \*(2001)  
Operations Superintendent  
Wisconsin Tissue Mills  
Chicago Operations  
13101 S. Polaski Road  
Alsip, IL 60658  
(708) 824-4397  
(708) 389-4901 FAX  
V-NISITA@NWU.edu

Dr. Paul R. Proxmire \*(2001)  
Research Associate  
Appleton Papers Inc.  
Post Office Box 359  
Appleton, WI 54912-0359  
(920) 730-7254  
(920) 991-7243 FAX  
pproxmire@appletonpapers.com

Mr. Thomas E. Rodencal \*(Alternate)  
Sr. Paper Mill Staff Engineer  
Georgia-Pacific Corporation  
133 Peachtree Street, NE  
18th Floor  
Atlanta, GA 30303  
(404) 652-4514  
(404) 584-1466 FAX  
terodenc@GAPAC.Com

## ***Papermaking PAC (cont.)***

Mr. Nickey J. Rudd \*(2002)  
Vice President, Special Projects  
BE&K Engineering Company  
Post Office Box 12607  
Birmingham, AL 35202-2607  
(205)969-3600  
(205) 972-6300 FAX

Mr. Ralf Sieberth \*(2001)  
Sr. Vice President, Market & Business Development  
Voith Sulzer Paper Technology North America Inc.  
Post Office Box 2337  
2200 North Roemer Road  
Appleton, WI 54913-2337  
(920) 731-0769  
(920) 731-1391 FAX  
rsieberth@voithsulzer.com

Mr. David G. Thurman \*(Alternate)  
Project Leader, Board  
Eka Chemicals Inc.  
1775 West Oak Commons Court  
Marietta, GA 30062-2254  
(770) 321-4138  
(770) 321-5880 FAX

Mr. James R. Watson \*(2001)  
Segment Manager - Printing & Writing Grades  
Eka Chemicals Inc.  
1775 West Oak Commons Court  
Marietta, GA 30062  
(770) 321-4142  
(770) 321-6451 FAX

Dr. Gary L. Worry \*(2001)  
Research Fellow  
Fort James Corporation  
1915 Marathon Avenue  
Post Office Box 899  
Neenah, WI 54957-0899  
(920) 729-8470  
(920) 729-8023 FAX  
gary.worry@fortjamesmail.com

Dr. Jay A. Shands \*(2001) (Chairman)  
Manager, Forming Systems  
Beloit Corporation  
Rockton Research Center  
1165 Prairie Hill Road  
Rockton, IL 61072-1595  
(608) 364-8501  
(608) 364-8600 FAX  
jashands@beloit.com

Mr. Frank J. Sutman \*(2002)  
Sr. Research Scientist  
Hercules Incorporated  
Pulp and Paper Division  
7510 Baymeadows Way  
Jacksonville, FL 32256  
(904) 733-7110  
(904) 448-4995 FAX  
frank.j.sutman@betzdearborn.com

Mr. Markku Tuderman \*(2002)  
Vice President, Research and Development  
UPM-Kymmene  
Eteläesplanadi 2  
P.O. Box 380  
FIN-00101 Helsinki, FINLAND  
358-204 15 111  
358-2041 50 507 FAX  
markku.tuderman@upm-kymmene.com

Mr. Lloyd O. Westling \*(1999)  
Vice President, Production Planning  
Longview Fibre Company  
Post Office Box 639  
Longview, WA 98632  
(360) 575-5259  
(360) 575-5926 FAX  
LOWestling@Longfibre.com





**PAPERMAKING  
PROJECT ADVISORY COMMITTEE MEETING**

*March 8-9, 2000*

**Institute of Paper Science and Technology  
Atlanta, Georgia**

**Location: S e m i n a r R o o m**

**March 8, 2000 - COMMITTEE DISCUSSIONS AGENDA**

7:30 a.m.	Coffee/Danish	
8:00 a.m. - 8:10 a.m.	Opening Remarks, Review of Antitrust Statement and Confidentiality Statement	Chairman
8:10 a.m. - 8:40 a.m.	Portfolio Management System and Project Scoring	Gary Baum, David Orloff
8:40 a.m. - 8:45 a.m.	Welcome	Fred Ahrens, Cyrus Aidun
8:45 a.m. - 9:30 a.m.	Project F048 Approach Flow Systems	Ted Heindel
9:30 a.m. - 10:15 a.m.	Project F022 Flow Through Porous Media	Seppo Karrila
10:15 a.m. - 10:30 a.m.	Break	
10:30 a.m. - 11:00 a.m.	Project F003 Fluid Dynamics of Suspensions	Cyrus Aidun
11:00 a.m. - 12:00 a.m.	Project F005 Headbox and Fluid Hydrodynamics	Cyrus Aidun
12:00 p.m. - 12:45 p.m.	Lunch and IPST Update	Gary Baum
12:45 p.m. - 1:30 p.m.	Project F039 Water Removal Limits	Tim Patterson
1:30 p.m. - 2:15 p.m.	Project F040 Press Dwell Time Limits	Paul Phelan
2:15 p.m. - 3:00 p.m.	Project F041 High Intensity Water Removal	Fred Ahrens
3:00 p.m. - 3:15 p.m.	Break	
3:15 p.m. - 4:15 p.m.	Project F021 & 4253 Drying Productivity	Fred Ahrens Tim Patterson
4:15 p.m. - 6:00 p.m.	Subcommittee Discussions of Projects & Preparation of Summaries	

NOTE: 10 minutes of project discussion time is included at the end of each presentation.

◆ *Dinner provided at 6:00 p.m.*



**PAPERMAKING  
PROJECT ADVISORY COMMITTEE MEETING**

*March 8-9, 2000*

**Institute of Paper Science and Technology  
Atlanta, Georgia**

**Location: R o o m 1 7 3**

**March 9, 2000 - COMMITTEE DISCUSSIONS AGENDA**

7:30 a.m.	Coffee/Danish	
8:00 - 8:10 a.m.	Convene - Antitrust Statement - Confidentiality Statement - New Members - Acceptance of Fall, 1999 minutes - Review of Agenda	Chairman
8:10 - 8:30 a.m.	F022 Flow Through Porous Media (Karrila)	<u>Chaudhuri</u> , Shands, Sieberth
8:30 - 8:50 a.m.	F048 Approach Flow Systems (Heindel)	<u>Hendrickson</u> , Westling, Bergin, Rudd
8:50 - 9:10 a.m.	F021 Drying (Ahrens/Patterson)	<u>Reese</u> , Worry, Beck
9:10 - 9:30 a.m.	F005 Headbox and Forming (Aidun)	<u>Anderson</u> , Devlin, Koukoulas
9:30 - 9:50 a.m.	F041 High Intensity Water Removal (Ahrens)	<u>Babinsky</u> , Watson, Kaufman
9:50 - 10:10 a.m.	F003 Fluid Dynamics of Suspensions (Aidun)	<u>Brown</u> , Maule, Proxmire
10:10 - 10:30 a.m.	Break	
10:30 - 10:50 a.m.	F039 Water Removal (Patterson)	<u>Cunnane</u> , Lacz, Haller
10:50 - 11:10 a.m.	F040 Press Dwell (Phelan)	<u>Kramer</u> , Palumbo
11:10 - 11:30 a.m.	Proposed Projects	IPST PI's
11:30 - 12:15 p.m.	PAC Discussion of Potential Projects	All
12:15 - 12:30 p.m.	Final Discussion/Adjourn	All

NOTE: Subcommittee chairs are indicated in underlined bold characters above.

◆ *Lunch provided.*



## TABLE OF CONTENTS

	<b>Page</b>
Project F048	Approach Flow Systems ..... 1
Project F022	Flow Thru Porous Media ..... 43
Project F003	Fluid Dynamics of Suspensions ..... 61
Project F005	Fundamentals of Headbox and Forming Hydrodynamics ..... 73
Project F039	Water Removal Limits ..... 85
Project F040	Press Dwell Time Limits ..... 127
Project F041	High Intensity Water Removal ..... 139
Project F021	Drying Productivity ..... 159



APPROACH FLOW SYSTEMS

STATUS REPORT

FOR

PROJECT F048

Ted Heindel (PI)  
Aklilu Giorges

March 8 – 9, 2000

Institute of Paper Science and Technology  
500 10th Street, N.W.  
Atlanta, Georgia 30318





**DUES-FUNDED PROJECT SUMMARY**

**Project Title:** Approach Flow Systems  
**Project Number:** F048  
**PAC:** Papermaking

**Project Staff**

**Principal Investigator:** Ted Heindel  
**Research Support Staff:** Aklilu Giorges

**FY 99-00 Budget:** \$75,007

**Time Allocation:**

**Principal Investigator:** 20%  
**Research Support Staff:** 50%

**1 RESEARCH LINE/ROADMAP: LINE #11**

Improve the ratio of product performance to cost for pulp and paper products by 25% by developing break-through papermaking and coating processes which can produce the innovative webs with greater uniformity than that achieved with current processes.

**2 PROJECT OBJECTIVE:**

The objective of this project is to provide recommendations to improve the spatial and temporal consistency and chemical uniformity of the stock leaving the approach flow area.

**3 PROJECT BACKGROUND:**

The PI in this project began the project on July 1, 1999. The initial focus was to review the work completed in a related project conducted by Dr. Xiaodong Wang (Project F004). Appendix A of this status report contains brief summaries of the various reports completed by Dr. Wang. Familiarization of other literature related to approach flow systems and pipe mixing was also completed. From this background, it was decided to focus this research on improving the spatial and temporal consistency and chemical uniformity in the approach flow area. The ultimate goal of this project is to be able to provide paper producers and suppliers with recommendations on approach flow piping configurations.

To accomplish the goal of providing approach flow recommendations to IPST Member Companies, this project will focus on developing and validating a model of the fiber mixing process. Once a model is validated, it can be used throughout the pulp and paper process where one constituent is mixed with another. The model will also provide a tool to paper producers to allow them to design approach flow configurations to optimize mixing performance given economic and space limitations. This effort will follow two parallel research paths, schematically represented in Fig. 1. The first path stresses the development of a new fiber mixing model, and the second addresses experiments to

study the mixing process and to validate the model. Since July 1999, a water/water mixing model for a concentric pipe mixer was developed and experiments in a similar system were completed. This work will be detailed in Section 10. Additionally, the initial stages of a water/fiber model and the accompanying experiments will be outlined in Section 10.

#### **4 MILESTONES:**

This project was initiated by this PI on July 1, 1999. In the Fall PAC meeting it was agreed that by June 2000, high speed video analysis of the concentric mixing process with velocity ratios of up to  $R_v \approx 5$  will be completed for a water/water system and a water/1% fiber system. It was further agreed that by June 2000, a model of turbulent fiber mixing in a concentric mixer will be developed. As of January 2000, water/water mixing experiments and numerical predictions have been completed for velocity ratios from 1 to 6, and a model of the fiber mixing process has been outlined. Details of this work are provided in Section 10.

#### **5 DELIVERABLES:**

The overall deliverable of this project is a validated model of the water/fiber concentric mixing process.

#### **6 STATUS OF GOALS FOR FY 99-00:**

The status of the goals for the current fiscal year, as of January 2000, are summarized as follows:

1. Review previous F004 work.  
Status: Completed
2. Become familiar with the approach flow and mixing literature.  
Status: Completed
3. Modify the current experimental facility.  
Status: Completed
4. Review CFD software options and purchase a new CFD software license.  
Status: Completed
5. Water/water concentric mixing:
  - a. Experiments  
Status: Completed
  - b. Computations  
Status: Completed
  - c. Comparisons between predictions and experiments  
Status: In progress
6. Water/1% hardwood fiber concentric mixing:
  - a. Model development  
Status: In progress
  - b. Experiments  
Status: Not yet begun
  - c. Computations  
Status: Not yet begun
  - d. Comparison between predictions and experiments  
Status: Not yet begun

7. Member Company Report  
Status: Not yet begun

## 7 SCHEDULE:

The project schedule for the current fiscal year is summarized in Table 1. The task numbers correspond to the goal numbers listed in Section 6 (above).

Table 1: Project F048 schedule for FY99-00.

Task Descriptions	1999 July - Sept	1999 Oct - Dec	2000 Jan - Mar	2000 Apr - Jun
1	---X			
2	-----X			
3	-----	---X		
4	-----	-----X		
5a		-----X		
5b		-----	----X	
5c			-----	
6a		-----	-----	-----
6b			-----	
6c			-----	-----
6d				-----
7				-----

## 8 SUMMARY OF RESULTS:

This project began with the current PI on July 1, 1999. Since that time, the current concentric mixing experimental facility has been modified to achieve velocity ratios of up to 6 without cavitation occurring at the trailing edge of the inner pipe. Using this facility, water/water mixing experiments have been completed. By increasing the velocity ratio from 1 to 6, the mixing distance was reduced by approximately 65%. Additionally, qualitative observations revealed that by increasing the velocity ratio, the inner jet spreading angle was found to be larger (i.e., the jet spread faster) and the downstream mixing region was more uniform.

New CFD software was also acquired for this project and turbulent water/water concentric mixing was modeled with the standard  $k-\varepsilon$  and realizable  $k-\varepsilon$  turbulence models. Numerical studies have shown that the closure constants in the turbulence models can influence the predicted mixing effects. Constant values of  $C_{1\varepsilon} = 1.7$  and  $C_{2\varepsilon} = 2.4$  for the standard  $k-\varepsilon$  model and  $C_2 = 2.2$  for the realizable  $k-\varepsilon$  model have been used to obtain reasonable qualitative agreement with the experimental data. It was further shown that qualitative differences between the two  $k-\varepsilon$  models were very small.

We are in the process of extending the mixing experiments to a water/fiber system, as well as developing a new model of water/fiber mixing. In the model, we propose to model the fiber mixing process by using a variable local shear stress (i.e., viscosity) which is a function of local fiber consistency and shear rate.

## 9 BULLETED KEY ACCOMPLISHMENTS:

- Water/water mixing experiments have been completed in a concentric mixer for velocity ratios between 1 and 6.
- Turbulence model closure constants affect the predicted mixing results. Thus, using the experimental results, the closure constants were determined.
- Reasonable qualitative agreement between experiments and numerical predictions have been obtained with water/water concentric mixing.
- A new method to model water/fiber mixing has been proposed.

## 10 DISCUSSION:

Details from work completed since July 1, 1999 are summarized below. Section 10.1 addresses the experimental work. Section 10.2 and 10.3 focus on modeling water/water mixing and water/fiber mixing, respectively, in a concentric pipe mixer.

### 10.1 Concentric Mixing Experiments

Concentric mixing is a simple and effective method to mix one constituent with another. It is a common process in many industries, including the pulp and paper industry. A schematic of a concentric mixing process is shown in Fig. 2. This process involves mixing a fluid from an inner pipe with diameter  $d$ , volumetric flow rate  $q$ , and mean fluid velocity  $u$ , with a fluid in an outer pipe of diameter  $D$ , volumetric flow rate  $Q$ , and mean fluid velocity  $v$ . Typically,  $u \geq v$  and the inner pipe fluid is referred to as the "primary fluid", while the outer pipe fluid is called the "secondary fluid". In many cases, the primary fluid has a specified species concentration  $C_p$  while the secondary fluid has a species concentration  $C_s$ . In this case, the purpose of the mixing operation is to provide a uniform species concentration downstream of the primary fluid inlet. As shown in Fig. 2, the jet issuing from the center pipe may be divided into two regions, the potential core region and the entrainment or mixing region. The characteristics of the potential core are identical to those of the primary fluid stream (e.g.,  $u$ ,  $C_p$ ), while the characteristics of the mixing region vary from those of the primary fluid to those of the secondary fluid.

This mixing process appears to be simple, but very complex flow phenomena occur to thoroughly mix the two fluid streams. When the two fluid streams enter the mixing region at different velocities, a high shearing region forms at the interface between the two fluid streams. Instabilities at this interface cause vortices to intertwine from each stream, enabling mixing. Depending on the mixing behavior, the two fluids may, or may not, mix completely or uniformly.

The degree of mixing in a concentric mixer depends on the following [1]: the ratio of inner-to-outer pipe diameter; the ratio of inner-to-outer pipe flow rates or velocities; the ratio of specific gravities between the two fluid streams; the inner and outer pipe Reynolds numbers; the pipe surface roughness; and any secondary pipe flows. When one of the constituents is a fiber suspension, additional parameters related to the fiber characteristics (e.g., fiber length, coarseness, flexibility, etc.) also affect the mixing process [2-5].

One of the important parameters in the mixing process is the velocity ratio between the primary and secondary fluid,  $R_v = u/v$ . In this research, initial experiments were

conducted in a water/water system in which  $1 \leq R_v \leq 6$  to determine the effect of  $R_v$  on mixing. In addition, these data will then be used in the model validation phase of this project.

#### 10.1.1 Experimental Equipment

A schematic of the former mixing system used by Dr. Wang is shown in Fig. 3. This system was composed of two transparent concentric pipes in the test section, a large mixing tank to hold the primary fluid, a smaller water tank to hold the secondary fluid, a large discharge tank, a pump, and the associated piping, valves, and flow meters. This system was designed to provide a constant head input into the test section and eliminate any pressure pulsations that may result from the system pump. With this setup, however, a maximum velocity ratio of  $R_v \approx 1.4$  was realized before cavitation occurred at the trailing edge of the inner pipe. This mean velocity ratio is much smaller than those in industry, as well as those recommended by others [5, 6].

To increase the possible velocity ratios, the flow loop was modified for this research program to allow the primary fluid to enter the test section directly from the pump (Fig. 4). This increased the maximum possible velocity ratio, but also introduced potential pressure pulsations from the pump, which were assumed to be acceptable if they were present. With this current configuration, a maximum water/water velocity ratio of  $R_v = 6$  was achieved.

The test section, pictorially represented in Fig. 5, consisted of a transparent inner pipe with inside diameter  $d = 2.54$  cm (1 in) and a pipe wall thickness of 0.3175 cm (0.125 in). The outer pipe was also transparent and had an inside pipe diameter of  $D = 6.35$  cm (2.5 in). As shown in Fig. 5, the inner pipe protruded into the outer pipe approximately  $\ell = 39.4$  cm (15.5 in) after the  $90^\circ$  bend. The outer pipe extended approximately  $L = 58$  cm (22.8 in) beyond the inner pipe trailing edge before exiting into the discharge tank. Although  $L = 58$  cm, the actual mixing region captured by high speed video was approximately 35 cm (13.8 in) downstream of the inner pipe trailing edge, corresponding to a mixing region of approximately  $5.5D$ .

The high speed video equipment used to capture the mixing process consisted of a Kodak Ektapro Motion Analyzer with a frame rate of 1000 frames/sec.

#### 10.1.2 Water/Water Mixing Experiments

Initial concentric mixing experiments were completed in a water/water system. To identify the primary fluid, red dye (rhodamine) was added to city water in the large mixing tank. This colored water was pumped through the inner pipe, while the outer pipe was supplied with clear city water from the elevated secondary fluid tank. High speed video images at 1000 frames/sec were then taken at the test section where the two fluid streams were allowed to interact. These images encompassed a mixing region of approximately  $5.5D$ .

During the experiments, the mean secondary fluid velocity was held constant at approximately  $v = 1.30$  m/s, while the mean primary fluid velocity was varied between  $1.35$  m/s  $\leq u \leq 7.76$  m/s. This corresponded to a mean velocity ratio range of  $1 \leq R_v \leq 6$ . Table 2 summarizes the actual flow conditions for each experiment.

Table 2: Flow conditions used in the water/water concentric mixing experiments.

Primary Volumetric Flow Rate, $q$ (gpm)	Secondary Volumetric Flow Rate, $Q$ (gpm)	Mean Primary Velocity, $u$ (m/s)	Mean Secondary Velocity, $v$ (m/s)	Mean Velocity Ratio, $R_v = u/v$
10.8	50.8	1.35	1.30	1.04
20.7	50.0	2.58	1.28	2.02
30.6	50.2	3.81	1.29	2.95
40.4	50.6	5.03	1.30	3.87
51.3	50.3	6.39	1.29	4.95
62.3	50.2	7.76	1.29	6.02

Figure 6 illustrates the flow structure of concentric water jets mixing when  $R_v = 1.04$ . The outer pipe boundary is clearly identifiable, and the tip of the inner pipe is captured on the left-hand side of the image. Each dark "+" mark on the outside of the outer pipe represents a distance of  $1D$ . The darker fluid is the colored primary fluid. The mixing process can be visually observed from the dispersion of the dye that was introduced in the center jet. As expected, the mixing region increases in the radial direction as the fluids evolve downstream. The actual mixing process can be attributed to flow and geometric factors that promote the interaction between the two fluid streams. A close visual inspection directly downstream of the trailing edge of the inner pipe in Fig. 6 points to a radial increase in the jet, even though the inner and outer jet mean velocities are nearly identical. This agrees with the flow character reported by Dahm et al. [7]. In their case, they concluded that the boundary layer on both sides of the inner pipe introduced a wake. This resulted in a velocity defect and caused the two fluid streams to intertwine at their interface, creating a vortex ring. In the current experimental geometry, boundary layers are present on both sides of the inner pipe, creating a velocity defect. Additionally, the inner pipe has a finite thickness, which results in wake formation at the pipe trailing edge. This wake also contributes to the interaction between the two fluid streams. Finally, through inspection of multiple images of the  $R_v = 1.04$  mixing process, the location at which the colored fluid stream contacts the outer pipe wall ( $L_w$  in Fig. 2) can be estimated. This will be further discussed below.

A representative image from the  $R_v = 2.02$  experiment is shown in Fig. 7. The location at which the colored fluid contacts the outer pipe wall has moved upstream compared to that at  $R_v = 1.04$ . For the relatively small velocity ratios depicted in Figs. 6 and 7, a large weave-like coherent structure is observed along the interface between the two fluids. This structure becomes unstable as it moves downstream, indicating that hydrodynamic instabilities, as well as small scale turbulent interactions, enhance the concentric pipe mixing process.

Figures 8 through 11 display representative images of the mixing process for  $R_v = 2.95, 3.87, 4.95,$  and  $6.02$ , respectively. As the mean velocity ratio increases, the inner jet angle increases. This increase in  $R_v$  also results in the decrease in the distance between the inner pipe exit and the location at which the colored fluid contacts the outer wall. The increase in jet spread also enhances the entrainment of the outer fluid and its mixing with the inner fluid. The inner jet and downstream mixing region also appear

darker and more uniform as the mean velocity ratio increases. This is the result of two factors: (i) the increase in center jet flow rate increases the dye concentration of the mixture causing the image to appear darker; and (ii) the large velocity difference between the inner and outer fluid enhance small scale turbulent mixing creating a more uniform mixture.

We define the dark region downstream of the inner pipe as the mixing region, and the distance between the inner pipe exit and the location at which the darker region contacts the outer pipe walls ( $L_w$  in Fig. 2) as the mixing distance. This distance has been estimated from Figs. 6-11, and has been nondimensionalized with respect to the outer pipe diameter,  $D$ . This nondimensional distance,  $L_w/D$ , has been plotted as a function of mean velocity ratio in Fig. 12. Increasing the velocity ratio from 1 to 6 reduces  $L_w/D$  by approximately 65%. This decline can also be used to obtain qualitative comparisons between experimental observations and numerical predictions and will be completed in Section 10.2.5.

Further analysis of multiple images from each test condition may also allow for qualitative identification of the local dye concentration through variations in the image intensity. This is currently under development and may be used for model comparisons if encouraging results are obtained.

### 10.1.3 Water/Fiber Mixing Plans

The next phase of experiments will be completed in the same flow loop and test section, but with 1% fiber suspension as the primary fluid. These experiments are currently planned for mid-March (after the Spring PAC meeting). It is hoped that a laboratory repulper and dewatering screw press that will assist with experimental preparation and cleanup will be approved and in place at this time. This equipment has been requested through IPST capital funds and is currently under review by IPST management. If this equipment is not in place by mid-March, the 1% fiber mixing experiments will still be completed, they will just be more time-intensive.

## 10.2 Numerically Modeling Water/Water Mixing

Water/water mixing was numerically modeled in an attempt to simulate the fluid flow in the water/water mixing experiments. Hence, the mixing process was simulated as two turbulent miscible fluids with the same density and viscosity, but with different concentrations of an inert tracer (e.g., a red dye). For this model, the governing equations and two turbulence models are summarized below. Selected numerical results and comparisons to experiments are also provided.

### 10.2.1 Governing Equations

The governing equations for conservation of mass, momentum, and tracer concentration for steady, incompressible, turbulent viscous fluid flow with constant fluid properties are

$$\frac{\partial u_i}{\partial x_i} = 0 \quad (1)$$

$$\rho u_j \frac{\partial u_i}{\partial x_j} = -\frac{\partial p}{\partial x_i} + \frac{\partial}{\partial x_j} \left[ (\mu + \mu_t) \left( \frac{\partial u_i}{\partial x_j} + \frac{\partial u_j}{\partial x_i} \right) \right] \quad (2)$$



$$\rho u_j \frac{\partial c}{\partial x_j} = \frac{\partial}{\partial x_j} \left[ \left( \frac{\mu}{Sc} + \frac{\mu_t}{\sigma_c} \right) \frac{\partial c}{\partial x_j} \right] \quad (3)$$

All quantities have been time averaged in the above equations, and  $u_i$  ( $i = 1, 2$ ) are the mean local velocity components in the axial and radial direction. Also,  $\rho$  is the fluid density,  $p$  is the time averaged pressure,  $\mu$  is the dynamic viscosity,  $\mu_t$  is the eddy (turbulent) viscosity,  $c$  is the time averaged local tracer concentration,  $Sc$  is the Schmidt number, and  $\sigma_c$  is the turbulent Schmidt number (specified as  $\sigma_c = 0.7$  in our calculations).

The governing equations are discretized and solved using Computational Fluid Dynamics (CFD) software. The particular software used in this study is called FLUENT, which uses a finite volume method to discretize the governing equations [8]. It was selected because it can be used to model the conservation equations of multiple fluid streams [9], which will be discussed in Section 10.3.

The eddy viscosity ( $\mu_t$ ) is specified through various turbulent models. Several models have been developed, but it is beyond the scope of this report to explain the advantages and disadvantages of each model. However, we present two turbulence models that are available in FLUENT v5 and were used to simulate the turbulent mixing process in this study.

#### 10.2.2 The Standard k- $\epsilon$ Model

The standard k- $\epsilon$  model [10] is widely used due to its robustness, computational economy, and reasonable accuracy for a wide range of engineering problems. The basis of the model is that the eddy viscosity is defined by

$$\mu_t = \rho C_\mu \frac{k^2}{\epsilon} \quad (4)$$

where  $C_\mu$  is an empirical constant and  $k$  and  $\epsilon$  are the turbulent kinetic energy and dissipation rates, respectively. These parameters are determined from the following transport equations

$$\rho u_j \frac{\partial k}{\partial x_j} = \frac{\partial}{\partial x_j} \left[ \left( \mu + \frac{\mu_t}{\sigma_k} \right) \frac{\partial k}{\partial x_j} \right] + G_k - \rho \epsilon \quad (5)$$

$$\rho u_j \frac{\partial \epsilon}{\partial x_j} = \frac{\partial}{\partial x_j} \left[ \left( \mu + \frac{\mu_t}{\sigma_\epsilon} \right) \frac{\partial \epsilon}{\partial x_j} \right] + C_{1\epsilon} \frac{\epsilon}{k} G_k - C_{2\epsilon} \rho \frac{\epsilon^2}{k} \quad (6)$$

where  $C_{1\epsilon}$  and  $C_{2\epsilon}$  are empirical constants, and  $\sigma_k$  and  $\sigma_\epsilon$  are the turbulent Prandtl numbers for  $k$  and  $\epsilon$ , respectively.

The  $G_k$  term represents the production of turbulent kinetic energy and is modeled by [9]

$$G_k = \mu_t S^2 \quad (7)$$

where  $S$  is the modulus of the mean rate-of-strain tensor defined by

$$S \equiv \sqrt{2S_{ij}S_{ij}} \quad (8)$$

with the mean strain rate given by

$$S_{ij} = \frac{1}{2} \left( \frac{\partial u_i}{\partial x_j} + \frac{\partial u_j}{\partial x_i} \right) \quad (9)$$

In the standard k- $\epsilon$  model, the following constant values are used as defaults in FLUENT v5:  $C_{\mu} = 0.09$ ,  $C_{1\epsilon} = 1.44$ ,  $C_{2\epsilon} = 1.92$ ,  $\sigma_k = 1.0$ , and  $\sigma_{\epsilon} = 1.3$ . Comments on the applicability of these values will be given below.

### 10.2.3 The Realizable k- $\epsilon$ Model

One variant of the standard k- $\epsilon$  model is called the realizable k- $\epsilon$  model [11]. This model differs from the standard k- $\epsilon$  model in two ways [9]: (i) the realizable k- $\epsilon$  model contains a new formulation of the eddy viscosity,  $\mu_t$ ; and (ii) a new transport equation for the dissipation rate,  $\epsilon$ , is used. One class of problems where the realizable k- $\epsilon$  model has been shown to be more accurate is the modeling of turbulent planar and round jets [9].

For the realizable k- $\epsilon$  model, the eddy viscosity given by Eq. (4) no longer has a constant value for  $C_{\mu}$ . Rather,  $C_{\mu}$  is now a complex function of the mean strain rate (Eq. (9)). This formulation can be found in FLUENT [9]. The turbulent kinetic energy equation for the realizable k- $\epsilon$  model is identical to that used in the standard k- $\epsilon$  model (i.e., Eq. (5)). The dissipation equation is given by

$$\rho u_j \frac{\partial \epsilon}{\partial x_j} = \frac{\partial}{\partial x_j} \left[ \left( \mu + \frac{\mu_t}{\sigma_{\epsilon}} \right) \frac{\partial \epsilon}{\partial x_j} \right] + \rho C_1 S \epsilon - \rho C_2 \frac{\epsilon^2}{k + \sqrt{\nu \epsilon}} \quad (10)$$

where S is given by Eq. (8),  $\nu$  is the kinematic viscosity ( $= \mu/\rho$ ),  $C_2$  is an empirical constant and

$$C_1 = \max \left[ 0.43, \frac{Sk/\epsilon}{(Sk/\epsilon) + 5} \right] \quad (11)$$

The default values for the realizable k- $\epsilon$  model in FLUENT v5 are  $C_2 = 1.9$ ,  $\sigma_k = 1.0$ , and  $\sigma_{\epsilon} = 1.2$ .

### 10.2.4 Numerical Results

Numerical simulations of the water/water concentric mixing phenomena have been completed using both the standard and realizable k- $\epsilon$  turbulence models available in FLUENT v5 [9]. The flow conditions were assumed to be axisymmetric to reduce the computational domain from three dimensions to two dimensions. The actual computation domain (Fig. 13) encompassed a radial distance of 3.175 cm and an axial distance of 44.45 cm, corresponding to a D/2 by 7D region. Note that the computations encompassed a 1D length upstream of the trailing edge of the inner pipe and a 6D length downstream. This region was discretized into a numerical computational grid of  $36 \times 300$  nodes, with a slightly higher node density near the inner pipe trailing edge.

It is well known that turbulence enhances the mixing process. Thus, the turbulence model used to simulate mixing plays a major role in determining realistic predictions. It

has also been shown that the values of the standard  $k$ - $\epsilon$  model constants,  $C_{1\epsilon}$  and  $C_{2\epsilon}$ , affect the relative concentration of the mixing streams [12, 13].

To identify the appropriate values for  $C_{1\epsilon}$  and  $C_{2\epsilon}$ , selected numerical experiments were completed at the velocity ratio extremes of this study ( $R_v = 1.0$  or  $6.0$ ). Figure 14 shows the concentric mixer concentration profiles predicted with the standard  $k$ - $\epsilon$  model when  $R_v = 1.0$ . Recall from Fig. 13 that each image shows the upper half of the concentric mixer, with the primary fluid entering from the lower left region and the secondary fluid entering from the upper left region. The isopleths in each figure represent lines of constant concentration. Therefore, at the trailing edge of the inner pipe wall, the closely packed lines of constant concentration represent a region of high concentration gradient. Downstream of the inner pipe, the concentration gradients are much less severe. The results with  $C_{1\epsilon} = 1.44$  and  $C_{2\epsilon} = 1.92$  (the FLUENT v5 default values) are shown in Fig. 14a. As  $C_{2\epsilon}$  increases (Figs. 14b, c), the length of the potential core of the inner jet (the region from the inner pipe to the first isopleth) decreases and the jet spread increases. Figures 14d-f represent calculations that were completed to identify the best values for  $C_{1\epsilon}$  and  $C_{2\epsilon}$ , and were completed in conjunction with the calculations at  $R_v = 6.0$ .

Figure 15 shows similar numerical experiments using the standard  $k$ - $\epsilon$  model and  $R_v = 6.0$ . An analogous trend is observed when  $C_{2\epsilon}$  is varied. By decreasing  $C_{1\epsilon}$ , the length of the potential core of the inner jet increases and the jet spread decreases. After several numerical experiments at  $R_v = 1.0$  and  $6.0$ , it was determined that  $C_{1\epsilon} = 1.7$  and  $C_{2\epsilon} = 2.4$  provide reasonable qualitative agreement to the experimentally observed jet shape. These constant values were used for all standard  $k$ - $\epsilon$  model calculations at the intermediate mean velocity ratios.

The realizable  $k$ - $\epsilon$  model was also tested to determine the effect of  $C_2$  variations on the mixing process. Figure 16b shows the predicted tracer concentration for  $R_v = 1.0$  when  $C_2$  is set to the FLUENT v5 default value of 1.9. Very little mixing between the inner and outer fluid streams is observed, even after six pipe diameters. By increasing  $C_2$ , the mixing is enhanced as shown by the increased jet spreading and the shortened potential core of the inner jet (Figs. 16c-f), while decreasing  $C_2$  results in less mixing and a larger potential core (Fig. 16a). Figure 17 shows similar results for  $R_v = 6.0$ . By comparing the experimental jet shape to the predictions in Figs. 16 and 17, a value of  $C_2 = 2.2$  was selected to yield the best qualitative agreement between the experiments and predictions. This value was used for all realizable  $k$ - $\epsilon$  model calculations of this study.

#### 10.2.5 Flow Visualization Comparisons

Calculations were completed using the standard  $k$ - $\epsilon$  model and the realizable  $k$ - $\epsilon$  model to predict the experimental jet shape at various  $R_v$  values. For the standard  $k$ - $\epsilon$  model,  $C_{1\epsilon} = 1.7$  and  $C_{2\epsilon} = 2.4$  were used for all calculations. For the realizable  $k$ - $\epsilon$  model,  $C_2 = 2.2$ . Figures 18-23 illustrate the numerical predictions with a representative high speed video image from the various  $R_v$  values for this study (Table 2). Each figure shows that there are only small qualitative variations between the two turbulence models. Further analysis is required to identify quantitative differences between the two numerical models, if any. In general, both models predict the qualitative shape of the mixing region between the colored and clear water streams. Figure 24 shows that the dimensionless mixing distance ( $L_w/D$ ) predicted by both turbulence models are similar, and they follow the experimental trend. However, exact lengths at which the inner fluid

stream contacts the outer pipe wall is a subjective measurement, and Fig. 24 shows only that the correct trend is predicted by each turbulence model.

The information determined in the water/water mixing experiments and computational simulations will be useful when extending the mixing system to water and fiber. However, the modeling of this mixing process will be much more complicated. Initial ideas in this area are presented next.

### 10.3 Modeling Water/Fiber Mixing

The mixing of a relatively thick fiber stream with a dilute fiber stream or white water is a very common process in the pulp and paper industry. This occurs in the approach flow area where thick stock is mixed with thin stock to dilute the fiber suspension to the proper headbox consistency. This also occurs when chemical additives are introduced into a pulp suspension moving through the mill. Modeling this mixing process is very complicated because the fiber suspension can behave as a Newtonian or a non-Newtonian fluid, depending on the fiber type, fiber consistency, flow conditions, and local shear rate. This section of the status report will summarize our progress in modeling this complex suspension flow. First, suspension flows without fibers will be briefly discussed. Then, fiber suspension flows will be addressed. Finally, a proposed new method to model the concentric pipe mixing process of two streams, one with fiber and one without, will be outlined.

#### 10.3.1 Suspension Flows Without Fibers

Suspensions of solid particles in fluids are commonly encountered in many engineering applications. For sufficiently dilute suspensions in a Newtonian fluid, the suspension behaves as a Newtonian fluid. As the solids loading increases, the viscous behavior of the suspension becomes non-Newtonian [14]. The point where this deviation occurs cannot be reliably predicted because it depends on the characteristics (i.e., size, shape, roughness, etc.) and concentration of the solid material, as well as the solid-solid and solid-fluid interactions [14, 15].

The rheological behavior of suspensions (and for that matter, all liquids) can be described by the deformation or shear rate ( $\dot{\gamma}$ ) as a result of a shear stress ( $\tau$ ). Several models that describe this viscous behavior for various fluids and suspensions are available [14-18]. The simplest case is for a Newtonian fluid where the shear stress is proportional to the shear rate. The proportionality constant is commonly called the dynamic viscosity,  $\mu$ . This relationship is described by

$$\tau = \mu \dot{\gamma} \quad (12)$$

For suspensions of dilute spherical particles, the interactions between particles can be neglected and the fluid will behave as a Newtonian fluid. Citing Frisch and Simka [19], Stein [18] describes the viscosity of such a system by the Einstein equation

$$\mu = \mu_f (1 + 2.5\phi) \quad (13)$$

where  $\phi$  is the volume fraction of the dispersed solids and  $\mu_f$  is the viscosity of the suspending medium. Additional models have been proposed to describe the viscous behavior of suspensions. Three of which are described below, which are summarized from Darby [14].

A power law fluid can be described by

$$\tau = m\dot{\gamma}^n \quad (14)$$

where  $n$  is the flow index and  $m$  is the consistency coefficient. A Newtonian fluid is described by  $n = 1$ , a shear-thinning fluid when  $n < 1$ , and a shear-thickening fluid when  $n > 1$ . Most fluids exhibit a power law region over a specified shear rate range, but the model fails at very high and/or low shear rates.

When a suspension is at rest, interparticle contact resistance may develop. Fluid motion will develop only after an apparent yield stress ( $\tau_y$ ) is reached. It is common to describe these fluid types as Bingham fluids with

$$\tau = \tau_y + \mu_\infty \dot{\gamma} \quad (15)$$

where  $\mu_\infty$  is a limiting viscosity.

Combining the power law model with a yield stress produces the Herschel-Bulkley model, described by

$$\tau = \tau_y + m\dot{\gamma}^n \quad (16)$$

This model is more flexible than the Bingham fluid model because it has three adjustable parameters ( $\tau_y$ ,  $m$ , and  $n$ ), but it still provides unrealistic behavior at high shear rates.

### 10.3.2 Suspension Flows With Fibers

The flow of cellulose fiber suspensions is different from other solid-liquid suspensions and conventional Newtonian or non-Newtonian fluids. The fibers inherently entangle and form structures, even at low fiber concentrations. According to Stenuf and Unbehend [3], the fibers rotate freely in a dilute suspension of fibers and transfer momentum from regions of high velocity to regions of low velocity. This momentum transfer produces additional drag forces which are proportional to the shear rate. The resulting system viscosity increases with increasing fiber concentration and length until a critical concentration is reached. Above this concentration, flocs form and may rotate freely. Further increases in fiber concentration produce a more continuous network which must yield or break down when flow begins. This produces a yield stress followed by a pseudo-plastic flow behavior. Because of this behavior, fiber suspensions have been described as Bingham fluids [17].

Previous investigators have studied the pipe flow behavior of fiber suspensions and it has been summarized in many articles [2, 3, 20-29]. From this information, a theoretical model of the effective viscosity can be identified [22]. The theoretical shear stress behavior as a function of shear rate is shown in Fig. 25. Location A in Fig. 25 represents the yield stress that must be overcome to produce fluid movement. Between A and B, the flow rheology may be described as a Bingham fluid. From B to C to D, the fluid becomes shear-thinning and a drag reduction region is identified, with the maximum drag reduction occurring at C. At location D, the shear rate is high enough that the flow is highly turbulent and the fiber suspension may be approximated as a Newtonian fluid. The theoretical behavior is shown in Fig. 25, but the actual locations of A, B, C, and D are dependent upon many factors including the fiber type, fiber consistency, and pulping process.

A successful model of the fiber suspension rheology must contain a majority of the characteristics found in Fig. 25. Wikström and Rasmuson [30] have numerically modeled a jet nozzle agitator in a large fiber suspension tank. A Bingham fluid model and a Hershel-Bulkley model of the fiber rheology was used in the numerical calculations. They concluded that there were no significant differences between the two rheology models because the dominating parameter was the yield stress. Furthermore, comparisons to experiments showed that the difference between the predicted and experimental velocities increased as the distance from the jet increased. Therefore, they concluded that a Bingham fluid model does not completely describe the fiber suspension rheology, and this was attributed to the shear-thinning behavior of the fiber suspension.

We believe that at least four significant behaviors must be incorporated into any model to accurately describe the fiber suspension rheology. These behaviors include:

- (I) A nearly rigid region where the shear stress is below the yield stress.
- (II) A low shearing rate region where the fiber suspension rheology is nearly linear once the yield stress of the fiber suspension is overcome.
- (III) A region where the shear stress is independent of shear rate (i.e., line BD in Fig. 25). This will provide a conservative estimate of the fluid viscosity in the shear-thinning region.
- (IV) A high shear rate region where the suspension behaves as a turbulent Newtonian fluid (i.e., turbulent water flow).

Region I and II can be successfully illustrated by modeling the suspension as a Bingham fluid. For this case, the yield stress is required for the fiber suspension. This value has been correlated for various fiber suspensions and has the form [28]:

$$\tau_y = \alpha C^\beta \quad (17)$$

where  $C$  is the fiber mass concentration and  $\alpha$  and  $\beta$  are empirical constants that depend on the fiber type. Hence, in modeling the fiber suspension mixing in this region, the local shear stress ( $\tau_{ij}$ ) can be modeled as

$$\tau_{ij} = \alpha C^\beta + \mu_{\text{eff}} \dot{\gamma} \quad (18)$$

where  $\mu_{\text{eff}}$  is the effective suspension viscosity.

In region III, the shear stress is described by the maximum shear stress obtained in region II. This relationship will be valid between locations B and D in Fig. 25, corresponding to critical shear rates  $\dot{\gamma}_{\text{cr1}}$  and  $\dot{\gamma}_{\text{cr2}}$ . At the second critical shear rate value,  $\dot{\gamma}_{\text{cr2}}$ , the shear stress once again becomes a linear function of shear rate. In this region (region IV), the flow may be approximated as highly turbulent Newtonian flow,

$$\tau_{ij} = (\mu + \mu_t) \dot{\gamma} \quad (19)$$

In summary, the shear stress for a fiber suspension flow may be modeled as

$$\text{Region I and II: } \tau_{ij} = \alpha C^\beta + \mu_{\text{eff}} \dot{\gamma} \quad \dot{\gamma} < \dot{\gamma}_{\text{cr1}} \quad (20a)$$

$$\text{Region III: } \tau_{ij} = \alpha C^\beta + \mu_{\text{eff}} \dot{\gamma}_{\text{cr1}} = \tau_{\text{max}} \quad \dot{\gamma}_{\text{cr1}} < \dot{\gamma} < \dot{\gamma}_{\text{cr2}} \quad (20b)$$

$$\text{Region IV: } \tau_{ij} = (\mu + \mu_t)\dot{\gamma} \quad \dot{\gamma}_{cr2} < \dot{\gamma} \quad (20c)$$

The challenging aspect of this simplified theory is identifying the appropriate values for  $\dot{\gamma}_{cr1}$  and  $\dot{\gamma}_{cr2}$ , which are likely to depend upon various parameters such as fiber type and consistency.

Additional characteristics of fiber suspensions, such as floc formation, are not included in the above discussion, but may be added at a later date. For example, the crowding factor, defined as [4]

$$N = \frac{5C_m L^2}{\omega} \quad (21)$$

where  $C_m$  is the fiber mass fraction in percent,  $L$  is the fiber length in m, and  $\omega$  is the fiber coarseness in kg/m. Kerekes and Schell [4] have shown that the crowding factor is a measure of the level of fiber-fiber interaction, and hence, the tendency to flocculate. The effect of  $N$  on the local shear stress is currently unknown. However, Steen [31] has concluded that the crowding factor and pipe Reynolds number were key variables that determine if the pipe flow conditions are either plug, turbulent, or mixed. This will ultimately affect momentum transport in the fiber suspension and possibly the mixing of a fiber suspension with a dilute fluid.

### 10.3.3 Modeling Concentric Pipe Mixing of Fiber Streams

In this study, we will consider the concentric pipe mixing process with the inner fluid consisting of a fiber suspension and the outer fluid corresponding to water (see Fig. 2). As previously discussed, the two fluids will respond differently to fluid shear. Water behaves a Newtonian fluid (Eq. (12)), while the fiber suspension is non-Newtonian (possibly described by Eq. (20)). As the two streams mix, the local viscous behavior of the suspension will change because it is a function of the *local* fiber consistency and the *local* shear rate, both of which vary throughout the mixing region. It is the goal of this research to identify the appropriate relationship that describes this variation.

Consider the simplest concentric mixing flow conditions, laminar flow in an axisymmetric (two-dimensional) mixer. The conservation of mass and momentum for a steady, incompressible fluid with constant properties is

$$\frac{\partial u_i}{\partial x_i} = 0 \quad (22)$$

$$\rho u_j \frac{\partial u_i}{\partial x_j} = -\frac{\partial p}{\partial x_i} + \frac{\partial \tau_{ij}}{\partial x_j} \quad (23)$$

where  $\tau_{ij}$  is given either by Eq. (12) for water or Eq. (20) for the fiber suspension. The conservation of fiber concentration can also be written for this process; however, we assume that fiber transport is governed by advection only and fiber diffusion is negligible. Therefore,

$$\rho u_j \frac{\partial c}{\partial x_j} = 0 \quad (24)$$

where  $c$  is the fiber mass fraction.

The solution to these equations is complicated because the fiber concentration equation (Eq. (24)) is coupled to the momentum equation through  $\tau_{ij}$ , where  $\tau_{ij}$  is a function of fiber consistency (Eq. (20)). The success of this model rests on the proper definition of  $\tau_{ij}$  as described in Section 10.3.2.

It is hoped that this simple model can be extended to the turbulent concentric mixing process.

#### 10.4 Goals for FY 00-01

Goals for the next fiscal year are based on a budget request of \$115,000 for this project. The goals include experimental concentric mixing studies with the primary fluid composed of 1 and 2% fiber suspensions. Two different fiber types will be studied in these experiments. These experiments will assist with model validation. Modeling of the concentric mixing process will also be continued. The model will be used to complete parametric studies of various factors that affect the mixing process. These studies will allow us to make recommendations for concentric mixing modifications and optimization.

The tasks for FY00-01 are given below. The numbers continue from those in Section 6.

8. Water/1% softwood fiber concentric mixing
  - a. Experiments
  - b. Computations
  - c. Comparisons
9. Water/2% hardwood fiber concentric mixing
  - a. Experiments
  - b. Computations
  - c. Comparisons
10. Water/2% softwood fiber concentric mixing
  - a. Experiments
  - b. Computations
  - c. Comparisons
11. March 2001 Status Report
12. Member Company Report on the experimental work
13. Numerical parametric studies
14. Member Company Report on the parametric studies

#### 10.5 Deliverables for FY 00-01

Two Member Company Reports will be completed during the next fiscal year. The first will address the experimental work and comparisons to the model predictions. The second will focus on numerical parametric studies of the mixing process.

#### 10.6 Schedule for FY 00-01

The proposed schedule for Project F048 for FY00-01 is provided in Table 3. The last three months of FY99-00 are also included. The numbers in the task column correspond to those in Section 6 and 10.4. The marks during any given time quarter represent some work will be performed during that time period, but they do not imply a full-time commitment.



Table 3: Project F048 schedule for FY00-01.

Task Descriptions	2000 Apr - June	2000 July - Sept	2000 Oct - Dec	2001 Jan - Mar	2001 Apr-Jun
6a	-----				
6b					
6c	-----				
6d	-----				
7	-----	--			
8a		----			
8b		-----			
8c		-----			
9a		--	----		
9b			-----		
9c			-----		
10a				----	
10b				-----	
10c				----	
11			--	-----	
12		----	-----	----	-----
13		-----	-----	-----	-----
14					-----

## 11 REFERENCES

- [1] Forney, L.J., "Jet Injection for Optimum Pipeline Mixing," *Encyclopedia of Fluid Mechanics Volume 2 - Dynamics of Single-Fluid Flows and Mixing*, N.P. Cheremisinoff, Ed., Gulf Publishing Company, Houston, 660-690 (1986).
- [2] Duffy, G.G., and Lee, P.F.W., "Drag Reduction in the Turbulent Flow of Wood Pulp Suspensions," *APPITA Journal*, **31**(4): 280-286 (1978).
- [3] Stenuf, T.J., and Unbehend, J.E., "Hydrodynamics of Fiber Suspensions," *Encyclopedia of Fluid Mechanics: Vol. 5 - Slurry Flow Technology*, N.P. Cheremisinoff, Ed., Gulf Publishing Company, Houston, 291-308 (1986).
- [4] Kerekes, R.J., and Schell, C.J., "Characterization of Fibre Flocculation Regimes by a Crowding Factor," *Journal of Pulp and Paper Science*, **18**(1): J32-J38 (1992).
- [5] Helmer, R.J.N., Covey, G.H., and Lai, L.C.-Y., "Laboratory Study of Co-axial Stock Mixing," *APPITA Journal*, **52**(3): 197-201 (1999).
- [6] Norman, B., and Tegengren, A., "Stock Preparation - A Key to Grammage Control," *Paper Technology*, 42-43 (January 1990).
- [7] Dahm, W.N., Frieler, C.E., and Tryggvason, G., "Vortex Structure and Dynamics in the Near Field of a Coaxial Jet," *Journal of Fluid Mechanics*, **241**: 371-402 (1992).
- [8] Patankar, S.V., *Numerical Heat Transfer and Fluid Flow*, Hemisphere Publishing Corp., New York, 1980.
- [9] Fluent Incorporated, "FLUENT 5 Users Guide," Lebanon, NH, Fluent, Inc. 1998.

- [10] Jones, W.P., and Launder, B.E., "The Prediction of Laminarization with a Two-Equation Model of Turbulence," *International Journal of Heat and Mass Transfer*, **15**: 310-314 (1972).
- [11] Shih, T.-H., Liou, W.W., Shabbir, A., and Zhu, J., "A New k- $\epsilon$  Eddy Viscosity Model for High Reynolds Number Turbulent Flows: Model Development and Validation," *Computers in Fluids*, **24**(3): 227-238 (1995).
- [12] Monclova, L.A., and Forney, L.J., "Numerical Simulation of a Pipeline Tee Mixer," *Industrial and Engineering Chemistry Research*, **34**(4): 1488-1493 (1995).
- [13] Georges, A.T., Forney, L.J., and Wang, X., "Numerical Study of Multi-Jet Mixing," *Industrial and Engineering Chemistry Research*, In review.
- [14] Darby, R., "Hydrodynamics of Slurries and Suspensions," *Encyclopedia of Fluid Mechanics: Vol. 5 - Slurry Flow Technology*, N.P. Cheremisinoff, Ed., Gulf Publishing Company, Houston, 49-91 (1986).
- [15] Ganani, E., and Powell, R.L., "Suspensions of Rodlike Particles: Literature Review and Data Correlations," *Journal of Composite Materials*, **19**: 194-215 (1985).
- [16] Hanks, R.W., "Principles of Slurry Pipeline Hydraulics," *Encyclopedia of Fluid Mechanics: Vol. 5 - Slurry Flow Technology*, N.P. Cheremisinoff, Ed., Gulf Publishing Company, Houston, 213-276 (1986).
- [17] Hubbard, D.W., "Diffusion and Mixing in Non-Newtonian Fluids," *Encyclopedia of Fluid Mechanics: Vol. 6 - Complex Flow Phenomena and Modeling*, N.P. Cheremisinoff, Ed., Gulf Publishing Company, Houston, 35-109 (1986).
- [18] Stein, H.N., "Rheological Behavior of Suspensions," *Encyclopedia of Fluid Mechanics: Vol. 5 - Slurry Flow Technology*, N.P. Cheremisinoff, Ed., Gulf Publishing Company, Houston, 3-48 (1986).
- [19] Frisch, H.L., and Simka, R., "Viscosity of Colloidal Suspensions and Macromolecular Solutions," *Rheology, Theory and Applications*, F.R. Eirick, Ed., Academic Press Inc., New York, 535-613 (1936).
- [20] Lee, P.F.W., and Duffy, G.G., "An Analysis of the Drag Reducing Regime of Pulp Suspension Flow," *TAPPI Journal*, **59**(8): 119-122 (1976).
- [21] Sharma, R.S., Seshadri, V., and Malhotra, R.C., "Drag Reduction in Dilute Fibre Suspensions: Some Mechanistic Aspects," *Chemical Engineering Science*, **34**: 703-713 (1979).
- [22] Gullichsen, J., and Härkönen, E., "Medium Consistency Technology - I. Fundamental Data," *TAPPI Journal*, **64**(6): 69-72 (1981).
- [23] Duffy, G.G., "The Optimum Design of Pipelines for Transporting Wood Pulp Fibre Suspensions," *APPITA Journal*, **42**(5): 358-361 (1989).
- [24] Duffy, G.G., "Flow of Medium Consistency Wool Pulp Fibre Suspensions," *47th APPITA Annual General Conference Proceedings*, 507-514 (1993).
- [25] Powell, R.L., Weldon, M., Ramaswamy, S., and McCarthy, M.J., "Characterization of Pulp Suspensions," *1996 Engineering Conference*, Chicago, TAPPI Press, 525-533 (September 16-19, 1996).

- [26] Kerekes, R.J., "Characterizing Fibre Suspensions," *1996 Engineering Conference*, Chicago, TAPPI Press, 21-28 (September 16-19, 1996).
- [27] Bennington, C.P.J., Kerekes, R.J., and Grace, J.R., "Motion of Pulp Fibre Suspensions in Rotary Devices," *The Canadian Journal of Chemical Engineering*, **69**: 251-258 (1991).
- [28] Bennington, C.P.J., Azevedo, G., John, D.A., Birt, S.M., and Wolgast, B.H., "The Yield Stress of Medium- and High-Consistency Mechanical Pulp Fibre Suspensions at High Gas Contents," *Journal of Pulp and Paper Science*, **21**(4): J111-J118 (1995).
- [29] Pande, H., Rao, N.J., Kapoor, S.K., and Roy, D.N., "Hydrodynamic Behavior of Nonwood Fiber Suspensions," *TAPPI Journal*, **82**(6): 140-145 (1999).
- [30] Wikström, T., and Rasmuson, A., "The Agitation of Pulp Suspensions with a Jet Nozzle Agitator," *Nordic Pulp and Paper Research Journal*, **13**(2): 88-94 (1998).
- [31] Steen, M., "On Turbulence Structure in Vertical Pipe Flow of Fiber Suspensions," *Nordic Pulp and Paper Research Journal*, **4**: 244-252 (1989).

12 FIGURES

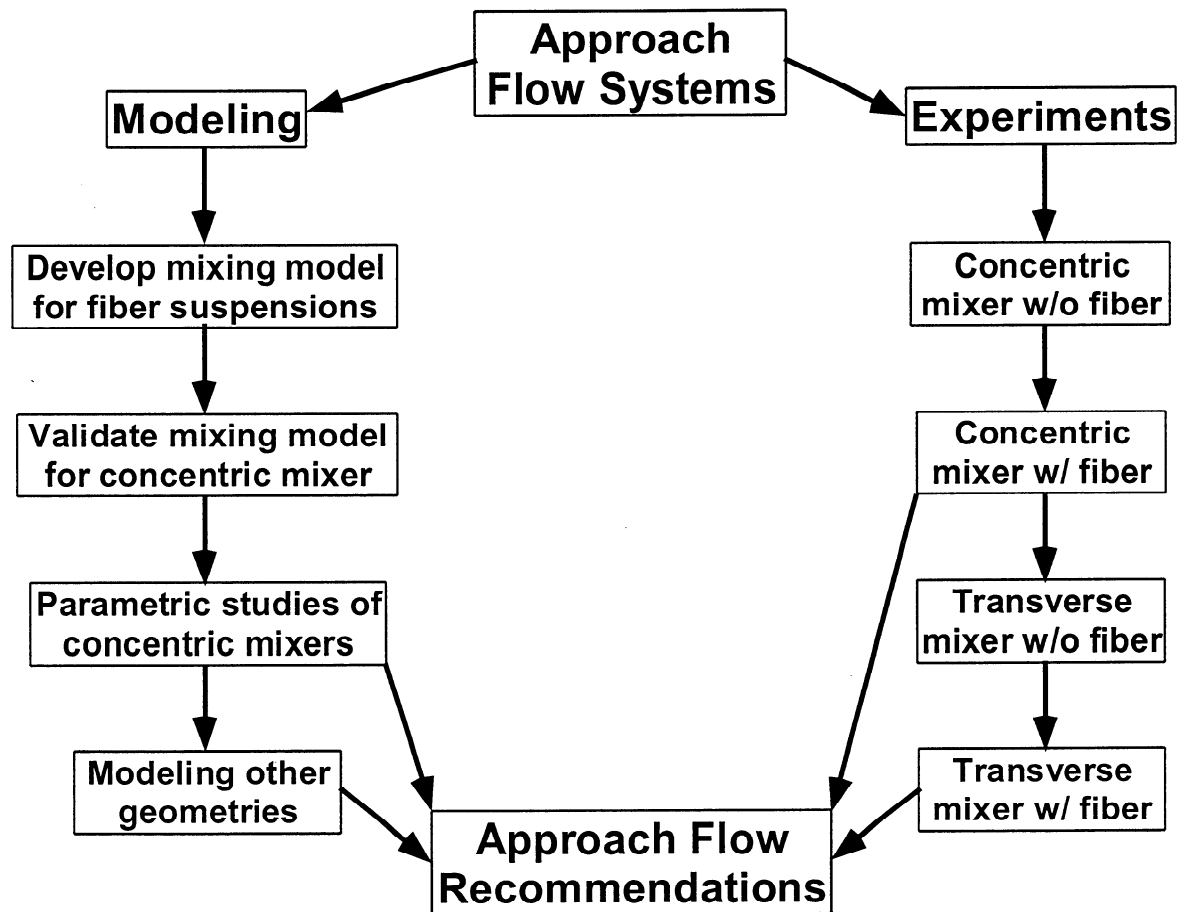


Figure 1: Research road map for Project F048.

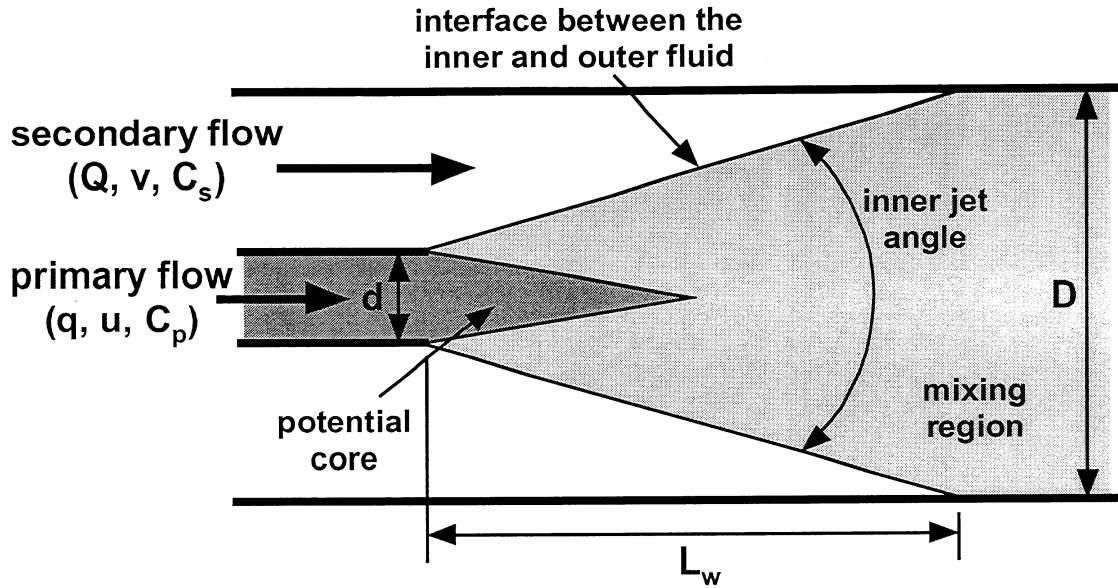


Figure 2: Schematic representation of the concentric mixing process.

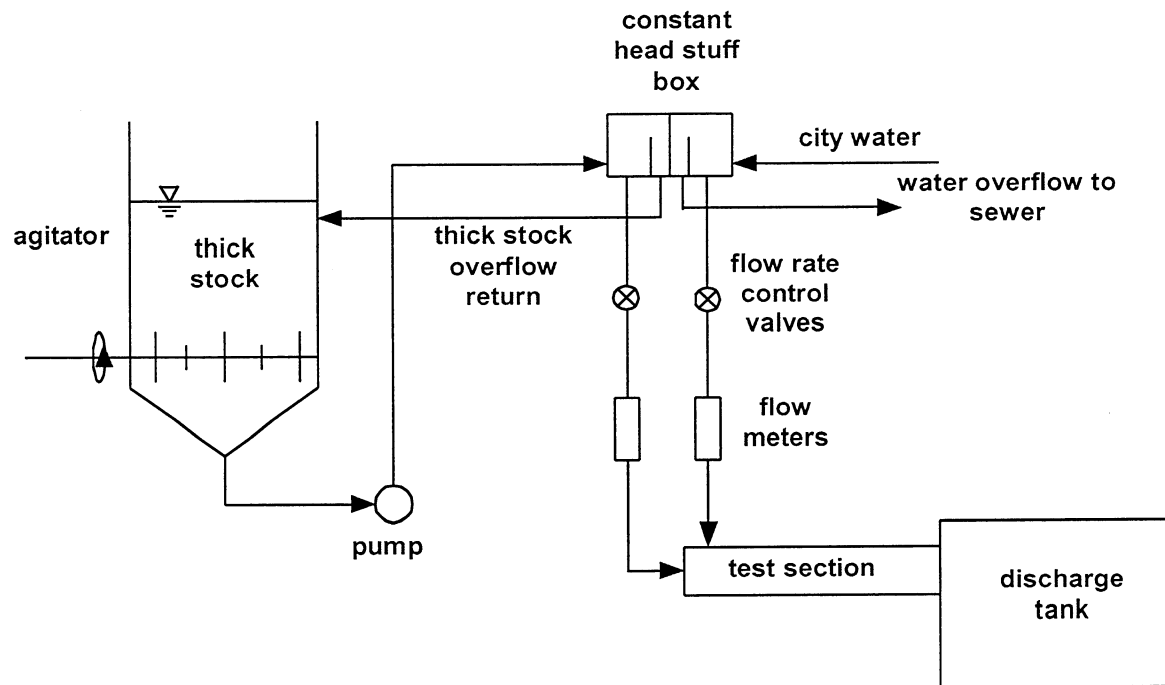


Figure 3: Former experimental mixing facility.

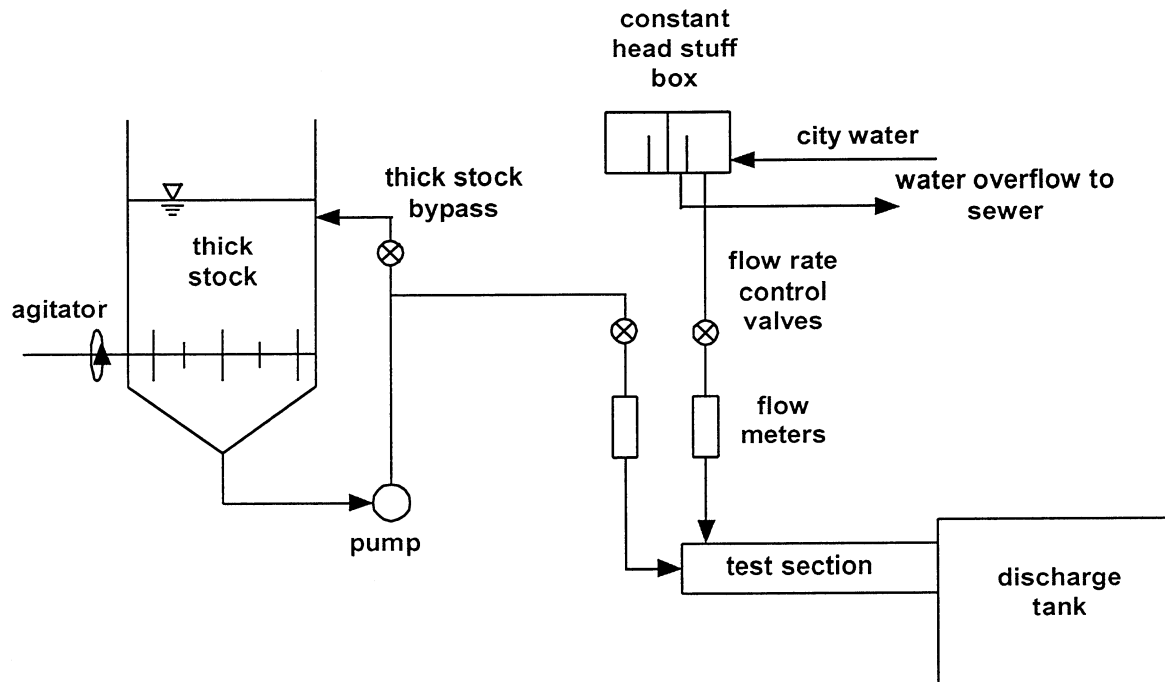


Figure 4: Modified experimental mixing facility.

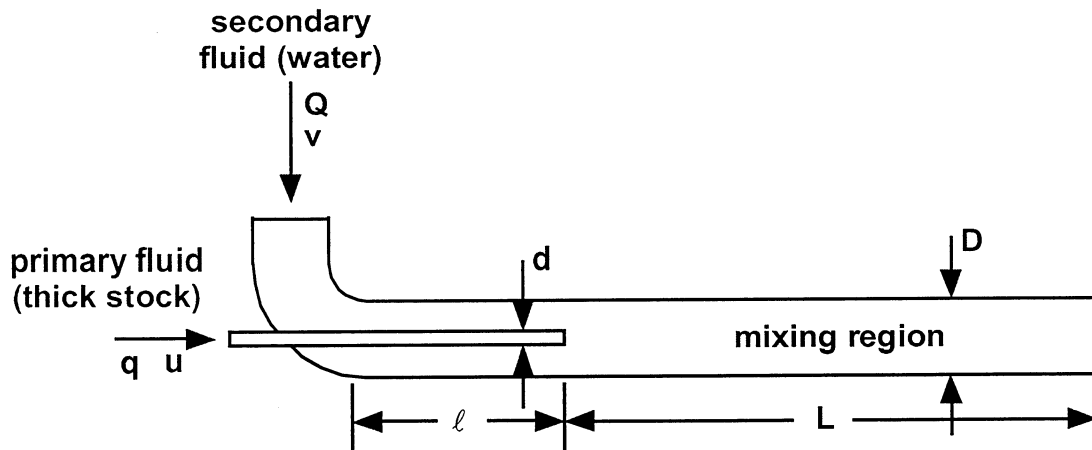


Figure 5: Concentric pipe mixer test section.

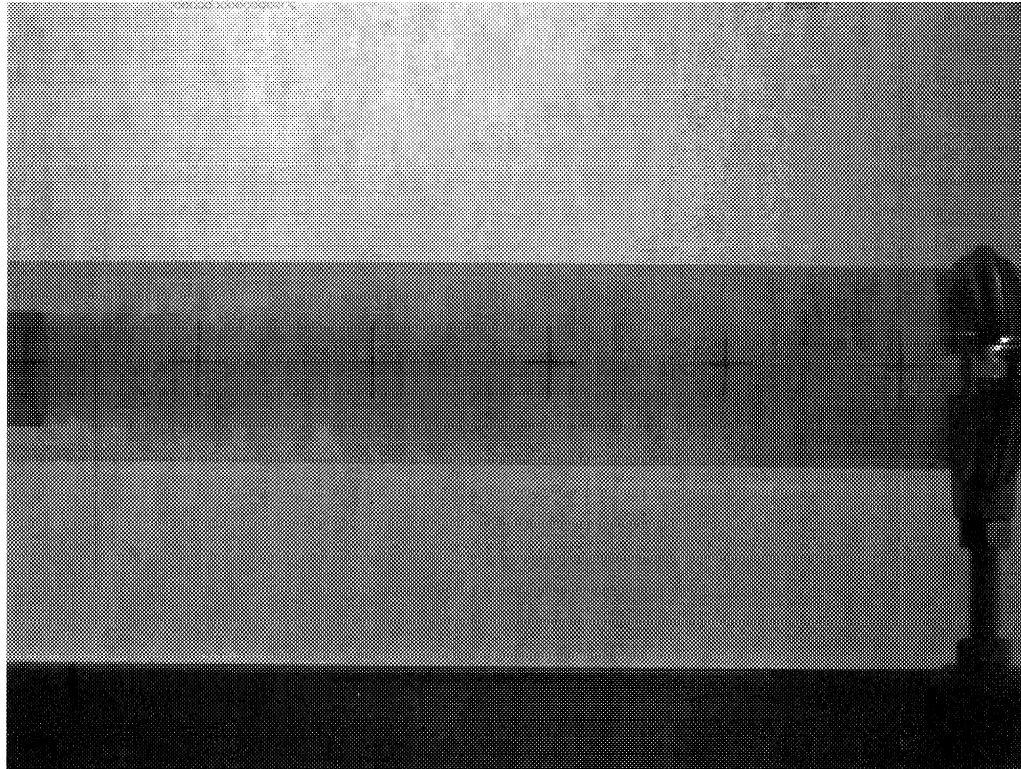


Figure 6: The mixing process at a mean velocity ratio of  $R_v = 1.04$ .

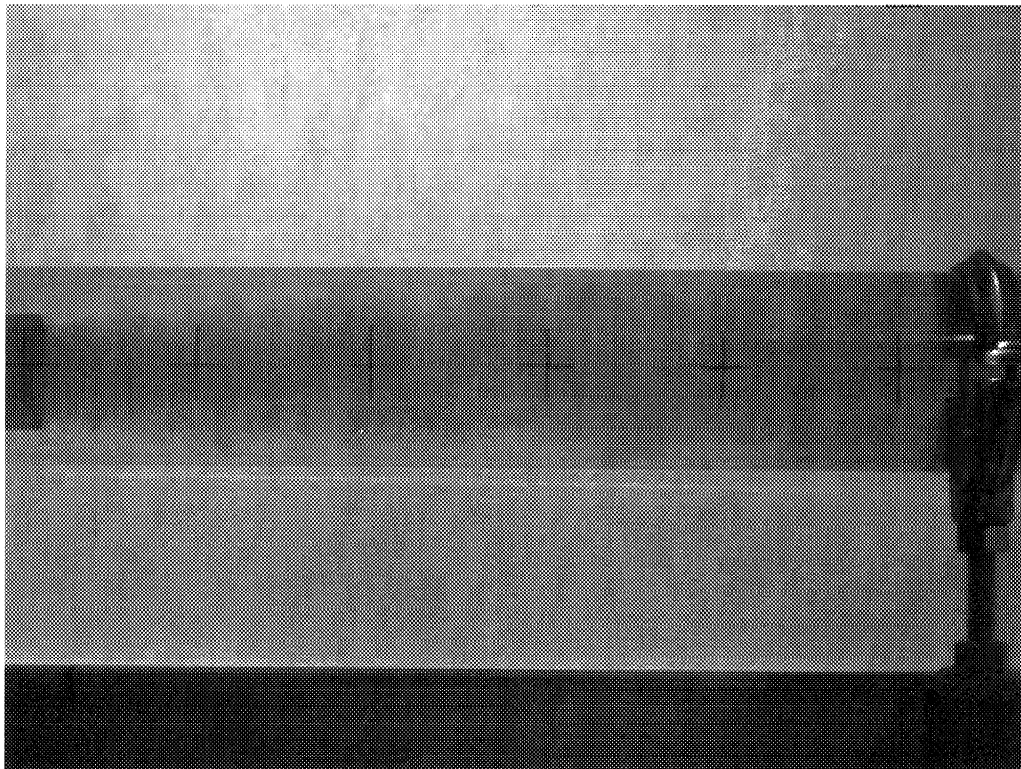


Figure 7: The mixing process at a mean velocity ratio of  $R_v = 2.02$ .

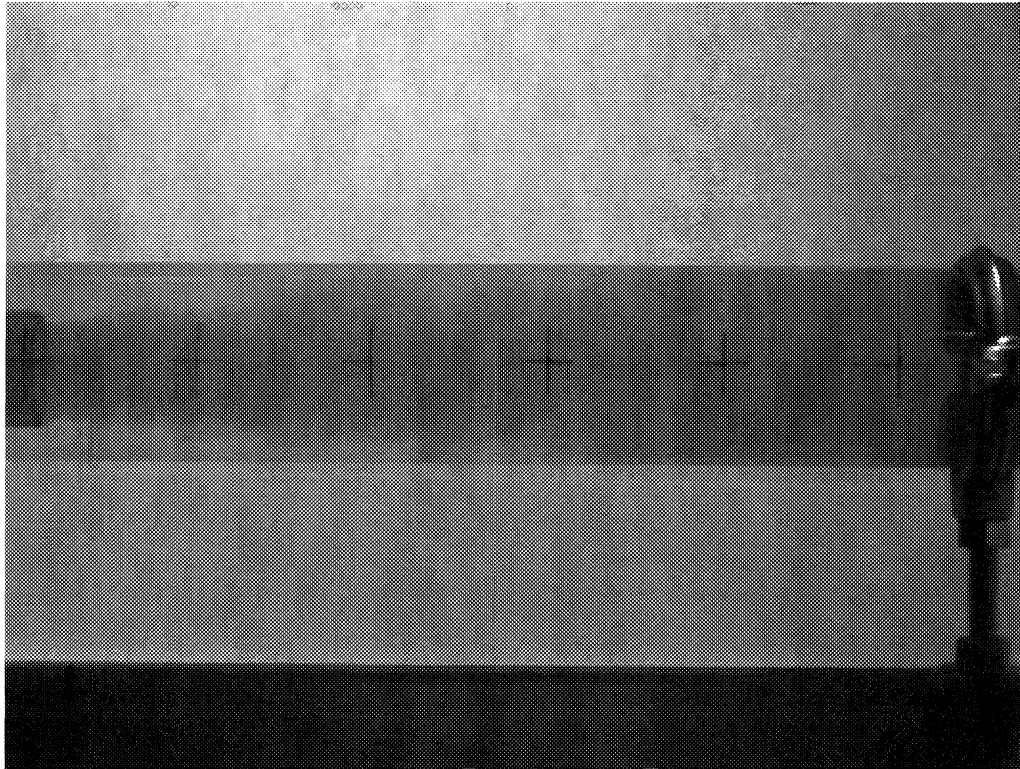


Figure 8: The mixing process at a mean velocity ratio of  $R_v = 2.95$ .

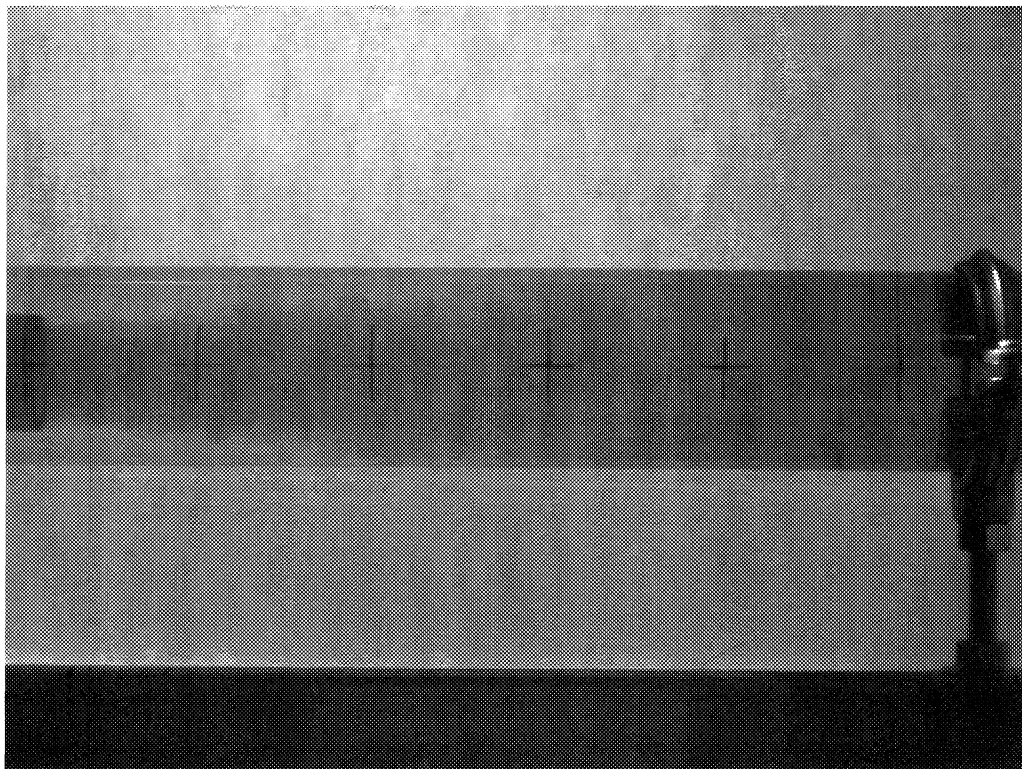


Figure 9: The mixing process at a mean velocity ratio of  $R_v = 3.87$ .



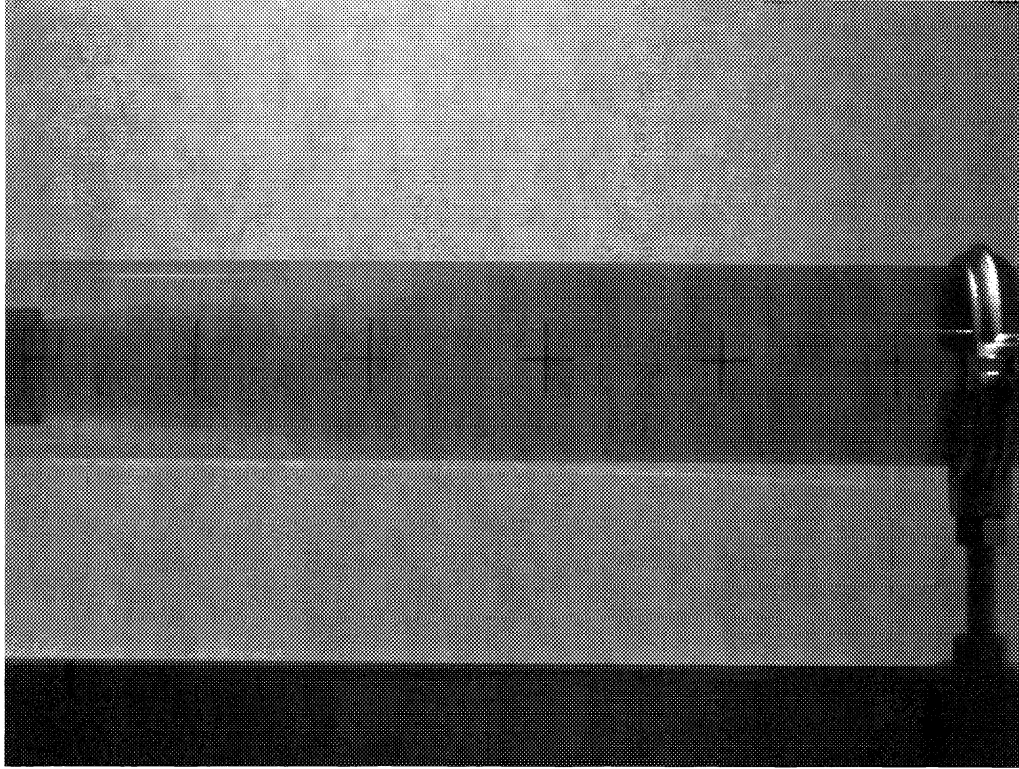


Figure 10: The mixing process at a mean velocity ratio of  $R_v = 4.95$ .

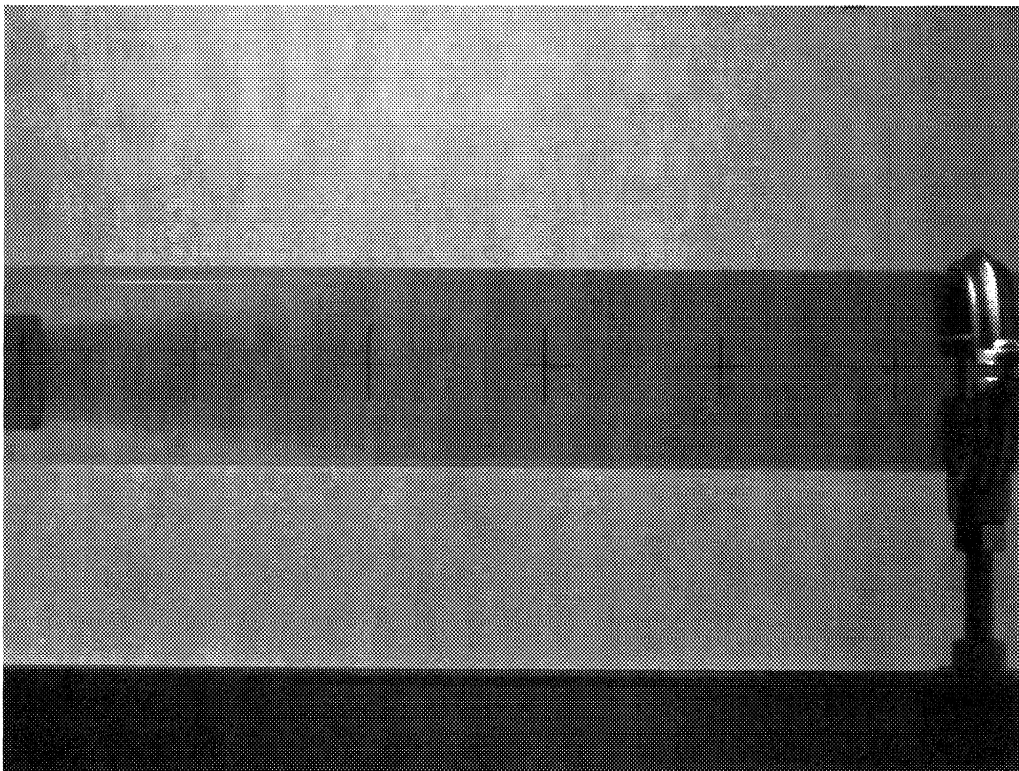


Figure 11: The mixing process at a mean velocity ratio of  $R_v = 6.02$ .

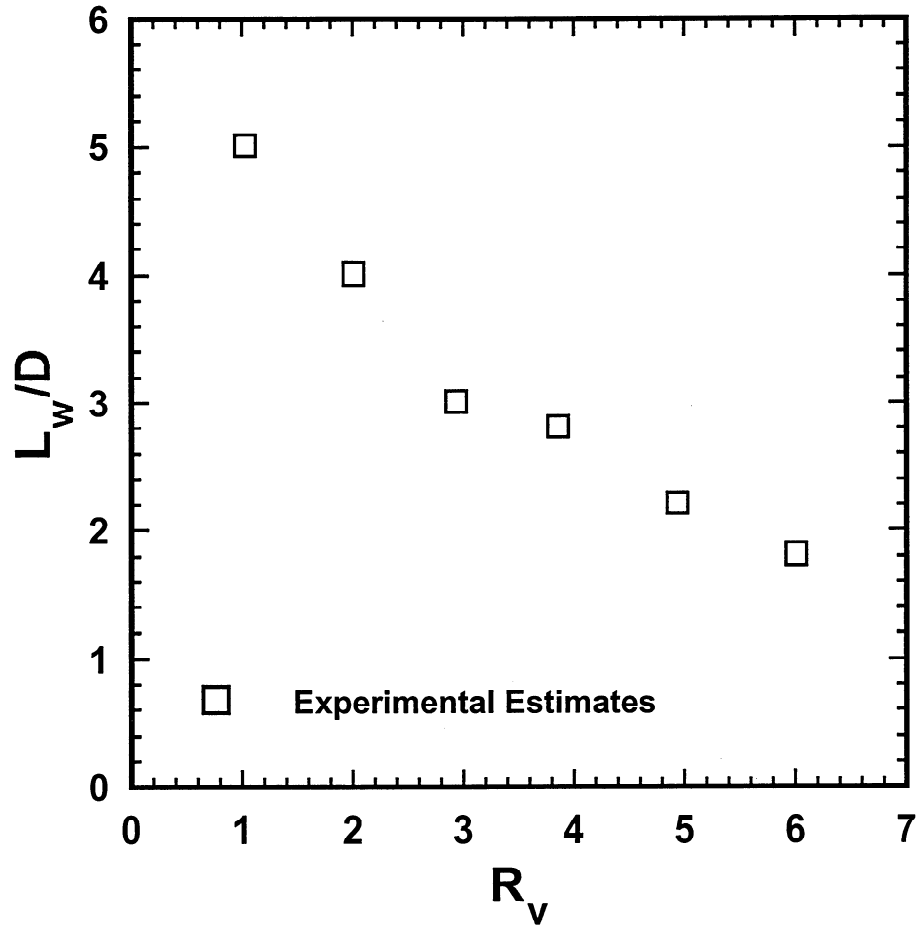


Figure 12: The effect of  $R_v$  on  $L_w/D$ .

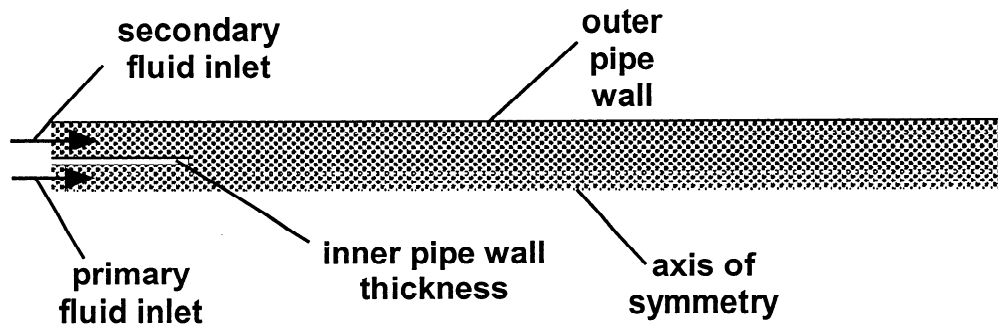


Figure 13: The axisymmetric computation domain.

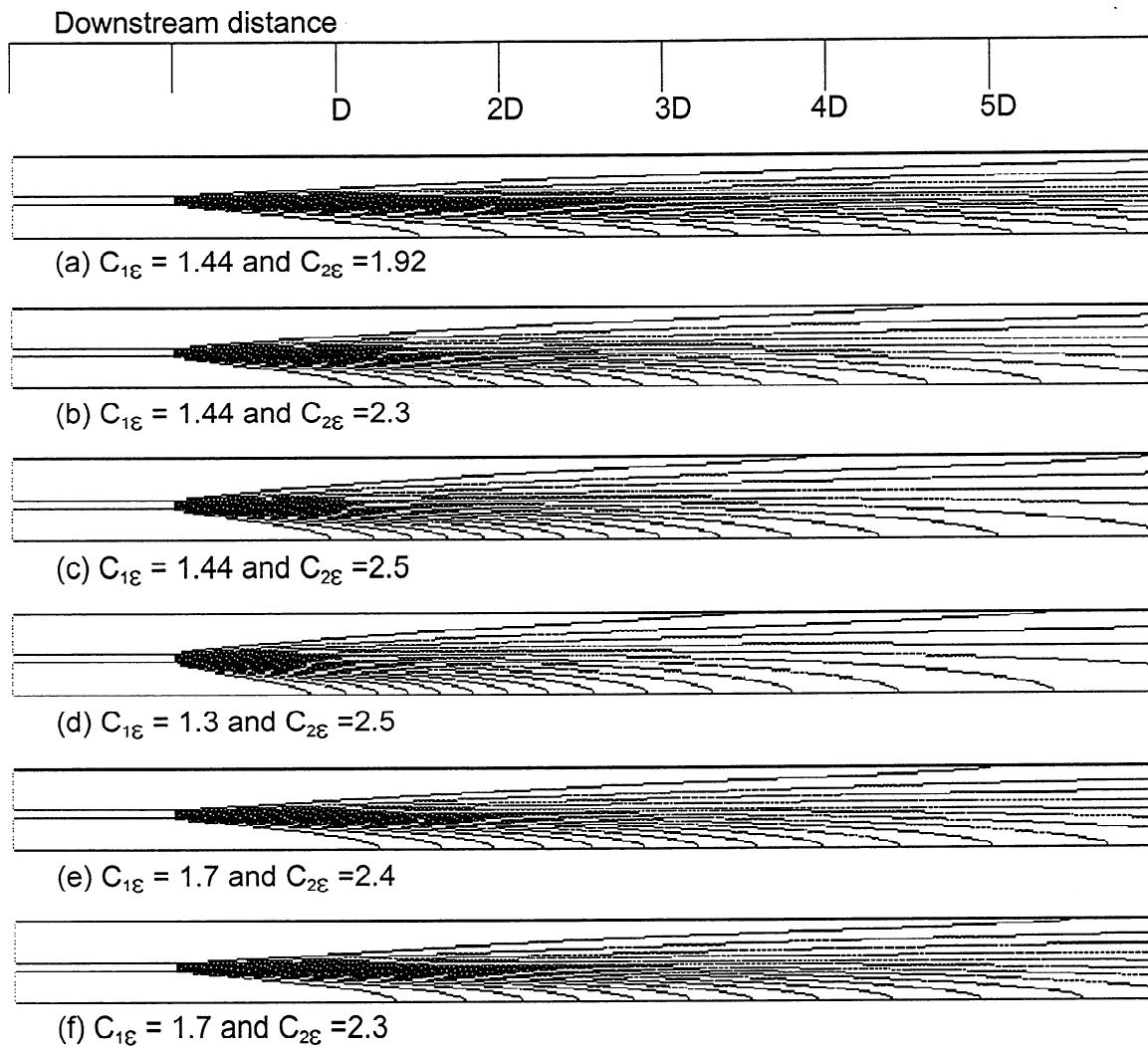


Figure 14: Concentric mixing predictions for  $R_v = 1.0$  by the standard  $k-\epsilon$  model for various  $C_{1\epsilon}$  and  $C_{2\epsilon}$  values.

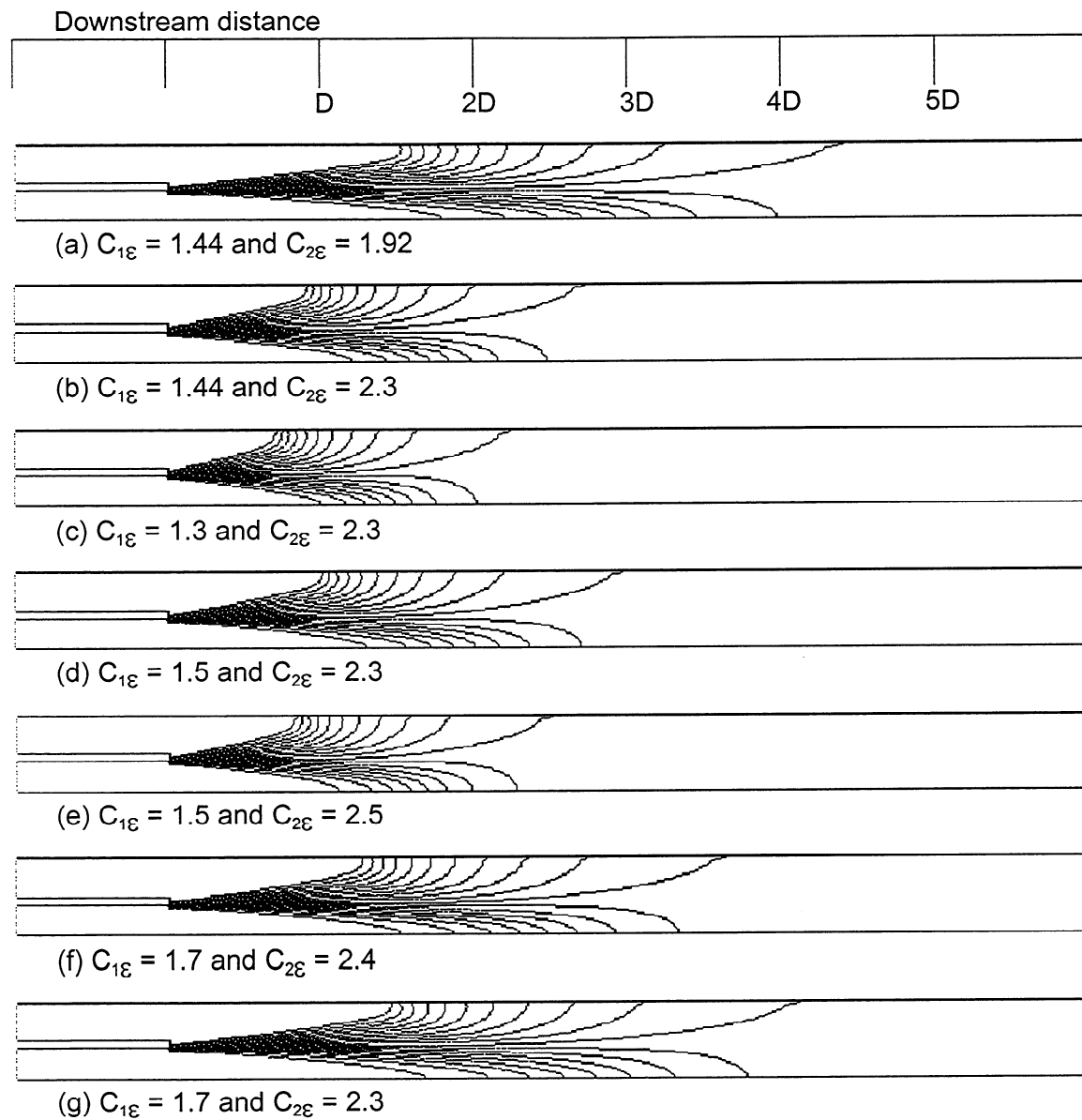


Figure 15: Concentric mixing predictions for  $R_v = 6.0$  by the standard  $k-\varepsilon$  model for various  $C_{1\varepsilon}$  and  $C_{2\varepsilon}$  values.

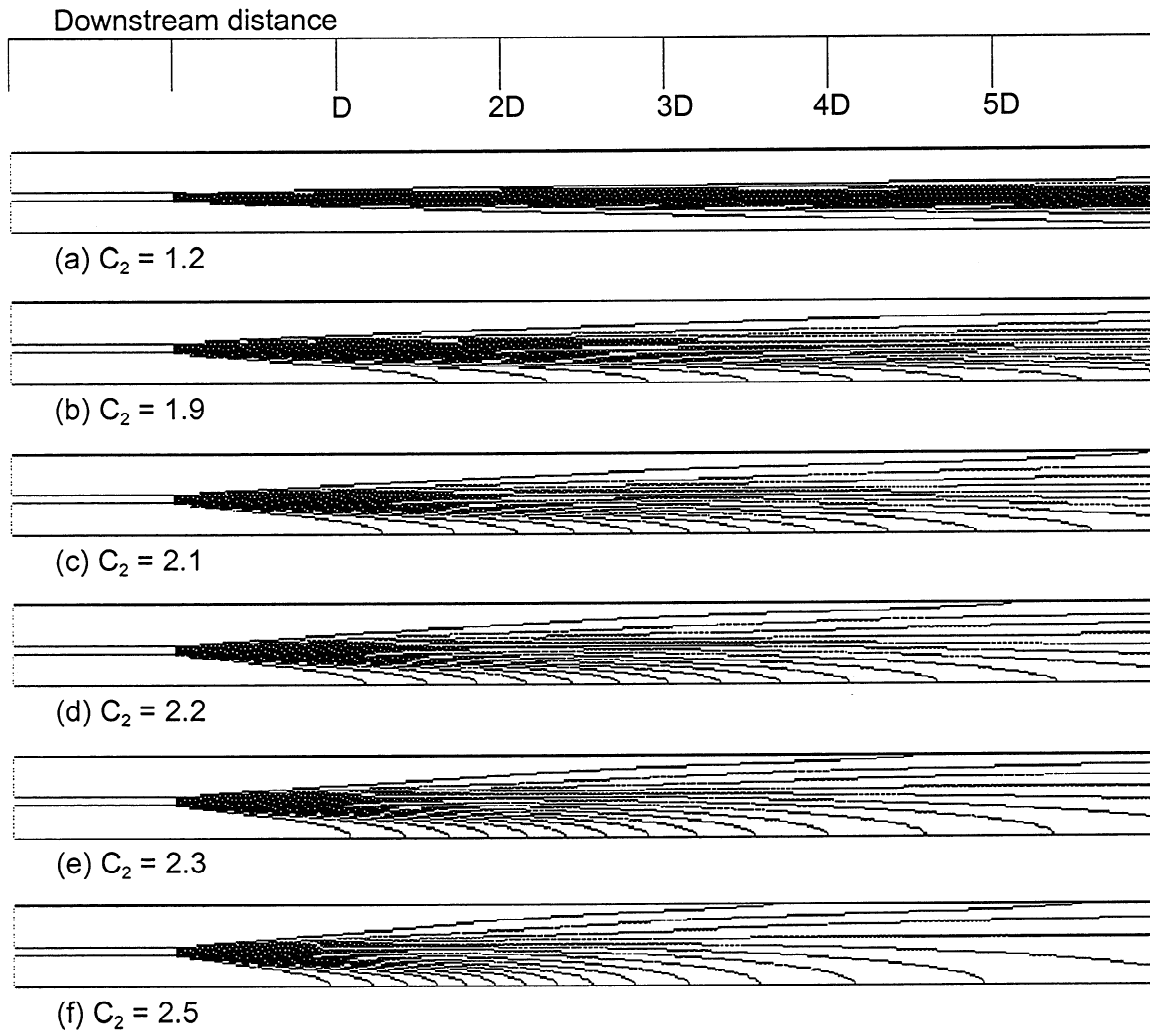


Figure 16: Concentric mixing predictions for  $R_v = 1.0$  by the realizable  $k-\epsilon$  model for various  $C_2$  values.

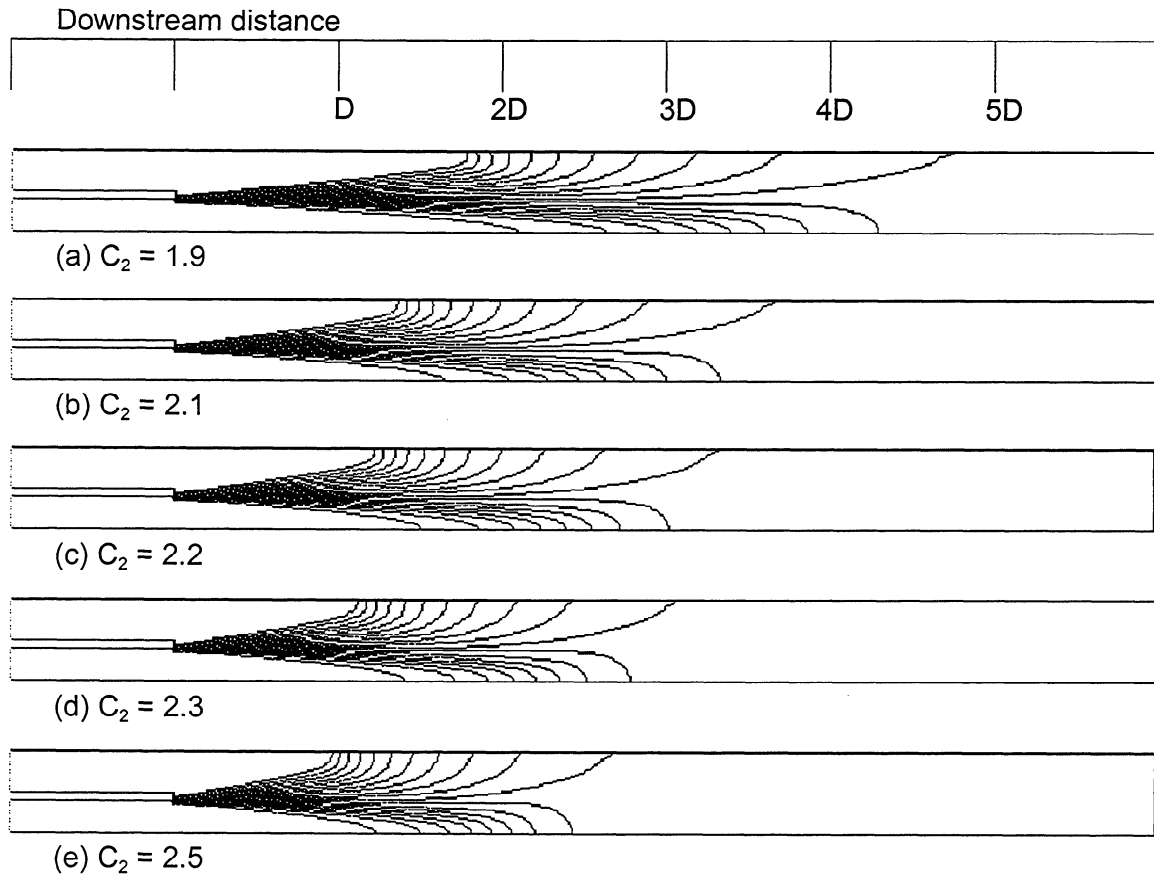


Figure 17: Concentric mixing predictions for  $R_v = 6.0$  by the realizable  $k-\epsilon$  model for various  $C_2$  values.

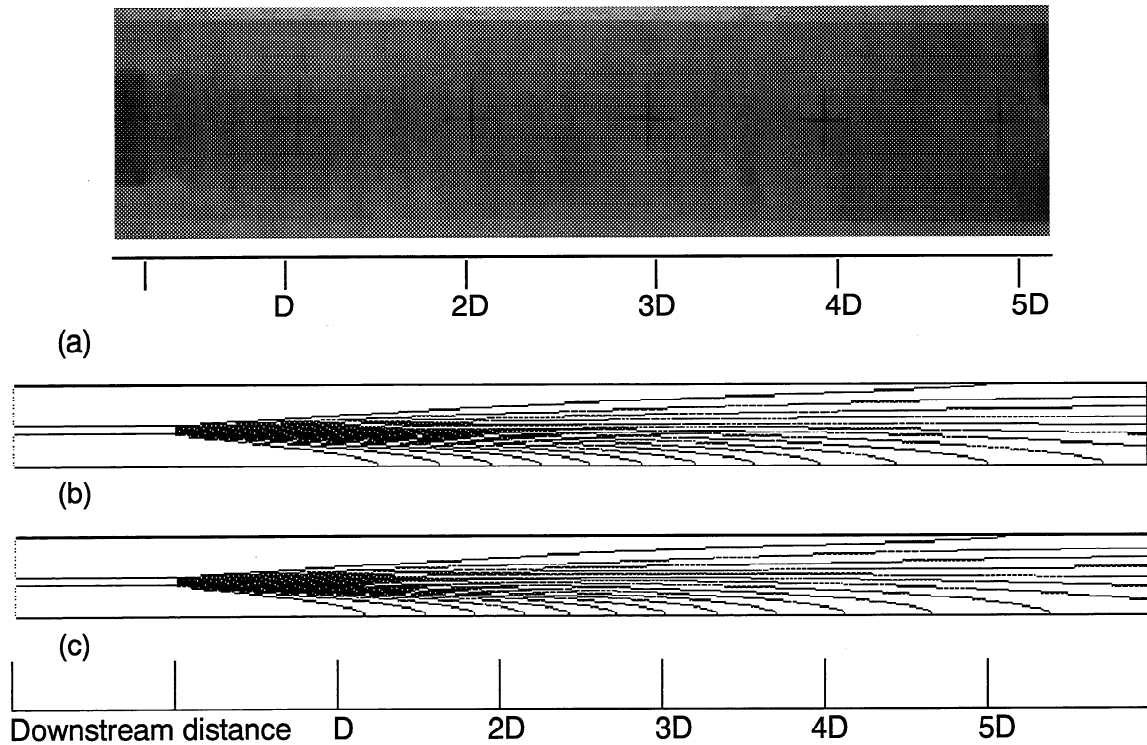


Figure 18: Comparisons between the experimental and predicted mixing regions for  $R_v = 1.04$ . (a) Representative experimental image, (b) standard  $k-\epsilon$  model predictions, and (c) realizable  $k-\epsilon$  model predictions.

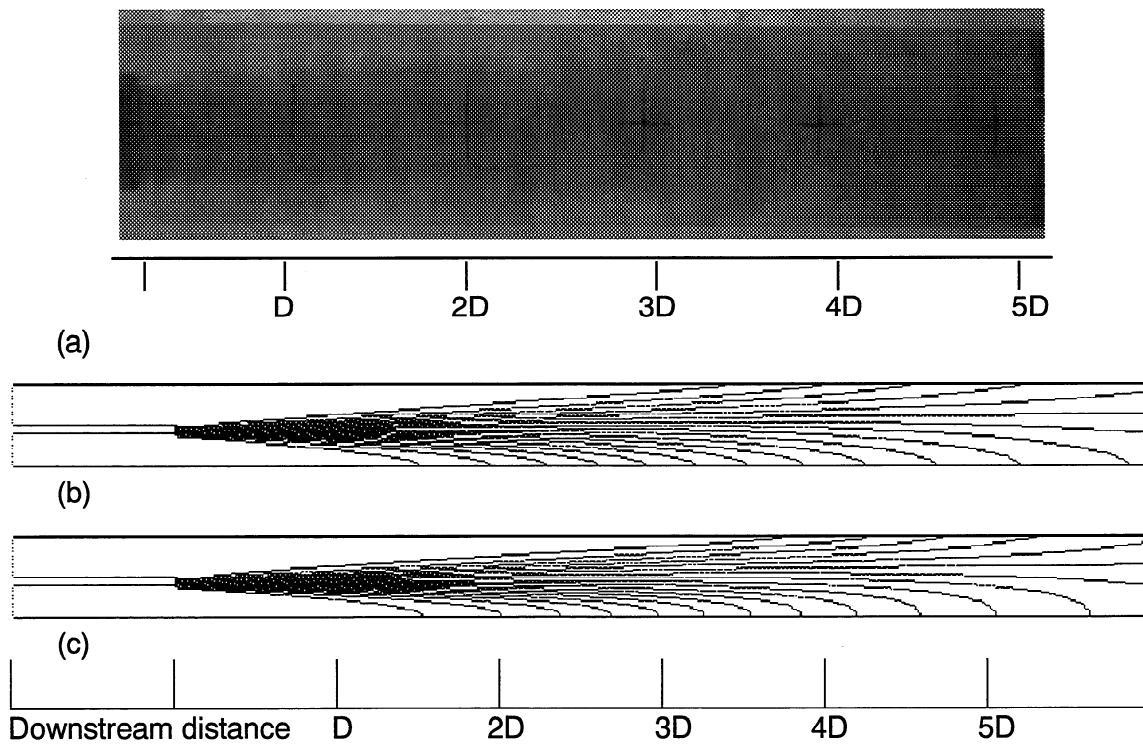


Figure 19: Comparisons between the experimental and predicted mixing regions for  $R_v = 2.02$ . (a) Representative experimental image, (b) standard  $k-\epsilon$  model predictions, and (c) realizable  $k-\epsilon$  model predictions.



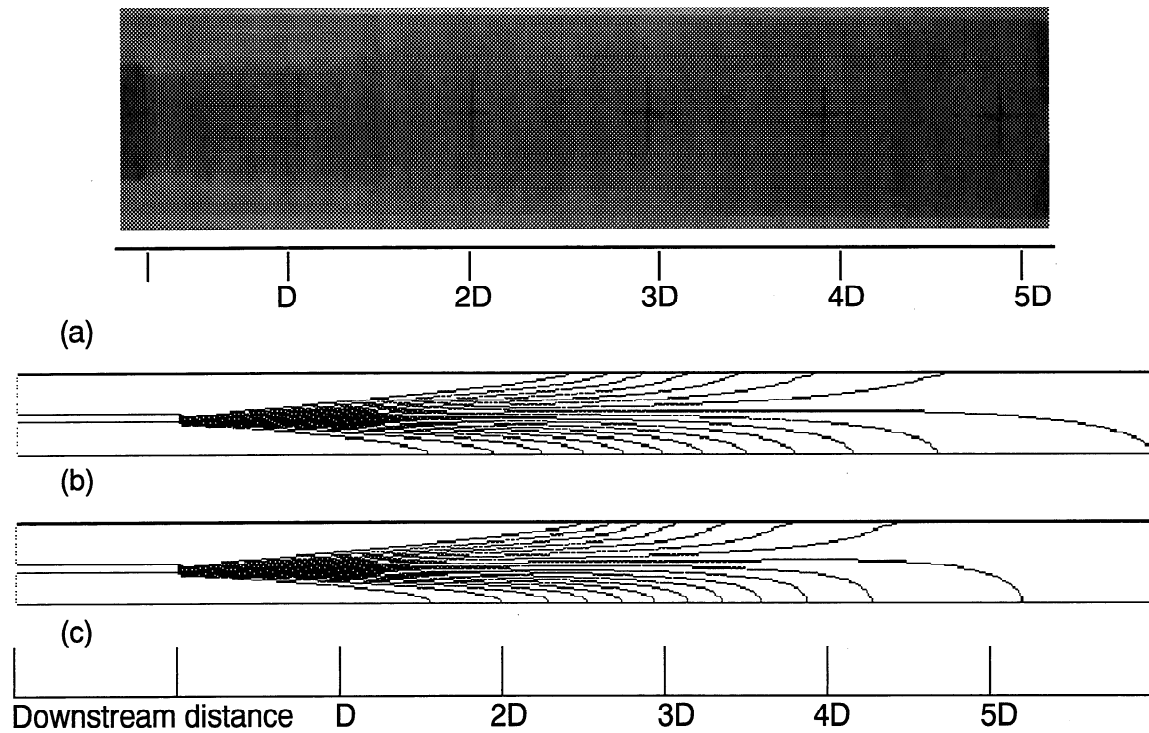


Figure 20: Comparisons between the experimental and predicted mixing regions for  $R_v = 2.95$ . (a) Representative experimental image, (b) standard  $k-\epsilon$  model predictions, and (c) realizable  $k-\epsilon$  model predictions.

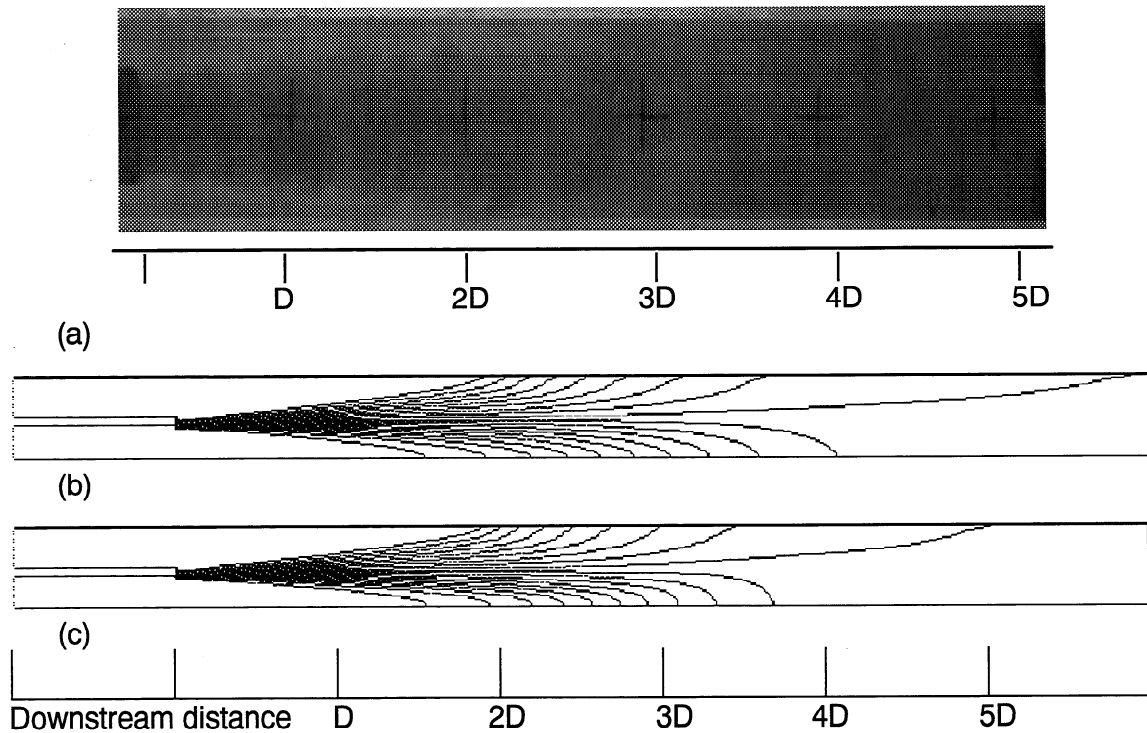


Figure 21: Comparisons between the experimental and predicted mixing regions for  $R_v = 3.87$ . (a) Representative experimental image, (b) standard  $k-\epsilon$  model predictions, and (c) realizable  $k-\epsilon$  model predictions.

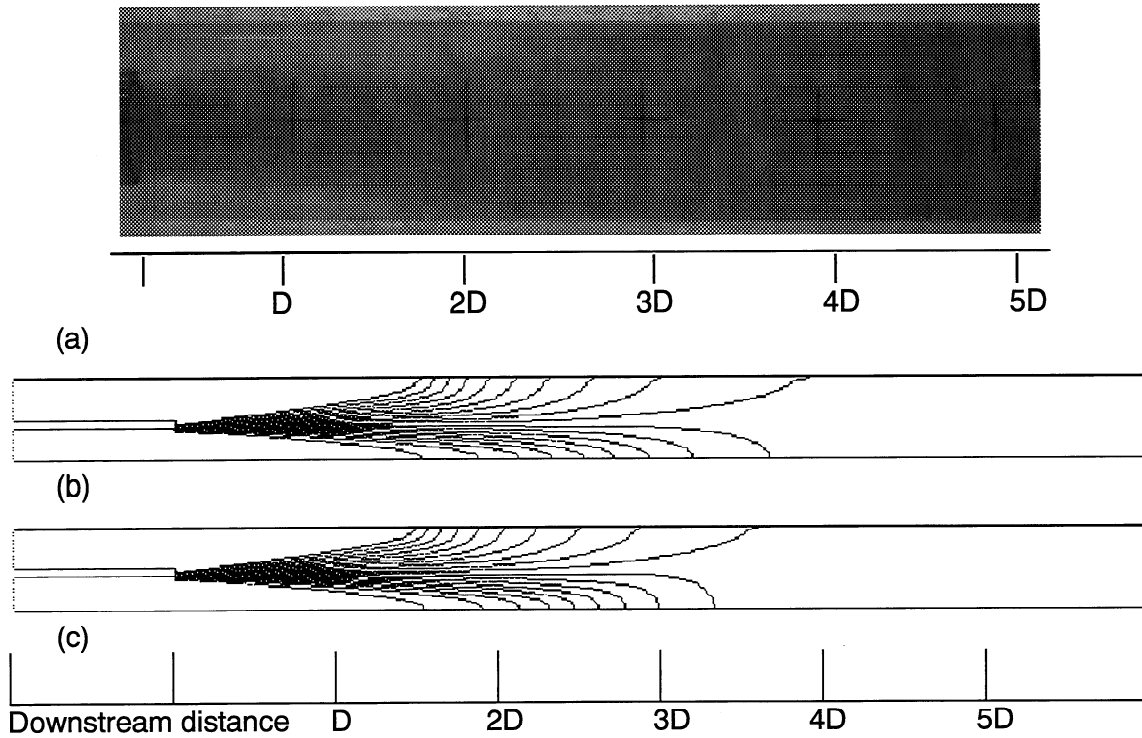


Figure 22: Comparisons between the experimental and predicted mixing regions for  $R_v = 4.95$ . (a) Representative experimental image, (b) standard  $k-\epsilon$  model predictions, and (c) realizable  $k-\epsilon$  model predictions.

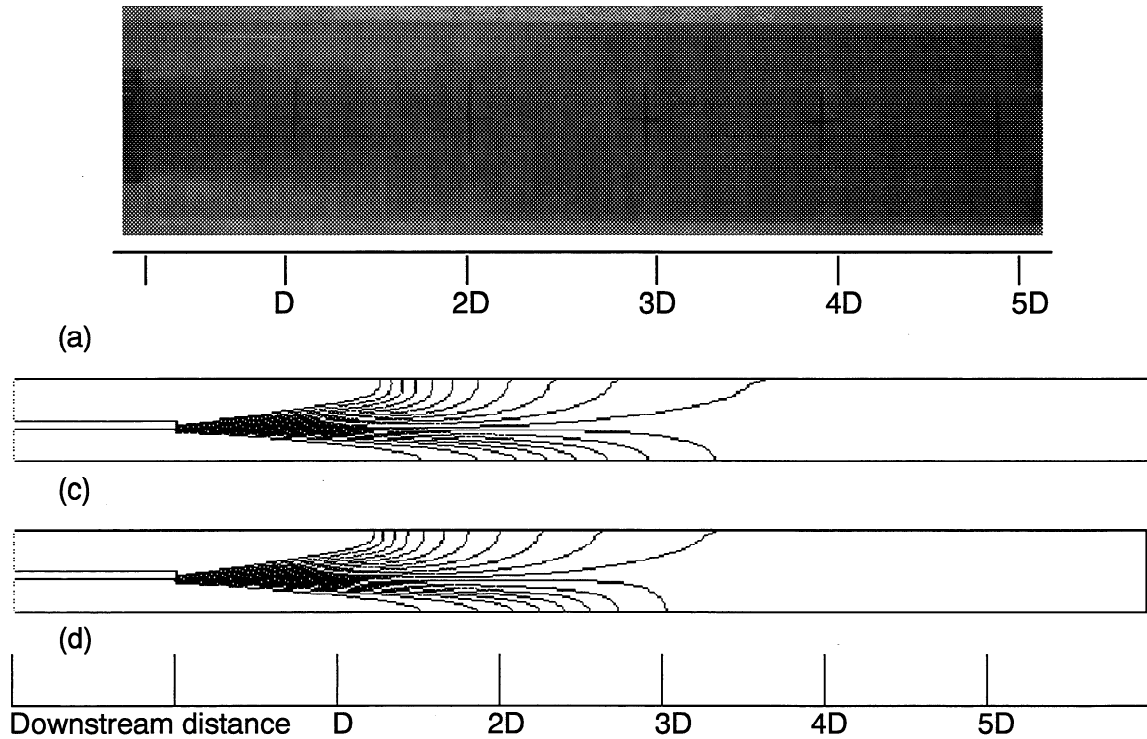


Figure 23: Comparisons between the experimental and predicted mixing regions for  $R_v = 6.02$ . (a) Representative experimental image, (b) standard  $k-\epsilon$  model predictions, and (c) realizable  $k-\epsilon$  model predictions.

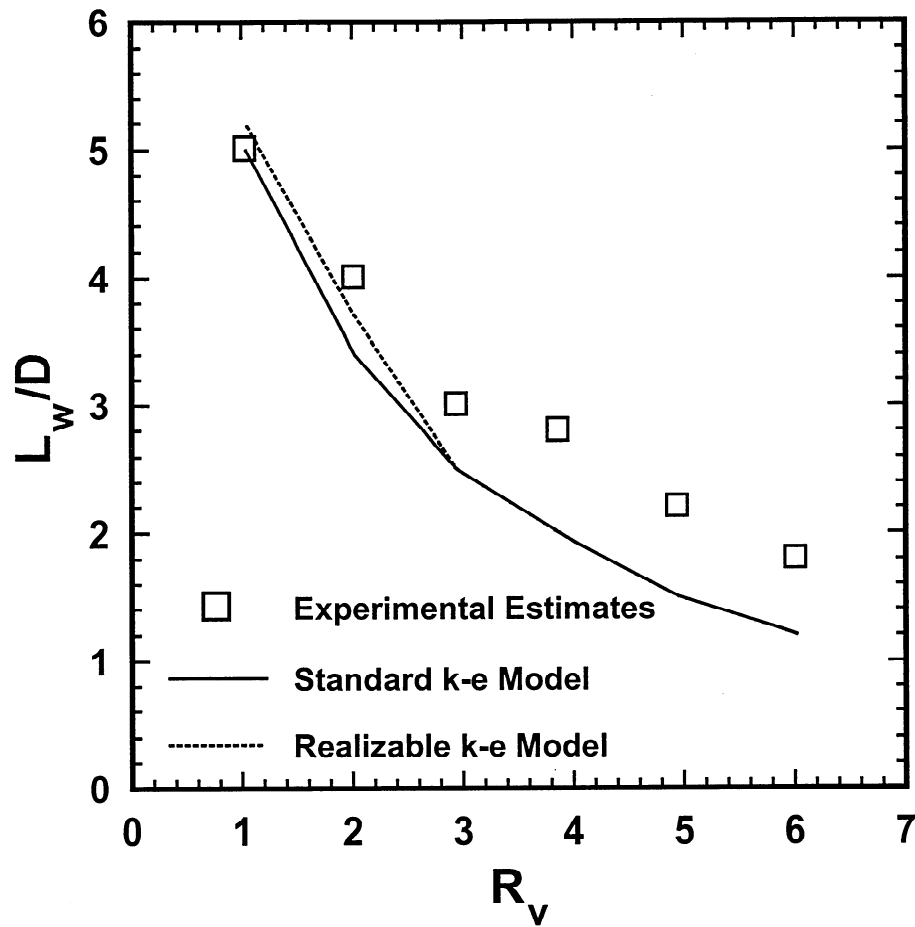


Figure 24: Qualitative comparisons between the experimental and predicted  $L_w/D$  values.

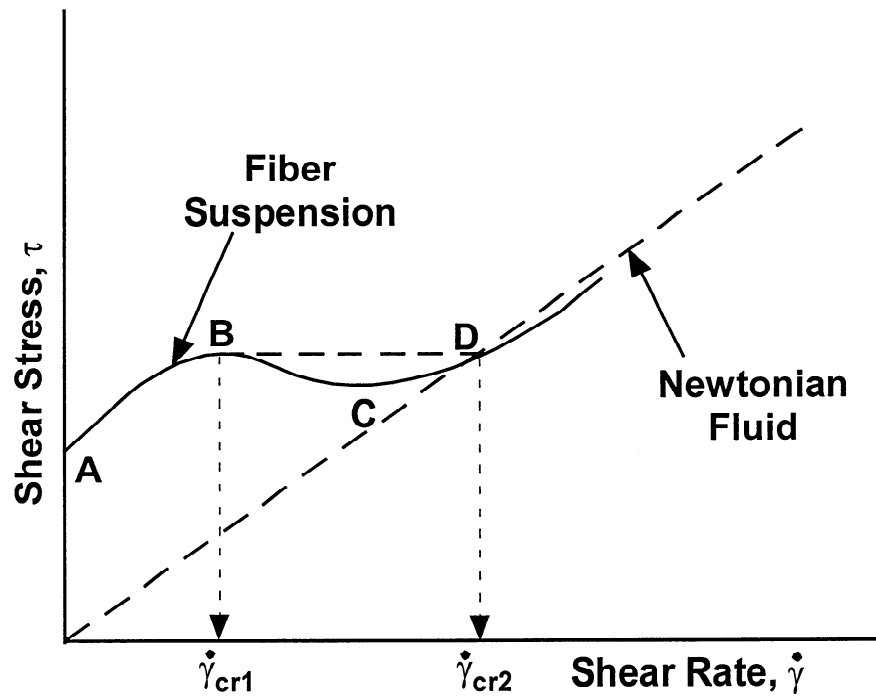


Figure 25: Theoretical model to the effective fiber viscosity.

## 13 APPENDIX A

This appendix contains summaries of the various reports completed by Dr. Wang as part of Project F004.

### 13.1 Report 1

Wang, X., "On the Research Areas of Approach Flow Systems", IPST Member Company Report, Project F004 Report 1, March 1996.

Report 1 provided an outline of potential research directions related to approach flow systems. It contained a brief summary of a telephone survey of various PAC members on approach flow problems. This survey was conducted in the Fall of 1995. The report also included current design recommendations from Voith, Beloit, Valmet, and TAPPI Technical Information Sheets. This report concluded by providing a research plan on approach flow systems.

### 13.2 Report 2

Wang, X., Anderson, T., Snyder, C., and Marziale, M., "On the Causes of Basis Weight Variability", IPST Member Company Report, Project F004 Report 2, September 1998.

This report analyzed various signals from a paper machine to try to determine precursors to basis weight nonuniformity. The recorded signals included thick stock flow rate, consistency at eight different stock locations, local inlet and exit pressure of the pressure pulsation attenuator, beta-gauge scanner position, and beta-gauge basis weight. The signals were sampled at a high frequency (100 Hz), and various signal analysis techniques were used to identify signal variances. Numerous peaks in the power spectrum were identified, but the associated causes were not discussed.

### 13.3 Report 3

Wang, X., Feng, Z., and Forney, L.J., "Computational Simulation of Turbulent Mixing with Mass Transfer", IPST Member Company Report, Project F004 Report 3, March 1998.

The use of ADINA software, and a  $k-\epsilon$  turbulence model to predict the three-dimensional mixing with mass transfer in various geometries was presented in this report. All calculations assumed that the rheology of a low consistency fiber suspension was similar to water. Therefore, the mixing process was modeled as two turbulent miscible fluids with the same density and viscosity, but with different concentrations of an inert tracer.

Modeling transverse mixing with various injection angles from 30° to 150°, in 30° increments, revealed a 90° pipe mixer provided the best mixing. However, these mixers, as well as those with injection angles greater than 90°, produced large scale vortices where flocs could form in actual approach flow systems. These mixer types may also impact the opposite pipe wall and create pressure pulsations in approach flow systems. Although jets with injection angles less than 90° are less efficient mixers, they are less likely to impact the opposite wall. This type of jet mixer was recommended for the pulp and paper industry, but a longer mixing length would be required to compensate for the loss in mixing efficiency.

Compared with a single 90° transverse jet mixer, the mixing efficiency of transverse multijet mixers, each with a 90° jet inlet, was much better. Multijet mixers with an even number of jets equally spaced around the pipe performed better than an odd number of jets. No explanation for this phenomena was provided.

Concentric pipe mixers were shown to be more effective than a single transverse mixer. Mixing was also shown to be unaffected by concentric mixer nozzle shape.

Finally, mixing in geometries that would represent pulp and paper silo operations entering a fan pump were completed. It was shown that increasing the outlet pipe length will improve the mixing efficiency. A corner cut in the silo was shown to reduce, rather than enhance, inert tracer concentration uniformity.

#### **13.4 Report 4**

Feng, Z., Wang, X., and Forney, L.J., "Single Jet Mixing at Arbitrary Angle in Turbulent Tube Flow", IPST Member Company Report, Project F004 Report 4, March 1998.

This report considered a transverse jet with injection angle  $\theta_0$ , with  $0^\circ < \theta_0 < 180^\circ$ , and derived asymptotic solutions for both jet trajectory and tracer concentration profiles in the region near the injection location. Both fluids were similar and the mixing occurred between different concentrations of an inert tracer. The asymptotic solutions matched the existing experimental data obtained from the literature.

#### **13.5 Report 5**

Wang, X., and Bloom, F., "Flow Induced Vibration of Submerged and Inclined Concentric Pipes with Different Lengths", IPST Member Company Report, Project F004 Report 5, May 1998.

This report presented a mathematical model for a submerged concentric pipe system with both confined and unconfined external flows (similar to silo flow right before the fan pump). The natural frequencies of the pipe system were determined and it was shown that the system contains low frequency oscillations around 1 Hz. This may cause low frequency vibrations in inner pipes containing thick stock. It was suggested that to minimize these oscillations, (i) the pipe mass per unit length should be reduced, (ii) the pipe flexural rigidity should be increased (or tapered pipes could be used), and/or (iii) various structural supports should be added to the piping system.

The criteria where buckling or flutter occurred was not detailed. However, additional conclusions in this report included: (i) the longer the outer pipe was, the more susceptible the inner pipe was to buckling or flutter; (ii) the pipe inclination angle and the depth of the submerged pipe system did not significantly influence the characteristic vibration behaviors; (iii) for a fixed volumetric flow rate, there was an optimal inner pipe radius to minimize buckling or flutter; and (iv) increasing the outer pipe diameter for a fixed volumetric flow rate reduced the inner pipe buckling or flutter.

#### **13.6 Report 6**

Wang, X., and Feng, Z., "A Note on Helmholtz Attenuators with Air Cavity and Membrane", IPST Member Company Report, Project F004 Report 6, September 1998.

This report presented a derivation of an analytical expression for the resonance frequency of Helmholtz resonators with an air cavity and membrane. This type of



resonator can be used to absorb pressure waves with frequencies similar to the membrane resonant frequency. Suggested design guidelines for these devices included (i) increasing the neck length will decrease the natural frequency, (ii) the membrane natural frequency should be as low as possible to minimize the resonance frequency, and (iii) the effect of changing the neck cross-sectional area depends on the membrane stiffness.

### **13.7 Report 7**

Wang, X., and Bloom, F., "Stability Issues of Concentric Pipes Conveying Steady and Pulsatile Fluids", IPST Member Company Report, Project F004 Report 7, April 1999.

This report extended the work of Report 5 and the mathematical modeling of a submerged concentric pipe system with both confined and unconfined external flows. The criteria when buckling and flutter occurs was also specified in this report. It was shown that frictional forces suppressed flutter instability, and the longer the outer pipe, the less likely flutter was to occur. Frictional forces also delayed buckling instability. However, it was shown that the longer the outer pipe length, the more susceptible the inner pipe was to buckling. It was also noted that for current pipe system designs in the pulp and paper industry with reasonable flow rates, the concentric pipe system was stable.

FLOW THRU POROUS MEDIA

STATUS REPORT

FOR

PROJECT F022

Seppo Karrila (PI)

March 8 – 9, 2000

Institute of Paper Science and Technology  
500 10th Street, N.W.  
Atlanta, Georgia



**DUES-FUNDED PROJECT SUMMARY**

**Project Title:** FLOW THRU POROUS MEDIA  
**Project Number:** F022  
**PAC:** PAPERMAKING

**Project Staff**

**Principal Investigator:** Seppo Karrila

**PAC Subcommittee** P. Chaudhuri, J. Shands,  
R. Sieberth

**FY 99-00 Budget:** \$104,000

**Time Allocation:**

**Principal Investigator:** 25%

**Supporting Research:**

**Special Students:** Andres Navia (MS)

**RESEARCH LINE/ROADMAP:** Line #11 - Improve ratio of product performance to cost for pulp and paper products by 25% by developing breakthrough paper making and coating processes which can produce the innovative webs with greater uniformity than achieved by current processes.

**PROJECT OBJECTIVE:** Improve control of the layered structure in thickness direction, by clarifying the mechanisms affecting formation and retention on the wire section. Strive to decouple formation and retention.

**PROJECT BACKGROUND:** *The SOTA was reviewed for formation-improving wire section elements as well as for splitting methods enabling layered analysis (tools needed for quantification of structure). Experiments with saturated in-plane flow on nip compression were reported. Drawings (in Finnish, European standards and parts list, with some needs for "debugging") for a pulsating handsheet former were acquired, with device construction dependent on budget allocation.*

**MILESTONES:**

*Implement pulsating handsheet forming capability at IPST.*

*Acquiring an MBDT (Moving Belt Drainage Tester) device is under way and will be accomplished by the end of this fiscal year (June 2000).*

*Quantify dominant benefits of research into wire-section phenomena.*

*Survey opinions from select DFRC members by Spring 2000 PAC.*

*Initiate numerical modeling of particle migration during forming.*

*The model is used to identify the dominant phenomena determining retention (layerwise), to design MBDT experiments and to interpret results. Blocks of the model will be presented in Spring 2000 PAC meeting.*

**DELIVERABLES:**Improved diagnostic laboratory methods for analyzing the structure of paper samples.

*Enabling characterization techniques necessary for quantitative experimental results are also coupled to troubleshooting printability and curl.*

Laboratory procedures for maximizing solids content off couch and tuning the stock composition.

*Development and validation of MBDT device and laboratory procedures for retention and drainage studies will enable fast laboratory studies improving dewatering and machine efficiency at a low cost and with a wide range of parameters, in comparison with pilot studies.*

Retrofit technology using next generation forming elements to decouple formation and retention.

*Opportunities are identified through mechanism studies and applied through innovations.*

**STATUS OF GOALS FOR FY 99-00:**March 2000 PAC goals.

Quantify dominant benefits of research into wire-section phenomena.

Identify key gaps in forming and dewatering on the wire section and estimate the economic implications. The survey will be reported in the Spring 2000 PAC meeting.

Initiate numerical modeling of particle migration during forming.

Phenomena and models related to particle migration have been reviewed to assess where improvement over published models is needed for papermaking application, and to enable composing an improved numerical model based on phenomenological equations describing the essential phenomena. The review is included in this report.

Current fiscal year goals. (Status will be reported in March 2000 PAC meeting.)

Implement pulsating handsheet forming capability at IPST.

IPST has made a capital allocation that enables construction of the MBDT device. The drawings have been reviewed in detail, improved where necessary, and organized into several subassemblies so that machining work can be subcontracted to external machine shops as separate sub-projects.

Develop experimental plan for application of the MBDT.

The direction taken is decided in the March 2000 PAC meeting, largely based on results of the survey mentioned above.

Adopt and improve dry splitting and image analysis techniques that are used as a tool to inspect wire-section effects on layered structure.

A set of pilot-run samples in which the jet/wire speed difference has been varied will be inspected. A flatbed scanner with through lighting capability has been acquired and is connected to an existing image analysis system at IPST. Intermediate status with these samples and techniques is reported in the March 2000 PAC meeting.

A supporting MS-project has been initiated, with focus on the curl of fine paper. In this project Andres Navia will apply layerwise analysis of paper samples from a collaborating mill to assess the root causes of curl.

Layerwise orientation and possibly also fines/filler distributions will be inspected.

**SCHEDULE:** The project schedule should tabulate the major tasks of the project that were scheduled to be worked on from the last spring PAC until the end of this fiscal year. The schedule should indicate the approximate dates when each task was to begin and when each task was scheduled to be completed. The completion of a major task is referred to as a project milestone. Time is usually expressed in quarters.

Task Descriptions (example)	1999 Apr - Jun	1999 July - Sept	1999 Oct - Dec	2000 Jan - Mar	2000 Apr-Jun
1. MBDT quotes, getting funding allocation		-----	----X		
2. Design "debugging"			-----	-----X	
3. Build Equipment				-----	-----X
4. Instrumentation					-----X
5. Initial testing					-----X
6. Initiate migration modeling				-----X	
7. Develop numerical model				-----	-----
8. PAC report				-----X	

#### **SUMMARY OF RESULTS:**

*Dry splitting of sheet samples was demonstrated in a troubleshooting case. Analysis of fiber orientation from thin peeled layers provided information not available from SEM microphotographs or from ultrasonic scans, and was helpful in solving the problem.*

*The construction of MBDT pulsating drainage device resumed after Fall 1999 PAC meeting; it was dropped in Spring 1999 due to budget constraints. Device is expected to be available for initial testing before the end of this fiscal year.*

*To enhance understanding of the mechanisms determining retention, and its layerwise profile in the paper web, numerical simulation of the particle migration phenomena is being initiated. Fundamental aspects related to building an appropriate model from the paper forming perspective are discussed in some detail within this report. The key element absent from earlier models with flow through formed web layers is the detachment of migrating particles. This appears to be the phenomenon responsible for filler depletion at the water exit surface of a formed web, possibly in combination with layerwise compression during a suction pulse.*

#### **SUMMARY OF KEY CONCLUSIONS:**

*A clear need for improvement in paper related particle retention modeling has been identified and will be pursued, to quantify the mechanisms determining thickness-direction filler profiles.*

## Particle migration during forming, review of fundamentals

- A. SIGNIFICANCE
- B. APPROACH
- C. RESULTS
  - Published models related to papermaking*
    - Deposition
      - Turbulent agitation without mat formation
      - Retention during drainage with mat formation
      - Filtration through preformed web
    - Steady models and survey data
  - Hydrodynamic particle release in general*
  - Entrapment of particles*
  - Interaction of migration with permeability*
  - Connections with industry practice*
- D. CONCLUSIONS
  - Scientific Conclusions*
  - Economics*
  - Deliverables*
- D. REFERENCES

### A. Significance

Dues-funded Project F022 at IPST seeks to improve the balance between retention and formation on the wire section. To achieve this goal, a mechanistic understanding of each of these is necessary to suggest developments in the equipment or operation practices.

A laboratory forming capability with pulsating dewatering—a so-called MBDT device—is under development at IPST. In practice, realistic z-direction profiles of pulp fines and fillers have only been observed when a web is formed under pulsating dewatering with somewhat realistic consistency; such capability is essential for inspecting the mechanisms affecting retention.

Conventional handsheet forming operates with smooth water removal and very low fiber consistency. This leads to an “inverted z-profile” of filler content, with enrichment on the wire side. Published modeling work appears capable of qualitatively matching this process, but unable to explain retention phenomena in a realistic situation. Still, models are the main tools needed to interpret experimental data, so an improved model is a necessity.

The purpose of this review is to inspect the fundamental phenomena and mechanisms in order to

- guide the design of experiments with the MBDT
- aid in interpreting results from experiments
- develop both qualitative and quantitative understanding of the active mechanisms, and facilitate numerical simulation of particle migration

A task agreed to with the subcommittee steering this project, for the March 2000 review, is to “initiate numerical simulation of particle migration during forming.” This review is part of the task mentioned, surveying available qualitative and quantitative information to be used in numerical simulation.

### **B. Approach**

Published literature is reviewed to collect submodels related to particle migration. These models will support numerical simulations for either qualitative trends to inspect the relative importance of various phenomena, or quantitative simulations and parameter identification based on experiments.

Even a qualitative model can provide insights for modifying the process—a well-known example is Wahlstrom's wet pressing theory and transversal flow presses.

A quantitative model should be able to predict the effects of changes in the dewatering profile on the thickness direction profile of migrating components in the web being formed, and on total retention. Calibrating the prediction could be based on current operating conditions on machine or on laboratory experiments that enable parameter identification.

### **C. Results**

To gain an understanding of what is missing from papermaking related models, first these are reviewed, and then more generic modeling of particle migration is inspected. The conclusions will emphasize the improvements considered necessary in modeling retention during paper forming.

#### Published models related to papermaking

The literature related to papermaking concentrates on the deposition of fillers. As noted, these models are good for steady forming at low fiber consistency, while pulsating forming at realistic consistency is still not well understood. The reader will observe that particle detachment in the paper-forming related models is only considered in cases where no web is formed and turbulent agitation is applied.

#### **Deposition**

The majority of papermaking related experiments have dealt with turbulent agitation of a suspension of fiber and filler and examination of filler content in samples devoid of fibers to assess the filler concentration in suspension as opposed to filler adsorbed on fibers.

In a case where web is formed, the options are to inspect retention in a realistic situation with simultaneous forming, or to assess the more well-defined, simpler situation with filtration through a preformed web. The simpler situation is naturally more amenable to modeling and interpretation of results.

#### Turbulent agitation without mat formation

These experiments are pertinent to stock handling prior to and within the headbox.

Alinec et al. provide a detailed derivation of an adaptation of Langmuir kinetics to model the deposition/detachment balance of filler on pulp fibers. He notes that aggregates of fillers will have both faster deposition rate and higher maximum coverage than well-dispersed filler [Alinec 91]. Causing aggregation of fillers prior to deposition would then seem kinetically advantageous, but avoiding aggregation maximizes the light-scattering effect of filler [Alinec 96].

The observations of Middleton et al. support the Langmuir-type deposition/detachment balance for turbulent suspensions; a static model under equilibrium is inspected



[Middleton 91]. The authors note that fiber consistency has a significant effect on the apparent retention, since increasing the amount of fluid with filler concentration in balance with some adsorption level on fibers means increasing the amount of filler not adsorbed but suspended in fluid. This matches the practical experience that forming at high consistency improves retention.

Kamiti et al. continued along the same lines, inspecting the effects of PEI with calcium carbonate, using the model provided by Alince. They once more confirmed the Langmuir kinetics for turbulent agitation without mat formation [Kamiti 94].

#### Retention during drainage with mat formation

van de Ven discussed the retention of small particles, such as dispersed filler, during forming. He concluded that particle attachment during forming is not significant, instead, most of the particles retained are deposited on the fibers earlier on in the process [Ven 84]. Note the assumption of fillers being in dispersed state; fillers attached to migrating fines or in agglomerated state may behave quite differently.

Wei et al. modeled the forming process in a handsheet mold, with analytical solutions reached using simplifying assumptions. The model predicts maximum deposition on the wire side, due to these layers “filtering” the suspension for a longer period of time than the top layers of the web. No effect of retention level on drainage through permeability changes is included. The mat is assumed incompressible in this work. Simulation results were compared with experimental observations published by others, and a satisfactory match was found [Wei 96].

Wildfong et al. developed a laboratory drainage tester operating at realistic consistency and drainage rate for forming low basis weight mats—pilot trial data is presented and was used to guide the design. A constant vacuum level drives the drainage, so the superficial flow rate is not constant. The flow resistance of the wire was accounted for on calculating the permeability of the formed mat, and a decreasing trend in permeability was observed with accumulation of formed web [Wildfong 98].

Further work with the same device showed that the fines content is the dominating factor determining permeability of formed webs. Observations were presented for furnishes with intentionally varied fines contents to examine this aspect. The authors conclude that compressibility effects are secondary in determining permeability, at least in comparison with fines retention [Wildfong 99]. Possibly for the case without fines, with a low basis weight, the compressibility effects on permeability are low—however, the experiments did not show that at a fixed fines content, compressibility effects would be absent.

Wildfong et al. also showed that the thickness direction retention profiles were almost uniform for both pulp fines and fillers, in spite of the rapid drainage rate affecting overall retention. Fines migration during forming was demonstrated experimentally by application of layerwise analysis of formed sheets [Wildfong 99b].

Sutman improved a pulsating drainage tester, which uses a rotating foil under the forming wire, by increasing the stock consistency to realistic level and adjusting the operating conditions to get realistic retention levels (coarser wire and moderate vacuum application during drainage). He developed various indicators that correlate with mill observations on the effects of additives, as regards drainage rate and formation [Sutman 99]. An interesting observation was the effect of peak vacuum level applied during drainage and dewatering on the final air permeability of the partially saturated sheet; this indicates that the compression level does cause a structure change affecting

permeability. The basis weights examined were above 50 gpsm, in reasonable alignment for comparison with Wildfong's results. Compression effects on permeability may well exist for webs formed with realistic fines content, under ordinary drainage conditions.

#### Filtration through preformed web

Ramarao developed a relatively complicated micro-model for particle deposition on fibers. Collection efficiency would describe the rate of capture onto a fiber from the set of bypassing particles [Ramarao 93].

Al-Jabari et al. presented a model in which the (in the plane of the web) nonuniform permeability of a preformed web was mathematically treated as axial dispersion. The mechanism by which this affected retention was through residence-time distribution of the filler-loaded liquid with the adsorbing fibers. Experiments showed that the breakthrough curves of particles passing through a fiber bed matched the model well for the most part [Al-Jabari 94 and 94b].

Vengimalla et al. used a continuum approach, matching model equations to experiments in a fiber-packed column. Pressure and porosity as well as filler concentration profiles were measured in a fiber bed during filtration. The permeability and retention aspects were uncoupled in the model: retention was assumed not to affect local permeability [Vengimalla 96]. Particle release was included in the model, but in a simplified form that did not consider hydrodynamically induced detachment.

#### **Steady models and survey data**

Webb has published a steady model, basically a species balance calculation, for inspecting the fluxes of the solids as well as chemicals that partly get adsorbed on fiber, fines, or filler, and partly remain in solution. The purpose of his model is to facilitate cost analysis of effluent treatment processes, and chemical or fiber gains from increasing retention. He states that the equilibration of the white-water system depends mainly on water consumption and single-pass retention (meaning the dynamics or time-constant of the system) [Webb 87].

Britt and Unbehend published in 1983 a survey of 43 commercial machines, examining their retention levels. The data showed single-pass retention of total fines being about 29% for twin-wire machines, ranging between 18 and 43%. Corresponding data for single-wire machines had, on average, 39% pulp fines retention and 29% filler retention, suggesting that the filler retention on twin-wire machines is only about 20% (filler retention is poorer than the retention of pulp fines or total fines). The loss of fines (out of the system instead of into the product) was about 24% for unfilled twin-wire cases [Britt 83].

The more recent survey of Korpi, concerning wood-containing grades in Finland, shows approximately similar retention levels [Korpi 92]. From a figure included in this publication, filler retention can be roughly estimated to be of the order 30%.

#### Hydrodynamic particle release in general

While papermaking related modeling has typically focused on particle capture and neglected particle release, the results have also been applicable only to handsheet forming. Typical "steady" handsheet forming will not show fines and filler depletion at the

wire side, instead, there will be enrichment due to more flow through the first formed layers of the web.

To make the models compatible with the commercially observed depletion on the wire side, either on fourdriniers or on using loadable blades with twin-wire forming, we need to incorporate detachment or release of particles. The particles may be pulp fines, fillers, or aggregates composed of these.

The fundamentals of hydrodynamically induced particle release have been studied by Hubbe, among others. After a discussion of the general phenomenology [Hubbe 84], he published results from a turbulent shear-flow experiment in a Couette-type device [Hubbe 85]. He also compared the hydrodynamic effects with centrifugal effects, to conclude that the mechanism of detachment is particle rolling (not sliding or lifting). In accordance, tangential forces are the most efficient for releasing particles attached to some surface.

Pendse used a rotating disk immersed in a beaker to impose hydrodynamic shear forces on particles adhering to the disk. He studied the effects of pH and salt concentration and how these would affect filler retention [Pendse 85].

Sharma confirmed the results of Hubbe by experiments with laminar Poiseuille flow compared with centrifugation. In particular, he discussed the effects of surface roughness and elasticity on the critical shear stress required for hydrodynamic detachment—it appears that elasticity and roughness are very significant factors in somewhat idealized model systems [Sharma 92]. Later on Das continued to refine the micromechanical theoretical aspects [Das 94].

In general it is agreed that for a single particle, there is a critical torque that initiates the rolling motion and detachment. This critical torque correlates with the average wall shear stress due to fluid flow, and so a critical shear stress is a sufficient descriptor. Similarly, a critical flow rate in some fixed geometry could be given. If the flow is turbulent, the fluctuations in fluid-particle interaction will impose a random component, and with a constant average flow field, there will be a detachment probability over any time step—a particle can remain attached for a while and then be detached after an apparent time delay. On the other hand, the particle-wall interaction through a fluid layer is strongly dependent on the gap size, so after particle detachment its initial motion will be slow, possibly giving the impression of some time delay.

Another component of randomness, also pertinent to laminar flow, is the distribution of attachment forces for a population of particles. The attachment forces depend strongly on local contact, with dependence on shape, roughness, and elasticity, even in a nearly ideal case (such as spherical particles on a plane surface). The critical shear stresses for the particle population have a corresponding distribution.

Finally, the “collectors” in a fibrous bed are nearly cylindrical, not planar. Even with laminar flow, the impaction probability and detachment forces will have a distribution around the cylindrical collector, which is typically oriented transverse to the flow direction. A change in flow direction will change these distributions and may lead to immediate detachment of a large amount of particles, due to local elevation of shear stress. The particle collection process should have much slower dynamics and will not react as quickly to changes in the flow field.

The references above provide some model equations that can be used in numerical simulations of particle detachment.

### Entrapment of particles

Once particles are released to migrate with the flow, either they will be entrapped and fixed in position, or they will be purged out of the fibrous web with drainage water. Particles that are large relative to the pore constrictions can be entrapped individually even from a very dilute solution, while small particles are susceptible to multiparticle blocking provided that their concentration in the liquid is sufficiently high. Multiparticle blocking has been observed for particles significantly smaller than the pore constriction, down to about 1% in diameter.

Concentration of the particles in the fluid is decisive for multiparticle blocking, also called bridging. Typically there exists a critical particle concentration in the suspension, above which a filter will tend to get plugged. Such plugging is observed by declining flow rate, which would translate to a drainage problem on a paper machine.

### Interaction of migration with permeability

It is well known that pulp fines significantly affect the specific surface of a fiber bed and have a strong influence on drainage resistance—a reasonable assumption is that the surface area depends linearly on the amount of fines, and affects permeability correspondingly (Cozeny-Karman model). The work of Wildfong et al. has confirmed that fines content in stock and its retention will strongly affect the intrinsic permeability of the formed web.

Also, it appears reasonable that the fillers attached on fiber or pulp fines will affect permeability only insignificantly. The only migrating component affecting permeability would then be the pulp fines. Due to their large surface area, these should be able to bond filler significantly, and the fines migration would also affect the filler distribution within the web.

Since entrapment will affect the permeability, which in turn will affect the flow rate as well as the release and migration of particles, we have a “feedback loop” requiring an iterative solution eventually. The flow and migration equations should be coupled in a model of general applicability.

Another aspect is the modification of void space by significant particle capture, leading to higher local flow rates in the pores even when the superficial flow rate is constant (e.g., in a constant-rate filtration experiment). The increasing flow rate should increase local particle detachment and limit capture.

### Connections with industry practice

Loadable blades are known to improve formation while retention deteriorates. Further, it has been noted with pilot experiments reported in literature that retention improvement due to increased roll dewatering may be set back by the drainage elements downstream in the wire section. These observations support the conclusion that strong flow (pulses) will deplete the migrating particles from the surface layers of the web.

Bachand notes in his review that positive pulses by blades lead to poor retention, which may be improved by replacement foils having a sharp leading angle doctoring the wire [Bachand 83]. This can be interpreted in two ways in terms of potential mechanisms. In a case where the formed web is incompressible, the positive pulse causes reversal of flow direction, releasing particles in areas where the shear stresses increased due to the change in flow. If, on the other hand, the positive pulse “loosens” the formed bottom

layers, the following drainage pulse would cause a sharp compression and an initially high flow rate, which will detach particles by strong shear forces.

#### ***D. Conclusions***

##### Scientific Conclusions

The fines and filler depletion observed on web surfaces created during forming is incompatible with results from models only considering particle collection. These models are sufficient to explain results from smooth slow drainage, with low fiber consistency, as in a regular handsheet mold.

The apparent retention of fines and fillers is, theoretically, strongly dependent on fiber consistency during forming; realistic forming experiments should be performed with realistic stock consistency when retention is inspected.

Even high drainage rate forming with steady vacuum and realistic stock consistency has shown almost uniform thickness direction profiles of fines and filler, in contrast with experience from machine formed samples. Apparently only pulsating forming causes realistic filler depletion on the water exit surface of the formed web. A theoretical basis exists for the phenomenological description of particle detachment caused by flow (hydrodynamically induced detachment), which could explain the phenomena due to flow pulses also. Such models have not been applied to papermaking but appear necessary for understanding the z-direction profiles of fines and filler created by various forming conditions.

Experiments with turbulent agitation without mat formation abound, and they are descriptive of filler attachment to fibers prior to forming on the wire. During forming the porous flow is expected to be laminar, not turbulent, and particle collection will likely take place mainly in the case of pulp fines, while particle release can concern both these and adsorbed filler.

The main causes of particle detachment include change in flow direction within the formed web, and fluid flow rates that exceed a critical detachment level. Detrimental effects on retention are associated with pulsating dewatering which may have two origins from the viewpoint of flow through a fibrous filter: the positive pulses on leading edges causing reversed flow and, possibly, loosening of the formed mat, and the initially high flow rates during mat compaction in the beginning of a suction pulse. A further possibility is that the formed fiber mat is redispersed by a positive pulse and then reformed.

If the fiber bed were homogeneous and incompressible and the flow unidirectional (no positive pulses), particle depletion at the surface of the web appears very difficult to explain. In reality the fiber/wire interaction makes the web inhomogeneous in thickness direction, but this effect is difficult to model and a first modeling attempt should neglect it. Whether the effects of positive pulses are dominating needs experimental inspection, using the pulsating drainage tester.

A homogeneous compressible fiber bed under pulsating drainage provides a reasonable explanation for filler depletion at the web surface, even without positive pulses. The surface layers get compressed and release water, leading to initially high flow rate at the surface. In upper layers there is initially not much relative motion of water and fiber, and the relative flow rates remain small because of the accumulated flow resistance of layers

below. The surface layers get a different treatment from the inner layers, when compressibility is assumed.

The only explanations for surface depletion that do not consider particle detachment are redispersion and inhomogeneity of fiber layers due to interaction with the wire. Modeling these aspects may be necessary if a simpler approach, using available fundamental and phenomenological knowledge, does not lead to reasonable results.

### Economics

To facilitate actual dollar value estimates of improved retention, this section presents some data available from the literature reviewed. As the value of improved quality is typically difficult to quantify, the data below relates to cost reduction.

Gavelin mentions several benefits of improved retention:

- decreased loss of solids
- lower headbox consistency improving formation
- lower load on saveall
- less renewed drainage with same fines and fillers recirculated
- less wire wear (due to quartz particles coming in with clay)

He also states that high filler content of white water causes serious operating problems [Gavelin 75].

Britt and Unbehend published data on the fines loss, meaning the difference of fines mass through the headbox and in the final sheet. This loss was of the order of 20% (somewhat lower for fourdrinier and higher for twin-wire) in unfilled cases, and increases with filler content [Britt 83]. Further, fines recirculation gives them an opportunity to adsorb colorant materials, which can lead to brightness loss. Additionally the recirculation increases deposits and loss of solids from the saleable product.

Webb's calculations indicate that when the degree of adsorption is 70%, the value of lost additive equals that of additive in the product when water consumption is about 20 tons water per ton of product. The lost additive amount is about half of that retained in the product, if the water consumption is lowered to 10 tons water per ton product [Webb 87]. The loss of chemical additives is then of the order of one third of purchase price. Webb also mentions the environmental cost of cleaning the mill effluent, and the effect of retention level on equilibration dynamics of the wet end.

### Deliverables

The review presented is used to design experiments with the MBDT and to examine the results of these experiments.

A simulation including detachment of particles will be constructed to examine the effects of drainage rate on filler profiles. It is expected that the simulation will show particle depletion on the wire side, and further there will exist a drainage rate above which this depletion leads to "frown-shaped" profiles.

**D. References**

## Alince 91

Alince, B.; Petlicki, J.; van de Ven, T.G.M.  
Colloids and Surfaces 59(1991) 265-277

## Alince 96

Alince, B.  
Tappi Journal 79, no. 3: 291-294 (March 1996).

## Al-Jabari 94

Al-Jabari, M.; van de Ven, T.G.M.; van Heiningen, A.R.P.  
Journal of Pulp and Paper Science 20, no. 9: J249-253 (September 1994).

## Al-Jabari 94b

Al-Jabari, M.; van de Ven, T.G.M.; van Heiningen, A.R.P.  
Journal of Pulp and Paper Science 20, no. 10: J289-295 (October 1994).

## Bachand 83

Bachand, J.P.  
TAPPI Wet-End Operations Seminar (Appleton, WI) Notes: 263-268 (May 8-13, 1983).

## Britt 83

Britt, K.; Unbehend, J.  
ESPRI Research Reports, 79:1 SUNY College of Environmental Science and Forestry (Syracuse) (NY) 78 (October 15, 1983).

## Das 94

Das, S.K.; Schechter, R.K.; Sharma, M.M.  
J. Colloid and Interface Science 164, 63-77 (1994).

## Gavelin 75

Gavelin, G.; Odell, P.O.; Vyse, R.N.  
Svensk Papperstid. 78, no. 11: 392-399 (Aug. 25, 1975).

## Hubbe 84

Hubbe, M.A.  
Colloids and Surfaces 12(1984) 151-178.

## Hubbe 85

Hubbe, M.A.  
Colloids Surfaces 16: 227-270 (1985).

## Kamiti 94

Kamiti, M.; van de Ven, T.G.M.  
Journal of Pulp and Paper Science 20, no. 7: J199-205 (July 1994).

## Korpi 92

Korpi, T.  
Wochenbl. Papierfabr. 120, no. 16: 638 (Aug. 31, 1992).

## Middleton 91

Middleton, S.R.; Scallan, A.M.  
CPPA Ann. Mtg. (Montreal) Preprints 77B: B35-46 (Jan. 31-Feb. 1, 1991).

## Pendse 85

Pendse, H.P.  
TAPPI Papermakers Conf. (Denver) Proc.: 259-264 (April 15-17, 1985).

## Ramarao 93

Ramarao, B.V.  
1993 Engineering Conference (Book 2), 455-476

## Sharma 92

Sharma, M.M.; Chamoun, H.; Sarma, D.S.H.S.R.; Schechter, R.S.

- J. Colloid and Interface Science Vol. 149, No. 1, March 1, 1992, 121-134.
- Ven 84  
van de Ven, T.G.M.  
J. Pulp Paper Sci. 10, no. 3: J57-63 (May 1984).
- Vengimalla 97  
Vengimalla, R., Chase, G., Ramarao, B., Das, S.  
1997 Engineering and Papermakers Conference, 1435-1449.
- Webb 87  
Webb, L. J.  
Paper Technol. Ind. 28, no. 3: 478-479, 481-483 (April 1987).
- Wei 96  
Wei, H., Kumar, B., Ramarao, B.V., Tien, C.  
J. Pulp and Paper Sci., 22(11), November 1996, J446-J451.
- Wildfong 98  
Wildfong, V.J., Shands, J.A., Genco, J.M., Bousfield, D.W.  
TAPPI 98 Proceedings Engineering Conference, 927-939.
- Wildfong 99  
Wildfong, V.J., Shands, J.A., Genco, J.M., Bousfield, D.W.  
TAPPI 99 Proceedings Engineering Conference, 1219- 1229.
- Wildfong 99b  
Wildfong, V.J., Shands, J.A., Genco, J.M., Bousfield, D.W.  
TAPPI 99 Engineering/Process and Product Quality Conference & Trade Fair,  
1173- 1180.



## **Some aspects of application potential of the MBDT**

### **A. Significance**

The Moving Belt Drainage Tester (MBDT) is being constructed at the IPST, and is expected to be available for initial testing before the end of current fiscal year. It provides exceptional capabilities in several respects, such as forming under conventional headbox consistency, applying controllable vacuum level and vacuum pulse rate during forming and dewatering, and providing timed mixing and agitation for chemicals addition prior to forming. In addition to final solids content after some dewatering sequence, the air flow through the wet web during high-vacuum dewatering (after the dry line) can be measured.

The device has been demonstrated for laboratory-measurement based prediction of on-machine high-vacuum dewatering, and due to realistic (fourdrinier-type) sheet structure – except for the isotropic fiber orientation distribution – can be used to characterize the effects of stock or fiber properties on paper properties.

An application in the project F022 is inspection of fundamental phenomena in fines migration during forming, but other aspects of value to the industry may be considered. The purpose of this document is to discuss earlier reported results that have a bearing on economic value estimates.

### **B. The MBDT principles**

In the MBDT drainage takes place under pulsating suction. Instead of having a moving wire the tester has a stationary wire and stationary suction box between which there is a moving cogged belt. At intervals in the belt there is a row of punched holes which expose the wire to the vacuum, experienced as vacuum pulses by "an observer fixed onto the wire". The belt speed is adjustable and the pulsation rate can be varied to a maximum of hundreds of pulses per second. It has been shown that a sheet formed under high pulsation rate possesses a similar structure, in terms of z-direction distribution of fines, to that of paper formed on a fourdrinier type paper machine. Vacuum level can be varied in a timed predetermined fashion during a single experiment.

Three injectors are included in the design for the dosage of chemical additives enabling the use of multi component retention aid systems. A variable speed stirrer provides shear forces simulating those to which a furnish is subjected in the approach flow. Vacuum level in the suction box and air flow rate through the formed sheet are measured during an experiment. With individual suction pulses being very short, of the order of 1ms, the dewatering on suction boxes and couch roll can be simulated. An earlier version of the MBDT has been applied in Finland for several years, with excellent results, in the following fashion. With a fixed vacuum level (a controllable parameter) the dewatering is measured as a function of vacuum application time. A set of such curves is constructed, and used in a calculation model to predict the dewatering profile, based on given vacuum levels and effective vacuum application times on machine. In this manner the effects of changes in the vacuum profile, or changes in the headbox stock, on the solids off the couch can be predicted.

### **C. Economic aspects**

A consulting company (Papes Oy) made use of the MBDT vacuum dewatering characterizations, in their projects on "Optimization of the use of energy in water removal on a paper machine wire section" and on "Mill measurements of a vacuum system and development of the analysing method" [Maijala 96]. The summary report on these projects indicates that using the current vacuum capacity, an average increase of 0.4%-points in the solids content of the web after the wire section could be achieved in the analyzed paper machines. Such an increase reduces the water load in the press section by about 4%, with the reduction concentrating on the first nips. The report states that the dewatering capacity of the beginning of the press section often limits the machine speed. If no change in solids content is desired, on an average an energy saving potential of 15% was observed.

The drive power requirements are of similar order of magnitude as energy used for vacuum pumping. In an energy optimization effort it is necessary to estimate the drive power requirement for the wire section, and how it depends on the vacuum profile. This is doable based on calibrating an estimation procedure with concurrent mill data. Economic aspects of retention have been discussed earlier on within this report. The MBDT has a significant bearing of retention studies, with timed mixing and agitation, and mat formation.

While the 0.4% increase in solids may seem small, the wet strength of a paper web has a strong dependence on the solids content, and the inertially caused tensile loads depend on the moisture content. In combination these effects can have a significant effect on runnability, in particular wet end breaks. On a single machine the cost of breaks (energy, lost production,...), with 30-minute break occurring three times per day, is of the order of a million dollars. Even a slight improvement has a significant economic impact.

The retention aspects are also connected with runnability and wet end breaks, through the stability of the white water recirculation.

Selection of furnish composition, based on inspection of both paper properties and drainage/dewatering, the MBDT provides good potential. One published study compared the drainage properties of different newsprint furnishes, SC and LWC base paper grades, with the result that TMP possesses an advantage over PGW [Raisanen 96]. Similar work can be envisioned with various fillers, retention, drainage or formation chemicals. No quantification of the value of such work is available at this time.

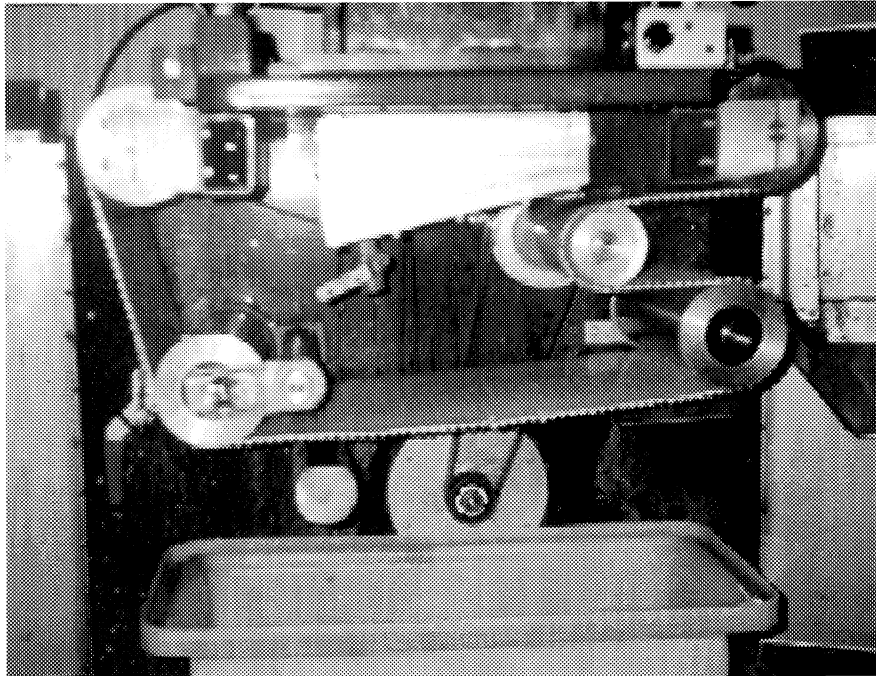
### **D. References**

#### ***Maijala 96***

Maijala, A.; Lahti, H., Report 10 of the "Sustainable paper" program, KCL 1996 (in Finnish)

#### ***Raisanen 96***

Raisanen, K., Appita '96, pp. 655-659.

**G. Figures**

The MBDT device at APPI has the same basic design as the device under construction at IPST. The belt loop is shown, with drive mechanism at the back wall and vacuum box inside the loop.

FLUID DYNAMICS OF SUSPENSIONS

STATUS REPORT  
FOR  
PROJECT F003

Cyrus K. Aidun (PI)  
E-Jiang Ding

March 8 – 9, 2000

Institute of Paper Science and Technology  
500 10th Street, N.W.  
Atlanta, Georgia 30318



**DUES-FUNDED PROJECT SUMMARY**

<b>Project Title:</b>	<b>Fluid Dynamics of Suspensions</b>
<b>Project Code:</b>	<b>FDS</b>
<b>Project Number:</b>	<b>F003</b>
<b>PAC:</b>	<b>Papermaking</b>
<b>Project Duration:</b>	<b>1999 - 2005</b>
<b>Project Staff:</b>	
<b>Faculty/Senior Staff:</b>	<b>C. Aidun</b>
<b>Staff:</b>	<b>E. Ding</b>
<b>Project Funding:</b>	<b>\$70,000 for 1999/00</b>

**RESEARCH LINE/ROADMAP:** Line 11. Improve the ratio of Product Performance to Cost – Models, algorithms, and functional samples of fibrous structures ..., break-through papermaking ...processes.

**BENEFITS TO INDUSTRY:**

To increase the market share and profitability of the member companies by understanding the physics of fiber suspensions in turbulent flow and optimizing the paper forming and coating processes through break-through technologies in suspension transport to enhance quality and reduce cost.

**PROJECT OBJECTIVES:**

- I. Investigate the effect of turbulent flow on individual and collection of fibers in the headbox and the forming section to find the most effective flow field for optimum forming process in various paper grades;
- II. Based on the information obtained through the first objective, develop an optimum forming process.

**PROJECT DELIVERABLES:**

1. *A direct method for investigation of individual and collection of fibers in turbulent flow of the headbox and the forming section,*
2. *Computational results of fiber orientation and interaction in the converging section of the headbox,*
3. *Optimum shape and design of a fiber network forming device and other flow parameters for most effective fiber distribution in the sheet;*

**SCHEDULE:** The project schedule to tabulate the major tasks of the project are:

Task Descriptions (example)	2000 Jan - Mar	2000 Apr - Jun	2000 Jul - Sep	2000 Oct - Dec	2001 Jan - Mar
1. Literature Survey	-----	-----X			
2. Computational method					
2.1 2-D	-----X				
2.2 CPU optimization	---	-----	-----X		
2.3 3-D			---	--X	
3. Include turbulent flow modeling			-----	-----	-----X
4. Experiments with fiber in a converging nozzle with turbulent flow		-----	-----X		
5. Comparison between computational & experimental results					-----X
6. Final report					-----X

## THE COMPUTATIONAL METHOD

The method being developed is a hybrid of the finite element and lattice-Boltzmann methods. In this method the motion of fiber in turbulent flow can be investigated in two steps: (1) first the fluid flow pattern is computed without any fiber recording the pressure and velocity at every node in the fluid; (2) the motion of the solid particle (i.e., the fiber) is obtained in the given flow. The first step of the study can be done by finite element method followed by an improved lattice-Boltzmann analysis of particle dynamics. The preliminary method for two-dimensional flows have been developed. Before running this code, two data files, FIINP and FIOUT, must be created by the finite element code, FIDAP. The first data file, FIINP contains locations of every element and their nodes, while FIOUT includes pressure and velocity at every node. The new code reads the information contained in these two files. The computational domain is confined in a small box containing the fiber under consideration. When the fiber moves in the fluid, the box moves simultaneously, keeping the fiber at its center. The pressure and velocity at the boundary are determined by the information contained in the two data files. When the computational domain is meshed by 4-node quadrilateral elements, the bilinear interpolation function is used to determine the pressure and velocity at any point on the boundary of the box.

An important step in development of any computational method is the estimate of the computational time required for analysis of practical problems. Assume that the lattice size equals  $\Delta x$  cm, and the time step in lattice-Boltzmann method is  $\Delta t$  sec, respectively. In this section, a subscript  $s$  is used for variables in CGS unit, while a subscript 1 is used for those in lattice-Boltzmann method.

The viscosity in CGS unit and lattice-Boltzmann method is related by

$$\nu_l = \frac{\nu_s \Delta t}{(\Delta x)^2} \quad (1)$$

And, the characteristic speed in the two unit systems is connected by

$$u_l = \frac{u_s \Delta t}{\Delta x}. \quad (2)$$

In lattice-Boltzmann method, values for  $\nu_l$  and  $u_l$  are confined in limited ranges. When  $\nu_l < 1/6$  the collision operator is over-relaxing, while  $\nu_l > 1/6$  corresponds to the under-relaxing collision operator.  $\nu_l = 1/6$  is the natural choice for the simulation, since the viscous stresses decay instantaneously. In computational analysis the range of  $\nu$  is usually from  $1/30$  to  $1/2$ . The characteristic speed,  $u_l$ , should remain small, because, in the current hybrid method, the lattice-Boltzmann calculation is carried out only in a small box, which contains the fiber. The influence of the flow outside the box on the suspended fiber is transferred with the speed of sound, as pressure pulses travel through fluid. If the box moved too fast in the fluid, the flow on the boundary of the box would change rapidly. However, the flow in the box could not change immediately, and the fluid around the fiber would remain at its previous velocity and pressure. Then the results of the calculation would no longer be reliable. Hence the speed of the box must be less than 0.1 in normalized units.

From relations 1 and 2, we find

$$\Delta x = \left( \frac{u_s}{u_l} \right)^{-1} \frac{\nu_s}{\nu_l}, \quad (3)$$

and

$$\Delta t = \left( \frac{u_s}{u_l} \right)^{-2} \frac{\nu_s}{\nu_l}. \quad (4)$$



The total CPU time for lattice-Boltzmann simulation,  $T$ , is proportional to  $(\Delta t)^{-1}$  and  $(\Delta x)^{-n}$  where  $n$  is 2 or 3 for two and three dimensional domains, respectively. Hence

$$T \propto \frac{(u_s / u_l)^{n+2}}{(v_s / v_l)^{n+1}}. \quad (5)$$

The following examples illustrate the accuracy of the new hybrid method.

#### EXAMPLE 1: A CIRCULAR CYLINDER IN A SHEAR FLOW

To verify the accuracy of the new code, the results for a freely suspended circular cylinder in a shear flow at the particle Reynolds number  $Re = 0.335$  have been obtained with three different computational approaches. The computational domain is shown in Figure 1. The channel is  $20cm$  long and  $4cm$  wide. The fluid density and viscosity is  $\rho = 1.3g/cm^3$  and  $\mu = 0.040625g/cm \cdot sec$ , respectively. Velocities of the two walls are  $\pm U = \pm 0.8cm/sec$ , respectively. The radius and density of the circular cylinder is  $r = 0.161875cm$  and  $\rho_s = 1.3g/cm^3$ , respectively. Initially the cylinder is at rest, and its center is at  $(x, y) = (1.625cm, 1.96875cm)$ .

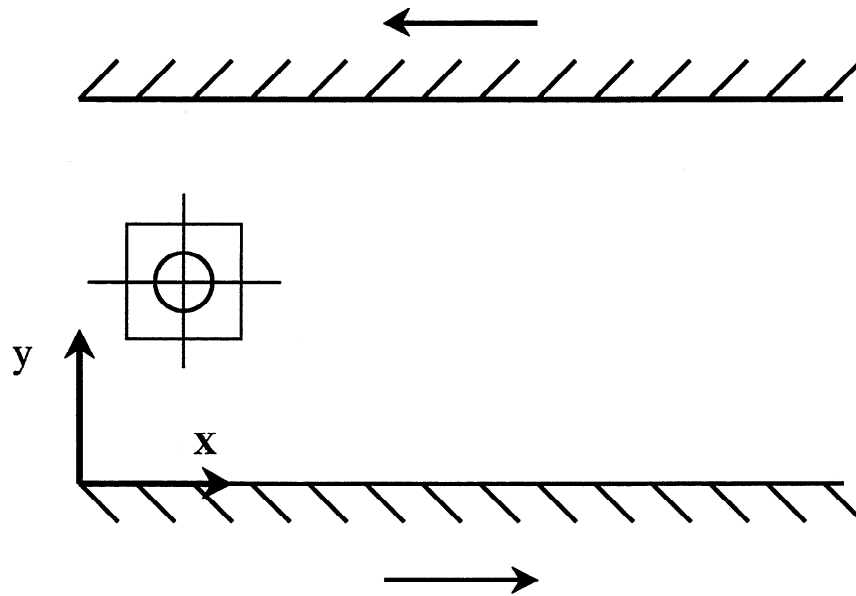


Figure 1. A circular cylinder in a shear flow.

(1) STANDARD LB

The first calculation is carried out by the standard lattice-Boltzmann method. The size of the channel is 320x64 lattice units. Results obtained by this calculation are presented with in Figures 2 and 3 showing the trajectory of the center of the cylinder, as well as the angular rotation rate of the cylinder, respectively. The rotation rate at steady state is  $0.201\text{sec}^{-1}$ . Since the standard lattice-Boltzmann method (ALD code) is accurate in simulating the motion of suspended circular cylinders in shear flow, the results of this calculation are reliable as well. Results obtained by the new hybrid method will be compared with these results, as well.

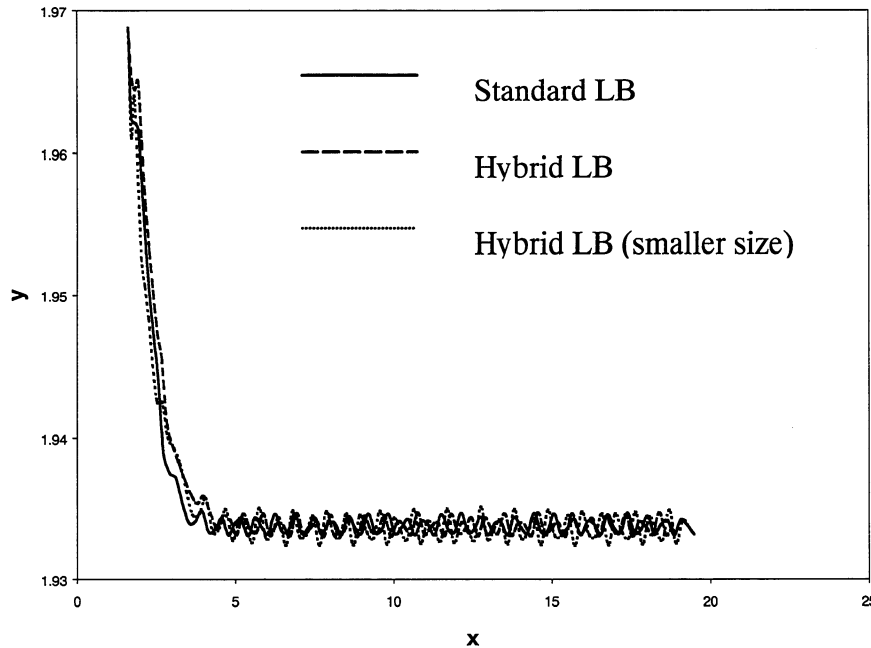


Figure 2: Trajectories of the circle in the channel.

## (2) HYBRID LB

The purpose of this calculation is to test the validity of the new hybrid code. The pressure and velocity fields are obtained by FIDAP. The size of the box covering the circular cylinder is 2 cm x 2 cm, i.e., 32x32 lattice units. The radius of the circular cylinder is  $r = 2.59$  lattice units. Results obtained by this calculation, presented in Figures 2 and 3, show good agreement with the previous methods. The rotating rate at steady state is  $0.207 \text{ sec}^{-1}$ , only 3% larger than the rate obtained by the standard LB.

## (3) HYBRID LB WITH SMALLER DOMAIN SIZE

In order to test the influence of the domain size on the accuracy of the simulation results, the size of the domain is reduced to be 1 cm x 1 cm, i.e., 16x16 lattice units. Results presented in Figures 2 and 3 compares fair with previous calculations. The rotating rate at steady state is  $0.20 \text{ sec}^{-1}$ , about 9% larger than the rate obtained by the standard LB.

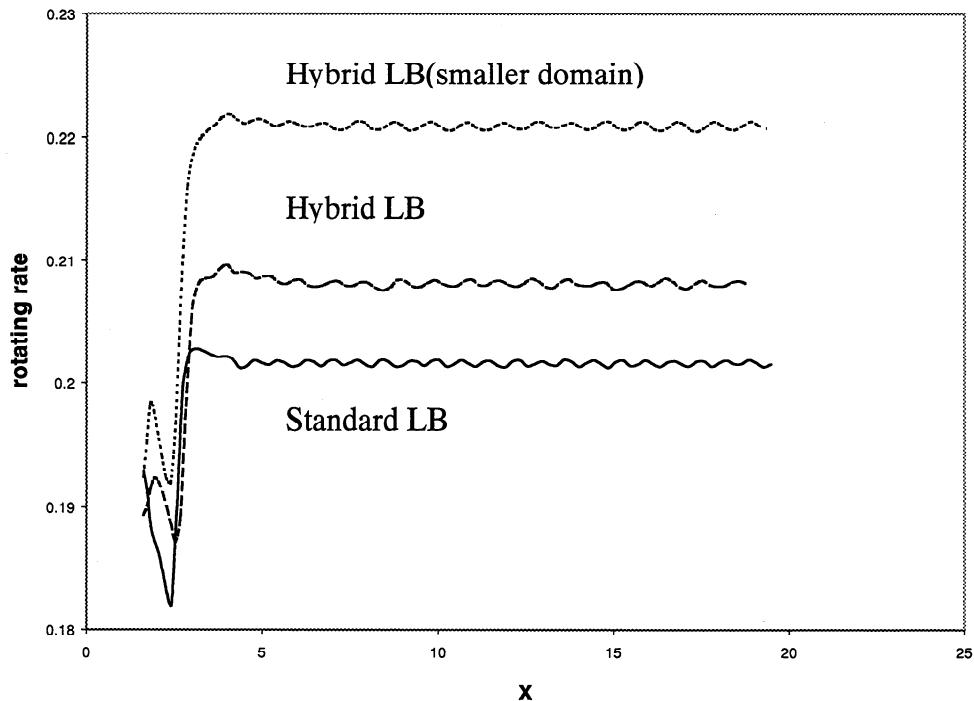


Figure 3: Rotating rate of the circle in the channel

#### EXAMPLE 2: DYNAMICS OF AN ELONGATED ELLIPSE IN A CONVERGING NOZZLE

Flow of particles in a converging nozzle takes place in many applications including headboxes and coater heads. A simplified version of this flow is used here as an example for application of the hybrid lattice-Boltzmann method. The computational domain, shown in Figure 4, is a converging channel 40cm long, where the inlet and the outlet are 10cm and 1cm wide, respectively. The fluid properties are that of water where viscosity is  $\nu = 0.01 \text{cm}^2 / \text{sec}$ , and density is  $\rho = 1 \text{g} / \text{cm}^3$ . A parabolic velocity distribution for  $u_x$  with a maximum velocity equal to 1cm/sec is imposed, and the inlet velocity  $u_y$  is zero. The major and minor axes of the elongated ellipse are  $b = 0.05 \text{cm}$  and  $c = 0.005 \text{cm}$ , respectively. The ellipse is neutrally suspended with density,  $\rho_c = 1 \text{g} / \text{cm}^3$ . Three initial positions at  $(x, y) = (0.1 \text{cm}, 1 \text{cm})$ ,  $(x, y) = (0.1 \text{cm}, 2 \text{cm})$ , and  $(x, y) = (0.1 \text{cm}, 4 \text{cm})$  are selected, where the initial angle from x-axis to the major axis of the is always  $\chi = \pi / 2$ .

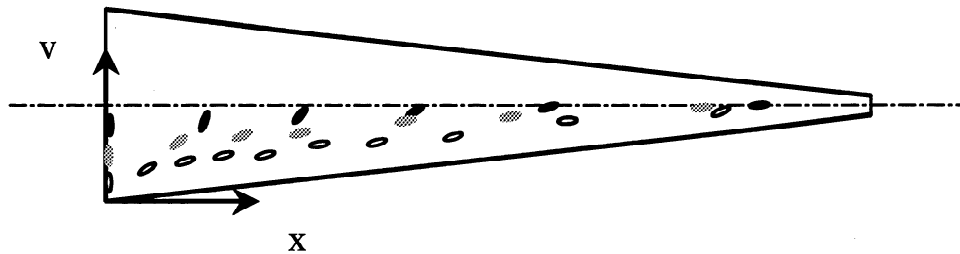


Figure 4. An ellipse in a converging nozzle. Positions and orientations of the ellipse at every 5 seconds are shown in this figure. Initial positions are at  $a=(0.1\text{cm},1\text{cm})$ (open ellipse),  $b=(0.1\text{cm},2\text{cm})$ (gray ellipse), and  $c=(0.1\text{cm},4\text{cm})$ (black ellipse), respectively.

The finite element computations with FIDAP gives the flow pattern in the channel with streamlines as shown in Figure 5. A total of 4049 nodes are used to grid the computational domain.

Following the finite element calculations, the lattice-Boltzmann computation of the particle dynamics with time step  $\Delta t$  is set to  $1.5\text{E-}05$  sec.,  $\Delta x$  is  $0.0015$  cm,  $v_1 = 1/16$ , and  $\tau = 0.6875$  is performed. The dimensions of the lattice Boltzmann computational domain are  $0.2 \times 0.2$  cm, or  $128 \times 128$  lattice units. The major and minor axes of the elongated ellipse are  $b = 32$  and  $c = 3.2$  lattice units, respectively. The particle at various initial positions generally accelerate to a maximum speed while drifting in the  $y$  direction to the centerline of the channel. The angle of attach  $\chi$  decreases until the major axis becomes parallel to the streamline. When near the outlet, the particles fluctuate in orientation about the fluid streamline. Only the particle at lowest initial position undergoes a full rotation by 180 degrees while turning with major axis parallel to the streamline.

The same problem will be simulated with the regular lattice-Boltzmann method to evaluate the accuracy and reliability of the hybrid technique. After this step, and after the computational

demand is reduced with the modified hybrid method, problems more relevant to headbox and flows in a gap former will be investigated.

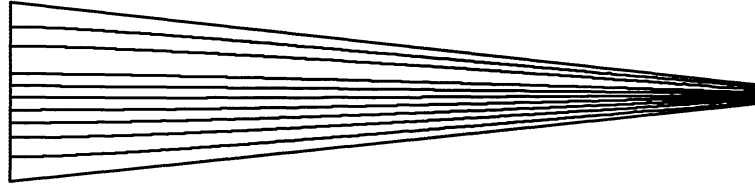


Figure 5: Streamlines in the converging nozzle.



FUNDAMENTALS OF  
HEADBOX AND FORMING HYDRODYNAMICS

STATUS REPORT  
FOR  
PROJECT F005

Cyrus K. Aidun (PI)  
Paul McKay

March 8 – 9, 2000

Institute of Paper Science and Technology  
500 10th Street, N.W.  
Atlanta, Georgia 30318





**DUES-FUNDED PROJECT SUMMARY**

<b>Project Title:</b>	<b>FUNDAMENTALS OF HEADBOX AND FORMING HYDRODYNAMICS</b>
<b>Project Code:</b>	<b>FORM</b>
<b>Project Number:</b>	<b>F005</b>
<b>PAC:</b>	<b>PAPER MAKING</b>
<b>Project Staff</b>	
<b>Principal Investigator:</b>	<b>Cyrus K Aidun</b>
<b>Co-Investigators:</b>	
<b>Research Support Staff:</b>	<b>Paul McKay</b>
<b>PAC Subcommittee Chairman</b>	<b>D. Anderson</b>
<b>FY 99-00 Budget:</b>	<b>\$219,000</b>
<b>Time Allocation:</b>	
<b>Principal Investigator:</b>	<b>25%</b>
<b>Research Support Staff:</b>	<b>95%</b>
<b>Supporting Research:</b>	
<b>Ph.D. Students:</b>	<b>C. Park, H. Xu, M. Brown</b>
<b>Special Students:</b>	<b>K. Ono</b>

**RESEARCH LINE/ROADMAP:** Line #11 - Improve the ratio of product performance to cost for pulp and paper products by 25% by developing break-through papermaking and coating processes which can produce the innovative webs with greater uniformity than that achieved with current processes

**PROJECT OBJECTIVES**

- I. Investigate the fluid flow interaction with fiber network in a headbox and the forming section; improve designs for reduction of floc formation and improvement of fiber dispersion in headbox and the forming section;
- II. Develop methods for measurement of the velocity profile in CD and MD of the forming jet and influence on physical properties. Use this method as a diagnostics tool for process optimization to improve formation and reduce consumption of raw material.

**PROJECT BACKGROUND**

*The two major areas in the project are to develop novel diagnostics methods for characterization of the forming jet, as well as methods to control the forming jet hydrodynamics. One such system for direct measurement of the forming jet velocity and the turbulent level has been completed to be used with commercial machines by a process engineer at the mill.*

*The other aspect of the project is to understand the behavior of the fiber network in various sections of the headbox.*

## SUMMARY OF RESULTS

*In this section, we summarize the results and their applications.*

### *IMMEDIATELY APPLICABLE RESULTS:*

- 1. Development of the Surface Pattern Image Velocimetry (SPIV) method based on two-dimensional cross-correlation of the high-speed digital images of the forming jet has been completed and tested for forming jet velocity measurements. Various techniques to increase the accuracy of the measurements have been used to provide more accurate measurement of the forming jet velocity profile. This method is now capable of surface velocity measurements with one percent (1%) accuracy.*
- 2. Automation of the SPIV method for the on-line measurement of the forming jet velocity has been completed. The mills can use this method for evaluation of the forming jet velocity profile.*

### PROGRESS TOWARD GOALS:

- 1. The two-component laser-Doppler velocity (LDV) measurements of the streamwise velocity and azimuthal component of the mean and turbulent fluctuations through the step expansion tube has been completed as part of a student project (CSP). These measurements provide details of the flow characteristics in a headbox tube. With this information, and visualization of the floc breakup and dispersion mechanism, the effectiveness of the headbox design can be examined.*
- 2. The floc dispersion mechanism at the step expansion section of the headbox tube has been examined. Methods to quantify the floc breakup and fiber dispersion as a function of flow rate and the dimension of the step change have been developed. The results show strong correlation between the mean axial velocity gradient through the transition from small diameter to larger diameter tube and the floc breakup and fiber dispersion. The fiber dispersion seems to be based on the turbulent eddy formation where the floc deformation, rupture and breakup are from the extensional flow and radial stresses.*
- 3. An automated SPIV system is constructed with the necessary software to use for on-line optimization of process parameters in the forming section.*
- 4. The SPIV method has been applied to a commercial system and results are used for optimization of the process parameters to improve the fiber orientation profile.*

## DELIVERABLES FOR by June 00:

1. *The velocity profile for the free-surface forming jet using the SPIV method;*
2. *An on-line method for measurement of the CD velocity profile on the surface of the forming jet as a diagnostics tool for process optimization,*

## DELIVERABLES FOR FY 00-01:

1. *Results from visualization of floc formation and breakup at various sections of the headbox as a mean to understand and optimize process parameters for best formation;*
2. *An on-line method for measurement of the velocity profile along the thickness of the forming jet from the slice to the impingement zone as a diagnostics tool for process optimization.*
3. *Relation between the mean and averaged velocity profile and streaks in the forming jet with the physical properties such as fiber orientation and dimensional instability;*
4. *The relation between velocity profile and the design features of the headbox;*
5. *Practical methods to optimize process parameters in order to minimize velocity profile nonuniformity, with the goal of improving uniformity of physical properties.*

**SCHEDULE:** The project schedule for each of the deliverables is provided below.

Task Descriptions (example)	2000 Apr - Jun	2000 July - Sept	2000 Oct - Dec	2001 Jan - Mar	2001 Apr-Jun
1. Floc dispersion/formation	-----	-----	-----X		
2. On-line vel. system					
2.1 Exp. setup	----	---X			
2.2 Experiments		-----	-----X		
2.3 data analysis			-----	---X	
2.4 interim report				---X	
3. Mean vel. and surface patterns				-----X	
4. Vel. profile				-----X	
5. Minimize Vel. Nonuniformity	-----	-----X			-----X
6. Annual Report					-----X

## RESULTS

The results are presented in this section with additional detail. The focus is on characterization of the forming jet and the headbox hydrodynamics. The first section outlines a method based on two-dimensional cross-correlation of the digital images to obtain the surface velocity profile of the forming jet. This method provides more detailed information on the forming jet hydrodynamics.

### 1.0 Introduction

The forming jet velocity profile has a significant impact on the physical properties of finished paper. It is believed that slight variations in the velocity profile can strongly affect fiber orientation, forming table streaks and other such properties. In order to achieve a desired jet-to-wire ratio, the forming jet velocity is typically controlled using feedback from a pressure transducer in the headbox with the jet velocity being calculated using Bernoulli's streamline equation. However with high levels of turbulence in the headbox the total head at the point of the pressure measurement includes a non-negligible velocity head that varies with the flow rate. Thus an equation for the total head of a free jet at a nozzle must include a term accounting for the significant head losses resulting from the turbulent flow through the nozzle. These losses vary for different headbox designs, flow rates and slice openings and the head-loss equations must be determined empirically. In practice it is difficult to obtain jet velocity measurement with accuracy better than two percent.

In order to study the impact of forming hydrodynamics on the physical properties of the sheet we need accurate measurements of the jet velocity profile. Laser Doppler Velocimetry (LDV) is a useful technique but it is limited in that it can only produce data for one physical point at a time and it cannot be used to analyze fiber suspension flows. Similarly there exist other methods that use point correlation to measure the surface velocity at a given point.

In order to obtain the surface velocity profile for a section of the forming jet we have developed a Surface-Pattern Image Velocimeter (SPIV) using cross-correlation methods and well-established Particle Image Velocimetry (PIV) technique. The PIV technique is a particularly powerful method for making velocity field measurements. This method is, however, limited to transparent fluids with well defined seed particles. The fiber suspension in the headbox and the forming section is not transparent and therefore cannot be measured using PIV methods. SPIV takes advantage of the non-uniform flow patterns on the surface of the forming jet by recording the positions of distinct flow patterns using a high speed digital camera and application of cross-correlation techniques between a sequential pair of images to determine the jet velocity profile. Various optimization methods are used in the calculations to maximize the signal to noise ratio.

### 2.0 The Theoretical Basis of SPIV

The SPIV method is based on the comparison of a pair of sequential images and the tracking of recognizable non-uniform patterns between the two images of known temporal separation. This is illustrated in Figure 1 below.

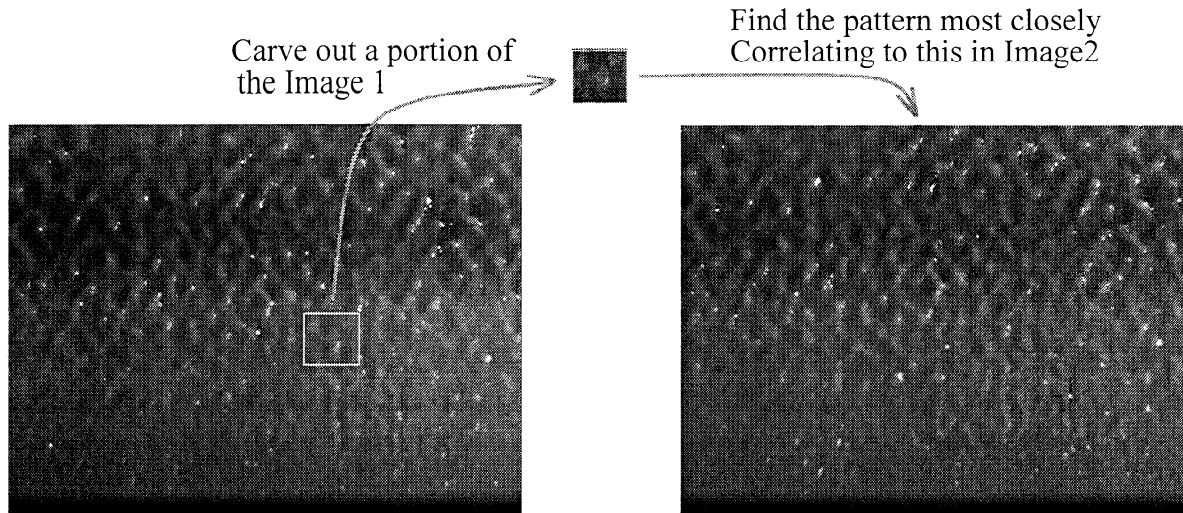


Figure 1 – Illustration of the basis of SPIV

## 2.1 The Cross Correlation Method

Each pattern in the image is represented by an array of gray scale numbers. To compare the two images, the cross correlation between the two images,  $D(i,j)$ , is computed according to Equation 1, below. The displacement during a time interval is determined by searching image 2 for the highest cross correlation value,  $D(i,j)$ , for each point  $(i,j)$  in image 1.

$$D(i, j) = \frac{\sum_{n=1}^N \sum_{m=1}^M \{v(m, n) - \mu_v\} \{u(m + i, n + j) - \mu_u\}}{\sqrt{\sum_{n=1}^N \sum_{m=1}^M \{v(m, n) - \mu_v\}^2} \sqrt{\sum_{n=1}^N \sum_{m=1}^M \{u(m + i, n + j) - \mu_u\}^2}} \quad - p \leq i, j \leq p \quad (\text{Eq. 1})$$

$D(i,j)$ : Cross correlation value

$v(m, n)$ : value of gray scale of Image 1 (0~255)

$u(m, n)$ : value of gray scale of Image 2 (0~255)

$\mu_v, \mu_u$ : Mean value of  $v(m, n), u(m, n)$  inside of the inspection box

$M, N$ : Size of inspection box

Without further optimization of the method, the accuracy would depend on the physical size of the pixels in the image. However, the accuracy is greatly improved by Sub-pixel analysis, presented in the next section.

## 2.2 Estimation of the Displacement at the Sub-pixel Level

This method has a limitation in resolution since the displacement is always measured in whole pixels. In order to obtain more accurate velocity measurements the resolution of the image must be improved or some additional filter must be added to the scheme of the calculation. The SPIV method overcomes this limitation and realizes sub-pixel accuracy in velocity measurement by

fitting the three points adjacent to the peak of the correlation distribution function with a Gaussian profile, as illustrated in Fig. 2. This method is used to reduce the digitization error that occurs whenever a continuous field is projected onto a discrete domain.

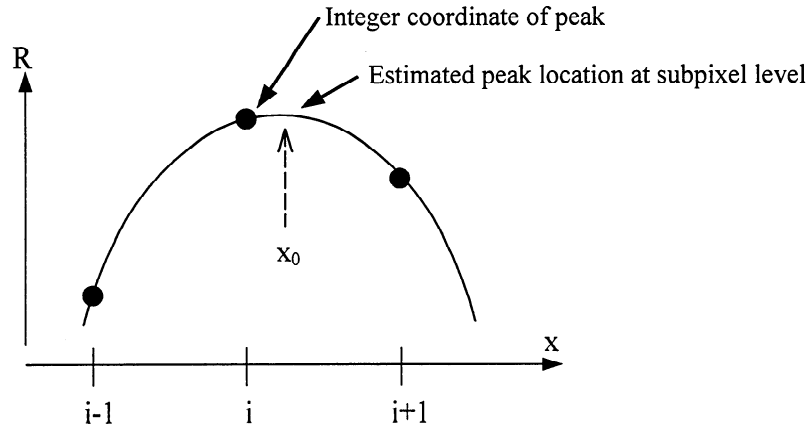


Figure 2 – Gaussian fit to the three points near the peak.

The application of the Gaussian equations, given by

$$f(x) = C \exp\left[\frac{-(x_0 - x)^2}{k}\right]$$

$$x_0 = i + \frac{\ln R_{(i-1,j)} - \ln R_{(i+1,j)}}{2 \ln R_{(i-1,j)} - 4 \ln R_{(i,j)} - 2 \ln R_{(i+1,j)}} \quad y_0 = j + \frac{\ln R_{(i,j-1)} - \ln R_{(i,j+1)}}{2 \ln R_{(i,j-1)} - 4 \ln R_{(i,j)} - 2 \ln R_{(i,j+1)}} \quad (\text{Eq. 2})$$

$(i, j)$ : integer coordinate of peak  
 $R_{(i,j)}$ : cross correlation value at  $(i, j)$

significantly improves the accuracy of the SPIV method. The range of the error is reduced by two thirds and the standard deviation of the error is reduced by approximately 80%. This increases the effective resolution of this technique by a factor of four to five over the resolution of the basic technique.

The results of these calculations often contain questionable data points that do not appear correct in relation to their neighbors. These questionable data points are eliminated in order that the velocity profile should vary continuously in space. The value calculated at each point on the image is compared to the average value of its eight neighbors and is discarded if it deviates from this average by more than a certain threshold value.

### 3.0 Automated SPIV method for On-line analysis

We have implemented the SPIV method in an automated system, as illustrated in Fig. 3, suitable for use in a mill. This system consists of three components for image acquisition, image transfer and real time image processing and analysis.

#### 3.1 Image Acquisition

The images are acquired using a Kodak high-speed digital video camera connected to a Kodak Ektapro Model 1000HRC Motion Analyzer. This system acquires and stores digital video images as a sequence of numbered eight-bit grayscale Bayer format images at a resolution of 512 by 384. These images may be acquired at a rate of up to 1000 frames per second and stored in the analyzer's online memory.

#### 3.2 Image Transfer

Currently the images for analysis are transferred using a SCSI optical disk drive as a SCSI buffer; necessary since SCSI can not be used for direct machine to machine data transfer. A set of two numbered sequential images is downloaded through the analyzer's built-in SCSI port and stored as TIFF files on a 1.3 GB optical disk. The SCSI drive is then reset to refuse interrupts from the analyzer and the files are read from disk by the image processing system.

#### 3.3 Image Processing and Analysis

The actual work of implementing the SPIV method has been programmed as a LabVIEW virtual instrument (VI) running on a Pentium III 500 MHz based Windows 98 notebook computer equipped with a PCMCIA based slim SCSI interface. The VI controls the analyzer's functions for image acquisition, storage and export through the analyzer's RS-232 compatible serial interface driven by the notebook's COM1 serial port. The images are acquired from the SCSI buffer through the PCMCIA slim SCSI card and read directly into the VI. Processing is handled through a series of sub-VIs and the final data is both saved as a text file for further post-processing and displayed as a set of charts in near real time.

Currently the system applies the SPIV method to a pair of images and calculates the surface velocity (in pixels per second) across the frame. It exports this data as a text file for post-processing including the plotting of vector diagrams to represent the velocity field overlain on the original image and suitable for animation. This post-processing is done using a custom Visual BASIC PC program and customized image analysis software on an SGI graphics workstation to build the animation files. It also calculates the average velocity along lines of constant CD and MD and plots this data in the VI's main window as plots of CD averaged velocity against MD and MD averaged velocity against CD. These plots may be printed or cut-and-pasted into a report. They may also be reconstructed in a plotting program from the main text file for a more detailed analysis. Elapsed time from the initiation of image recording through the generation of the final plots and export of data is approximately four minutes with default settings.

The VI allows the inspection box (that is the area of the image used for pattern recognition) to be adjusted from the default and for MD and CD offsets to be set to allow for imperfectly centered images. It also has a setting to allow for images with flow running either vertically or horizontally through the frame. Changing these settings, especially the inspection box size, from



the defaults can significantly alter the time required to process the images as well as affect the resolution of the velocity plots.

### 3.4 Future Plans

Development of this system is a continuing effort. While all of the first objectives are met there are plans to greatly enhance the utility of this system. These can be divided into three areas; ease of use, instantaneous analysis and time dependent analysis.

To improve the ease of use of the system we plan to look into eliminating the need to reset the SCSI bus through direct machine-to-machine transfer of the TIFF images. While this will not appreciably affect system performance it will eliminate one step requiring operator intervention and will remove one piece of equipment from the system.

To the current system allowing instantaneous analysis (that is analysis of a set of two images) we plan to add features allowing the plotting of velocity along arbitrary lines and to allow the calculation of FFTs across lines of constant CD.

We also plan to enable the system to deal with a time series of more than two adjacent images. It will repeat it's set of calculations between each adjacent image in the set and display the velocity data as a function of time. This will be more suitable for a post-processing situation as it will appreciably increase the required processing time.

## IPST Surface Pattern Image Velocimetry System

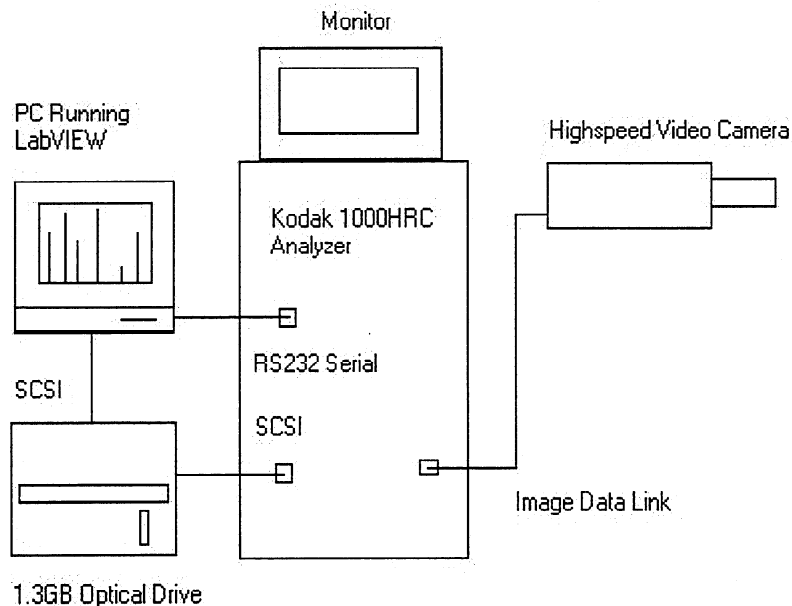


Figure 3. A schematic of the current on-line SPIV system.

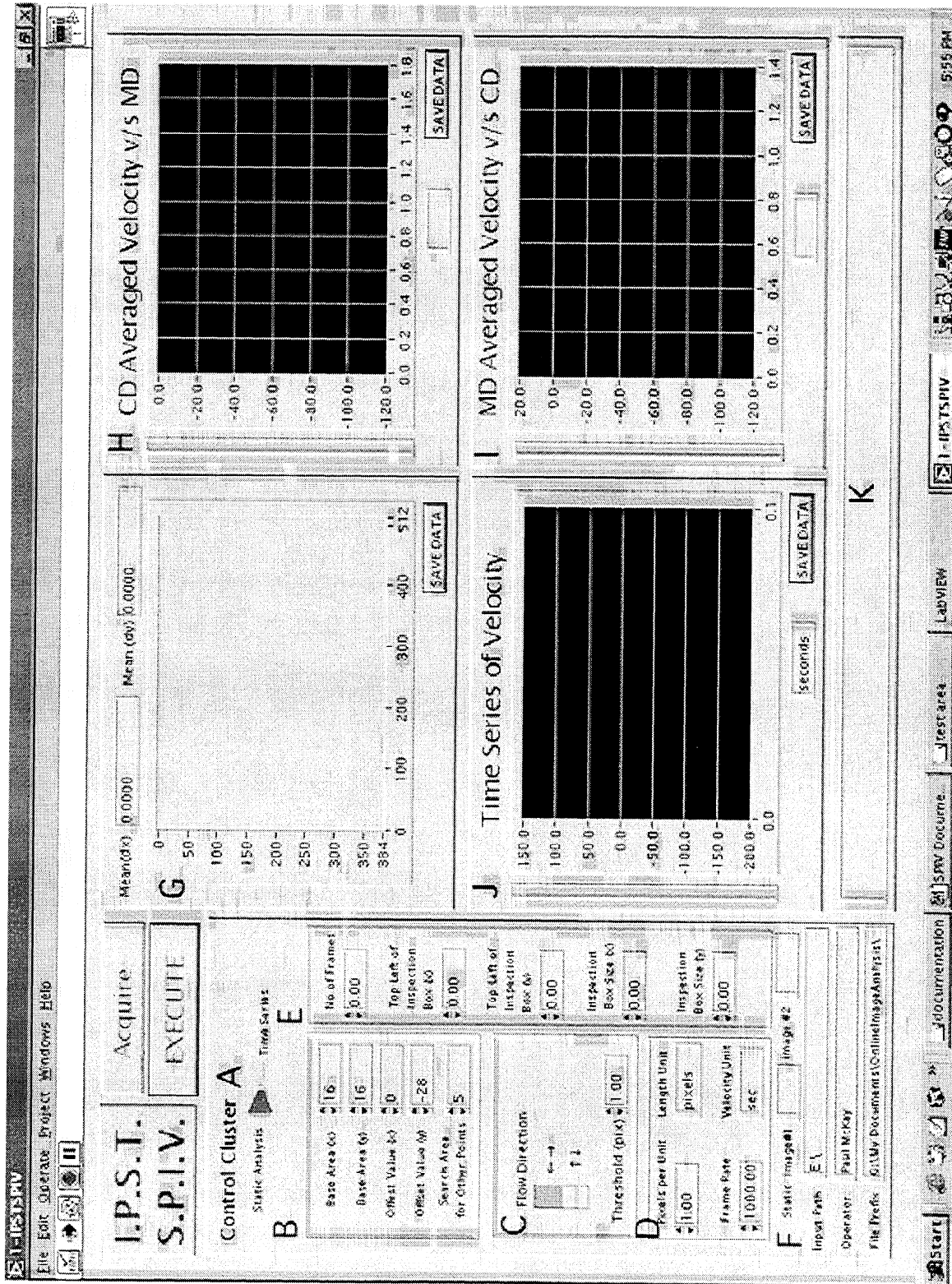


Figure 4. The front page of the On-line SPIV system



OVERCOMING THE FUNDAMENTAL WATER REMOVAL LIMITATIONS  
OF CONVENTIONAL WET PRESSING

STATUS REPORT  
FOR  
PROJECT F039

Timothy F. Patterson (PI)  
Isaak Rudman  
Daniela Edelkind

March 8 – 9, 2000

Institute of Paper Science and Technology  
500 10th Street, N.W.  
Atlanta, Georgia 30318



**DUES-FUNDED PROJECT SUMMARY**

<b>Project Title:</b>	<b>Overcoming the Fundamental Water Removal Limitations of Conventional Wet Pressing</b>
<b>Project Number:</b>	<b>F039</b>
<b>PAC:</b>	<b>Papermaking</b>
<b>Project Staff</b>	
<b>Principal Investigator:</b>	<b>Timothy Patterson</b>
<b>Co-Investigators:</b>	<b>None</b>
<b>Research Support Staff:</b>	<b>Isaak Rudman, Daniela Edelkind</b>
<b>PAC Subcommittee</b>	
	<b>F. Cunnane</b>
	<b>D. Lacz</b>
	<b>T. Haller</b>
<b>FY 99-00 Budget:</b>	<b>\$96,000</b>
<b>Allocated as Matching Funds:</b>	<b>0%</b>
<b>Time Allocation:</b>	
<b>Principal Investigator:</b>	<b>20%</b>
<b>Co-Investigators:</b>	<b>0%</b>
<b>Research Support Staff:</b>	<b>I. Rudman 25%</b> <b>D. Edelkind 50%</b>
<b>Supporting Research:</b>	
<b>Special Students:</b>	<b>None</b>
<b>External (Where Matching Is Used):</b>	<b>N/A</b>

**RESEARCH LINE/ROADMAP:** Line #7 - Increase paper machine productivity by 30% over 1997 levels via focus on breakthrough forming, dewatering, and drying concepts.

**PROJECT OBJECTIVE:** Develop through theoretical, experimental and pilot scale studies a non-drying, dewatering technology that will produce sheet solids levels that equal the theoretical maximum for non-drying methods.

**PROJECT BACKGROUND:** Project was initiated July 1, 1999.

**MILESTONES:**

Identify and quantify opportunities for improving wet pressing water removal. (To be Completed by March 2000)

- Review published literature.
- Review unpublished IPST research from previous DFRC projects.
- Identify and prioritize alternative water removal methods and opportunities.
- Evaluate potential methods at laboratory scale. (Schedule to be determined in consultation with sub-committee and PAC)

- Implement method(s) at an appropriate scale to convincingly demonstrate the method.

**DELIVERABLES: Deliverables for March 2000**

Overall Deliverable - Establish the path forward for the research project.

- Literature search directed at understanding the current limitations on wet pressing and possible methods for overcoming those limitations. Completed literature search will be submitted as an IPST Member Report.
- Review of previous IPST research, specifically;
  - Member company surveys completed for F021 - use information to establish pressing baseline.
  - Steambox (F002) and Impulse Drying (F001) - for permeability data, pore size data, compressibility data.
- Use literature and previous IPST research to create a solids profile vs nip curve pressure profile and solids profile vs press position.
- Identify and prioritize water removal methods and opportunities.

**STATUS OF GOALS FOR FY 99-00:**

- Review the literature and previous IPST research to establish the magnitude of the gain that can be obtained by overcoming the current fundamental limitations on wet pressing (To be completed by March 2000).
- Prioritize, based on potential gain and technical feasibility, the possible methods for overcoming current limitations on wet pressing (To be completed by March 2000).
- In consultation with the PAC sub-committee develop an experimental plan for evaluating potential methods (To be completed by March 2000).
- Goals for the remainder of the FY99-00 to be decided at Spring PAC meeting (March 2000).

**SCHEDULE:**

Task Descriptions	1999 July - Sept	1999 Oct - Dec	2000 Jan - Mar	2000 Apr-Jun
1. Literature Survey	-----	-----	x	
2. Write up of Lit Survey			----- x	
3. Review Prev. IPST Research		-----	----x	
4. Develop Press Solids Profile		-----	----x	
5. Prioritize Potential Methods			----x	
6. Develop Experimental Plan			-----x	
7. Setup Experiment Equip.				
8. Perform Experiments				
9. Write yearly report				-----x

#### SUMMARY OF RESULTS:

- A literature review directed at understanding the current limitations on wet pressing and possible methods for overcoming those limitations was initiated.
  - Conventional pressing is not capable of producing sheet solids levels that approach the theoretical maximum for non-drying methods. Sheet and fiber compressibility limit the maximum sheet solids.
  - Attaining solids levels that approach the theoretical maximum for non-drying methods will require the use of alternative "driving forces" that are not the result of the application of mechanical pressure, e.g. conventional pressing.
- A review of the literature, previous IPST research, and the potential mechanisms for sheet dewatering yielded several possibilities:
  - Fiber modification.
  - Ultrasound application during pressing.
  - A modified form of displacement dewatering.
- Given the fundamental mechanisms operating, displacement dewatering has the greatest potential.

#### SUMMARY OF KEY CONCLUSIONS:

- Conventional pressing is not capable of producing sheet solids levels that approach the theoretical maximum for non-drying methods. Overcoming those limitations will require the use of alternative "driving forces".
- A modified form of displacement dewatering appears to have the greatest potential, based on the fundamental mechanisms operating, for overcoming the current limitation on wet pressing water removal.



**DISCUSSION:**

## 1. INTRODUCTION

The start date for this project was July 1999. Between the project start and the present time, the primary effort was to identify and prioritize potential methods for significantly enhancing the water removal of wet pressing. This effort had three parts:

1. A survey of the open literature.  
Objective: Determine the following
  1. Where in the sheet is the water held during the pressing process?
  2. What are the forces holding the water in the sheet during pressing?
  3. What can be done to reduce the forces holding the water?
  4. What can be done to increase the forces driving water from the sheet?
2. A review of an earlier paper machine survey (Project F021)  
Objective: Determine if
  1. Sheet solids vs press section location can be determined.
3. A review of earlier steambox (F002) and impulse drying (F001)  
Objective: Determine the following
  1. Can representative average sheet pore diameters be determined from existing water permeability data?
  2. Can average sheet pore diameter be used to determine the capillary forces in the sheet at various points in the pressing process?
  3. Can sheet compression data, obtained from previous sheet displacement experiments, be used to estimate sheet solids vs nip position?
  4. Can additional insight into the mechanisms controlling the press dewatering process be obtained?

The primary results of the above work were:

1. Press dewatering is limited by sheet compression and the resultant decrease pore spaces. As the sheet compresses it becomes stiffer limiting further compression. The decreased pore size causes increased resistance to water flow.
2. Displacement dewatering, employed in a manner that takes advantage of initial sheet compression that occurs in the early part of the pressing process, has the greatest potential for yielding significantly increased water removal.
3. The paper machine survey data was not sufficient to obtain position in the machine vs sheet solids correlations. However, the data did show that many machines deliver low solids sheets to the dryer section.
4. Using theoretical considerations, water permeability data, and sheet displacement data it is possible to calculate the pneumatic pressure required for displacement dewatering, the optimum point in the nip to initiate displacement dewatering, sheet solids vs compression level, and sheet apparent density vs nip location (up to maximum compression). Compression data for the entire pressing process can be obtained and used to analysis the process.

The work is described in the following sections.

## 2. LITERATURE SURVEY

At the beginning of the project, two different general means of enhancing press dewatering were considered. These were, change the sheet/fiber ability to hold water and increase the forces or use alternative forces to remove water from the sheet/fiber. Therefore, a first step was to understand the forces holding the water in the sheet and the forces acting during standard wet pressing. The following subject areas were investigated: wet pressing theory, wet pressing practice, web compression, fiber structure, fiber-water interaction, web-water interaction, WRV test, FSP test, rewet, displacement dewatering, and press felts.

While a number of methods were found that could yield incremental increases in water removal, i.e., more uniform pressure application, heating, increased press load, optimized pressing pulse, longer pressing pulse, and improved felts, only three methods appeared to have any potential for significantly increasing water removal. These were, fiber modification to reduce fiber swelling and water content, application of ultrasound during pressing, and displacement dewatering.

In standard wet pressing the amount of water removed from the sheet corresponds to the amount of water normally held in the inter-fiber spaces. This does not imply that only inter-fiber water is removed during wet pressing, earlier research has shown that intra-fiber water can be removed by wet pressing. However, if the fiber held less water the wet pressing process should result in greater solids contents at the end of the process. Thus, fiber modification (reduction in fiber swelling and water content) via the addition of chemicals to pulp prior to pressing was considered. There are a few disadvantages to this approach. Previous research indicated that the sheet strength tended to decrease as a result of treatments to reduce fiber swelling. There were also some contradictory results in the literature. In addition, it appeared that different treatments would be required for different furnish types.

Several Russian researchers studied the use of ultrasound during and prior to the pressing process. These researchers filed a number of patents and claimed significant increases in water removal. The pressing application involved superimposing an ultrasound induced force on the standard pressure applied during wet pressing. A drawback to this research was that the fundamental mechanism causing the increased dewatering was not identified. The mechanism may have been a phenomena known as ultra sound induced capillary pressure. When a capillary is exposed to ultra sound the capillary pressure is increased. This could in theory, result in water being forced from inside the intra-fibers pores or from the inter-fiber pores. However, no mention of this phenomena was made by the Russian researchers. The subject deserves further investigation to determine the potential magnitudes of ultrasound induced capillary pressure. However, the lack of a clearly identified fundamental operating mechanism made this approach less promising.

The final area was displacement dewatering. Several researchers have done work in this area. However, most of the work was directed at maintaining bulk and not at optimizing water removal. Based on some preliminary calculations there appeared to be the potential for potentially significant increases in water removal if displacement

dewatering were employed in the proper manner. There was also the additional possibility of limiting rewet. The last section of this report presents a theoretical derivation on how to employ displacement dewatering in an optimum manner. This derivation was developed by Isaak Rudman, and utilizes the previous literature, water permeability data from F001 and F002, and sheet displacement/compression data from F001.

A report covering the entire literature search is being written at this time. A section covering rewet is complete. The report will be submitted as an IPST Member Report.

## MACHINE SURVEY

As part of project F021 a survey of a large number of linerboard, medium, and fine paper machines was undertaken. The objective of the survey was to obtain data on the operation and problems encountered in the dryer section. The survey included a number of questions about the operation of the press section. The data on the press section had not previously been studied. It was hoped that an analysis of the data would yield a press section position vs sheet solids relationship. This relationship would potentially help prioritize potential methods of enhancing water removal in the press section.

A review of the data showed that there was not enough information to produce a position vs solids correlation. However, there were some interesting results. The level of solids at the press section exit was not high for any of the furnishes.

In the case of the fine paper machines (see Table 1), no machine produced greater than 44% solids at the press section exit. Also, the sheet temperature tended to be rather low, for most machines it was around 38 °C. The low level of solids and the low sheet temperature were probably the result of constraints on sheet quality and the resultant limiting of press loading and sheet heating.

In the case of linerboard (see Table 2), the exit press solids tended to be slightly higher than for the fine paper machines. However, the exit solids were all less than 45% except for two medium machines. Sheet temperatures and press loading tended to be higher than those for the fine paper machine, and are probably the main reason for the higher solids levels.

While no quantitative data was derived that could help with the current project, the results do demonstrate that there is significant room for improvement in water removal on most machines.

#### 4 SUPPORTING THEORY FOR DISPLACEMENT DEWATERING

The work presented in the following subsections is an attempt to provide a motivation for the optimal use of displacement dewatering based on fundamental concepts and existing experimental data. The work is not intended to be exhaustive nor complete, but rather to demonstrate there is an optimum manner for implementing displacement dewatering. And, that its implementation can be guided by understanding the physical mechanisms that are at work and by utilizing data from carefully formulated experiments.

##### The Mechanism of Water Removal - Limits Imposed by Conventional Pressing.

In conventional pressing, water removal is induced by compressing the sheet. Sheet compression results in a decrease in average pore size and increase in apparent density. These changes decrease sheet compressibility and as a result decrease the potential for water removal. Using peak pressures of up to 1000 psi, the maximum solids attainable in most press sections is 45-50%. This solids level represents about the same amount of water as is found in the inter-fiber pores, i.e. inter-fiber water or free water, (Maloney et al. 1998).

Inter-fiber water is contained in the pore spaces between the fibers, these pores generally have diameters of 1 micron or greater. Intra-fiber water (or swollen water) is the water contained in pores that exist in the fibers. These pores generally have diameters of less than 0.05 microns. The intra-fiber water consists of water that is bonded to the fiber through hydrogen bonding and water that is not bonded to the fiber and can be removed mechanically. The amount of intra-fiber water determines the Fiber Saturation Point (FSP) and is about 1.4-1.5 g/g (Lindstrom 1986). If only free water is removed in press section the sheet solids should be 40-42%. Outgoing solids on most modern presses is in this range or slightly higher. Some of the latest machines may produce solids in the range of 50%, however, the quality constraints on many grades prevent the level of press loading required to attain those solids levels.

Is only inter-fiber water removed in press section? Experiments indicate that intra-fiber water is also removed in the nip (Carlsson 1983, Laivins and Scallan 1993). Therefore, the low solids levels attained in conventional pressing imply that the water removal process is not a serial process - all the free water is removed and then the intra-fiber water is removed. As the sheet is compressed some intra-fiber water is pushed into the inter-fiber spaces and a portion of it may reach the felt. Some of the inter-fiber water also enters the felt, however some of the inter-fiber water may be absorbed by the fibers, thus becoming intra-fiber water. This process is beneficial for development of sheet strength but at the same time limits water removal by conventional pressing.

A number of researchers have studied different approaches to increasing water removal in the press section. Peak pressure and nip dwell time can be increased to increase dewatering (Busker and Cronin 1982, Pikulik et al. 1996, Springer et al. 1991). The uniformity of pressure application can be enhanced with improved felts, thus increasing water removal for many grades (McDonald et al. 1999, Oliver and Wiseman 1978, Sze 1986, Szikla 1991, Vomhoff et al 1997). Also, the pressure pulse can be optimized (Schiel 1973). While the earlier work did show that improvements could be made, no

significant breakthrough is expected by using conventional pressing at room temperatures. Some researchers have suggested fiber treatments to decrease fiber swelling and, therefore the amount of intra-fiber water in the sheet. These treatments may negatively affect the mechanical strength of paper (Swerin et al. 1990, Strom and Kunnas 1991).

#### Limit of Water Removal by Mechanical Means

A portion of intra-fiber water (about 0.4 g/g) forms hydrogen bonds with the fibers and is contained in the fiber wall in pores smaller than 25 Å (or 0.0025 microns) (Stone et al. 1966). This water is sometimes referred to as non-freezing water. The amount of hydrogen bonded water varies insignificantly for different pulps. The amount of this water is affected by neither beating, nor drying. It does not depend on the sheet treatment. This water cannot be removed mechanically, as its removal requires heating to break the hydrogen bonds. It constitutes the limit of water removal by mechanical means and represents a sheet solids content of  $1/(1 + \text{moisture ratio}) = 1/(1+0.4) = 0.71$ . Thus, it appears that there is a significant potential to increase water removal from the present level of outgoing solids (40-45%) to magnitudes that are closer to the maximum limit on mechanical water removal, about 70% of solids.

#### Alternative Water Removal Methods.

Most alternative water removal methods rely on applying a pneumatic pressure differential to the sheet and on minimizing sheet compression. Earlier techniques associated with this concept involve displacement dewatering (Sprague 1986, Lindsay 1991), capillary dewatering (Chuang et al. 1997, Lee 1995), and blow-through dewatering (Kawka 1979). In the case of displacement dewatering the applied pressure differential acts against the capillary pressure resistance and drives the water out of the sheet. Capillary dewatering counteracts the sheet capillary pressure with a larger imposed capillary pressure. Blow through dewatering depends on water evaporation and water entrainment. All three methods minimize sheet compression in the nip to keep more pores open and increase the water removal rate.

Pore size determines capillary pressure to be overcome by the driving pressure used to induce water removal. Pore size decreases with sheet compression. Thus, more efficient water removal can be expected if the sheet is not significantly compacted during application of driving pressure differential. In general, the pores of interest for all three methods are the inter-fiber pores. The intra-fiber pores are extremely small and result in correspondingly high capillary pressures, pressures that would be difficult to produce and maintain.

#### Displacement Dewatering Concept.

Displacement dewatering involves sheet prepressing and subsequent application of a driving air pressure. If displacement dewatering is to be efficient, it is necessary to determine the optimal combination of compressive and driving air pressure. Application of the proper compressive pressure ensures that the sheet is in saturated condition and serves to move some of the water in the sheet from intra-fiber pore spaces to inter-fiber pore spaces. Maintaining the sheet in a saturated condition can reduce the occurrence

of fingering. Fingering results when there are small areas in the sheet that present less resistance to water flow than the remainder of the sheet. Given an equal pneumatic pressure applied to the sheet and the inter-fiber water, the water will follow these "paths of least resistance" quickly creating a path through the sheet that is not blocked by water. The driving air then flows through those paths creating fingering and localized blow through. The problem is the pneumatic pressure on the remainder of the sheet is relieved, stopping the water removal, and significant amounts of air can escape. If all the paths through the sheet were comprised of equal diameter pores, pores producing the same level of capillary pressure, there would be no fingering and blow through. Elimination of blow fingering can be also achieved by applying foam to the sheet surface (Skelton 1987). As the compressive pressure increases, the size of the pores available for water flow decreases, the capillary pressure resistance increases and the driving pneumatic pressure must increase.

Inter-fiber water and intra-fiber water are held by capillary forces. This water can be removed mechanically when an applied pneumatic,  $P$ , exceeds the capillary resistance which is given by

$$P = 2 \gamma \cos \theta / r,$$

where  $\gamma$  is surface tension of water (at room temperature  $\gamma = 0.073$  N/m);  $r$  is average pore radius; and  $\theta$  is the contact angle, usually varying within the range from 0 to 60 degrees (Hodgson and Berg 1988). Thus capillary pressure resistance depends on the wetting fluid, which determines surface tension and contact angle, and on average pore size. Effective use of displacement dewatering requires that approaches be found to determine necessary compressive and driving pressures in terms of their magnitudes and time distribution in the nip.

#### Role of Water Permeability for Determining Pore Size.

There is an experimentally observed and theoretically substantiated link between permeability and average pore size (Bliesner 1964, Dullien 1986, Hoyland and Field 1976). This link makes it possible to obtain an estimate of average pore size and capillary pressure resistance using the water permeability test (Appendix 1). Thus, required driving pressure can then be calculated.

An analysis of the available water permeability measurements conducted at IPST over the years was made. These measurements were routinely performed to estimate specific surface area of the water swollen fibers in the sheet, a measure thought to be correlated with critical temperature of impulse drying. No research specifically targeting effect of the applied pressure within the range encountered in the press nip (up to 500 – 1000 psi) was conducted using the water permeability test. However, tests were conducted at lesser applied pressures and the data is valuable to the current research.

A summary of the available water permeability results is presented in Table 3. It indicates that at high applied pressures the pore size for the sheets, made from different furnishes, converges to approximately the same value regardless of their basis weights and permeabilities in uncompressed state. The coefficient of variation of average pore

size decreases as the applied pressures increases from 10 to 1000 psi and then levels off (Figure 1). The average pore size in highly-compressed sheets is about 36 Å, which is close to the pore size in which hydrogen-bonded water is contained (about 25 Å). This water cannot be removed mechanically and determines the limit of pressing.

During the water permeability test, the overall sheet compression is measured by monitoring the separation of the press platens. Using this information, sheet compressibility results can be measured which enables a calculation sheet elastic modulus as a function of the sheet strain, or apparent density as a function of applied pressure. While the compression process used in the sheet is not identical to that encountered in the press nip, this information can be used to estimate sheet compression in the nip. Also the development of the solids as a function of compressive pressure can be described.

#### Role of Thickness Measurements in the Nip

A system developed to measurement the displacement of metal targets, placed on and within sheets, was used from April to June 1997 for an investigation of sheet compression and expansion during conventional pressing and impulse drying. A schematic is shown in Appendix 1. The system was used in conjunction with an MTS computer controlled hydraulic press. Various furnishes and impulses were tested, all tests used a felt to ensure the compression process was as realistic as possible. Some of the results obtained with this system were reported by Orloff et al. 1998, Table 4 shows the test conditions.

Displacement measurement system, in general, worked well within certain limitations. The system used eddy current sensors to measure the displacement of the metal targets. Due to the errors inherent to this measurement method, reliable data could not be obtained from low thin sheets. The minimum sheet thickness for repeatable data was 100 - 150 microns. Thus, sheets or layers within a sheet that had basis weights less than 100 gsm had poor reproducibility. In addition, if the sheet layers were made from sheets of different basis weights cause the prepressing sample preparation process to produce a non-uniform sheet density profile.

Figure 2 shows parameters that can be calculated using the displacement measurements. The case shown used a shoe press impulse. Sheet strain, as a function of dwell time, was calculated as follows:

$$\Delta\varepsilon(t) = [L_0 - L(t)] / L_0$$

where  $L_0$  is initial (ingoing) thickness of the sheet;  $L(t)$  is the sheet thickness at a given time,  $t$  of the nip. The corresponding compression rate is  $-dL/dt$ .

Analysis of the pressure and compression rate curves makes it possible to single out four intervals within the nip which were qualitatively outlined in some publications associated with fundamentals of wet pressing (Carlsson 1983, Wahlstrom 1969, Wrist 1964). The first three intervals characterize the compressive phase of the nip, while the last characterizes the expansion phase of the nip. A more detailed description of the



pressure nip intervals is presented in Appendix 2. Some other results are described below.

The MTS presses the sheet under dynamic conditions. The water permeability test apparatus presses the sheet under static, saturated sheet conditions. It is generally acknowledged that static pressing produces higher solids levels than dynamic pressing. Results from the two pieces of equipment can be used to compare sheet compression and solids during static and dynamic pressing. The development of the solids under static and dynamic pressing conditions is presented in Figure 3. It demonstrates the significant difference in outgoing solids attained by static and dynamic compression. An increase of platen temperature makes it possible to diminish this difference.

Using the plot of sheet thickness as a function of time it is possible to determine the time and amount applied pressure which brings the sheet to a saturated state. Once the sheet is completely saturated, significant water removal can begin. This pressure can be considered as the minimum pressure required to avoid the fingering effect during displacement dewatering. Reaching this pressure can be thought of as a pre-pressing for displacement dewatering. The maximum of pre-pressing pressure is determined by the point at which the compression rate becomes small. After this point, water removal by sheet compression is not efficient and displacement dewatering by pneumatic pressure should be least susceptible to fingering and have the greatest potential for dewatering. The average pore size will dictate the magnitude of pneumatic pressure required. A point in favor of delaying the application of displacement dewatering until the this point is that as the sheet is compressed the pore size distribution decreases, thus further reducing the potential for fingering.

#### Estimate of Water Removal in the Nip

To determine the optimum relationship between pre-pressing and driving pressure in displacement dewatering, an estimate of water removal with respect to nip position should be made. This would also allow a comparison of water removal in displacement dewatering and in conventional pressing. A theoretical derivation is presented in the following paragraphs. Within the limits of the assumptions made in the derivation, the result can serve as a guide for determining the point at which to initiate displacement dewatering.

The velocity of the water flow during pressing is determined by the sheet compression rate. Since the area available for water flow in any cross section is the area not occupied by the fibers, the absolute velocity of water inside the sheet is given by the expression:

$$U = (dL/df) / (1-v c),$$

where  $v$  is the specific volume of swollen fibers and  $c = m_f / (A L)$  is the apparent density of the sheet.

The velocity of the water relative to the fiber network is

$$U_r = (dL/dt) / (1-v c) - dL/dt \\ = (dL/dt) \{v c / (1- v c)\} .$$

In the case of laminar flow, according to Poiseuille's Law, viscous resistance to the compression-induced water flow through the fiber network can be expressed as

$$P_v = 8 L \mu U_r / R^2 ,$$

where  $\mu$  is the dynamic viscosity of water and R is the average hydraulic radius of the pores for water flow.

Since R can be expressed as

$$R^2 = 8 K / \varepsilon \\ = 8 K / (1 - v c) ,$$

where K is the permeability for water flow, the equation for viscous resistance can be rewritten as

$$P_v = L \mu U_r \varepsilon / K$$

Using the relationship for  $U_r$  the expression for the viscous resistance becomes

$$P_v = L dL/dt \mu v c / K.$$

It is important to note that although no pressure differential is applied to the sheet in the nip, the resistance to compression-induced water flow is the same as for Darcian flow.

where

$$L = W / c,$$

and W is the oven-dry basis weight. Substituting the Darcian expression L and differentiating yields,

$$P_v = (- \mu W^2 v) (dc/dt) / (c^2 K).$$

Water permeability K can be found as a function of apparent density using regression analysis of experimental data and the relationship

$$K = k_1 c^{k_2} .$$

The viscous resistance in the sheet is balanced by the portion of applied pressure that is equal to  $P - P_c$ , where P is the total applied pressure and  $P_c$  is the pressure compressing the fibers. Thus,  $P_v$  can be stated as

$$P_v = P - P_c$$

where  $P_c$  is the compression pressure which is usually found as a power function of apparent density (Ingmanson et al. 1959, Wrist 1964)

$$P_c = p_1 c^{p_2}$$

Finally, an equation for the calculation of apparent density as a function of the nip position at which water flow out of the sheet begins is obtained by combining the expressions for  $P_v$  and  $P_c$

$$(p_1 c^{p_2} - \mu W^2 v) (dc/df) / (c^2 k_1 c^{k_2}) = P$$

Nilsson and Larsson (1968) concluded that measurements of flow resistance and compressibility do not give enough quantitative information to estimate water removal in the nip after the point of maximum compression. The relationship is suitable for estimates of water removal prior to that point. Additionally, time-dependent functions can be used if required (Wrist 1964).

The solution of this equation can be easily found by coding it in an Excel Spreadsheet. As estimate indicate, the assumption about sheet saturation results in marginal error at high compressive pressures, because the volume occupied by compressed air is negligible.

A sample calculation, for portion of compressive phase of the nip where water removal takes place, was performed for a sheet pressed at room temperature. The following parameters were used:

$$\begin{aligned} k_1 &= 0.01 \times 10^{-15} \text{ m}^2 / (\text{g}/\text{cm}^3); \\ k_2 &= -4.463 \\ p_1 &= 2.75 \text{ MPa} / (\text{g}/\text{cm}^3); \\ p_2 &= 3.175; \\ \mu &= 0.00995 \text{ (dynes/sq.cm) sec}; \\ W &= 0.01874 \text{ g}/\text{cm}^2 \\ v &= 1.03 \text{ cm}^3/\text{g}. \end{aligned}$$

The result is plotted in Figure 3. This example calculation illustrates that the suggested approach produces a reasonable match of experimental and calculated results.

### Conclusions.

An analysis of the amount water held in the inter- and intra-fiber of a wet sheet, indicates that there is an opportunity to increase water removal in the press from the current level of about 45% of solids to the levels approaching 70% of solids. The main factor which impedes attaining higher levels of solids during conventional pressing is the extent of sheet compression required. The compression is attained through high press loads. Compression of the sheet reduces the average inter-fiber pore size and restricts water flow. Thus, to achieve higher solids, water removal should not be accompanied by excessive compression of the wet web, which in turn requires an alternative driving force for removing the water.

Displacement dewatering in the press section appears to be a promising method for attaining higher water removal. Displacement dewatering involves sheet prepressing and subsequent application of a driving pneumatic pressure. Optimum displacement dewatering requires pre-pressing that saturates the sheet, removes some water from the fibers, but does not "excessively" compress the sheet. It then requires the application of the pneumatic driving force at the point in the nip when the compression rate is low, but not negative.

The experimentally observed and theoretically substantiated link between permeability and average pore size makes it possible to use water permeability test for an estimate of average pore size and capillary pressure resistance. Thus, the required pneumatic driving pressure can be calculated.

Additionally, an analysis of the available water permeability measurements shows that at high applied pressures the average pore size for sheets made from different furnishes converges to approximately the same value regardless of basis weights and permeabilities in uncompressed state. The amount of water contained in the pores at this convergent condition is approximately to the amount of water held by hydrogen bonds. This water cannot be removed mechanically and determines the limit of pressing. The convergence of permeabilities to approximately the same value at high applied pressures also supports the observation that the limit of water removal by pressing is independent of permeability in the uncompressed state.

Dynamic measurements of the sheet thickness in the nip make it possible to determine the time and value of applied pressure which brings the sheet into a saturated state and the time and applied pressure that initiate significant water removal due to compression. This pressure can be considered as a minimum pre-pressing pressure for avoiding the fingering effect that can occur during displacement dewatering. The maximum pre-pressing pressure is determined at which the compression rate becomes small. After this instant of time, water removal by sheet compression is not efficient and displacement dewatering provides an alternative driving force for dewatering.

Table 1. Fine Paper Machines

Machine	Operation							1st Press			3rd Press			4th Press						
	Basis weight (g/m <sup>2</sup> )	Speed (m/min)	Speed (m/min)	Press Exit Solids	Press Exit Temp	Number of Presses	Former	Press Load (Mpa)	Top Felt (1=yes)	Bottom Felt (1=yes)	Press Load (Mpa)	Top Felt (1=yes)	Bottom Felt (1=yes)	Press Load (Mpa)	Top Felt (1=yes)	Bottom Felt (1=yes)				
<b>Fine Paper</b>	Basis weight less than 50 gsm																			
47	45	2200	671	39.1	95	2	fourdrinier		yes	0	--	--	yes	--	--	--	0	--	--	
29	49	1401	427	38	90	2	fourdrinier	1.31	--	yes	2.41	yes	--	--	--	--	0	--	--	
32	49	1500	457	36		2	fourdrinier	1.03	--	yes	2.76	yes	--	--	--	--	0	--	--	
<b>Average</b>	<b>48</b>	<b>1700</b>	<b>518</b>	<b>38</b>	<b>93</b>	<b>2</b>		<b>1.17</b>			<b>2.58</b>						<b>0.00</b>			
<b>Std. Dev.</b>	<b>2</b>	<b>436</b>	<b>133</b>	<b>2</b>	<b>4</b>	<b>0</b>		<b>0.19</b>			<b>0.24</b>						<b>0.00</b>			
<b>Fine Paper</b>	Basis weight less than 70 gsm and greater than 50 gsm																			
19	55	2644	806	43	120	3	top wire	2.76	yes	0	3.93	yes	--	4.14	--	yes	--	--	--	
46	66	2676	816	41	125	3	top wire	1.72	yes	yes	2.93	--	yes	3.10	--	yes	--	--	--	
30	67	1392	424	39	90	2	fourdrinier	2.41	yes	0	2.41	yes	--	--	--	--	--	--	--	
38	74	1550	473	38		2	fourdrinier	2.41	0	yes	2.76	yes	--	--	--	--	--	--	--	
8	75	1800	549	35	110	2	fourdrinier	2.41	yes	yes	3.10	--	yes	--	--	--	--	--	--	
36	75	1200	366	41		2	fourdrinier	1.72	0	yes	3.10	yes	--	--	--	--	--	--	--	
39	75	1960	598	38	96	2	fourdrinier	2.41	yes	0	2.76	--	yes	--	--	--	--	--	--	
41	75	2850	869	40	109	3	top wire	2.41	yes	yes	3.10	yes	--	4.31	yes	--	--	--	--	
9	76	2750	838	42	105	3	top wire	2.76	yes	yes	3.45	yes	--	4.14	yes	--	--	--	--	
42	75	3050	930	44	105	4	top wire	2.21	yes	yes	3.86	yes	--	4.14	yes	--	4.47	--	yes	
<b>Average</b>	<b>75</b>	<b>2883</b>	<b>879</b>	<b>42</b>	<b>106</b>	<b>3</b>		<b>2.46</b>			<b>3.47</b>			<b>0.00</b>			<b>0.00</b>			
<b>Std. Dev.</b>	<b>0</b>	<b>153</b>	<b>47</b>	<b>2</b>	<b>2</b>	<b>1</b>		<b>0.28</b>			<b>0.38</b>			<b>0.00</b>			<b>0.00</b>			
<b>Fine Paper</b>	Basis weight less than 100 gsm and greater than 80 gsm																			
1	83	2403	733	42.5	98	3	fourdrinier	0.28	yes	0	0.15	yes	0	0.15	yes	yes	--	0	0	
37	88	910	277	41	115	2	fourdrinier	1.72	0	yes	3.10	yes	0	0	0	0	--	0	0	
33	90	1569	478	36	100	2	fourdrinier	1.90	0	yes	2.41	yes	0	0	0	0	--	0	0	
20	93	2100	640	43	112	3	fourdrinier	3.10	yes	0	5.51	yes	0	5.17	0	yes	--	0	0	
<b>Average</b>	<b>90</b>	<b>1526</b>	<b>465</b>	<b>40</b>	<b>109</b>	<b>2</b>		<b>2.24</b>			<b>3.68</b>			<b>0.00</b>			<b>0.00</b>			
<b>Std. Dev.</b>	<b>2</b>	<b>596</b>	<b>182</b>	<b>4</b>	<b>8</b>	<b>1</b>		<b>0.75</b>			<b>1.63</b>			<b>0.00</b>			<b>0.00</b>			

Table 2. Linerboard and Medium Machine

Machine	Operation						1st Press			2nd Press				3rd Press				Shoe Press
	Basis Weight (g/m <sup>2</sup> )	Speed (m/min)	Press Exit Solids	Press Exit Temp (F)	Number of Presses	Former	Press Load (Mpa)	Top Felt (1=yes)	Bottom Felt (1=yes)	Press Load (Mpa)	Top Felt (1=yes)	Bottom Felt (1=yes)	Pre Dryer (1=yes)	Press Load (Mpa)	Top Felt (1=yes)	Bottom Felt (1=yes)	Pre Dryer (1=yes)	
<b>Linerboard</b>																		
34	127	516	36	113	2	Fourdrinier	3.45	1	0	4.14	--	1	--	--	--	--	--	--
17	166	710	43	125	3	Fourdrinier	3.45	1	1	4.14	1	--	--	41.35	1	1	--	3rd Press
27	171	762	38	135	2	Multi-Fourdrinier	6.89	1	1	13.09	1	1	--	--	--	--	--	2nd Press
14	176	626	44	140	2	Fourdrinier	8.62	1	1	12.06	1	1	--	--	--	--	--	
43	186	550	39	138	3	Fourdrinier	1.72	--	1	2.41	--	1	--	6.89	--	1	--	
28	269	693	43	145	2	Multi-Fourdrinier	9.30	1	1	37.91	1	1	--	--	--	--	--	2nd Press
16	269	520	41	140	3	Fourdrinier	4.14	1	1	5.51	--	1	--	8.27	--	1	--	
24	298	76	42	149	2	Fourdrinier	1.45	--	1	1.45	--	1	--	--	--	--	--	
Average	208	557	41	136	2		4.9			10.1				18.8				
Std. Dev.	62	215	3	12	1		3.0			12.0				19.5				
<b>Bleached Linerboard</b>																		
15	205	427	37	--	3	Fourdrinier	1.90	--	1	1.90	--	1	7	2.48	--	1	1	
21	288	277	46	109	2	Fourdrinier	2.41	--	1	2.41	--	1	--	--	--	--	--	
Average	247	352	42	109	3		2.2			2.2				2.5				
Std. Dev.																		
<b>Medium</b>																		
12	127	595	45	135	2	Fourdrinier	6.89	1	1	8.27	1	1	--	--	--	--	--	
13	127	762	47	130	2	Fourdrinier	4.14	1	1	41.35	1	1	--	--	--	--	--	2nd Press
23	127	638	44	140	2	Fourdrinier	4.82	1	1	6.89	1	1	--	--	--	--	--	
45	127	637	41	140	2	Fourdrinier	5.51	1	1	13.78	1	1	--	--	--	--	--	
44	127	762	44	120	3	Fourdrinier	4.14	1	1	4.14	1	--	--	6.89	1	1	--	
18	161	510	42	135	2	Fourdrinier	3.10	1	--	5.51	1	1	--	--	--	--	--	
Average	133	651	44	133	2		4.8			13.3				6.9				
Std. Dev.	14	98	2	8	0		1.3			14.1								

IPST Confidential Information - Not for Public Disclosure  
(For IPST Member Company's Internal Use Only)

Table 3. Average Pore Size Based on Permeability Measurements

Case	Oven Dried Basis Weight	Specific Surface	Permeability x 10 <sup>15</sup>	Average Pore Diameter (from Permeability Data)	Average Pore Diameter (Calculated from Regression Analysis)					Comments	
					68.9 kPa	68.9 kPa	689 kPa	3450 kPa	6890 kPa		20700 kPa
					m <sup>2</sup> /g	m <sup>2</sup>	µm	µm	µm		µm
1	79.2	5.41	25.14	0.8969	0.0885	0.0175	0.0087	0.0029	Unbleached North-American Pulp.		
2	93.4	10.95	4.749	0.3898	0.0613	0.0168	0.0096	0.0040	Unbleached North-American Pulp.		
3	94.3	6.51	12.89	0.6421	0.0669	0.0138	0.0070	0.0024	Unbleached North-American Pulp.		
4	96.5	15.94	1.182	0.1945	0.0334	0.0097	0.0057	0.0025	Bleached		
5	102.6	3.24	40.4	1.1365	0.1205	0.0251	0.0128	0.0044	Unbleached North-American Pulp.		
6	104.4	3.17	30.19	0.9828	0.1166	0.0263	0.0138	0.0050	Unbleached North-American Pulp.		
7	109.6	18.14	2.041	0.2556	0.0259	0.0052	0.0026	0.0009	Bleached		
8	113.6	36.16	0.5853	0.1369	0.0277	0.0091	0.0056	0.0026	Unbleached North-American Pulp.		
9	119.1	1.37	574.5	4.2877	0.2928	0.0448	0.0200	0.0056	Unbleached North-American Pulp.		
10	131.4	1.82	651.1	4.5647	0.2872	0.0415	0.0181	0.0048	Unbleached North-American Pulp.		
11	147.6	9.04	16.46	0.7257	0.0565	0.0095	0.0044	0.0013	Unbleached North-American Pulp.		
12	150.4	9.90	9.624	0.5549	0.0606	0.0129	0.0066	0.0023	Unbleached North-American Pulp.		
13	153.1	28.50	1.426	0.2136	0.0302	0.0077	0.0043	0.0017	Unbleached North-American Pulp.		
14	197.8	61.61	0.286	0.0957	0.0264	0.0107	0.0073	0.0039	Unbleached North-American Pulp.		
15	201.3	35.00	0.501	0.1267	0.0336	0.0133	0.0089	0.0047	Unbleached North-American Pulp.		
16	204.6	70.99	0.268	0.0925	0.0233	0.0089	0.0059	0.0030	Unbleached North-American Pulp.		
17	205.3	36.30	0.655	0.1448	0.0316	0.0109	0.0069	0.0033	Bleached		
18	205.5	33.30	0.567	0.1347	0.0236	0.0070	0.0041	0.0018	Bleached		
19	210	9.66	0.296	0.2959	0.0528	0.0158	0.0094	0.0041	Unbleached North-American Pulp.		
20	239.3	25.61	0.223	0.2228	0.0577	0.0224	0.0149	0.0078	Non US Furnish		
21	435.1	92.54	0.252	0.0898	0.0319	0.0155	0.0114	0.0069	Unbleached North-American Pulp.		
Maximum	435.1	92.54	651.1	4.5647	0.2928	0.0448	0.0200	0.0078			
Minimum	79.2	1.373	0.223	0.0898	0.0233	0.0052	0.0026	0.0009			
Average				0.7707	0.0738	0.0164	0.0090	0.0036			
Standard Deviation				1.2569	0.0773	0.0106	0.0047	0.0018			
Coefficient of Variation				1.6308	1.0480	0.6445	0.5233	0.4971			

IPST Confidential Information – Not for Public Disclosure  
(For IPST Member Company’s Internal Use Only)

**Table 4. Experimental Conditions for Displacement Measurements**

	Condition 1 Conventional Pressing	Condition 2 Shoe Press.	Condition 3 Shoe Press w/ Ramp
Peak pressure, MPa	4.82	5.39	5.55
Pressure impulse, kPa s	37.9 - 41.3	117.2	137.8 – 151.6
Dwell Time, ms	19 - 20	46 - 47	40
Ramp Duration, ms	0	0	15 runs 4,5 26 runs 1,2 43 runs 3
Furnish	Repulped Liner 30% OCC 660 ml CSF	Repulped Liner 30% OCC 660 ml CSF	OCC 620 ml CSF
Press Platen Temperatures, °C	21 200 250	21 100 200 300	275 250 300 325 350
Ingoing Solids, %	35	35	40
Layering, gsm	51, 51, 51, 51	51, 51, 51, 51	15, 30, 30, 30, 100



Figure 1. Average Pore Diameter and Coefficient of Variation vs. Compressive Pressure.

Basis Weights = 80 - 435 gsm  
Furnishes: Bleached and Unbleached Pulp

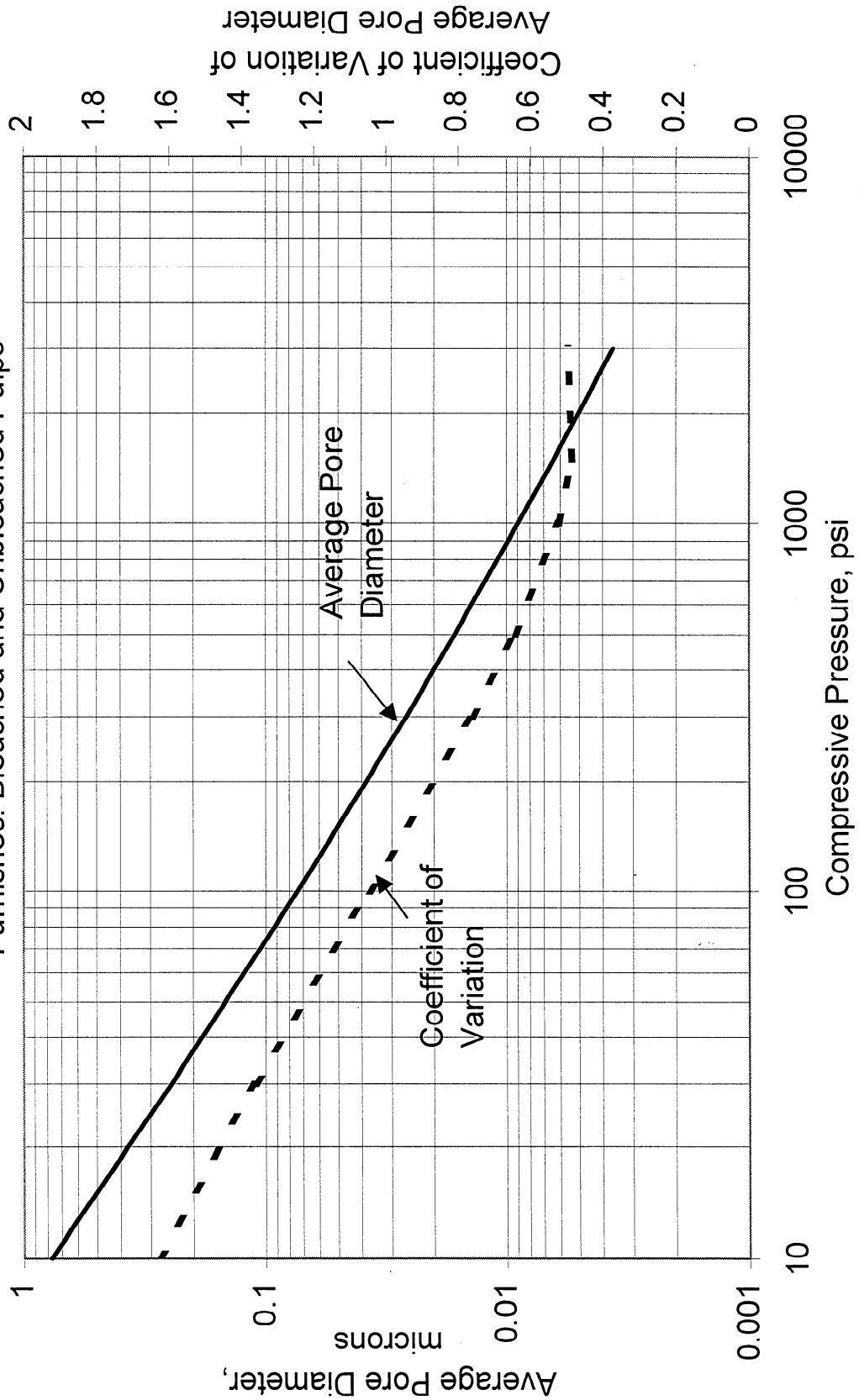


Figure 2. Displacement Results for MTS Pressing at Room Temperature

Compression Rate =  $-dL/dt$

Strain =  $(L_0 - L) / L_0$

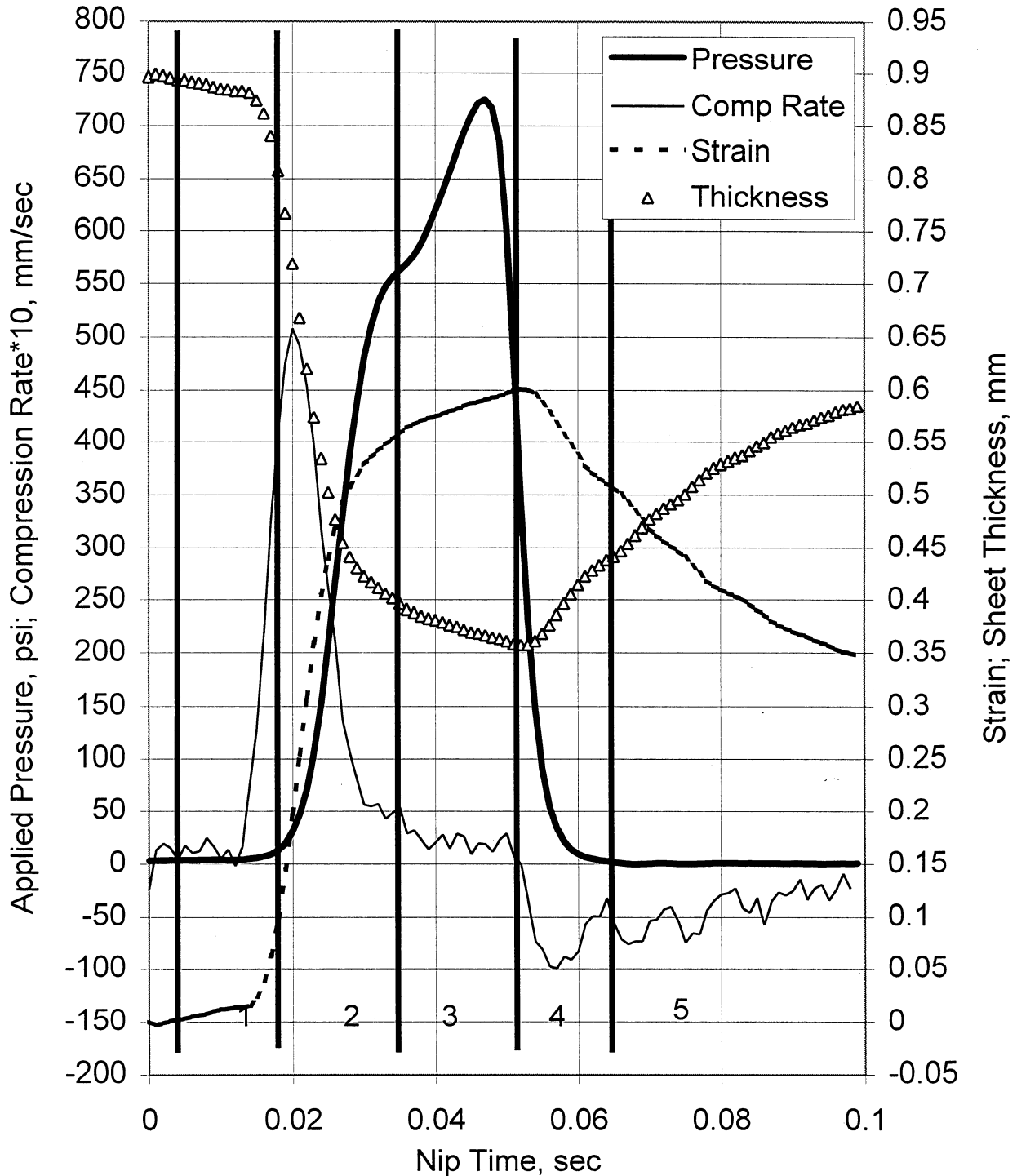


Figure 3. Compressive Pressure vs. Solids from Water Permeability (Static Data) and Sheet Displacement Measurements (Dynamic Data)

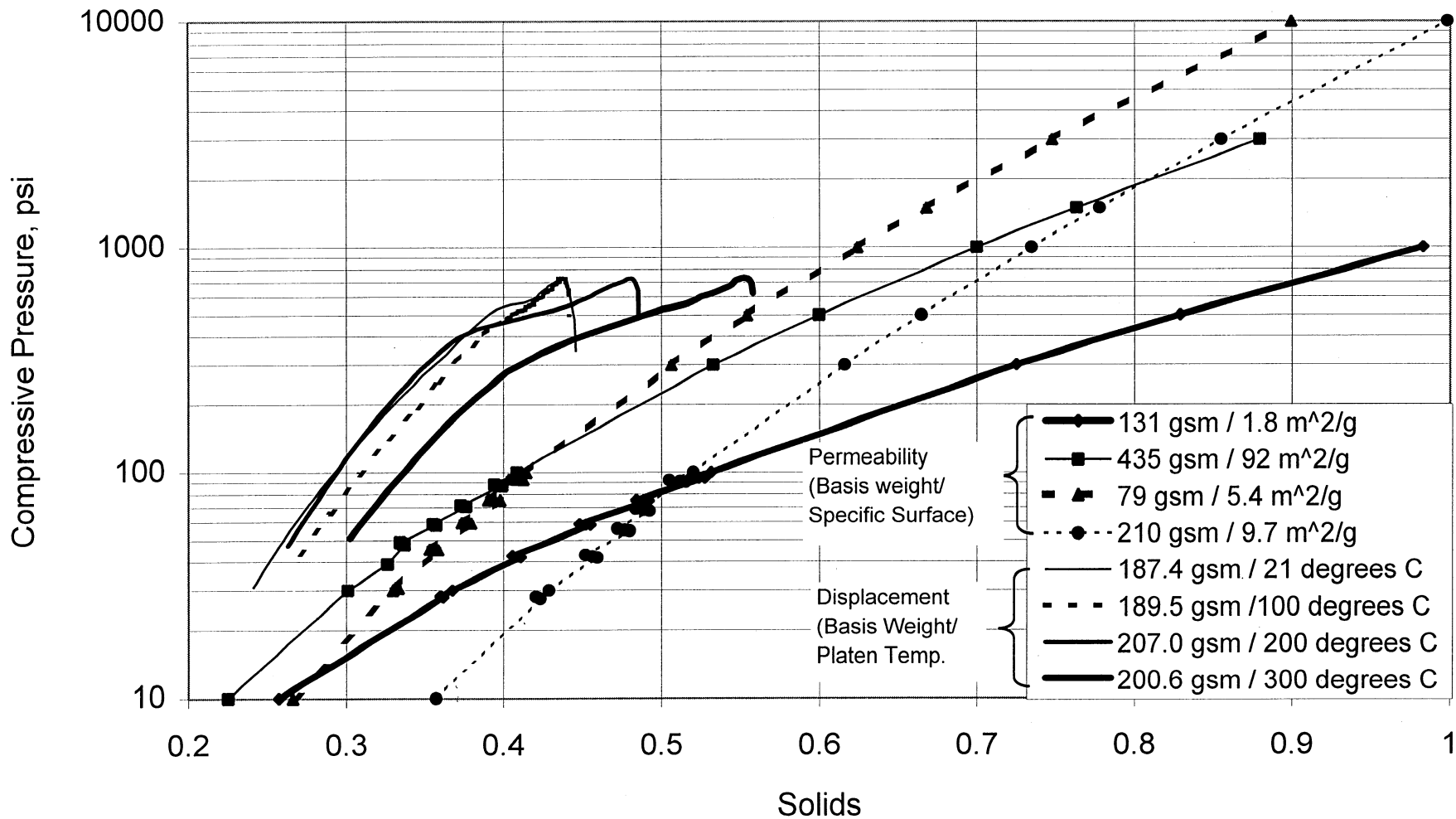
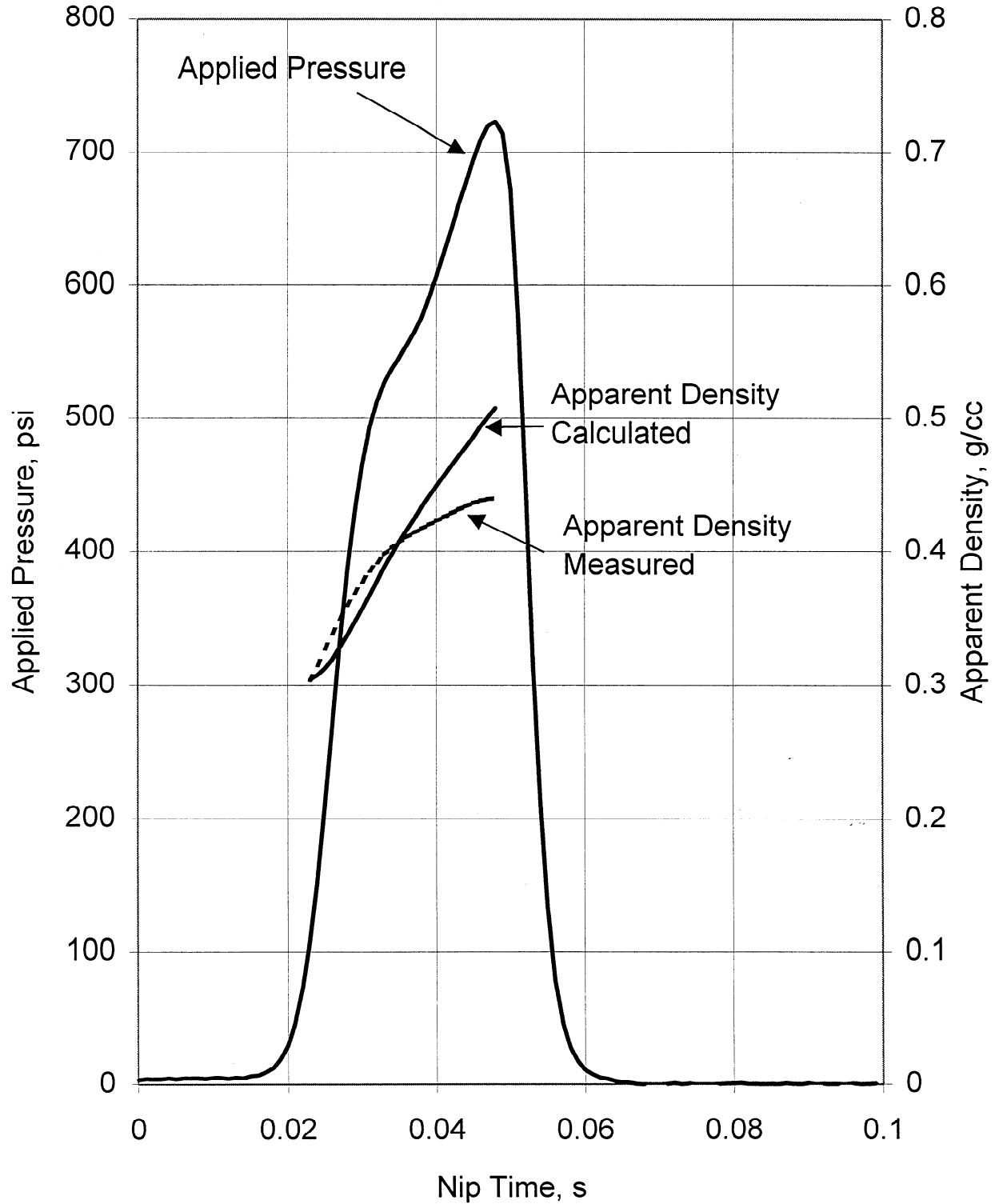


Figure 4. Experimental and Calculated Apparent Densities



## LITERATURE CITED

- Bliesner, W.C. A Study of the Porous Structure of Fibrous Sheets Using Permeability Techniques. Tappi J., 47(7): 392-400 (July, 1964).
- Burns, J.R., Conners, T.E., and Lindsay, J.D. Dynamic measurement of density-gradient development during wet pressing. Tappi J., 73(4):107-113(1990)
- Burton, S.W., and Sprague, C.H. The Instantaneous Measurement of Density Profile Development During Web Consolidation. Journal of Pulp and Paper Science:Vol.13, No.5, September 1987.
- Busker, L.H. and Cronin, D.C. The Relative Importance of Wet Press Variables in Water Removal. 1982 Int. Water Removal Symp., 25-34.
- Carlsson, G. Some fundamental aspects of the wet pressing of paper. Doctoral Thesis, Stockholm, 1983.
- Chuang, S., Kaufman, K., Schlessler, R. Capillary Dewatering Method and Apparatus. U.S. pat. 5,701,682. Issued December 30, 1997.
- Dullien, F.A.L. Porous Media: Fluid Transport and Porous Structure.
- Hodgson, K.T. and Berg, J.C. Dynamic Wettability Properties of Single Wood Pulp Fibers and Their Relationship to Absorbency. Wood and Fiber Science, Vol.20 (1), 3-17, January, 1988.
- Hoyland, R.W, and Field, R. A review of transudation of water into paper – in five parts. Part 3. Some principles of flow & their application to paper. Paper Techn. and Industry, December 1976, 291-299.
- Ingielewicz, H; Kawka, W. INVESTIGATION ON INTENSIVE DEWATERING AND DRYING OF POROUS PAPERS. Paper (London) 191, no. 10: 618, 621-622 (May 21, 1979).
- Ingmanson, W.L., Andrews, B.D., and Johnson, R.C. Internal Pressure Distribution in Compressible Mats under Fluid Stress. TAPPI, Vol.42, #10, 840-849, October 1959.
- Kawka, W., Szwarcosztajn, E. SOME RESULTS OF INVESTIGATIONS ON THE EQUIPMENT FOR INTENSIVE DEWATERING AND DRYING OF POROUS PAPERS. EUCEPA Conf. (London) 18, Paper No. 31: 17 p. (May 21-24, 1979).
- Laivins, G.V. and Scallan, A.M. Removal of Water from Pulps by Pressing – Part 1: Inter and Intra Wall Water. Tappi Eng.Conf, 1993, Orlando, Florida: 741 – 748.
- Lee, C. A. Method for Dewatering a Porous Wet Web. U.S. pat. 5,445,746. Issued August 29, 1995.

Lindsay, J.D. Displacement dewatering to maintain bulk. Paperi ja Puu, Vol.74, #3, 232-242, 1992.

Lindstrom, T. The Concept and Measurement of Fiber Swelling. Pp.75-97 in monograph edited by Bristow, J.A. and Kolseth, P. "Paper Structure and Properties", 1986.

Maloney, T.C., Todorovic, A., and Paulapuro, H. The effect of fiber swelling on press dewatering. Nordic Pulp and Paper Res. J., Vol.33, #4, 1998, 285-291.

McDonald, J.D., Pikulik, I.I., Ko, P.L., and Owston, T.H. Optimizing Market Pulp Felt Design for Water Removal. 85<sup>th</sup> Annual Meeting, PAPTAC, Jan.28-29, 1999, A243-A250.

Nilsson, P. and Larsson, K.O. Paper Web Performance in the Nip. Pulp and Paper Mag. of Canada, December 20, 1968: 68 – 73.

Oliver, J.F. and Wiseman, N. Water Removal in Wet Pressing: The Effect of Felt Roughness. Transactions of the Technical Section, TR104-TR109, December 1978.

Orloff, D., Rislakki, M., Rudman, I. Impulse Drying of Board Grades: Status of Commercialization. IPST Technical Paper Series, #715, April, 1998, 8p.

Pikulik, I.I., McDonald, J.D., and Gilbert, D. Pressing of Market Pulp. 1996 Eng. Conf. Proc., 735-740.

Schiel, C. Optimizing the Nip Geometry of Transversal-Flow Presses. Pulp and Paper Mag. of Canada, March 7, 1969, 73-78.

Skelton, J. Foam-Assisted Dewatering - New Technology Emerges. Paper Technol. Ind. 28, no. 2: 431, 434-436 (March 1987).

Sprague, C.H. New Concepts in Wet Pressing. Final Report. March, 1986. Institute of Paper Chemistry.

Springer, A., Nabors, L.A., and Bhatya, O. The influence of fiber, sheet structural properties, and chemical additives on wet pressing. Tappi J., 221-228, April 1991.

Stone, J. E.; Scallan, A.M.; Aberson, G.M.A.; The Wall Density of Native Cellulose Fibres; Pulp and Ppr. Mag. Can. T263-T268 (May 1966)

Strom, G.; Kunnas, A. Effect of Cationic Polymers on the Water Retention Value of Various Pulps. Nord. Pulp Pap. Res. J. 6, no. 1: 12-19 (April 1991).

Swerin, A.; Lindstrom, T.; Odberg, L.; Deswelling of Hardwood Kraft Pulp Fibers by Cationic Polymers: Effect on Wet-Pressing and Sheet Properties; Nord. Pulp Pap. Res. J. 5, no. 4: 188-196 (Dec. 1990).

Sze, D. Measuring wet press felt pressure uniformity and its effects on sheet solids. Tappi J., April 1986, 120-124.

Szikla, Z. Role of felt in wet pressing. Paperi ja Puu, 73 (1991):2, 160-168.

Vomhoff, H., Norman, B. Model Experiments on Wet-Pressing-the Influence of Felt-Surface Structure; Nordic Pulp & Paper Research Journal 1, no. 12: 54-60 (March 1997).

Wahlstrom, P. B. OUR PRESENT UNDERSTANDING OF THE FUNDAMENTALS OF PRESSING. Pulp Paper Mag. Can. 70, no. 19: 76-96 [T349-69] (Oct. 3, 1969).

Wrist, P.E. The Present State of Our Knowledge of the Fundamentals of Wet Pressing. Pulp and Paper Mag. of Canada, T284-T296, July 1964.

## APPENDIX 1 - Water Permeability, Average Pore Size, and Capillary Pressure

In conventional wet pressing, the applied pressure drives water from the sheet by compression. Sheet compression results in a less compressible mat and a decrease in average pore size. Thus, pore diameter in the compressed state is a factor controlling dewatering. Average pore diameter can be evaluated based on an analogy between laminar flow in a channel and Darcian flow in the porous medium (Dullien 1986, Hoyland and Field, 1976).

The expression for driving pressure in a circular channel is:

$$\Delta P = U \mu L / (2 D_h^2/64).$$

The Darcy equation for driving pressure is:

$$\Delta P = U \mu L / K.$$

Setting the two equations for  $\Delta P$  equal to one another yields an expression which relates permeability to hydraulic diameter of the pores

$$K = D_h^2/32.$$

An expression, derived from by alternative means, that links permeability and pore size for a bundle of parallel capillaries is essentially the same

$$K = \varepsilon D_h^2/32,$$

where  $\varepsilon$  is porosity indicating volume of the mat available for water flow. This equation can be also obtained from the using the channel flow/Darcy analogy if one takes into account that flowing water is affected by the fraction of pressure differential equal to  $\Delta P$   $\varepsilon$ .

Capillary pressures, calculated as a function of pore diameter and contact angles of zero and sixty degrees are plotted in Figure A1.1. The intervals of pore sizes for inter-fiber water and intra-fiber water are also shown. Inter-fiber water is contained in the pores greater than 1 micron diameter. Intra-fiber water is contained in the pores having diameters below about 0.05 microns. The graph shows that in order to express free water, the driving pressure should be within the range 2-40 psi. Removal of the intra-fiber water requires driving pressures in the range of 300 to 40000 psi. Removal of the water from the pores less than 25 Å which would produce solids more than 70% requires pressure more than 8500 psi.

Bliesner did some earlier work on determining average pore size. The method used for that work was to measure "breakthrough pressure". This work produced pore size distribution curves and permeability measurements. From these results hydraulic diameter was calculated. A comparison of Bliesner's results and the results obtained from previous IPST work is shown in Figure A1.2. The trends for the two sets of data are similar.



IPST accumulated a considerable data base of water permeability measurements during various projects over the past 4-5 years, a sample of these tests are tabulated in Table A1.1. The majority of these test were performed at compressive pressure of 0.02 to 2.0 MPa. From the available water permeability data three data sets were selected, the sets represented low, average, and high water permeability. Permeability as a function of compressive pressure was then determined using a power function regression

$$K \times 10^{12} [\text{m}^2] = a P^b,$$

where compressive pressure is taken in psi. Using the formula

$$K = D_h^2/32,$$

pore diameter as a function of compressive pressure for the sheets having low, average and high water permeability were calculated and plotted in Figure A1.1. Note that the plotted compressive pressures (70 MPa) are well above those used to obtain regression formulae which may result in some inaccuracies.

The results in Table A1.1 and Figure A1.1 suggest that at high compressive pressures, permeabilities for any sheet converges to approximately the same number which is about  $(20-50) \times 10^{-20} \text{ m}^2$ . The average pore diameter at such permeabilities is about 25-40 Å, which is the upper bound of the pores in the fiber wall which contain hydrogen-bonded water.

Using the permeability data, a regression function was determined to relate the values of apparent density to sheet solids. At high compressive pressures, apparent density of the sheet

$$c = BW/L$$

should approach the wood fiber density equaled to about 1.55 g/cc. As the experimental data were obtained within the range of 0.2 to 2.0 MPa, extrapolation to the pressures up to 7-70 MPa may result in inaccuracies. In some cases the values of apparent density exceeded their theoretical maximum.

Plots of apparent density vs. compressive pressure can be translated into the functions of compressive pressure vs. solids in the nip which are frequently used in calculating water removal for wet pressing. An equation that links the apparent density and solids,  $s$ , can be obtained for a saturated sheet and has the form

$$s = c / (c + \rho_w - c \rho_f)$$

where  $\rho_w = 1\text{g/cc}$  and  $\rho_f = 1.55 \text{ g/cc}$ . Which leads to the following formula linking apparent density and solids

$$s = c / (0.355 c + 1).$$

Graphs reflecting effect of static compressive pressure on the average pore size and outgoing solids for cases of different basis weights and specific surfaces (Data from Table 1) are plotted in Figure A1.2. Convergence of the average pore size is again confirmed. Even using static compression outgoing solids of about 70% can be obtained only at pressures in excess of 7 MPa. Thus, current machine solids levels of about 45% are quite understandable.

The results plotted in Figure A1.1 can be used to determine the required pressure differential to displace water from the sheet when the sheet is also subjected to a compressive load. The results can also be used to determine the suitability of sheet with a given permeability for displacement dewatering.

For the purposes of illustration, let's assume that in order to bring the sheet to a saturated state, the sheet to be subjected to displacement dewatering is precompressed by the compressive pressure of 0.7 MPa. The range of capillary resistance pressure at this compressive pressure is given in Table A1.2.

Table A1.1

Parameter	Low Permeability	Average Permeability	High Permeability
Oven-Dry Basis Weight, gsm	203.7	150.4	177.4
Coefficient a in regression $K \cdot 10^{12} = a \cdot (P^b)$	0.0052196	0.79691	55.005
Coefficient b in regression $K \cdot 10^{12} = a \cdot (P^b)$	-1.1737	-1.9204	-2.5965
Measured specific surface, $m^2/g$	62.97	9.9	2.156
Measured specific volume, $g/cc$	0.73	1.03	1.405
Permeability $\cdot 10^{15}$ , $m^2$ @10 psi	0.35	9.572	1329.8
Average pore diameter, A, @ 10 psi	1060	5538	66799
Permeability $\cdot 10^{15}$ , $m^2$ @3000 psi	0.000433	0.000167	0.000515
Average pore diameter, A, @ 3000 psi	37.25	23.16	40.63

Table A1.2

Permeability	Low Permeability	Average Permeability	High Permeability
Capillary resistance pressure at compressive pressure of 100 psi	800 - 1600	340 - 680	64 - 128

Figure A1.1. Capillary Pressure vs. Average Pore Diameter. Average Pore Diameter vs. Compressive Pressure from Water Permeability Measurements

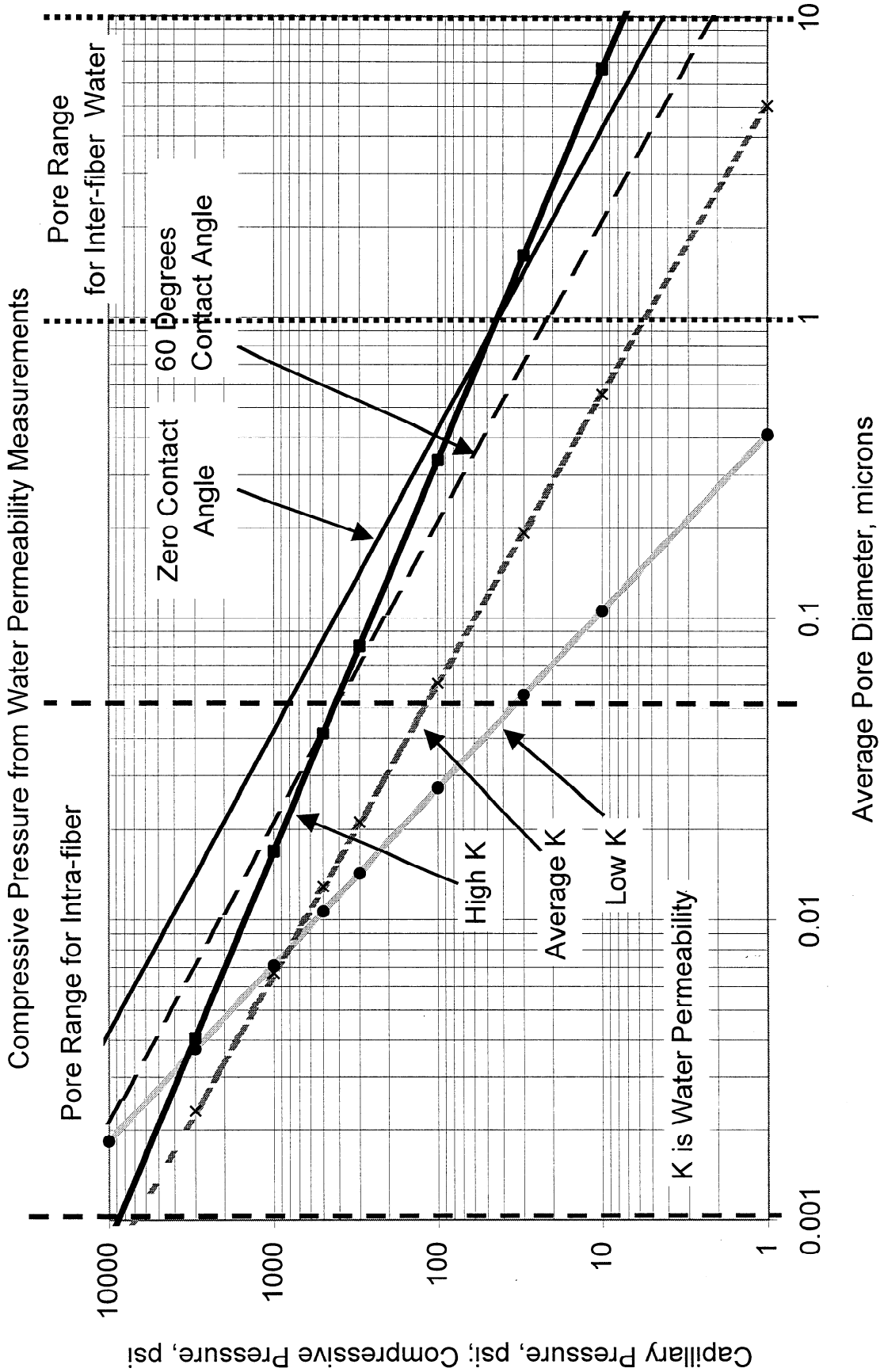
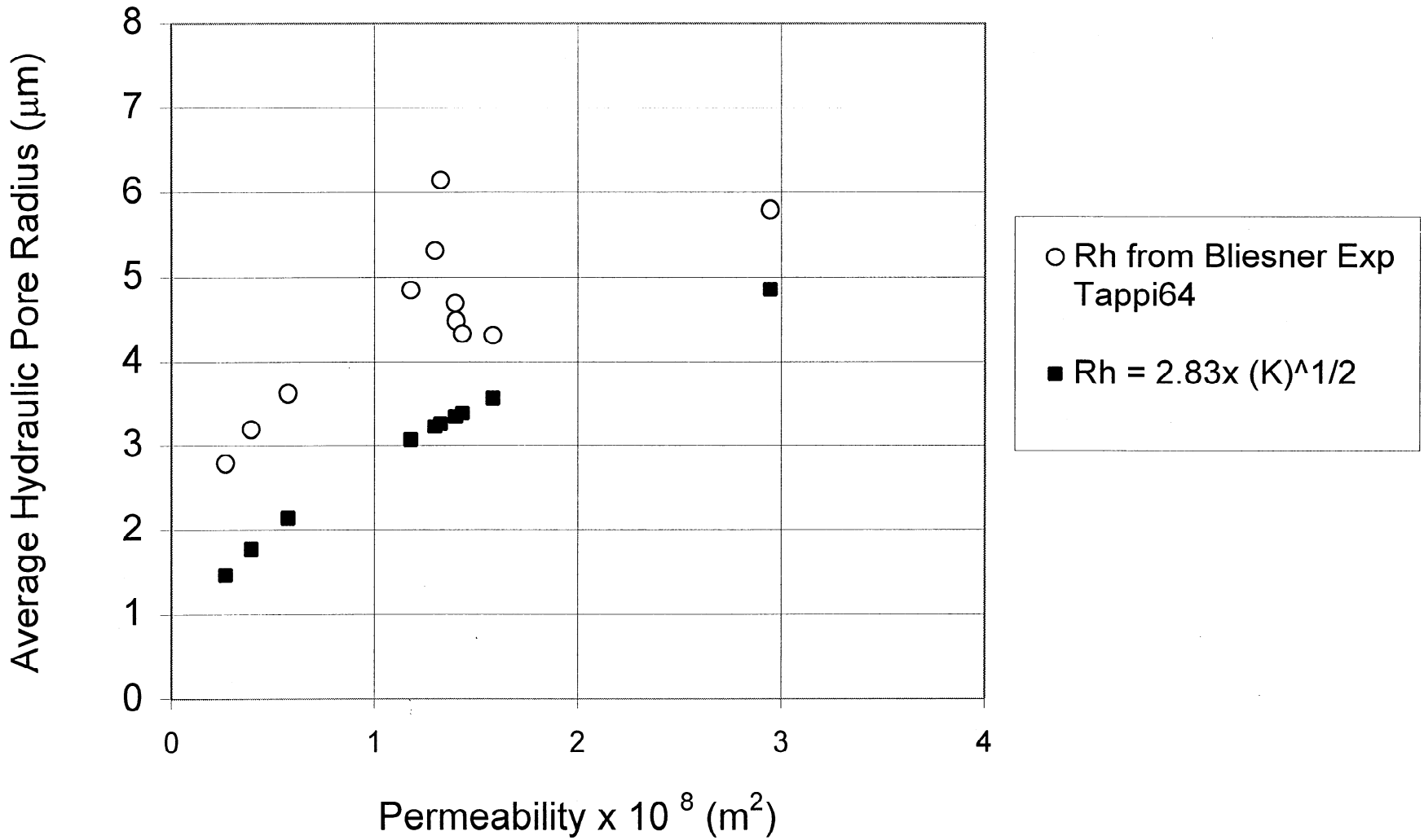


Figure A1.2. Average Hydraulic Pore Radius vs. Permeability



## APPENDIX 2. Displacement Measurement Results.

The displacement measurement system used eddy current sensors and perforated copper target disks. These disks were either embedded in the sheet or placed at the top and bottom surfaces of the sheet. This is the same approach as used by Burns et al. 1990, Burton and Sprague 1987. The displacement measurement system was used between April and June 1997 for an investigation of sheet compression and expansion in the nip during conventional pressing and impulse drying. A felt water receiver was used in all cases. A schematic of the experimental setup is shown in Figure A2.1.

Typical results of displacement measurements on the MTS press at room and elevated temperatures of the platen for extended nip (2<sup>nd</sup> set of experiments) are plotted in Figure A2.2 – A2.5. Analysis of the pressure and compression rate curves makes it possible to single out 4 intervals within the nip. First three intervals characterize compressive phase of the nip, while the last characterizes expansion phase of the nip.

### Interval 1: From the entrance of the nip to the point at which a rapid decrease in compression rate occurs

During this period of the nip, the compression rate in flow-controlled nip is usually very high, because sheet is easy compressible. Part of the applied pressure is balanced by fiber network, while the rest of applied pressure is balanced by air which is contained in the pores. No water or a negligible amount of water is removed from the sheet and, thus, the hydraulic component of total pressure is close to zero.

At a known ingoing sheet weight and solids content, the sheet thickness at zero porosity can be evaluated by using the formula

$$L=1/A (m_f/\rho_f + m_w/\rho_w)$$

where

$m_w$  and  $m_f$  are mass of water and fiber in the sheet respectively;  $\rho_w$  and  $\rho_f$  are the densities of water and fiber respectively.

By comparing the calculated and measured sheet thickness it can be established that air is present in the sheet at the end of this interval.

Interval 2: From the point at which a rapid decrease in compression rate occurs to the point at which slows to slightly greater than zero. At a point, when the pressure inside the sheet becomes higher than capillary pressure resistance, the water starts to flow out of the sheet. This point corresponds to a quasi-inflection point in compression rate curve. It is thought that during this period, water in the inter-fiber space is pushed from the sheet.

Interval 3: from quasi-inflection point of compression rate curve to zero compression rate (or the minimum of sheet thickness in the nip). In this interval compression rate is very low which indicates that primarily intra-fiber water is removed during this period. As

sheet compressibility is low at high pressures, water removal in this interval is marginal. An increase in the duration of this interval will not produce a noticeable increase in water removal.

Interval 4: from minimum of the sheet thickness to exit of the nip (pressure is about zero). In this interval the spring force of the compressed sheet exceeds applied pressure and sheet recovers. The compression rate becomes negative. Reducing the duration of this period should reduce rewet.

Sheet recovery continues after the nip exit. If the sheet is not separated from the felt, post-nip rewet may occur. No thickness measurements of completely recovered sheet were conducted to determine total springback.

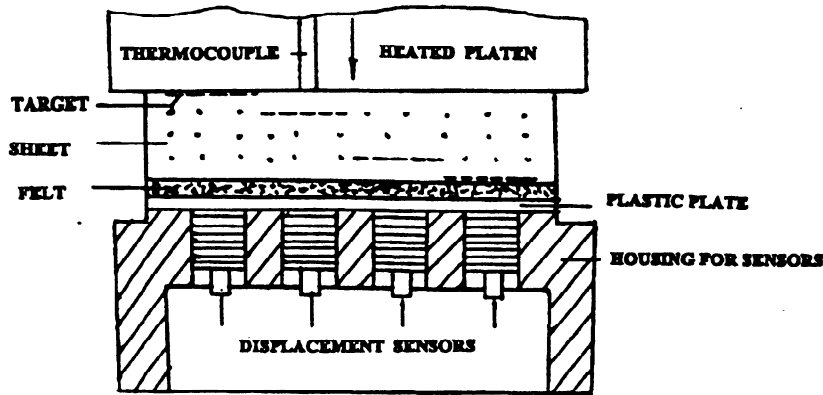


Figure A2.1 Displacement Measurement Device



Figure A2.2 Displacement Results for MTS Pressing at Room Temperature

Compression Rate =  $-dL/dt$ , Strain =  $(L_0 - L) / L_0$

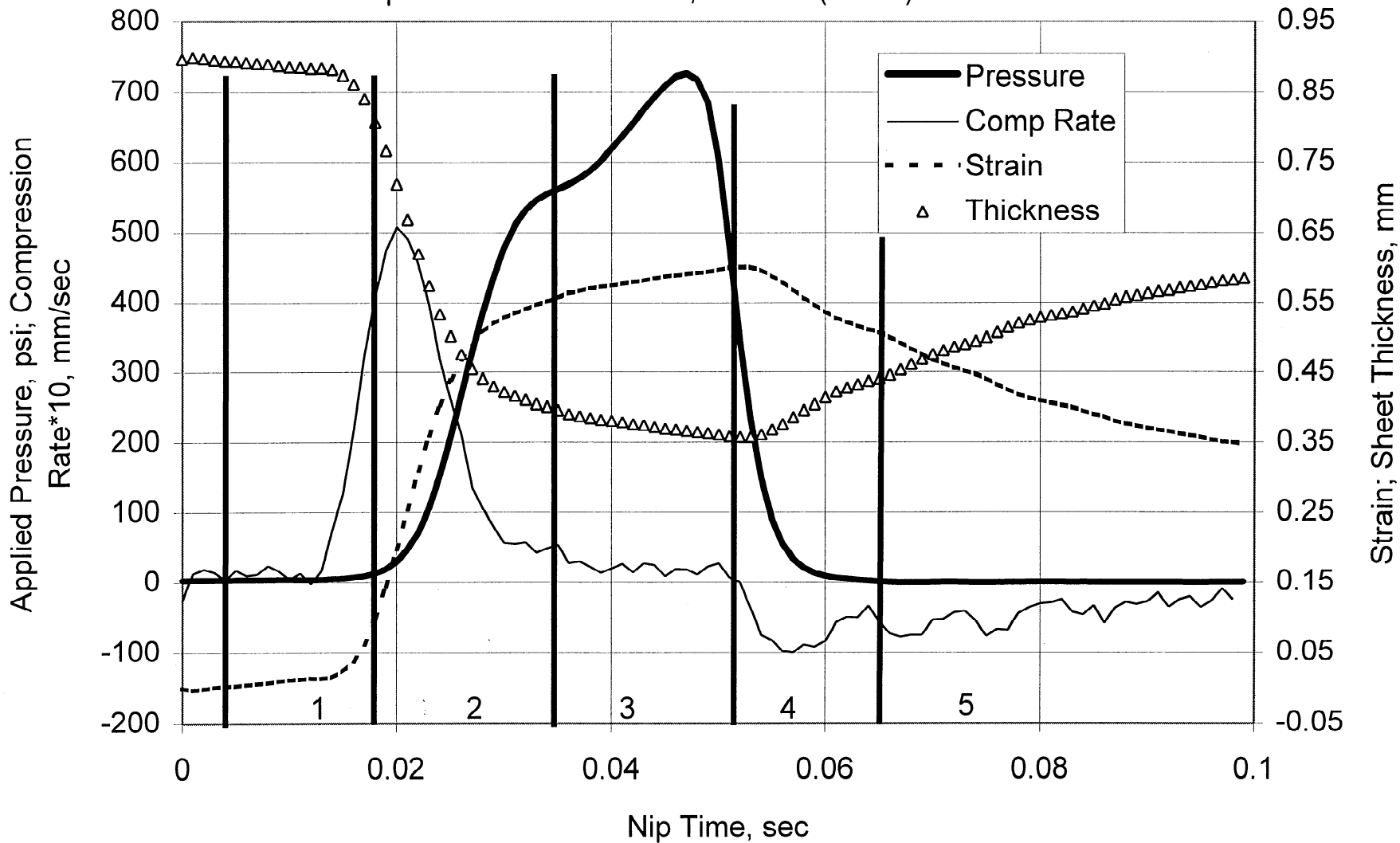


Figure A2.3. Displacement Results for MTS Pressing at Platen Temperature of 100 °C

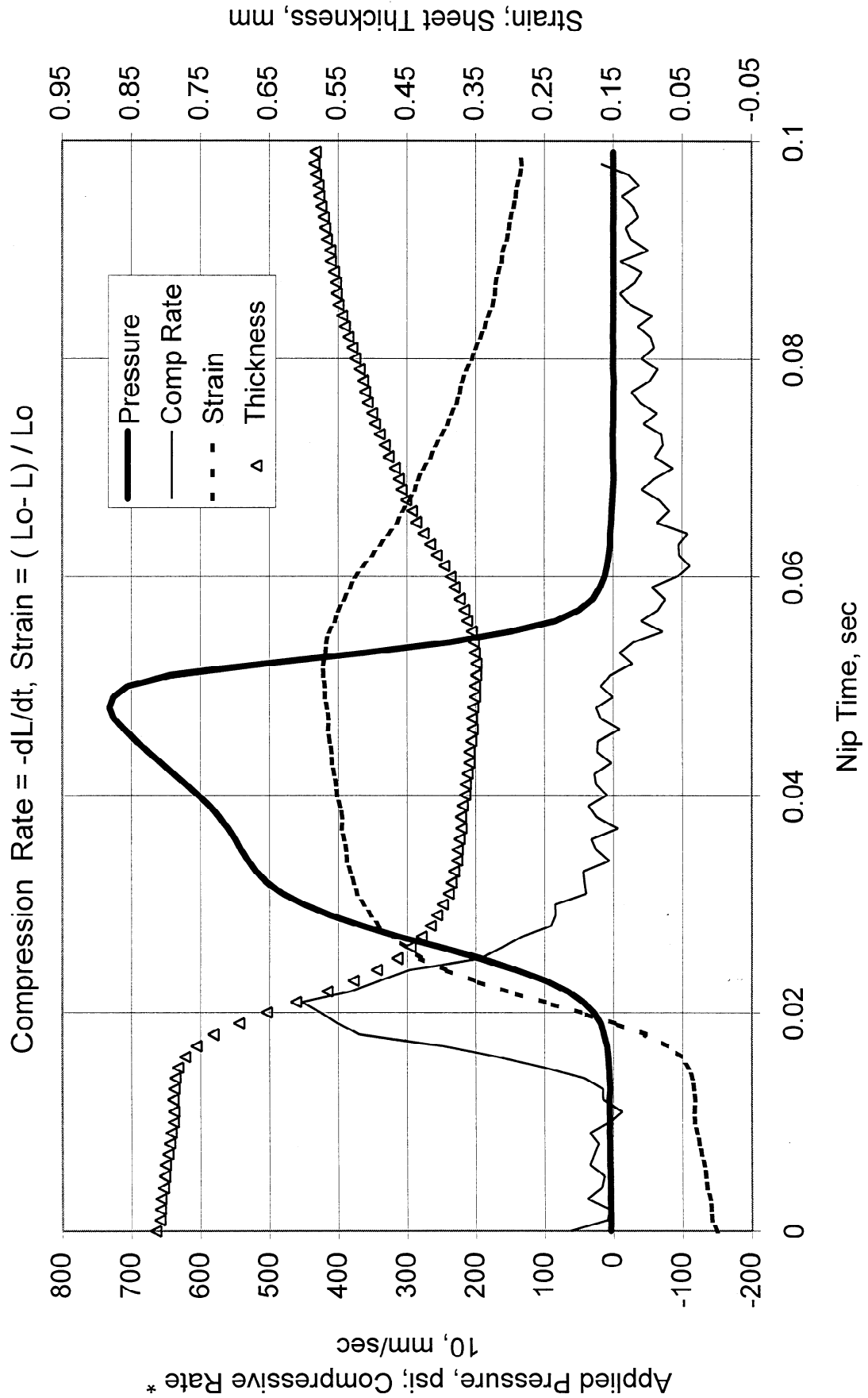


Figure A2.4. Displacement Results for MTS Pressing at Platen Temperature - 200 °C

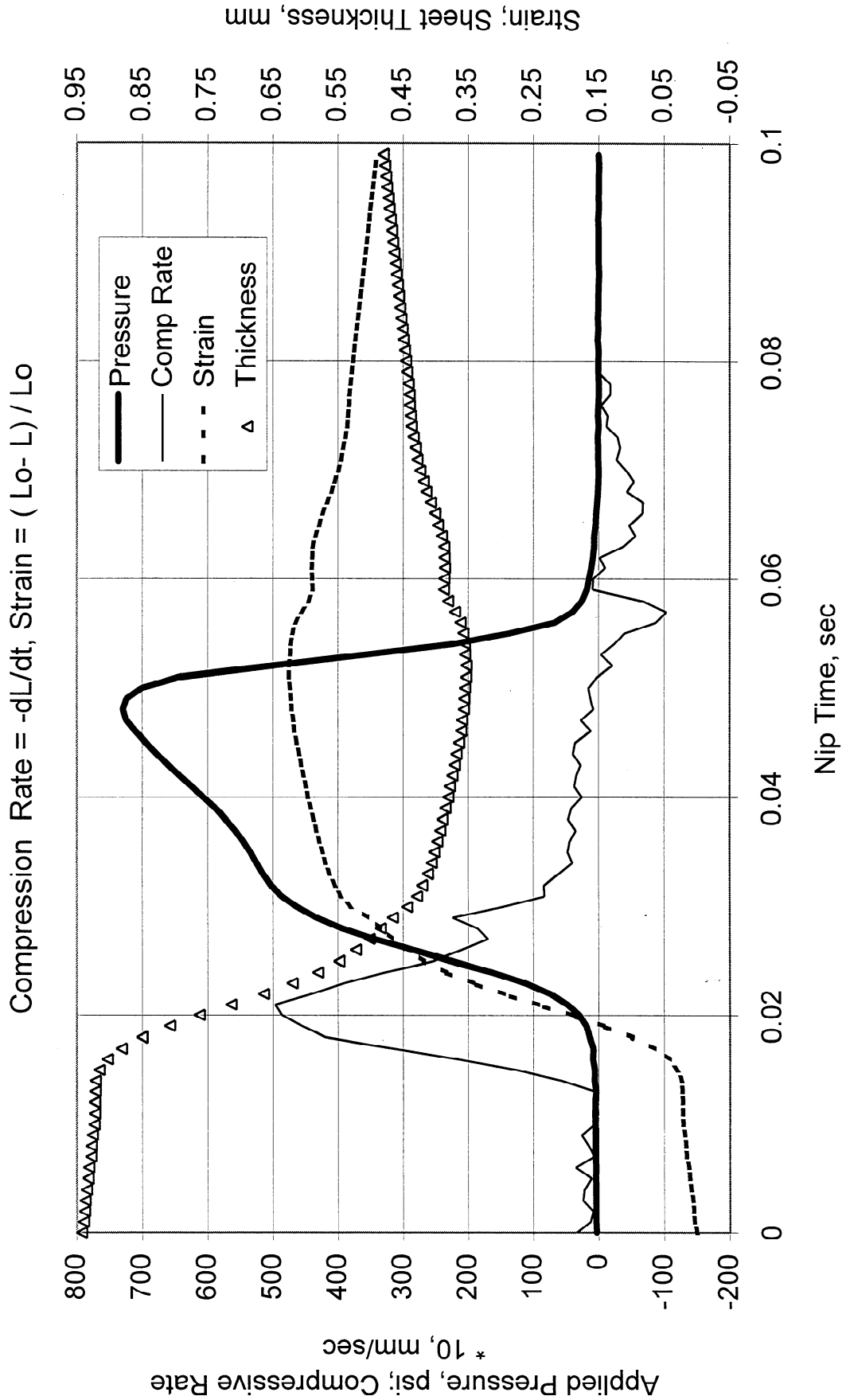
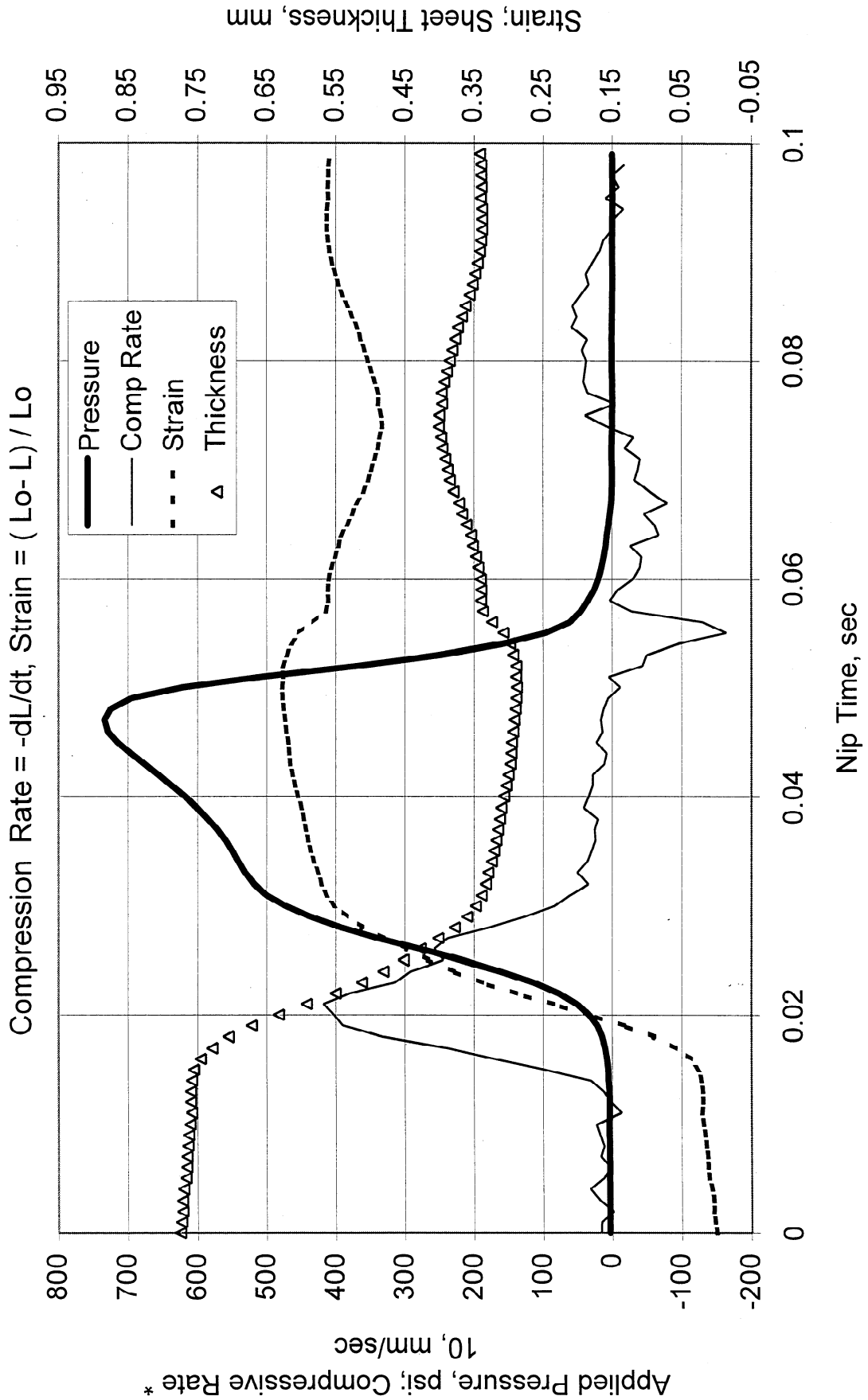


Figure A2.5. Displacement Results for MTS Pressing at Platen Temperature of 300 °C





REMOVING LIMITATIONS ON DWELL TIME OF WET-PRESSES,  
IMPULSE DRYERS, AND DISPLACEMENT DEWATERING

STATUS REPORT  
FOR  
PROJECT F040

Paul Phelan (PI)  
Isaak Rudman  
Marcos Abazeri  
Edward Lindahl

March 8 – 9, 2000

Institute of Paper Science and Technology  
500 10th Street, N.W.  
Atlanta, Georgia 30318



**DUES-FUNDED PROJECT SUMMARY**

<b>Project Title:</b>	<b>REMOVING LIMITATIONS ON DWELL TIME OF WET-PRESSES, IMPULSE DRYERS, AND DISPLACEMENT DEWATERING TECHNOLOGY</b>
<b>Project Code:</b>	<b>LONG DWELL</b>
<b>Project Number:</b>	<b>F040</b>
<b>PAC:</b>	<b>PAPERMAKING</b>
<b>Project Staff</b>	
<b>Principal Investigator:</b>	<b>P. Phelan</b>
<b>Research Support Staff:</b>	<b>I. Rudman, M. Abazeri, E. Lindahl</b>
<b>PAC Subcommittee</b>	<b>C. Kramer, F. Palumbo, N. Rudd</b>
<b>FY 99-00 Budget:</b>	<b>\$143,052</b>
<b>Allocated as Matching Funds:</b>	<b>None</b>
<b>Time Allocation:</b>	
<b>Principal Investigator:</b>	<b>50%</b>
<b>Research Support Staff:</b>	<b>Technician (50%)</b>
<b>Supporting Research:</b>	
<b>Special Students:</b>	<b>None</b>
<b>External (Where Matching Is Used):</b>	<b>None</b>

**RESEARCH LINE/ROADMAP:** Line #7 - Increase paper machine productivity by 30% over 1997 levels via focus on breakthrough forming, de-watering, and drying concepts.

**PROJECT OBJECTIVE:** The objective of this work is to improve productivity by increasing water removal while maintaining and/or improving bulk and other sheet properties. This will be achieved by increasing the effective dwell time of wet presses, impulse dryers, and displacement de-watering devices (FY 99-00 focus is on wet pressing). Technical approaches to implementing the technology may be evaluated.

**PROJECT BACKGROUND:** This is a new project for FY 99-00. The P.I. was changed from D. Orloff to P. Phelan in November, 1999.

**MILESTONES:** The following tasks were presented at the Fall '99 PAC meeting.

1. Survey the literature on shoe press technology with an emphasis on current and projected use in the manufacture of grades other than linerboard and corrugating medium. (Completed by first quarter, FY 99-00)
2. Determine how existing shoe press technology can be best utilized in the manufacture of bulk sensitive printing and writing grades. (Rejected by the PAC)



3. Determine if there is justification for developing a "Super-Long Nip High-Load" press. (Completed by fourth quarter, FY 99-00) **Note:** The PAC suggested that this task be the focus for fiscal year 99-00.
4. Identify and resolve the technical barriers to the development of a SLN-HL press. (Completed by fourth quarter, FY 00-01)
5. Design, build and evaluate a prototype with respect to technical and economic factors important to commercialization. (Completed by fourth quarter, FY 01-02)

**DELIVERABLES:** The PAC agreed on experiments to justify the use of a SLN-HL press for a copy paper grade. Initial experiments will look at the impact of a third position SLN-HL press on water removal and sheet property development. The experiments should be completed and reported to the PAC at the Spring '00 meeting with an economic analysis of the impact. The PAC will recommend continuation or termination of the project based on the results.

**STATUS OF GOALS FOR FY 99-00:** The goal for the Spring, '00 PAC meeting is to complete initial experiments justifying a SLN-HL third press for copy paper at two refining levels and report the results. Experiments were completed in January, 2000.

Proposed goals for completion by the end of the fiscal year are to conduct the same experiment with the SLN-HL press in the first press position and write a member report on all of the results obtained in 1999-00. Production of Formette sheets are to begin in February, 2000.

**SCHEDULE:**

Task Descriptions (example)	1999 July - Sept	1999 Oct - Dec	2000 Jan - Mar	2000 Apr-Jun	2000 -01	2001 -02
1. Literature Survey	-----X					
3a. Justification at Third Press		-----	-----X			
3b. Justification at First Press(proposed)			-----	-----X		
4. Identify & Resolve Technical Barriers					-----X	
5. Build & Evaluate Prototype						-----X
6. Write yearly report (proposed)				-----X		

**SUMMARY OF RESULTS:** Experiments were completed using a copy paper furnish at two levels of freeness and 40% ingoing solids. Five different cases of peak pressure and impulse, for the same basic shoe press profile, were tested for each freeness level. The following results were obtained.

- The 400 ml CSF furnish was predominantly flow-controlled.
- The 500 ml CSF furnish was predominantly pressure-controlled.
- Density is a linear function of water removal (outgoing solids).
- Tensile apparently increases with increasing density, but the change is slight.
- Brightness and opacity are apparently unaffected, but there is a large amount of scatter in the data.
- There is no apparent trend for Sheffield roughness.

#### **SUMMARY OF KEY CONCLUSIONS:**

- As a third press a SLN-HL press can remove more water at higher impulses than a “standard” shoe press. There is a corresponding increase in density, but the increase does not appear to affect optical properties.
- Estimated payback periods for a runnability-limited machine range from 4 to 46 years.
- Estimated payback periods for a dryer-limited machine range from 0.5 to 6.2 years.
- There may be more potential for increased water removal, while maintaining bulk, if the SLN-HL press was in the first position, before the sheet is densified by roll presses. Additionally, a SLN-HL press, potentially, may be used to reduce the number of press nips, reducing rewet.

#### **DISCUSSION:**

##### **Experimental Plan and Procedures**

**Furnish:** The furnishes made for this trial simulate copy paper and were made using the Formette Dynamic at 900 m/min. The pulp was a blend of 75% hardwood and 25% softwood. Each pulp was refined to two freeness levels, 400 and 500 ml CSF and then blended. Table 1 lists the additives used.

**Plan:** The Formette sheets were cut into 5-inch diameter test samples for pressing. Table 2 shows the MTS conditions used. After pressing the samples were dried under constraint and tested as shown in Table 3.

Figures 1 and 2 show examples of the type of generic shoe press pulses that were used. All of the pulses had the same relative shape, except that the depressurization part of the pulse was the same for all cases. The exact shape was determined when the MTS is programmed. Cases 1, 2 and 3 had the same peak pressure, but the dwell time was varied to correspond to the different shoe lengths. Cases 1, 4 and 5 had the same impulse, but different dwell times and peak pressures.

## **Results**

The outgoing solids levels, for each furnish, are shown in Figures 3 and 4. For the 400 ml CSF furnish, water removal is flow-controlled, as shown by the increase in solids with increasing impulse but with little change with increasing pressure. However, the 500 ml CSF furnish is predominantly pressure-controlled with a slight increase in solids with increasing impulse and a greater increase with increasing pressure.

Figures 5 and 6 further indicate that the 500 ml CSF furnish is pressure-controlled by showing a stronger influence of pressure than impulse on density. On the other hand, the density for the 400 ml CSF furnish has little dependence on pressure, but increases with increasing impulse. Both furnishes have a linear relationship between density and outgoing solids as shown in Figure 7.

Most strength properties increase with increasing density. However, the paper used in this experiment had low overall strength for reasons unknown at this time. Figure 8 shows that the geometric mean tensile index for both furnishes only has a slight increase with increasing density. Also plotted, for comparison, are the results of a commercially available copy paper tested at the same time. The MIT fold data were so low that the results are meaningless, most counts were less than 10 and the highest was 14. None of those data are in this report.

In Figure 9 the Gurley porosity data for the 500 ml CSF furnish increases with increasing density and are relatively low indicating an open furnish. For the 400 ml CSF furnish the data are more scattered and have no correlation with density. Data for Sheffield roughness, ISO brightness, and opacity do not show any significant trends or have large scatter. All of the data are summarized in Table 4.

## **Conclusions**

### **Scientific**

Operating as a third press, a Super-Long Nip High-Load press must operate at high pressures and impulses (cases 2 or 3) to increase water removal. For a flow-controlled furnish this will result in a substantial increase in sheet density, while for a pressure-controlled furnish the density increase is minimal. Data from this experiment are inconclusive about the detrimental effect of increased density on opacity, but there are indications that the change is insignificant. Therefore, the use of a Super-Long Nip High-Load press would result in a net benefit based on increased productivity.

Squeezing more water out of the web by using high pressures has economic benefits by increasing productivity. For a bulk sensitive furnish, it would be better to remove water without increasing density. Using a Super-Long Nip High-Load press as a first press may accomplish this with a long dwell, low pressure pulse (cases 4 and 5).

### **Economic**

Using the IPST Economic Model developed for project ROCIT, two economic scenarios were investigated. Both assumed a papermachine producing 75.2 gsm copy paper. The base case assumed a machine speed of 3300 fpm and a production of 842 FMT/day. For each of these scenarios, it was assumed that the press section could be rebuilt at three levels of capital investment, \$5M, \$10M, or \$15M. The differential increase in gross profits was calculated for each improvement in capabilities. The estimated capital cost of rebuilding the press section was divided by the differential profit to obtain an estimated payback (in years).

The first scenario was for a runnability-limited machine with 3.0% downtime due to sheet breaks. Higher outgoing solids from the press section would reduce the number of breaks resulting in higher overall productivity. Table 5 lists the estimated payback periods calculated.

The second scenario was for a dryer-limited machine with press section outgoing solids of 42.0%. Using the rule-of-thumb that for a dryer limited machine, each percentage point of increased solids out of the press section results in a 4% increase in machine speed, payback periods were calculated for up to 4-percentage points of increased dryness. The results are in Table 6.

### **Suggested Future Work**

The potential for removing water while maintaining bulk by using a Super-Long Nip High-Load press as a first press should be investigated by repeating this experiment with a lower ingoing solids level and no prepressing. Without the prepressing to densify the sheet, a low pressure SLN-HL press could gently squeeze out water while maintaining bulk. To maximize water removal, it is suggested that the experiment use double felted pressing with a grooved platen on the top and bottom.

Another potential benefit of using a Super-Long Nip High-Load press would be to eliminating press nips. Each nip has the potential to introduce rewet as the web exits the nip. Eliminating nips has the potential of increasing the final outgoing solids from the press section, even with the same total impulse. Using a Super-Long Nip High-Load press with an optimized profile may reduce the press section to a single nip with resulting capital and space savings. A proposed experiment would compare two nips to a single long nip.

**Figures**

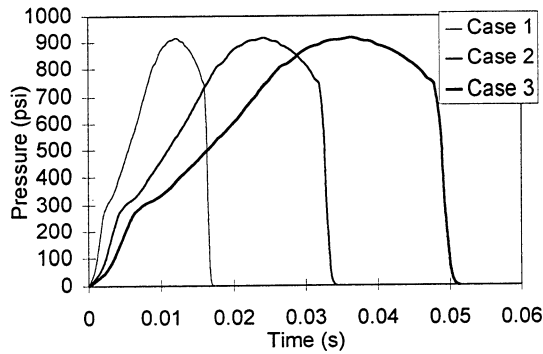


Figure 1. Pulses with same peak pressure.

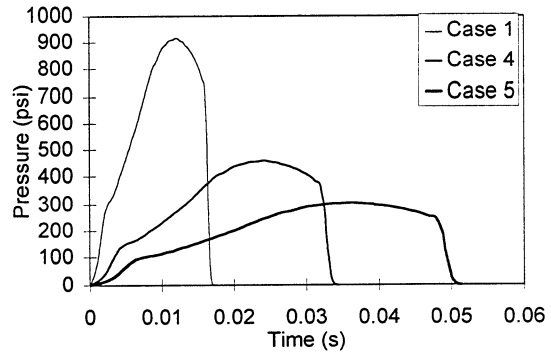


Figure 2. Pulses with same impulse.

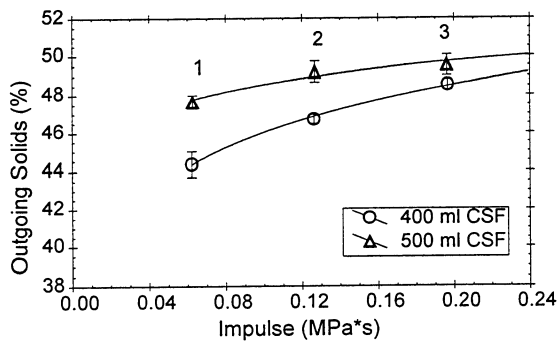


Figure 3. Outgoing solids for cases 1, 2, and 3.

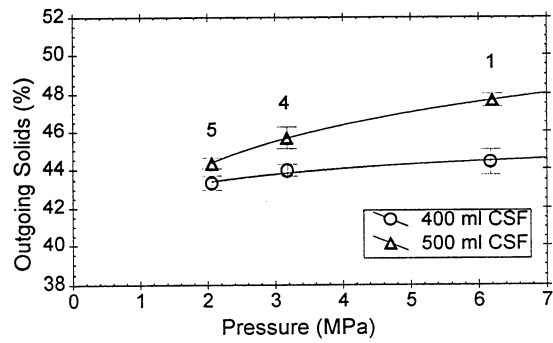


Figure 4. Outgoing solids for cases 1, 4, and 5.

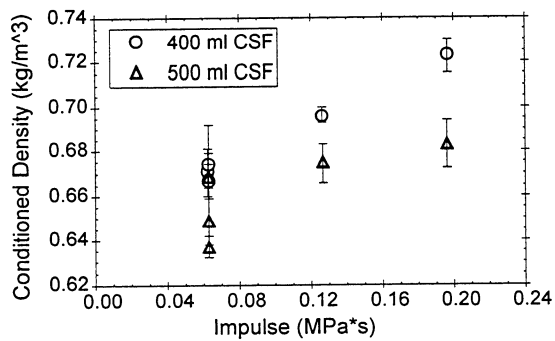


Figure 5. Density versus impulse for all cases.

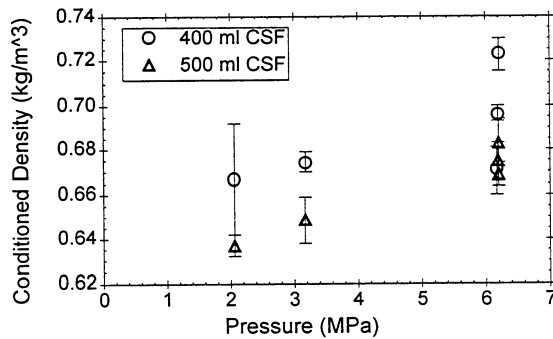


Figure 6. Density versus peak pressure for all cases.

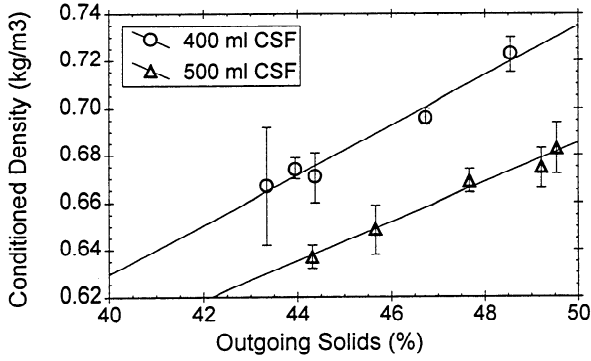


Figure 7. Density versus outgoing solids for all cases.

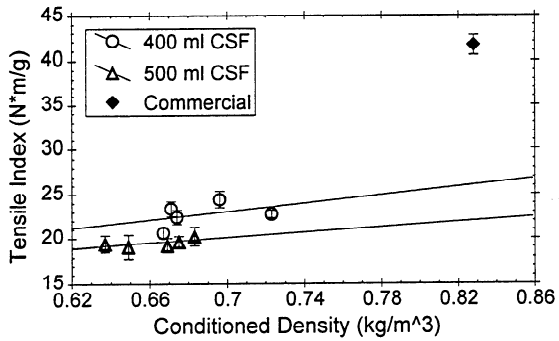


Figure 8. Geometric mean tensile index versus density for all cases.

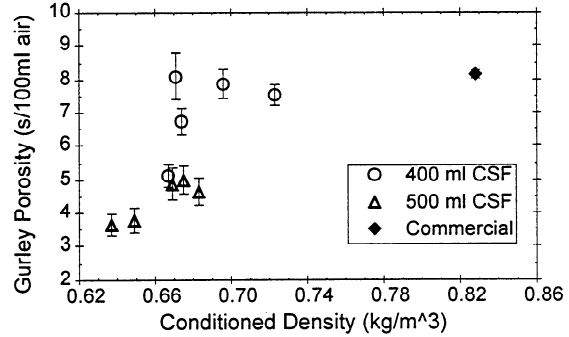


Figure 9. Gurley porosity versus density for all cases.

**Tables**

Table 1. Sheet additives.

Additive	Amount
PCC	15% of dry weight
Optical Brightener	2 lbs./ton
AKD	3 lbs./ton
Starch	12 lbs./ton
Retention Aid	2 lbs./ton

Table 2. MTS process conditions.

Condition	Value
Platen	Beloit J
Nip Length	10, 20, and 30 inches
Machine Speed	3000 ft/min (914 m/min)
Basis weight	67 gsm OD
Pulses	Single-felted wet pressing simulated shoe press
'Standard' Press load (Case 1)	4500 pli (788 kN/m)
Freeness	400 and 500 ml CSF
Ingoing solids	40%
Preheat	none
Felts	Fine Paper felt, preconditioned
Ingoing Felt Moisture	20%
Repeats per Case	30

Table 3. Testing.

Non-destructive Tests	Destructive Tests
Gurley Porosity (T460)	MD and CD Tensile, 4-inch span (T494) MD and CD MIT Fold (T511) OD weight (basis weight, bulk)
Opacity (T519)	
ISO Brightness (T534)	
Sheffield Roughness (T538)	

Table 4. Average values for physical properties.

Case	1	2	3	4	5	1	2	3	4	5	Com.
Freeness (ml)	400	400	400	400	400	500	500	500	500	500	-
Dwell Time (ms)	17	35	52	33	49	17	35	52	33	49	-
Peak Pressure (MPa)	6.17	6.19	6.21	3.18	2.06	6.20	6.19	6.20	3.17	2.05	-
Impulse (MPa*s)	0.062	0.126	0.197	0.063	0.063	0.063	0.127	0.196	0.063	0.063	-
Basis Weight (gsm)	66.74	66.21	66.69	67.05	66.85	68.41	68.02	65.90	67.35	68.34	72.71
Ingoing Solids (%)	39.02	39.29	39.47	39.45	39.67	40.13	40.49	40.69	40.34	40.39	-
Outgoing Solids (%)	44.37	46.73	48.55	43.95	43.34	47.67	49.21	49.54	45.66	44.31	-
Soft Platen Caliper ( $\mu\text{m}$ )	105.7	100.9	97.8	105.5	106.8	108.3	106.5	102.3	110.3	114.0	94.1
Cond. Density ( $\text{kg}/\text{m}^3$ )	0.671	0.696	0.723	0.674	0.667	0.669	0.675	0.683	0.649	0.637	0.828
Cond. Bulk ( $\text{m}^3/\text{kg}$ )	1.493	1.436	1.385	1.483	1.504	1.495	1.483	1.465	1.543	1.570	1.208
Gurley Por. (s/100ml)	8.09	7.87	7.53	6.73	5.13	4.88	5.00	4.65	3.78	3.64	8.16
Top Sheffield (ml/min)	1778	1763	1692	1780	1519	1598	1648	1647	1750	1786	1492
Bot. Sheffield (ml/min)	2190	2151	2078	2077	1732	1959	1958	1928	1904	1912	1347
MD Tensile Index ( $\text{N}^*\text{m}/\text{g}$ )	34.83	36.48	34.93	32.05	31.14	29.37	29.18	30.00	28.71	30.58	64.43
CD Tensile Index ( $\text{N}^*\text{m}/\text{g}$ )	15.69	16.38	14.83	15.70	13.68	12.64	13.21	13.65	12.76	12.37	26.88
GM Tensile Index ( $\text{N}^*\text{m}/\text{g}$ )	23.38	24.44	22.76	22.43	20.64	19.27	19.63	20.24	19.14	19.45	41.62
ISO Brightness	87.72	87.92	88.47	88.27	88.59	88.66	88.51	88.10	88.63	88.53	84.15
Opacity	88.86	88.23	88.69	89.07	89.36	88.96	88.84	88.15	88.54	88.70	89.11

Table 5. Estimated payback periods (years) for a runnability-limited machine.

Breaks (%)	Capital Costs		
	5,000 k\$	10,000 k\$	15,000 k\$
3.0	-	-	-
2.5	15.4	30.9	46.3
2.0	7.7	15.4	23.2
1.5	5.2	10.3	15.5
1.0	3.9	7.7	11.6

Table 6. Estimated payback periods (years) for a dryer-limited machine.

Solids Increase (% Points)	Capital Costs		
	5,000 k\$	10,000 k\$	15,000 k\$
0	-	-	-
1	2.1	4.1	6.2
2	1.0	2.1	3.1
3	0.7	1.4	2.1
4	0.5	1.0	1.6





EXTENDING HIGH INTENSITY WATER REMOVAL PRINCIPLES  
INTO THE DRYER SECTIONS

STATUS REPORT  
FOR  
PROJECT F041

Fred Ahrens (PI)  
Paul Phelan  
Isaak Rudman  
Edward Lindahl

March 8 – 9, 2000

Institute of Paper Science and Technology  
500 10th Street, N.W.  
Atlanta, Georgia 30318



**DUES-FUNDED PROJECT SUMMARY**

**Project Title:** **Extending High Intensity Water Removal Principles into the Dryer Section**

**Project Number:** **F041**

**PAC:** **PAPERMAKING**

**Project Staff**

**Principal Investigator:** **F. Ahrens**

**Co-Investigators:** **P. Phelan, I. Rudman**

**Research Support Staff:** **Lindahl**

**PAC Subcommittee** **Babinsky, Kaufman, Watson**

**FY 99-00 Budget:** **\$86,000**

**Allocated as Matching Funds:** **0%**

**Time Allocation:**

**Principal Investigator:** **15%**

**Co-Investigators:** **25%**

**Research Support Staff:** **20%**

**Supporting Research:**

**Students:** **N. Alaimo (M.S.)**

**External (Where Matching Is Used):** **None**

**RESEARCH LINE/ROADMAP:** Line #7 - Increase paper machine productivity by 30% over '97 levels via **focus on breakthrough** forming, dewatering, and **drying concepts** [faster drying]

**PROJECT OBJECTIVE:** Demonstrate/verify a high intensity drying concept that provides the basis for a feasible, high productivity, capital/space/energy effective dryer system. Provide the data and understanding needed for development.

**PROJECT BACKGROUND:** New DFRC project in FY 99-00 (started July 1999)

**MILESTONES:**

- Identification of promising conditions and configurations for initial laboratory high intensity drying experiments [by Mar. 2000]
- Completion of high intensity drying experiments to demonstrate the drying rate potential and guide concept development [First phase by Mar. 2000]
- Development of promising concept(s) [ based on systematic application of fundamentals and analysis of experimental results] [review - Mar. 2000]
- Development of plan to refine the concept(s) [Q4, FY 99-00]

- Identification of equipment and clothing issues/requirements [Q4, FY 99-00]
- Completion of preliminary technical/economic assessment [Q4, FY 99-00]

**DELIVERABLES:**

- High intensity dryer concept(s) [Mar. 2000]
- Results of laboratory simulation and technical analysis of promising concept(s) [Q4, FY 99-00]
- Results of preliminary technical and economic analysis [Q4, FY 99-00]
- Definition of most promising concept and applications [FY 00-01]
- Data and understanding needed for scale-up [FY 00-01]
- Model of PAPRICAN's high intensity (impingement) drying concept [via proposed collaboration with PAPRICAN] {proposed new task}

**STATUS OF GOALS FOR FY 99-00:**

- Identify promising conditions and configurations for drying experiments: [completed Fall '99]
- Conduct high intensity drying experiments to demonstrate the drying rate potential and guide further concept development: [ First phase completed]
- Develop promising concept(s) based on systematic application of fundamentals and analysis of experimental results: [Progress review at March PAC meeting]
- Develop plan to refine the concept(s): [Spring 2000]
- Submit pre-proposal to Agenda 2020 Capital Effectiveness Program: [Nov.1999]
- Model of PAPRICAN's high intensity (impingement) dryer concept [via proposed collaboration with PAPRICAN]: [proposed new task - under development]

**SCHEDULE:**

Task	FY 99-00				FY 00-01			
	Q1	Q2	Q3	Q4	Q1	Q2	Q3	Q4
Define initial experiments	X	X						
Perform initial experiments		X	X					
Develop promising concept		X	X	X				
Plan for concept refinement				X				
Identify equipment/clothing issues			X	X				
Preliminary technical/economic evaluation				X				
Data for scale-up					X	X	X	X
Model of PAPRICAN concept				X	X			

**SUMMARY OF RESULTS:**

- Preliminary/simplified concept definition: Heat input via multiple long, moderate pressure nips, with interspersed vapor removal areas, on high temperature cylinders. The sheet would be restrained by a suitable fabric or felt.
- Initial MTS experiments demonstrated very large (heat input based) drying rates (1000's of kg/hr/sq m) for simulated copy paper and linerboard, over an applied pressure range of 10 to 1000 psi (applied in one or two 20 ms pulses), with surface temperatures of 149 to 233 °C, for initial solids levels of 50% and 70%.
- In response to an inquiry from PAPRICAN, a preliminary proposal for interaction with the PAPRICAN high intensity (impingement) drying effort (for printing grades) has been developed. Focus is on development and pilot machine verification of a computer model of the concept.

**SUMMARY OF KEY CONCLUSIONS:**

- According to the initial laboratory simulation results, it should be possible to accomplish (via multiple cycles of intense heat input and vapor removal on a high temperature cylinder) drying equivalent to that normally associated with several/numerous dryer cans and their open draws.
- A wide range of "shoe press" loadings and surface temperatures appear to be useful, offering the opportunity to identify a technically and economically feasible design.
- The vapor removal and sheet restraint strategies still need attention and development.

## DISCUSSION and ADDITIONAL DETAILS

### INTRODUCTION

The dryer sections prevalent for most grades of paper and board are based on use of contact heat transfer from numerous steam heated dryer cans and movement of large volumes of heated air for vapor removal. Dryer sections have undergone evolutionary changes in recent years [e.g., recent developments include the single-tier configuration and the incorporation of impingement units at selected stations in the dryer section], but are still limited to rather low overall drying rates, resulting in very long, expensive systems and only modest-to-good energy efficiency.

In view of the industry need for increased productivity, improved capital effectiveness, and reduced energy use, it is timely to seek to apply the principles and techniques associated with high-intensity heat transfer and water removal (including, but not limited to, adaptations of technology developed for impulse drying) to the challenging task of making beneficial step increases in drying rates for paper and board. In this project we intend to bring together available technical tools and new ideas for implementing high-intensity heat transfer and water removal principles, in order to overcome the heat and mass transfer impediments associated with current approaches to drying. The goal of the work is to develop a feasible high-intensity **drying** concept having the potential to make the paper machine dryer section at least an order of magnitude smaller, and significantly more energy efficient, than a conventional dryer section of the same capacity. Preliminary analysis and literature review in Fall 1999 indicates that it should be possible to achieve drying rates well in excess of those offered by the best currently available technologies (impingement drying and Condebelt), and points toward a particular implementation concept.

The benefits from successful commercial implementation of expected project results are as follows. For retrofit of existing machines, it will be possible to install significant extra capacity in a smaller space and at lower capital cost than for comparable conventional capacity. For new machines, greatly reduced space and capital cost, and increased energy efficiency, will be achieved; the very low drying rates and enormous dryer sections of today will be avoided (e.g., using 2 to 4 larger, high drying rate cylinders rather than 40 to 100 standard dryer cans).

### TECHNICAL BASIS FOR SUCCESS

Conventional paper drying involves low-pressure (<1 psi) thermal contact between the sheet and numerous steam-heated cylinders for heat input, with low intensity convective mass transfer (drying via evaporative cooling) in the draws between these cylinders (as well as on the lower cylinders, in single-tier dryer sections). Although paper drying is always a combined heat and mass transfer process, in the conventional dryer section there is only a relatively minor amount of evaporation while the sheet is covered by a fabric on the dryer cylinder. Therefore, conventional paper drying can be viewed as a cyclic process [cycles of heat transfer to the sheet (heat-up) followed by mass transfer from the sheet (accompanied by cooling of the sheet)]. The use of a hot air impingement unit over the fabric-covered sheet (on the dryer cylinder) would introduce a greater component of simultaneous heat and mass transfer to the drying process, via increasing the extent of vapor removal while the sheet is on the dryer cylinder. Additionally, the unit would increase the total rate of heat transfer to the sheet. Consideration of these principles (cyclic vs. simultaneous heat and mass transfer) should be useful in helping to establish and discuss a preliminary concept for a high intensity dryer.

Mention of a key concept relevant to development of a high intensity dryer is believed important, at this point. That is, there are two distinct modes by which mass transfer from a paper web can take place. The dominant one in nearly all current drying processes is diffusion of vapor within the web, coupled with convective diffusion from the web surface to the surroundings. The driving force for this process is a vapor partial pressure gradient. This mode occurs when the web temperature is below the ambient boiling point (which is the case in the conventional dryer section). The web temperature is, of course, influenced by heat transfer rate. The resistance to mass transfer in the web and in the adjacent boundary layer is a major factor limiting drying rate.

The other mode for mass transfer can be called bulk vapor flow. Here, the driving force is a total pressure gradient. It occurs if the web temperature exceeds (even slightly) the ambient boiling point. In this case, the only resistance to mass transfer is inside the web, and it is inversely related to the vapor permeability. This resistance is typically negligible compared to the diffusional resistance mentioned above. Therefore, it tends to be only heat transfer factors that limit the drying rate. However, very intense heat transfer to the web is needed to enter into this regime (which can, therefore, be defined as the **high-intensity drying** regime). An early description of the transition from conventional drying to high intensity drying can be found in Ref. 1. The Condebelt process is the only known commercial process in which the bulk flow mode of vapor removal occurs (in it, the vapor leaving the sheet condenses on a cooler adjacent surface). A consequence of the bulk flow mode of vapor transport is that the energy transport within the web is enhanced by intense 'heat pipe effects' (evaporation-flow-condensation). This implies that temperature differences in wet portions of the web tend to be small (provided the permeability does not become too low).

As a point of technical interest, one other statement can be made concerning the drying process. That is, pure impingement drying (i.e., simultaneous convective heat and mass transfer) can, at best, provide wet web temperatures equal to the 'wet bulb temperature', which can only approach the ambient boiling point. Thus, although relatively high drying rates may be possible with this technique, it is not an example of high-intensity drying, as defined here. This statement is not intended to imply that impingement heat and/or mass transfer should be disregarded as a potentially useful tool in achieving a successful high intensity dryer concept.

It might be noted that example calculations of mass transfer rates for both modes, and other information on transport phenomena in the web, were included in the Fall 1999 Project F041 presentation to the Papermaking PAC. This material will not be repeated here, but it is believed to support the preliminary concept definition given below.

Although, the high intensity mode has excellent potential for increasing drying rate, its limitations should be noted. If web vapor permeability does become small (perhaps due to the web moisture content being high and/or due to high levels of compression), the internal vapor pressure can become large (relative to the ambient pressure). In this case, if the web has insufficient restraint (relative to its cohesive strength), delamination can occur. A less serious phenomenon (liftoff, a loss of thermal contact between the sheet and the hot surface) is also believed possible under some conditions. A further limitation to high intensity drying is that a dry layer tends to develop in the sheet (adjacent to the hot surface); its thickness increases with contact time, tending to gradually reduce heat transfer rate (2). A successful dryer concept would need to manage this effect.



## PRELIMINARY CONCEPT DEFINITION

Since mass transfer impediments can be removed by operating in the high-intensity drying mode, concepts compatible with that regime have been given primary attention. With heat transfer-related factors tending to control drying rate in the high-intensity drying regime, they represent a major focus of the preliminary concept definition effort.

The two most important factors for high heat transfer rate to the web are large temperature difference (driving force) and low thermal resistance between the hot surface and the web. These factors point toward use of high-surface-temperature dryer (using an as yet unspecified heat source) and higher than conventional mechanical pressure (to increase the contact heat transfer coefficient). Loading considerations will, of course, place a limit on the combinations of pressure level and contact area at pressure that are feasible. A further, direct restriction on mechanical pressure level could come from either its impact on sheet bulk or its related impact (via web vapor permeability) on the possibility of blistering/delamination.

The phenomenon mentioned earlier concerning a dry layer, of continuously increasing thickness, developing during the high intensity drying process suggests two other considerations. It may be desirable to interrupt the regions of intense heat transfer periodically to allow some z-directional redistribution of moisture to occur. It may also be desirable to alternate heat input from one surface of the sheet to the other at reasonable intervals.

The first of these points is compatible with the use of shoe press-like devices at intervals around the cylinder. In this context, the term 'shoe press-like' refers to the general configuration, but is certainly not intended to imply that the pressure levels and clothing employed should be similar to those associated with shoe presses for wet pressing or impulse drying. In fact, it is believed that the best range of pressure for high intensity drying may be well below that for wet pressing. The purposes are quite different. In the drying application, we are not seeking to squeeze water from the sheet, but to improve heat transfer. It can be expected that vapor removal via the bulk flow mechanism (i.e., flow from the sheet into the felt) would occur while the sheet is being intensely heated in the shoe press nip zone. After the sheet leaves the nip, it may evaporatively cool to temperatures below the ambient boiling point. In this between nip region, an appropriate sheet-restraining fabric may be needed to provide restraint against shrinkage effects, as well as to promote a continuation of heat transfer to the sheet (possibly at a reduced rate due to the reduced applied pressure). Also in the between nip region, impingement could potentially be employed to increase the local mass transfer (drying) rate.

## INITIAL HIGH INTENSITY DRYING EXPERIMENTS

As suggested by the above description of high intensity drying principles, and the preliminary concept definition, adaptation of shoe pressing techniques, coupled with higher than conventional dryer surface temperatures, should offer an opportunity to achieve large heat transfer and drying rate increases. The experiments described here were intended to provide an initial, relatively broad, overview of the effects on water removal of "shoe press" variables (pressure level, number of pressure pulses [1 vs. 2]), surface temperature, initial sheet solids level and grade. The particular objective of these initial (heated MTS press) experiments is to demonstrate and quantify the drying rate (heat transfer aspects) potential, and to guide the development of high intensity drying concepts that integrate multiple "shoe pressing" nips (to intensify heat transfer) and higher than conventional surface temperatures into the drying process. A limitation of this initial work is that short dwell times between pressure pulses were not achievable on the MTS [2 sec was shortest].

## Experimental Plan

### **Test Conditions:**

Samples: These were 4" diameter circular discs cut from handsheets.

#### 1. Linerboard-like sheets:

- 205 gsm
- 100% unbleached softwood kraft
- 500-550 CSF
- 50% initial solids (via pressing to at least 45%, followed by air drying, if necessary)

Initial sheet solids: 2 levels: 50% and 70%

Surface Temperature: 2 levels: 300 F and 450 F [149 C and 232 C]

Dwell times:

- single nip: 20 ms
- multi-nip: 2 hits at 20 ms each, with 1 level of dwell (minimum possible) in between [about 2 sec]

Applied Pressure Pulse: 3 levels: 10, 100, 1000 psi

Repeats: 10, for each test condition

#### 2. Copy paper-like sheets:

- 70 gsm
- 75% BHWK/25% BSWK
- 450 CSF
- 50% initial solids (via pressing to at least 45%, followed by air drying)

Initial sheet solids: Mainly 50%; limited 70% solids runs at one pressure

Surface Temperature: 2 levels: 300 F and 450 F [149 C and 232 C]

Dwell times:

- single nip: 1 level: 20 ms
- multi-nip: 2 hits at 20 ms each, with 1 level of dwell (minimum possible) in between [about 2 sec]

Applied Pressure Pulse: 3 levels: 10, 100, 1000 psi

Repeats: 10, for each test condition

### **Procedures:**

- Each sample was supported on a "dry" felt, which was resting on the lower platen of the MTS press. The dry felt presses the sheet against the hot platen, serves as a water receiver, and permits some vapor venting to occur.
- In a limited number of runs, fine thermocouples were placed between the sheet and felt, to provide some insight on the heat transfer process.

## Experimental Results and Discussion

The above experimental program has recently been completed. The primary results and observations are presented here. Analysis and interpretation of these results is still in progress, but some preliminary discussion is included.

For each experimental condition, the water removal data were used to calculate a drying rate based on residence time in the shoe press nip period(s) (i.e., either 20 ms or 40 ms). The drying rate defined in this manner represents an upper bound on the actual drying rate that occurred in the experiment, or on that achievable in practice. It represents the (heat transfer based) drying rate for an ideal situation in which vapor removal (evaporation) is instantaneous. In effect, this rate definition also corresponds to the assumption that the sample is in good thermal contact with the hot surface only during the pressure pulse(s) (perhaps not always the case in practice).

The drying rates, as defined above, are presented in Figures 1, 3 and 4 [some limited additional data, for the bleached, 70 gsm samples, at 10 psi peak pressure and 70% initial solids, appear in Table 1]. For the bleached, copy paper-like sheets, the total water removal was sufficiently large as to make it interesting to present the final sheets solids data, as well (see Fig. 2). Over the entire range of the experimental program, the nip residence time based drying rate ranged from 1100 to about 9700 (kg/h/sq m)<sup>1</sup>. For reference, note that typical 'TAPPI drying rates' are in the 15 to 30 kg/h/sq m range, impingement units provide rates of about 60 to 110 kg/h/sq m, and Condebelt rates can likely be as high as 150 kg/h/sq m.

The actual drying rate based on total residence time in the dryer, comprising both periods in the shoe press nip(s) and time between/after nips [e.g., available for vapor removal from the web], will be less than that based on nip residence time, alone. The relationship is:

$$DR_{actual} = DR_{nrt} * NRT / TRT$$

where:

$$DR_{actual} = \text{actual} - \text{drying} - \text{rate}$$

$$DR_{nrt} = \text{nip} - \text{residence} - \text{time} - \text{based} - \text{drying} - \text{rate}$$

$$TRT = NRT + ANRT$$

TRT= total residence time

NRT= nip residence time

ANRT= after-nip residence time (= between nip time, for a multi-nip dryer)

The rates presented in Figs. 1,3 and 4 are all in the range of about 10 to 100 times greater than the actual rates typical for either impingement drying or Condebelt drying. Therefore, if the time needed for vapor removal (ANRT) can be kept to less than about 10 to 100 times the nip residence time, respectively, the actual drying rates for the high intensity dryer concept envisioned here should exceed those for the fastest currently available technologies (impingement drying and Condebelt). Intuitively, it would seem likely that ANRT/NRT ratios considerably shorter than 10 should be adequate for vapor removal. This is one topic meriting investigation in the near future. The amount of heat transfer occurring (and contributing to the actual drying rate) via post-nip contact also needs to be investigated.

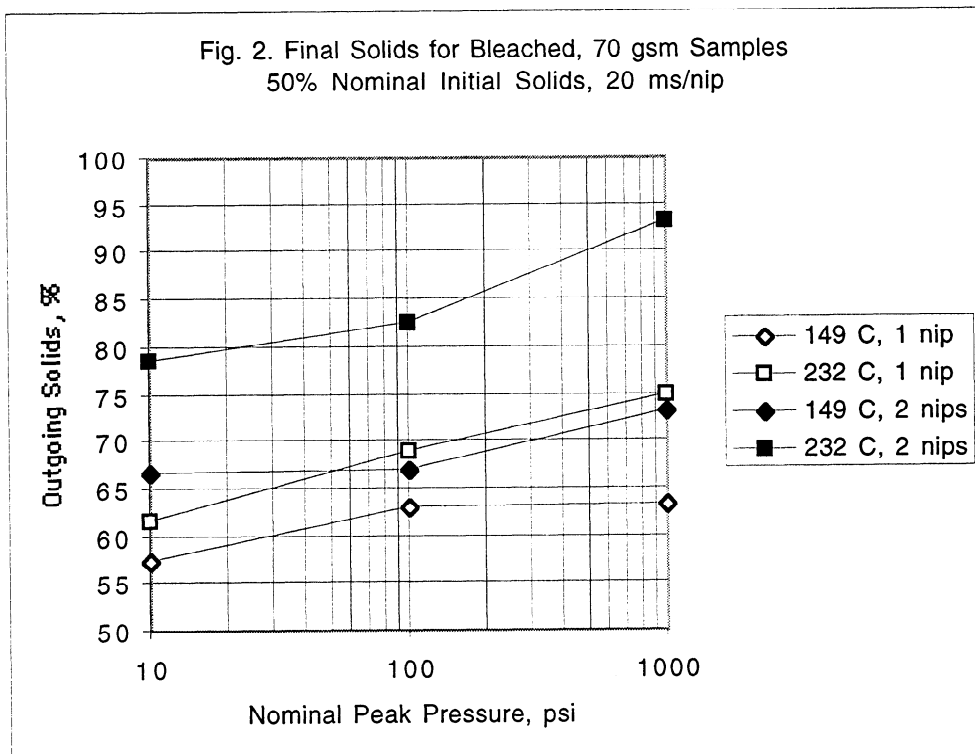
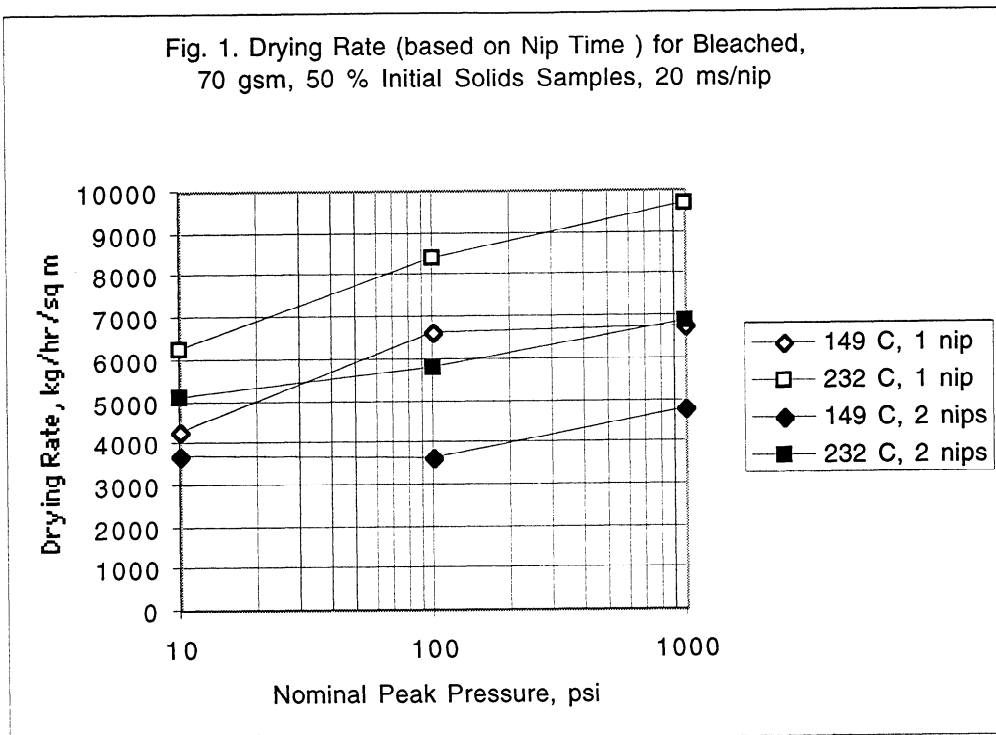
<sup>1</sup> Note: dividing drying rate in (kg/h/sq m) by 4.88 converts it to (lb/h/sq ft).

Inspection of the drying results in the cited figures reveals the following:

- The rate increases with surface temperature and applied pressure. These results are compatible with the elementary heat transfer concepts of thermal driving force and of pressure-dependent contact resistance, respectively.
- The rate decreases for two nips, compared to one nip. This is compatible with the existence of a dry layer near the hot surface impeding heat transfer in the second nip.
- The rate is less for a 70% ingoing solids level than for 50% ingoing solids. This is compatible with the expectation that drier paper is a better insulator than wetter paper.
- The drying rate for the 70 gsm web is greater than that for the 205 gsm web. This may be due to a greater part of the heat input being needed for sensible heating, in the case of the heavier web.
- For the bleached, lighter weight sheets, the high intensity drying experiments led to very high final solids levels (Fig. 2).

Another aspect of the experimental program involved tracking the sticking and blistering tendencies of the paper samples. A summary of these observations is provided in Tables 1 and 2. The first point to be made about these results is that blistering/delamination was found to occur at only the most intense condition (232 C, 1000 psi), and only for the 205 gsm samples at 50 % initial solids. Thus, there seems to be plenty of opportunity to apply high intensity drying ideas without undue concern about delamination.

Sticking was more frequently observed, but the practical significance of these observations is not yet clear. The tendency for sticking was greater for the linerboard than for the copy paper-like samples. The tendency was also greater for 50% initial solids cases than for 70% initial solids. In any of the double nip cases where only between nip sticking was observed, there is probably no cause for concern relative to potential applications, since such sticking would likely promote improved heat transfer in the between nip section.



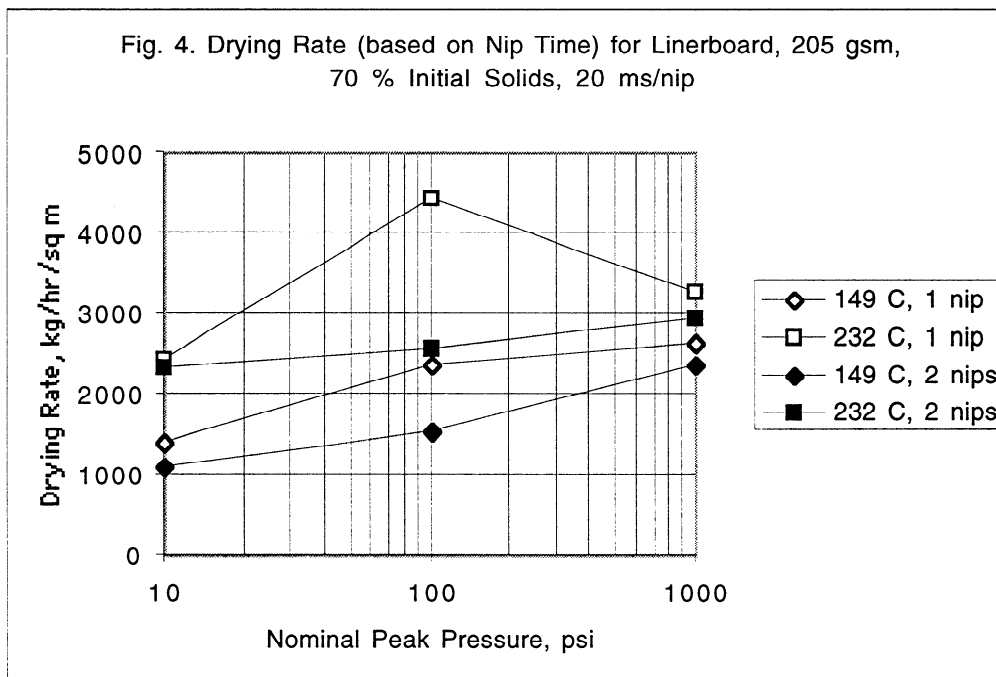
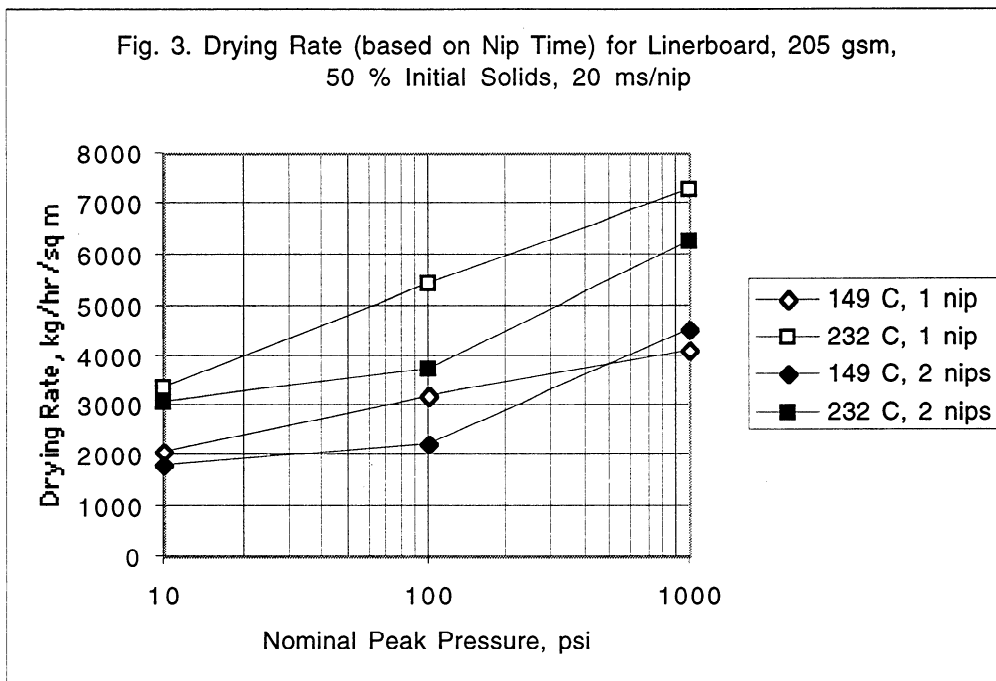


Table 1. Bleached 70 gsm Samples: Degree of Sticking

<u>nips</u>	<u>Nominal Initial Solids</u>	<u>Surface Temperature</u>	<u>Peak Pressure</u>	<u>Drying Rate kg/h/sq_m</u>	<u>Degree of Sticking</u>
1	50%	149 C	10 psi	4290	varied
1	50	149	100	6610	edge
1	50	149	1000	6769	varied
1	50	232	10	6257	severe
1	50	232	100	8439	very slight
1	50	232	1000	9673	slight
2	50	149	10	3663	moderate
2	50	149	100	3605	between hits
2	50	149	1000	4760	between hits
2	50	232	10	5077	none
2	50	232	100	5818	between hits
2	50	232	1000	6890	none
1	70	149	10	2961	varied
1	70	232	10	3740	none
2	70	149	10	2183	none
2	70	232	10	2775	none

Table 2. Linerboard: Degree of Sticking

<u>nips</u>	<u>Nominal Initial Solids</u>	<u>Surface Temperature</u>	<u>Peak Pressure</u>	<u>Drying Rate kg/h/sq_m</u>	<u>Degree of Sticking</u>	
1	50%	149 C	10 psi	2069	severe	
1	50	149	100	3198	moderate	
1	50	149	1000	4082	mod/sev	
1	50	232	10	3321	none	
1	50	232	100	5385	slight/mod	
1	50	232	1000	7238	hi severe*	*1 of 10 blistered
2	50	149	10	1800	slight	
2	50	149	100	2218	varied	
2	50	149	1000	4506	severe	
2	50	232	10	3076	slight	
2	50	232	100	3687	severe	
2	50	232	1000	6258	severe*	*most shts blistered
1	70	149	10	1412	none	
1	70	149	100	2381	varied	
1	70	149	1000	2628	varied	
1	70	232	10	2442	none	
1	70	232	100	4421	very slight	
1	70	232	1000	3267	varied	
2	70	149	10	1102	none	
2	70	149	100	1531	none	
2	70	149	1000	2382	varied	
2	70	232	10	2320	none	
2	70	232	100	2578	none	
2	70	232	1000	2938	between hits	



## CONCEPT DEVELOPMENT ISSUES AND PLANS

The work to date has likely generated more questions than answers. Hopefully, it has also given some initial support for the value and direction of this project.

The following list, which is neither complete nor prioritized, is intended to give an idea of the types of issues that need to be addressed as the project goes on. Work in the coming period to refine the concept presented here will be guided by these issues and questions.

- Number of shoe press nips per cylinder vs. length of nips
- Number of cylinders vs. size of cylinders
- Ratio of total nip length to total contact length
- Temperature-pressure tradeoffs (drying rate and paper properties aspects)
- Vapor removal requirements
- Clothing issues and desirable characteristics (interaction with sheet surface properties, sheet restraint strategies, operating temperatures, vapor removal, etc.)
- Equipment issues and limitations (including technical and economic impacts of mechanical pressure and surface temperature levels, etc.)
- Heat sources
- Paper properties impacts
- Fillers and additives impacts
- Economic issues, tradeoffs and feasibility

### **PROPOSED NEW PROJECT TASK: Development/Verification of a Model of the PAPRICAN High Intensity (Impingement) Dryer Concept**

It is quite well known that PAPRICAN is active in the development of a 'high intensity dryer' concept (although they are not necessarily using the same definition as given in this report) involving impingement heat transfer to the sheet on a large diameter cylinder. The work is focused on drying of printing grades. Recently, they initiated communication with IPST regarding potential collaboration on one aspect of this work (development and verification of a computer model of the concept, which would be useful for scale-up, etc.). Since such collaboration could provide a way to gain understanding of the merits and potential of impingement techniques in the dryer section, it would seem compatible with the other aspects of this DFRC project. A proposal for moving forward in this endeavor has been prepared (see APPENDIX A). Feedback from the Papermaking PAC on this proposed work would be appreciated.

## REFERENCES

1. Ahrens, F., Kartsounes, G. and D. Ruff, "A Laboratory Study of Hot-Surface Drying at High Temperature and Mechanical Loading", PULP & PAPER CANADA 85(3):T63-67 (March 1984).
2. Ahrens, F. and Åström, A., "High-Intensity Drying of Paper", DRYING TECHNOLOGY 4(2): 245-270 (1986).

**APPENDIX A****Proposed Interaction with PAPRICAN in the Area of High Intensity Drying****F. Ahrens, Water Removal Unit, IPST**

The purposes of this document are: to present an opportunity for a limited (but significant) interaction between IPST and PAPRICAN in an area of mutual activity (high intensity drying processes) and to outline an approach to implementing this interaction that provides benefits to both of our organizations (and their memberships). An overall Proposed Path Forward is also provided.

**Background**

There are several background points that contribute to this opportunity and/or to its value:

- PAPRICAN is working on a “high intensity dryer” concept involving inserting larger than conventional diameter steam cylinders (e.g., one or two), fitted with hot air impingement hoods, at selected points in the dryer section (for printing grades). The sheet is believed held to the dryer surface by adhesion rather than by fabric tension. In essence, the configuration is that of a Yankee dryer. A major purpose is to achieve a large increase in drying rate. They will begin evaluating the concept on their new medium/high-speed pilot machine this year.
- Several supplier companies (Beloit, ABB, Valmet) are promoting various ways of introducing impingement units into the dryer section, as well.
- IPST has initiated a DFRC project (F041) in July 1999 on “Extending High Intensity Water Removal Principles into the Paper Machine Dryer Section.” The scope of this project is currently broader than that of the PAPRICAN project (i.e., it is not limited to use of impingement techniques). In spite of that, it would be desirable to gain access to the PAPRICAN work and, more generally, to develop a better understanding of the potential and the limitations of impingement techniques in the dryer section.
- At the recent (5 Jan. 2000) ‘IPST Forum,’ one of the highly rated areas for IPST improvement in the new decade was “improving interactions with our sister organizations” (of which PAPRICAN is an important one).
- The author has extensive experience in computer modeling of the Yankee dryer (for towel and tissue machine applications). The author’s current model is based on fundamental heat and mass transfer equations, together with various empirical correlations developed from published (non-proprietary) information. However, the model would likely require some modification to make it better suited to simulation of the drying of printing grades. In particular, the variation of sheet temperature and moisture in the z-direction can be (and was) neglected for tissue drying, but these variations should be included in modeling the behavior of heavier grades. Also, some of the empirical correlations used in the model may need to be adjusted.
- Most importantly, Dr. Ivan Pikulik (responsible for the PAPRICAN project) has approached the author with the question as to whether the author would be able to work with PAPRICAN in applying/adapting the Yankee dryer model to

the evaluation of their high intensity dryer concept and its further development and application. Part of the effort would be to use data from trials with the pilot machine high intensity dryers to verify and tune the computer model. A copy of Dr. Pikulik's initial e-mail inquiry is in the **Attachment**. According to that e-mail, it appears that the PAPRICAN management is inclined to be favorable to the proposed interaction. A subsequent e-mail, received in early January of this year, reaffirms the PAPRICAN interest in pursuing this interaction. Apparently, they do not currently have access to a suitable model, and cannot justify developing one of their own 'from scratch.' Dr. Pikulik has expressed interest in having long term direct access to the version of the model resulting from the proposed collaboration.

### **Proposed Approach**

In view of the background presented, it seems that there is a sound basis for mutually beneficial cooperative work in development of a computer simulation of the PAPRICAN high intensity dryer concept. The proposed approach would include the following steps:

- Initial meeting at PAPRICAN to review the current Yankee dryer model, to inspect the pilot machine dryers, to establish requirements for the proposed high intensity dryer model, and to develop a more detailed project scope and timing.
- Create an initial high intensity impingement dryer computer model that is incorporates useful portions of the current Yankee dryer model, but is focused on the PAPRICAN application. Some of the new features believed needed were mentioned in the Background section. **It is proposed that this work would be considered part of the DFERC F041 project.** It is expected that this step would take about one man-month of effort.
- Conduct pilot machine trials at PAPRICAN to provide data sufficient for verification and tuning of the model. It is expected that this experimental work would be performed and paid for by PAPRICAN. However, the author would participate in planning the trials.
- Use the experimental data to verify and tune the model. This would likely be a joint effort, with the model tuning being done by the author.
- Make the model user-friendly, and train the PAPRICAN team in its use.

### **Expected Benefits**

For IPST and its members, the potential benefits of this work include:

- A deliverable (validated computer model) would be produced that could be made available to interested member companies. The model would be structured in a general way, to make it useful for scale-up and investigation of design variations. As a result, the model could later be applied/adapted to the evaluation of the impingement ideas being promoted by the various equipment suppliers.
- Access to the PAPRICAN pilot machine dryer system and associated performance data. The extent of this would have to be negotiated.

- Establishment of working relationships that could lead to additional cooperation in the water removal area. For example, if work on Project F041 at IPST produces promising concepts beyond impingement, they could potentially be evaluated within the PAPRICAN pilot machine dryer system in the future.

For PAPRICAN and its members:

- Availability of a validated computer model that adequately simulates their high intensity drying concept, without having to fully pay for its development.
- Long term access to the model so that they can apply it to the design and economic assessment of future (commercial) installations. The form of this access would have to be negotiated.
- Hopefully, establishment of working relationships with IPST that could lead to additional beneficial cooperation in the water removal area.

### **Proposed Path Forward**

The following steps appear to be needed prior to beginning the proposed work:

- IPST management reviews this proposal and approves proceeding to next step (**completed** 21 Jan. 2000)
- Papermaking PAC F041 Subcommittee reviews this proposal (Jan. 2000)
- Initial meeting with PAPRICAN to develop more detailed scope and timing (Feb. 2000)
- Papermaking PAC reviews scope of proposed interaction (Mar. 2000)
- Veda Christmas (Legal) and Marsha Gill (Contracts) develop appropriate agreements with PAPRICAN (Mar. 2000)
- PAPRICAN and IPST reach final agreement and proceed with the work (April 2000).

**Acknowledgement:** Thanks to David White for encouragement and for helpful comments on a draft of this proposal.

**Attachment: e-mail from I. Pikulik**

From: ipikulik@paprican.ca  
To: Fred.ahrens@ipst.edu  
cc: jhamel@paprican.ca, npoirier@paprican.ca, jrogers@paprican.ca  
Date: Tue, 2 Nov 1999 17:07:45 -0500  
Subject: Cooperation on modeling high-intensity drying

Dear Fred,  
During the Engineering Conference I told you that we would be very interested in using your Yankee simulation model to evaluate the drying rate during High-Intensity drying (HID) of printing papers. I have checked with Paprican management, and there is no objection to us establishing a co-operation on a project of our mutual interest. At this time I am not sure what form would could take such a co-operation.

Presently, our pilot paper machine is in the start-up phase. By the end of the year we intend to start up the dryer section, consisting of two HID units. One of machines first tasks will be further to develop the HID technique and to demonstrate these units at commercial speeds. Our dryers are highly instrumented - much more than any commercial installation. This will allow us to examine the effects of various parameters on drying rates, paper quality and energy efficiency. This might be an excellent opportunity for you to verify your model. We might gain a tool to estimate the effect of an HID installed in a commercial machine, before the decision about such an installation is made. Can we find on this basis a room for co-operation?

Perhaps it would be useful to meet and to discuss these possibilities in more details. Perhaps the PAPTEC Paper Week held in Montreal at the end of January, beginning of February 2000 would be a good opportunity for such a meeting. Friday morning of that week we might demonstrate the machine for various visitors and it might be an opportunity to see it in action.

Ivan Pikulik

DRYING PRODUCTIVITY

STATUS REPORT

FOR

PROJECT F021

Fred Ahrens (PI)  
Tim Patterson (PI)  
Hiroki Nanko  
Yulin Deng  
Shana Mueller  
Marcos Abazeri

March 8 – 9, 2000

Institute of Paper Science and Technology  
500 10th Street, N.W.  
Atlanta, Georgia



**DUES-FUNDED PROJECT SUMMARY**

<b>Project Title:</b>	<b>DRYING PRODUCTIVITY</b>
<b>Project Number:</b>	<b>F021</b>
<b>PAC:</b>	<b>PAPERMAKING</b>
<b>Project Staff</b>	
<b>Principal Investigators:</b>	<b>F. Ahrens/T. Patterson</b>
<b>Co-Investigators:</b>	<b>H. Nanko, Y. Deng</b>
<b>Research Support Staff:</b>	<b>S. Mueller, M. Abazeri</b>
<b>PAC Subcommittee</b>	<b>Reese, Worry, Beck</b>
<b>FY 99-00 Budget:</b>	<b>\$141,000</b>
<b>Allocated as Matching Funds:</b>	<b>70%</b>
<b>Time Allocation:</b>	
<b>Principal Investigators:</b>	<b>25%</b>
<b>Co-Investigators:</b>	<b>10%</b>
<b>Research Support Staff:</b>	<b>50%</b>
<b>Supporting Research:</b>	
<b>Students:</b>	<b>None</b>
<b>External (Where Matching Is Used):</b>	<b>Project 4253 (DOE-\$400,000)</b>

**RESEARCH LINE/ROADMAP:**

Line 7 - Increase paper machine productivity by 30% over '97 levels via focus on breakthrough forming, dewatering, and drying concepts [faster drying and improved runnability/quality]

**PROJECT OBJECTIVE:**

Understand and reduce the impediments (e.g., picking/sticking, surface deposits, cockle, sheet sealing) to the use of higher surface temperatures in the first dryer section. Provide fundamental knowledge and tools needed to design new technologies that will allow ultra high speed web transfer.

**PROJECT BACKGROUND:**

Project F021 was connected to DOE Project 4253 in Oct. 1998. 70% of F021 funding represents cost share to DOE project.

**MILESTONES:**

- Establish baselines on current operations:
  - Drying strategies and problems [Q1, FY 99-00]
  - Roll/dryer can contamination/topology [Q3, FY 99-00]
- Develop experimental equipment:
  - Contamination Test Stand (CTS) [Q3, FY 99-00]
  - Web Adhesion and Drying Simulator (WADS) [Q3, FY 99-00]



- Develop empirical data and models:
  - contamination
  - picking/adhesion
  - cockle[Q1, FY 00-01]
- Develop and verify web transfer model for high speed machine operation [Q3, FY 00-01]
- Develop/evaluate:
  - surface conditioning technologies
  - improved drying strategies [Q4, FY 00-01]

**DELIVERABLES:**

- Summary of baseline information [Q4, FY 99-00]
- Experimental equipment: CTS and WADS [Q3, FY 99-00]
- Understanding and data on factors influencing picking/sticking, cockle, and surface deposits/contamination [Q1, FY 00-01]
- Dryer section operating strategies relative to picking/sticking, cockle, and surface contamination problems [Q3, FY 00-01]
- Surface conditioning technologies [Q4, FY 00-01]
- Web transfer model for high speed operation [Q3, FY 00-01]

**STATUS OF GOALS FOR FY 99-00:**

- Summarize and analyze the Questionnaire results to guide project work and to characterize the opportunity for improved productivity by grade [further analysis put on hold at Fall '99 PAC mtg.]
- Collect meaningful surface contamination and topological data from mills [complete for 3 grades]
- Design, construct and debug a **Web Adhesion and Drying Simulator** for use in investigating effect of sheet and drying conditions on sticking and picking [complete]
- Design and construct a **Contamination Test Stand** for use in providing model contaminated surface coupons for use in the WADS [complete; working out contamination procedures]
- Use WADS to quantify sticking/picking for clean and contaminated surfaces [trial plan in place; ready to begin]
- Investigate the extent to which drying-related variables influence cockle [in collaboration with the Project F020 team] [first trial complete]

**SCHEDULE:**

Task	FY 99-00				FY 00-01			
	Q1	Q2	Q3	Q4	Q1	Q2	Q3	Q4
Summarize/analyze Questionnaire results	X			?				
Collect dryer contamination/topology info.	X	X	X		X			
Develop experimental equipmt: WADS, CTS	X	X	X					
Web adhesion/picking experiments			X	X	X			
Cockle experiments		X	X	X				
Develop web transfer model					X	X	X	
Develop/evaluate improved drying strategies				X	X	X	X	
Develop/evaluate surface conditioning technologies					X	X	X	X

**SUMMARY OF RESULTS:**

- Questionnaire results indicated that **picking/sticking, surface deposits, and cockle** are believed to be the biggest problems influenced by drying strategy in the first dryer section, and confirmed that some degree of temperature graduation is used on most machines, regardless of grade.
- Mill visits [conducted under Project 4253] have provided data on the nature and extent of surface deposits on dryer cans, for three grades.
- Contamination Test Stand [designed and constructed under Project 4253] is now available to provide model contaminated surface coupons for use in the WADS.
- The checkout and development of experimentation procedures for the Web Adhesion and Drying Simulator is nearly complete. Investigation of picking and sticking can begin (trial plan in place).
- Data on effect of drying variables (surface temperature, applied pressure, fabric design, proportion of drying under restraint, and heat flux uniformity) on cockle severity have been obtained.

**SUMMARY OF KEY CONCLUSIONS:**

- The Questionnaire results support the value of Project F021
- The Web Adhesion and Drying Simulator checkout process revealed that accurate measurement of the low level adhesion forces occurring under typical drying conditions will require integrated analysis of tension data and video recordings of the peel event

- The cockle results to date are consistent with (but do not yet prove) the statement that high surface temperature in the first dryer section can aggravate cockle problems
- Non-uniform heat transfer (e.g., from surface deposits) was shown to increase cockle severity.
- Surface deposits problems appear to be prevalent in the first dryer section

## DISCUSSION and ADDITIONAL DETAILS

### Topology of Dryer Roll Surfaces

#### Significance

It is anticipated that the roughness of underlying cast iron surface has a role in determining the topology of contaminated surfaces and the amount of contaminant that deposits. These relationships have as yet to be confirmed.

#### Results

##### Work reported at the fall'99 PAC

In previous work, reported at the fall 1999 Paper making PAC, we have made roughness measurements on cleaned dryer cylinders from two mills making fine paper. For this purpose, we utilized an epoxy material to obtain replicas of the surfaces. We utilized the services of CyberMetrics to characterize the topology of these surfaces. They used a non-contact method to measure the one-dimensional roughness of the replicas. Analysis of the results suggested that the surfaces on paper machine B were generally rougher than was observed on paper machine C.

##### Work during this period

During this period we have extended our topological measurements to include the cleaned dryer cylinder surfaces from a paper machine making three-ply linerboard (designated PHL) and a paper machine that produces medium (designated PHM). In addition, we have also characterized the topology of curved cast iron coupons that are being used in our laboratory experiments. These included two cases, coupons with a smooth finish (designated CI (smooth)) and coupons that exhibited machining scratches (designated CI (scratched)). Topology measurements were obtained from epoxy replicas for the linerboard and medium machines while direct measurements were made on the cast iron coupons.

In an effort to obtain more accurate data, we obtained both one and two-dimensional roughness measurements. Figure 1 shows one-dimensional measurement of some key roughness parameters for the earlier reported fine paper machines as well as the data from the linerboard and medium paper machines and the laboratory coupons.

We observe that the topologies of B and PHL are similar and the topologies of C and PHM are similar. We also observe that the smooth cast iron coupons show similar topological characteristics to the linerboard machine and the scratched coupons are similar to the medium machine.

Figure 2 shows the two dimensional measurements for the cast iron coupons as well as for the linerboard and medium machines. We observe similarities between the coupons and the commercial surfaces.

**Conclusions**

We have shown that the topology of our curved cast iron coupons is within the range of topologies observed on commercial paper machines. Hence, we may utilize these coupons in future laboratory experiments.

**Figures: Topology of Dryer Roll Surfaces**

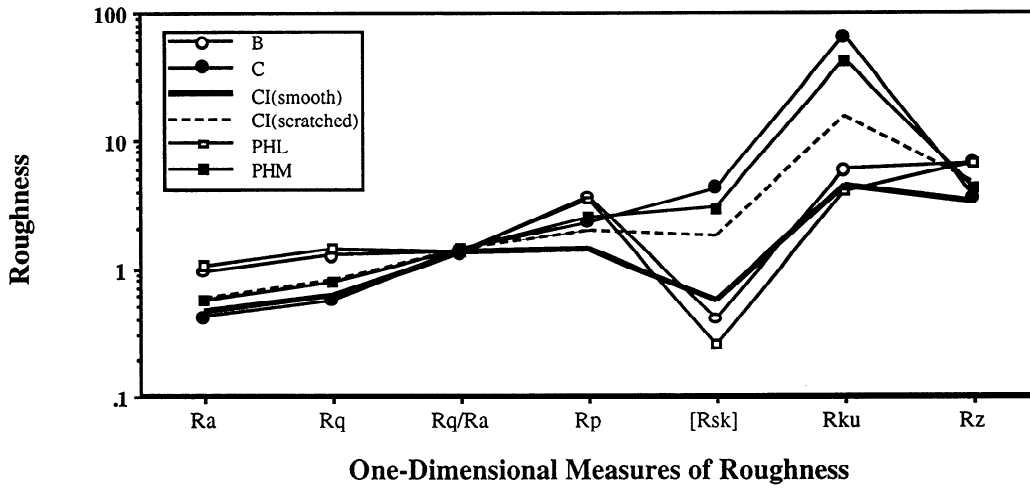


Figure 1. One Dimensional Measurements of Roughness

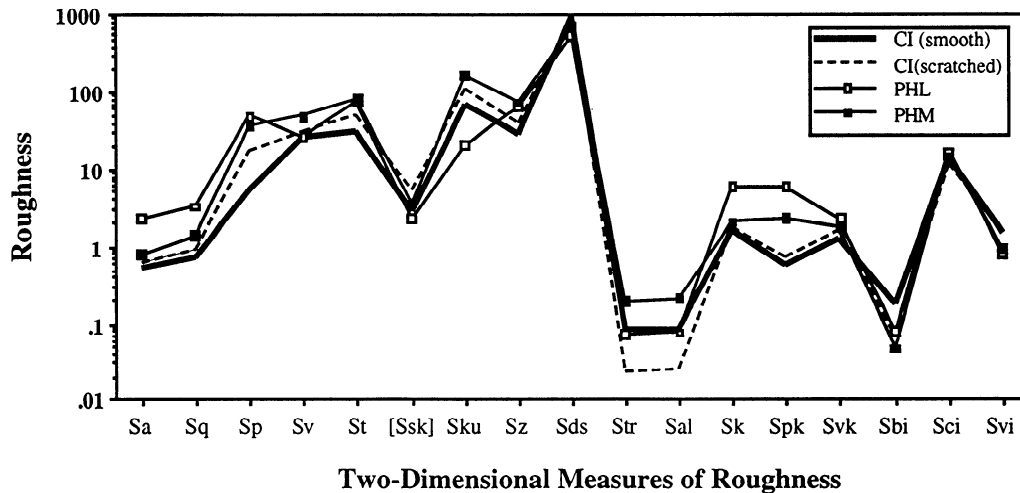


Figure 2. Two Dimensional Measurements of Roughness

## Dryer Roll Deposit Composition

### Significance

It is anticipated that chemical deposition on dryer rolls can play a significant part in reducing paper machine productivity and paper quality. Deposition of chemical contaminants onto dryer roll can lead to sticking and picking which adversely impacts paper surface properties and paper machine runnability. To reduce these effects, papermakers routinely reduce dryer roll temperatures, which negatively impact machine productivity. Contamination is often found to be non-uniformly deposited on dryer cylinders. These non-uniform deposits can lead to non-uniform heat transfer, which may lead to paper defects such as cockle. Ultimately we wish to be able to determine the adverse economic impact of dryer deposits and to develop technologies to reduce these chemical depositions and their impact.

### Results

#### Work reported at the fall'99 PAC

Samples of deposits were taken from the surface of dryer cylinders from two commercial fine paper machines. Our purpose was to estimate the range of contaminant loading and identifying the chemical composition of the deposits. We found that contaminant loading on paper machine B ranged from 3.8 g/m<sup>2</sup> to 8.7 g/m<sup>2</sup>, and that on paper machine C was from 0.01 g/m<sup>2</sup> to 1.4 g/m<sup>2</sup>. We observed that the contamination was uniformly deposited on each cylinder of paper machine B and was deposited in MD streaks on cylinders of paper machine C.

The primary purpose in characterizing the chemistry of the deposits was to develop a model contaminant mixture for future laboratory experiments. The work at this early stage was primarily qualitative. A battery of tests including wet chemical analysis, inorganic elemental analysis and microscopy were conducted. On both machines we observed large amounts of fiber and fines, latex, starch, kaolin clay, titanium dioxide and calcium carbonate. In some cases we also found smaller amounts of glue, styrene, talc, and rust.

An attempt was made to also characterize the surface energy of the collected deposits. For this purpose, samples of deposits from each cylinder were compacted and formed into flat surfaced pellets. The contact angle (water) of deposits from paper machine B ranged from 75° to 78°, while that from paper machine C ranged from 98° to 115°. For comparison we measured the contact angle of clean cast iron as 77°.

#### Work during this period

The focus of work during this period was on characterizing the deposits that were sampled from the surfaces of dryer cylinders of a linerboard machine and a medium machine.

### General Background

The linerboard machine used a double felted first press and a double felted Beloit extended nip second press followed by a smoothing press. The Black Clawson dryer section was configured such that the bottom dryer cylinders (even numbered) were without dryer fabrics while the top dryer cylinders (odd numbered) had dryer fabrics. Doctors were located at the end of each dryer section. Hence, cylinders 5, 17, 31, 43, 55, 67 were doctored.

The linerboard that is produced is three-ply with 50% OCC and 50% Virgin Kraft in the middle ply. A small amount of recycle is in the side of the liner that is in contact with the top dryer cylinders, while the bottom cylinders contact the side of the liner that is 100% Virgin Kraft.

The mill reports the use of the following chemicals in the manufacture of the linerboard; Alum, Sulfuric Acid, a defoamer (Callaway 8514 supplied by Calloway Chemical Company, Columbus Georgia), and felt cleaners (feltECCel 231, 455, and 465 supplied by ECC International, and TWI C505 supplied by The Way, Metairie, Louisiana),

The mill reports picking problems only when the steam pressure is increased in the first dryer section. Cockle problems have not been reported.

Typically they do not clean the dryer cylinders. When there is a break they will use caustic on the dryer fabrics. Also, once a month they spray Fast Foam (a commercial caustic) on all parts of the machine and then rinse with water.

The dryers on the medium machine are configured into four sections. The first section includes cylinders 1 through 9. The top cylinders (odd numbered) in the first section were all doctored. A single dryer fabric wraps each of the cylinders in the first section. In later sections, separate top and bottom dryer fabrics are utilized. Dryer cylinders 10, 12, 14, 23, 37, and 51 are doctored.

Chemicals utilized in the manufacture of medium include a defoamer (Callaway 8514), a wetting agent (Callaway 5507), and felt cleaners (feltECCel 231, 455, and 465 and TWI C505).

#### Dryer Cylinder Surface Temperatures

Dryer temperature surveys were conducted by the mill on the linerboard machine in October of 1999 while it was producing 42# liner and on the medium machine in August of 1999 while it was producing 26# medium. Surface deposits were collected by IPST during shutdowns in November of 1999. Average infrared surface temperatures are shown in Figures 1 and 2.

#### Dryer Cylinder Deposit Loading

During machine shutdowns, we scrapped a one square foot area of some of the cylinder surfaces to determine deposition loading, deposit chemistry and underlying cylinder topology. The deposit loading results are shown in Figures 3 and 4. We took samples in the first dryer section on the linerboard machine and found a range of loading from 1.2 g/m<sup>2</sup> to 6.5 g/m<sup>2</sup>. We took our samples later on in the drying process on the medium machine as the area around cylinder 16 showed particularly heavy contamination. Unfortunately, the region of greatest contamination on cylinder 16 was not close enough to the catwalk for us to safely obtain a scrapping of a fixed area. As a result we do not have a measurement of loading on cylinder 16. We were able to obtain a sample for chemical analysis and estimate the thickness of the deposit to be of the order of a sixteenth of an inch.

## Dryer Cylinder Deposit Chemistry

Samples of the deposits from the liner and medium machine were analyzed by IPST research services. The weight percent of various organic and inorganic components are shown in Figures 5 and 6.

Figure 5, for the linerboard machine, shows that Polyvinyl Acetate was a main component of the deposit on cylinder 1 while it was absent on cylinders 2 and 4. This is consistent with the fact that cylinder 1 was in contact with a side of the sheet that contained OCC while cylinders 2 and 4 were in contact with a side that contained 100% Virgin Kraft. In contrast, we observe a high concentration of calcium carbonate and silicates on cylinders 2 and 4 while these are in much lower concentration on cylinder 1.

The polyvinyl acetate probably comes from the adhesives used in making the manufacturers glue joint of the corrugated containers that form the OCC. The silicates could be coming from the defoamers or from sand. The mill reports high levels of sand in the cleaner rejects. The calcium carbonate may relate to occasional lime mud carryover problems that the mill has experienced.

Figure 6, for the medium machine, shows a high concentration of Styrene-Butadiene in the sample from cylinder 16. This component is absent from cylinders 22 and 26. Similar to the linerboard results, we observe high concentrations of silicates in the samples from cylinders 22 and 26.

The styrene-butadiene could be coming from pressure sensitive adhesives brought in by waste materials, 20-30%OCC, used in making up the medium furnish.

## Conclusions

The loading and chemical composition data should give us sufficient information to establish model contaminant mixtures for each of the three grades. Once we have defined these models we can use them to develop an understanding of the deposition process and allow us an opportunity to prepare contaminated coupons for adhesion and picking experiments on the laboratory web adhesion and drying simulator (WADS).



**Figures: Dryer Roll Deposit Composition**

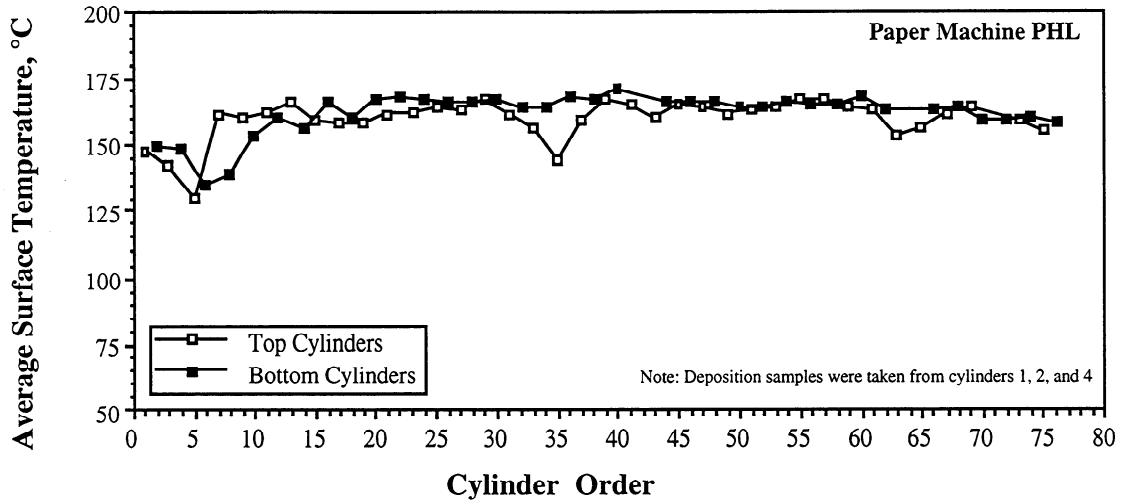


Figure 1. Average Surface Temperature for Dryer Cylinder on the Commercial Paper Machine Making Linerboard

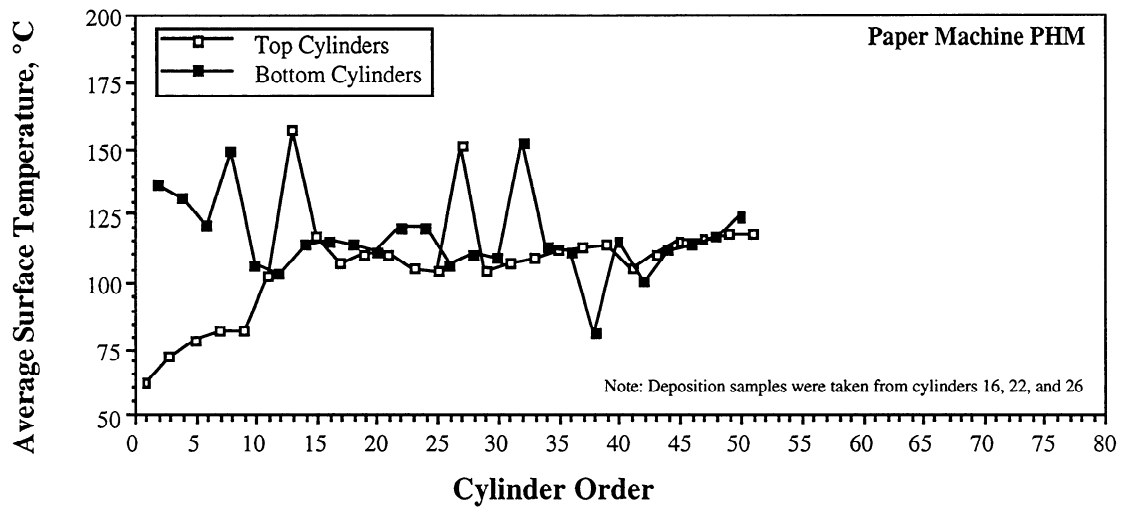


Figure 2. Average Surface Temperature for Dryer Cylinder on the Commercial Paper Machine Making Medium

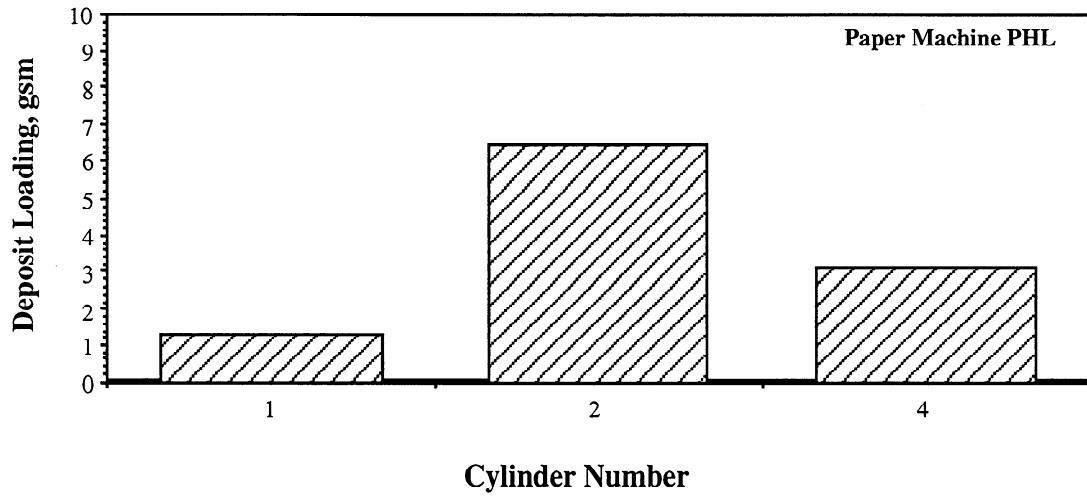


Figure 3. Deposit Loading for Dryer Cylinders on the Commercial Paper Machine Making Linerboard

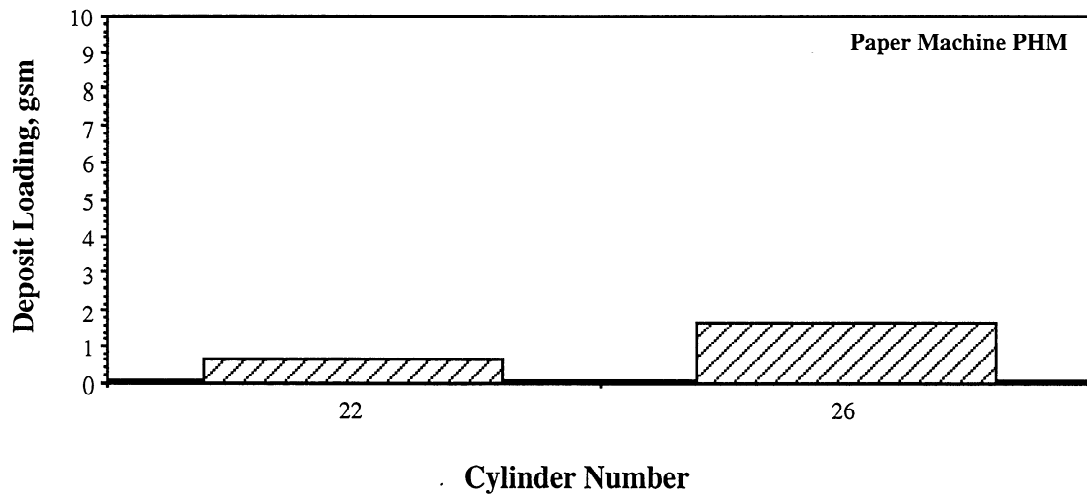


Figure 4. Deposit Loading for Dryer Cylinders on the Commercial Paper Machine Making Medium

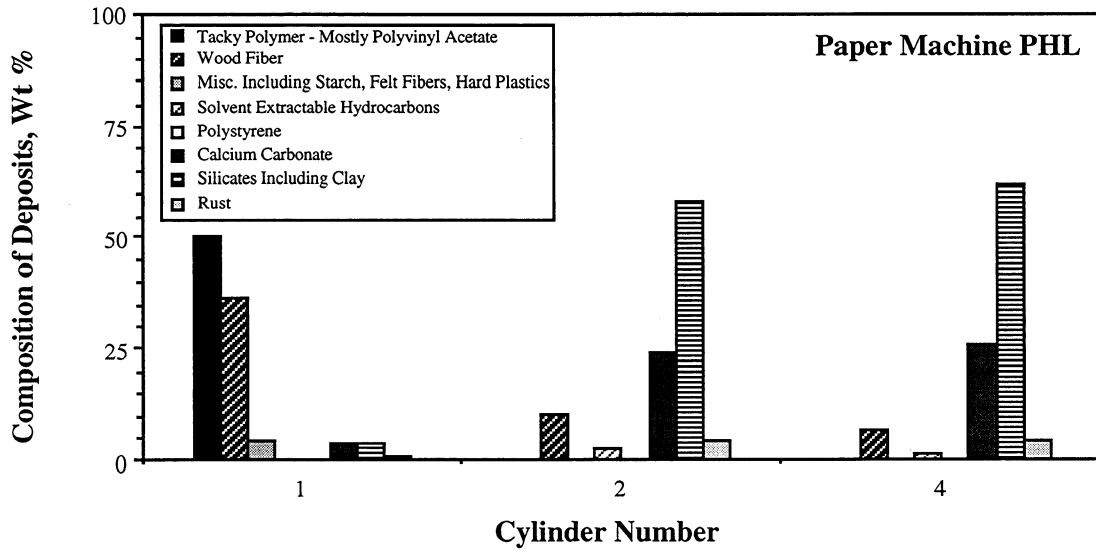


Figure 5. Composition of Deposits from Dryer Cylinders on the Commercial Paper Machine Making Linerboard

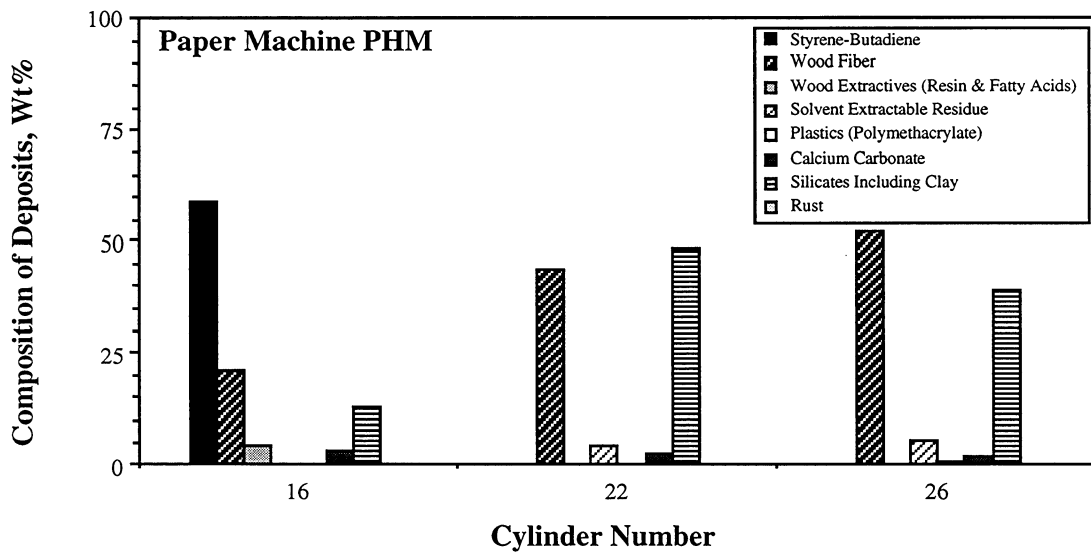


Figure 6. Composition of Deposits from Dryer Cylinders on the Commercial Paper Machine Making Medium

## Web Adhesion and Drying Simulator (WADS)

Project F021 was initiated in order to study methods of increasing paper machine productivity by using high temperatures in the first dryer section. Currently, the use of elevated temperatures is limited by various interactions between the paper and drying roll surfaces which cause picking/sticking of the web. Furthermore, contamination of the dryer roll surfaces may have an effect on the degree of picking/sticking. A review of the relevant literature has revealed that no quantitative analysis of this problem has been undertaken. A Web Adhesion and Drying Simulator (WADS) was thus designed and constructed (via Project 4253 funding) to better understand the mechanisms behind the picking/sticking phenomena so that solutions can be developed to increase product quality and paper mill productivity.

The WADS unit provides a direct measure of the peel force under simulated dryer conditions. Through the use of the Mardon equation shown below, the peel force can be correlated to the Work of Adhesion [1].

$$T' = \frac{W''}{1 - \cos \phi} + mV_1^2$$

$T'$  = Tension (g/cm)

$W''$  = Work of Adhesion (g/cm)

$m$  = Mass per unit area (g/cm<sup>2</sup>)

$V_1$  = Velocity (cm/s)

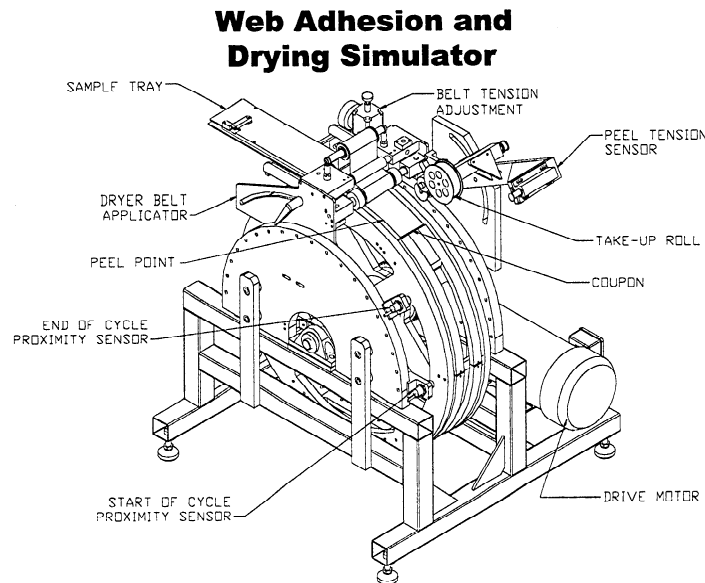
$\phi$  = Peel Angle

The Work of Adhesion is a more fundamental parameter which depends on a number of factors including surface topology, surface materials, surface energy, contaminants, fiber characteristics, application pressure, surface and sheet temperature, and moisture content. Picking/sticking occurs when the adhesion between the web and the dryer roll surface is of the same order of magnitude as the cohesion of the web. By characterizing the work of adhesion, ways of preventing and reducing picking/sticking can be determined.

### WADS Unit

The WADS system, shown below in Figure 1, consists of a belt driven flywheel to which a removable cast-iron "coupon" is attached. The coupon can first be installed in the Contamination Test Stand (CTS) to acquire a layer of surface contamination, and then can be transferred to the WADS system for peel testing. Therefore, the WADS can be used to test the effect of surface conditions, particularly contamination, on the peel force and work of adhesion. Various surface materials and surface treatments can be investigated as well.

Figure 1: WADS Unit



Unlike Mardon's sheet stripper apparatus [2], the WADS has the ability to control and vary the surface temperature which is necessary in order to simulate realistic dryer roll conditions. A range of peel angles, peel velocities, web application pressure (controlled by belt tension), and dwell times are available. The sample inlet (web) temperature, which plays a role in the degree of sticking, can also be adjusted.

During an experiment, the coupon makes one revolution from its start position at a set peel speed. The dryer belt acts to laminate the web (pulled in from the sample tray) onto the coupon as it makes its way around the wheel. The speed of the wheel and length of this dryer belt, both user specified parameters, determine the dwell time. In addition, web application pressure is adjusted with the belt tension. After passing through the applicator section, the paper is pulled from the coupon at the specified peel angle and peel point with a length of tape that is tracked over the tension sensor. The sensor records the peel force (tension) required to pull the paper from the coupon. Upon completion of the peel event, a proximity sensor triggers the brake. The data acquisition program collects the peel speed, tension, belt application pressure, and coupon surface temperature throughout the course of an experiment.

Initial experiments on the WADS unit showed a significant level of noise with the tension sensor. Viscoelastic vibration damper material was used to mechanically isolate the frame which supports the sensor. In addition, a low pass filter was installed into the system to electronically reduce noise. Static calibration of the sensor demonstrates that readings are accurate within  $\pm 0.1$  g. Dynamic tests show a consistent 1g frictional drag of the tape over the sensor apparatus which increases the tension output. This factor will be incorporated into the data analysis to determine the real peel force.

## WADS Checkout Runs

Paper samples of a bleached pulp blend (75% BHWK/25%BSWK) were prepared in the Formette for the development and testing of the WADS system. Linerboard samples were also used for initial development because of its superior durability and sticking ability. For preliminary runs, equipment settings are shown below in Table 1.

Table 1: Initial WADS Setup

Parameter	Setting
Peel Angles	60°, 45°, and 15°
Peel Speeds	50 ft/min & 150 ft/min (0.25 & 0.50 m/s)
Coupon Temperature	250 °F (121° C)
Sample Temperature	approx. 150° F (66 °C)
Application Pressure	0.47 psi (3240 Pa)
Dwell Time	0.271 s – 0.407 s (depending on speed)

A plot of tension vs. time for a typical experimental run using the bleached sample is shown in Fig 2. There is a start-up and shutdown period of transience in each run before and after the actual peel event which is indicated by the arrows.

Figure 2: Typical Experimental Run (Tension vs. Time)

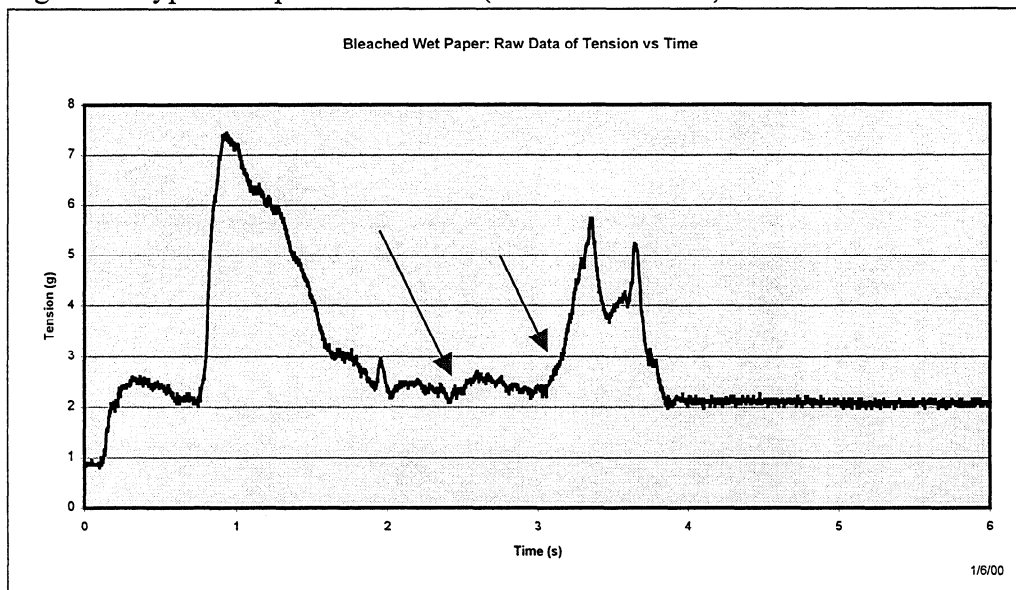
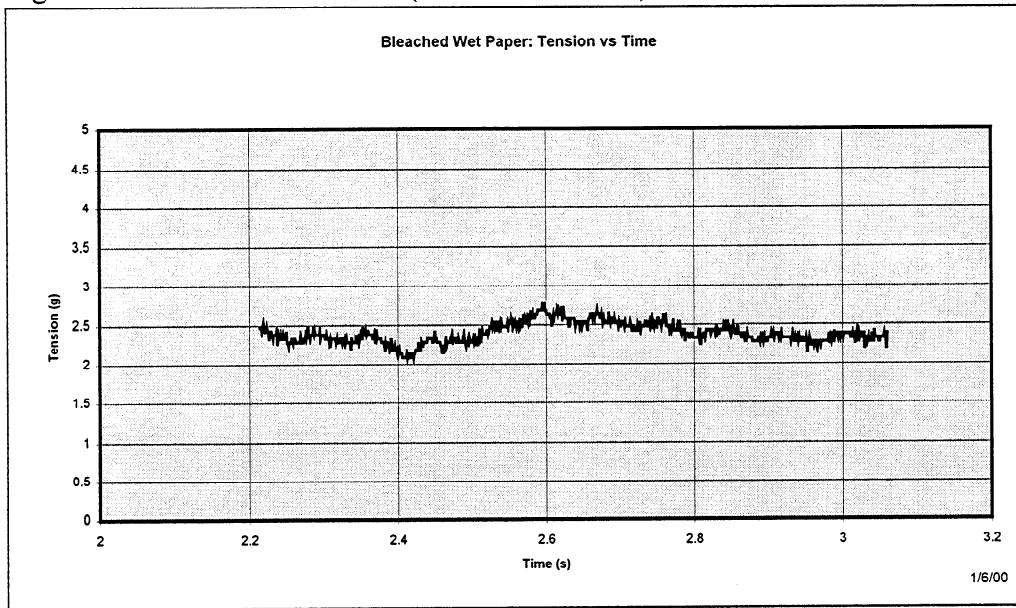


Figure 3: Extracted Peel Event (Tension vs. Time)



For the data analysis, the actual peel event, shown in Fig. 3, is extracted from the raw data file (which records a user specified number of points and sampling rate). For the preliminary runs, extraction of the peel event was difficult because there was no time stamp in the data showing the onset and end of the peel. A method of extraction was found while performing the simulated experiments (as explained in the next section) and was used on previously gathered data.

The data must be corrected for various factors including zero value, paper/tape weight and friction. During an experiment, the tape is being retracted and the paper sample is being added as the paper sample is pulled off the coupon. These two factors contribute to the tension sensor output and must be accounted for when determining the actual peel tension. Given the constant speed of the paper sample around the wheel, a linear function describes the change in weight of the paper (and tape) sample. The resulting weight is subtracted from the tension value to give the peel tension. The contribution of friction mentioned earlier must also be accounted for in the final data analysis.

Initial results revealed problems with producing adequate sticking to the clean coupon surface. A study was done to correlate solids content with optimal sticking for the bleached Formette sheets. Results showed similar sticking behavior for a range of inlet solids content, 30-60%. Tension values appeared to be quite low, in the 0.5-3.0 g range, making it very difficult to assess equipment performance. Setup conditions were modified to maximize sticking by moving to low angles and intermediate temperatures. However, only minor improvement was observed.

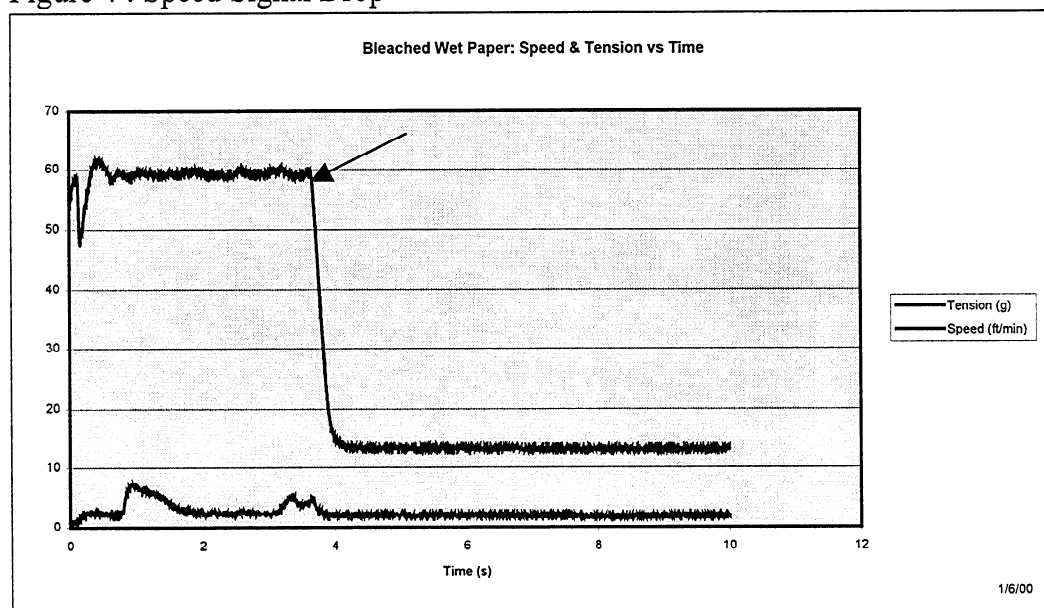
## Simulated Runs

In order to verify equipment capability and understand the peel, simulated experiments were performed using dry paper (copy and blotter paper). By using double-sided tape on the coupon, an artificial sticky surface was created. Video documentation was made of each run in order to correlate the data with the actual peel event.

A number of important observations resulted from these simulated tests. First of all, at higher peel angles, frame-by-frame video analysis showed that the actual peel angle varied greatly from set point. For example, for a peel angle of  $60^\circ$ , the actual angle ranged from  $18^\circ$ - $24^\circ$ . This is primarily due to the fact that the paper does not peel from the coupon surface at a sharp angle. Rather, there is some curvature due to lack of adhesion and inherent stiffness of the paper creating this discrepancy. Since the peel angle is required in the Mardon Equation to solve for work of adhesion, an accurate angle measurement is necessary. Similar results were observed by Mardon who found that at set points of  $90^\circ$ , the actual angle was about  $45^\circ$  [3]. He used a Fastex camera to account for the actual angle in the calculations. For the WADS system, the implication is that videotaping of each run is necessary to record accurate peel angles. The Mardon equation must then be applied locally for each discrete point.

In addition, the actual peel event can be extracted by using the drop in the speed signal as shown in Fig.4. The motor cut off is triggered by a proximity sensor at which time the speed signal begins to drop. The distance between the sensor and the peel point allows the start time of the peel to be determined. The length of the peel is simply based on the linear speed and length of paper sample. This method of analysis proved to be highly accurate in locating the actual peel event, with the start time varying only  $\pm 0.02s$ . Recently, another proximity sensor has been added to the system in order to provide a measure of the exact time at which the peel event takes place.

Figure 4 : Speed Signal Drop





Tension and peel angle data collected using this method were used in the Mardon equation to calculate the work of adhesion. A plot of the work of adhesion is shown in Figure 5. Units of work are shown in g/cm which is numerically approximately the same as the SI units of  $J/m^2$  (0.98 conversion factor).

Figure 5 : Work of Adhesion during the Peel Event

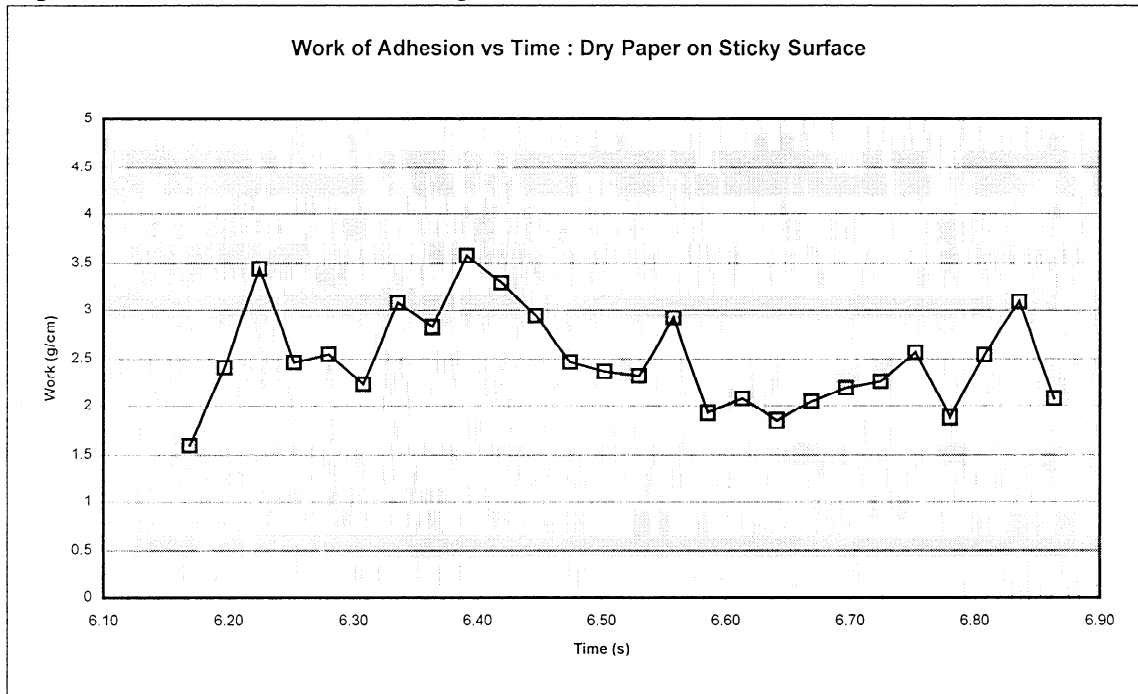
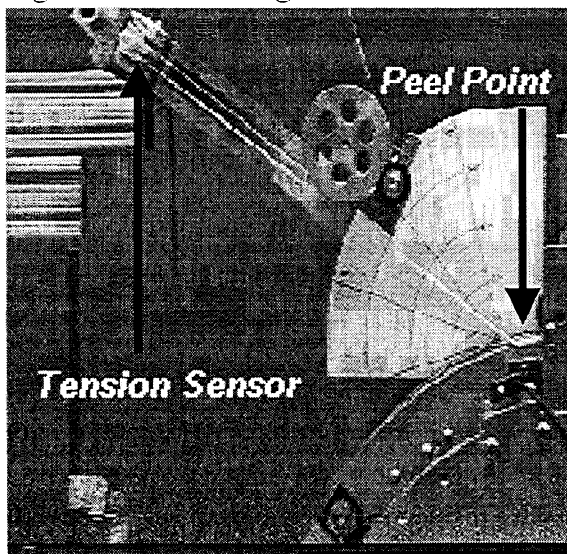


Figure 6 is a video image of an actual peel event for one of the dry paper runs. Tension values of 10-40g, significantly higher than with the wet paper on the clean coupon, were found with the tape runs.

Figure 6 : Video Image of Peel Event



### Picking/Sticking Experiments

The first part of the WADS testing involves clean coupon measurements of tension and a characterization of the work of adhesion at a range of speeds, coupon and sample temperatures, and dwell times. Initial experiments were used to verify and define the operating range of the WADS equipment. Currently, the dwell time has a range from 0.14s to 1.20s. The speed can likewise be varied from 25ft/min to approximately 200 ft/min. While the WADS does not provide peel speeds similar to actual paper machines, it does nevertheless provide dwell times in the range of the paper-to-dryer contact times at real machine speed. Consequently, the picking/sticking data can be expected to be highly meaningful.

In addition to determining work of adhesion, another goal of this work is to quantitatively describe the picking/sticking phenomena. Previous work by Meinecke [4] showed that the degree of picking depends on surface temperature, peel speed (dwell time) and inlet solids. However, the amount of picking was not quantified nor was it related to the work of adhesion. The WADS, on the other hand, should be capable of providing data for a quantitative map relating the regions of greatest picking/sticking. A detailed procedure is being developed in order to collect and measure the amount of picking. A qualitative visual rating will also be used.

The Clean Coupon experiments will employ the following conditions:

Parameter	Setting
Coupon Surface Temperature	194° F, 248° F, 302° F (90° C, 120° C, 150° C)
Dwell Time	0.17s, 0.5 s
Initial Sheet Temperature	100° F (38 °C), 150° F (66°C)
Initial Sheet Solids	40%, 50%, 60%
Peel Speed	50 ft/min, 150 ft/min (0.25 & 0.50 m/s)
Peel Angle	fixed at 30 degrees
Paper Type	Copy Paper and Liner Board

Once these experiments are complete, contaminated coupons from the CTS can be installed on the WADS to test the effect of surface condition on work of adhesion as well as on picking/sticking. The same conditions as those listed above will be analyzed.

### References

1. Mardon, J., "The Release of Wet Paper Webs from Various 'Papermaking Surfaces'," *APPITA*, Vol. 15, No. 1, pp.14-34. (July 1961)
2. Ibid
3. Mardon, J., "Theoretical and experimental investigations into the peeling of paper webs from Solid Surfaces," *Paperi ja Puu*, No. 11, pp.797-815 (1976)
4. Meinecke, A., Chau Huu, T., and Loser, H., "Neue Erkenntnisse über die Papiertocknung mit Trocken-zylindern," *Das Papier*, 42(10A), pp.159-165 (1988)

## Cockle Investigation

### Background

One of the several reasons given for the use of temperature graduation in the dryer section (i.e., use of low temperatures in the first dryer section) is that heating/drying the sheet too quickly can increase the likelihood/severity of cockle. Another problem associated with high initial dryer temperatures is increased surface deposits. Since deposits can easily be non-uniform, they are expected to contribute to cockle due to the associated non-uniformity of heat flux to the sheet.

Qualitative studies of the influence of initial moisture and heating non-uniformities on the cockle developed in paper as a result of drying, were performed by Brecht, et al (1). A discussion of some of the results is given in the paper by Gallay (2).

D. Coffin's team has developed a technique to quantify the degree of cockle in a paper sample (shadow Moiré technique), and applied it in initial experimental studies of the factors believed to influence cockle [Project F020]. Some of the factors investigated were the degree of restraint during drying, formation uniformity, dryer surface temperature (over a rather narrow range), pressing level and basis weight.

The capability of an existing dryer simulator has been upgraded to aid in conducting a further investigation of the extent to which drying-related variables influence cockle. The dryer simulator now has two heated surface options, a uniform cast iron platen and a cast iron platen having a pattern of epoxy-filled depressions to simulate non-uniform surface deposits. The simulator offers control over surface temperature, dwell time, and restraint pressure. Furthermore, the sheet can be lightly pressed against the hot surface with samples of real dryer fabrics (which apply somewhat non-uniform pressure to the sheet).

### Initial Cockle Experiments

In keeping with the input from the Papermaking PAC, some new cockle experiments relevant to Project F021 have been planned and executed, in collaboration with D. Coffin's team. The basic strategy developed for the trial is to generate samples that have been dried to various extents (in terms of moisture ratio) under selected conditions in the dryer simulator (i.e., with some restraint), and to let the drying be completed via unrestrained air drying. It was hypothesized that the amount of cockle in the final sheets would be dependent on the proportion of drying occurring in the simulator, as well as on the drying conditions. The trial plan developed is as follows.

#### Trial Objectives

- To quantify the effects of surface temperature and applied pressure on cockle
- To investigate the effect of heat flux non-uniformity on cockle

#### Experimental Plan

There are 4 parts to this trial: (1) generation of drying curves (i.e., moisture ratio vs. time) to provide input to Parts 3 and 4; (2) control runs; (3) drying runs with uniform heat flux; (4) drying runs with non-uniform heat flux.

**Test Conditions:**

Samples: These will be cut (5"x5" squares) from some of the existing Formette sheets that were initially made for use in WADS adhesion experiments:

- 70 gsm
- 75% BHWK/25% BSWK; with appropriate additives to simulate a copy paper furnish (see Table 1)
- 450 CSF
- Tensile Ratio: about 2.0
- Initial Solids Level: 45% (via pressing)

Table 1. Sheet additives.

Additive	Amount
PCC	15% of dry weight
Optical Brightener	2 lbs./ton
AKD	3 lbs./ton
Starch	12 lbs./ton
Retention Aid	2 lbs./ton

## Part (1): Drying Curves:

- Dwell time in dryer simulator: 10 levels, TBD
- Surface temperature: 2 levels, 110 C and 170 C
- Mechanical pressure: 0.2 psi and 1.0 psi [covering the range corresponding to the pressure created by fabric tension on a dryer can]
- Platens: uniform surface and non-uniform surface
- No. of runs per condition: 1

## Part (2): Controls:

- entirely air dried without restraint: 10 samples
- completely dried with high restraint in the dryer simulator:
  - 5 samples using uniform platen [for one combination of surface temperature, mechanical pressure and fabric]
  - 5 samples using non-uniform platen [for one combination of surface temperature, mechanical pressure and fabric]

## Part (3): Drying runs with uniform heat flux (uniform surface):

- Final moisture ratio (for dryer simulator runs): 3 levels, about 0.7, 0.3, 0.1 g/g
- Surface temperature: 2 levels, 110 C and 170 C {possibly one extra level at the final moisture condition giving worst cockle}
- Mechanical pressure: 0.2 psi and 1.0 psi
- Dryer fabric: 2 fabric designs
- Completion of drying after removal from dryer simulator: unrestrained air drying in a 50% RH/22 C lab
- No. of runs per condition: 5

Part (4): Drying runs with non-uniform heat flux (non-uniform surface):

- Final moisture ratio (for dryer simulator runs): 3 levels, about 0.7, 0.3, 0.1 g/g
- Surface temperature: 2 levels, 110 C and 170 C
- Mechanical pressure: 0.2 psi and 1.0 psi
- Dryer fabric: one design
- Completion of drying after removal from dryer simulator: unrestrained air drying in a 50% RH/22 C lab
- No. of runs per condition: 5

**Test Runs:**

Part (1): Trial and error (and consultation with F. Ahrens) should be used to select about 10 different dwell times that define the moisture ratio vs. time curves over the range from about 1.2 g/g down to about 0.05 g/g.

Parts (3) and (4): The drying curves will be used to determine the dwell times needed to achieve the target moisture levels for the dryer simulator runs. The sheet and fabric MD's need to be aligned. After initial drying in the dryer simulator, to their established moisture targets, the completion of the drying of samples will be done via air drying without restraint, in a room at 50%RH/22 C.

**Data Collection/Handling:** Record all test conditions; give samples unique, easily understood code designations; record initial and final (after dryer simulator) weights. After the air drying (unrestrained) step is complete (24 hrs. at 50% RH), submit samples to Kennisha Collins for cockle analysis. After cockle analysis, oven dry samples and calculate initial and final (after dryer simulator) solids levels.

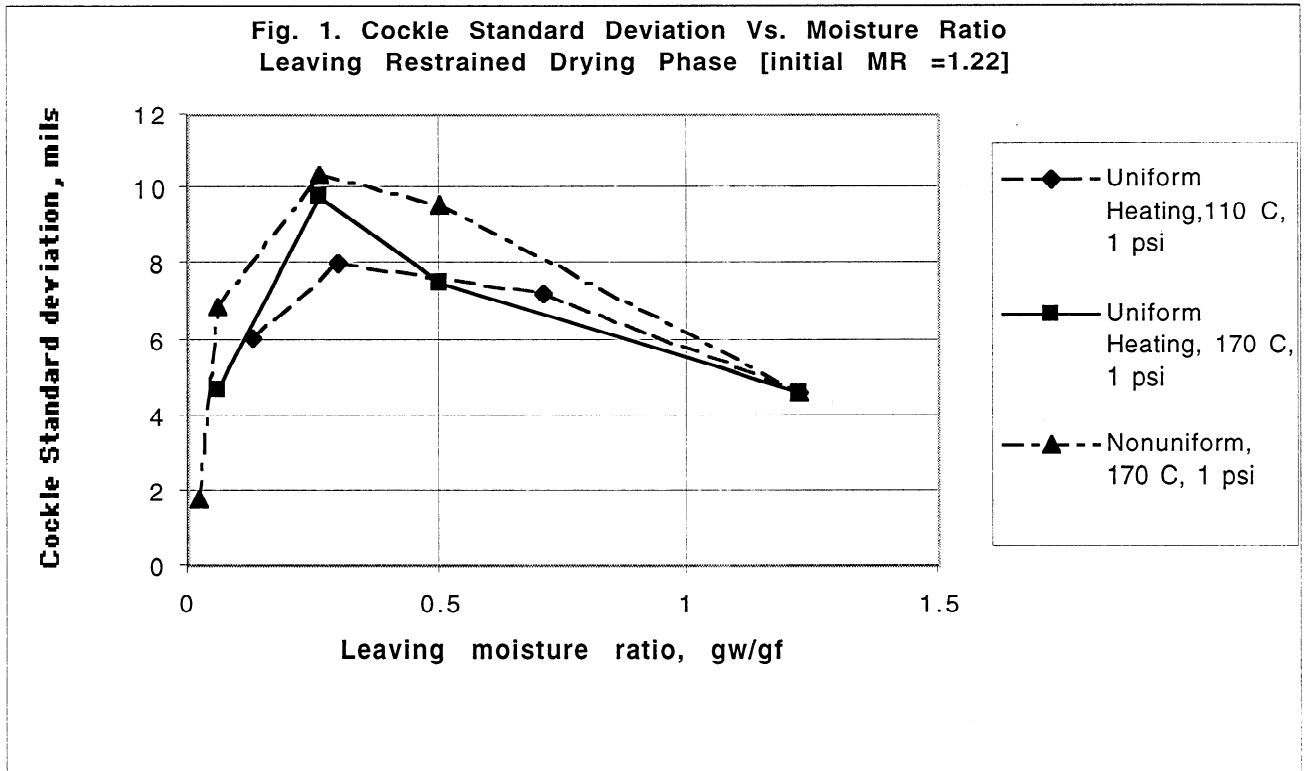
For Part (1), plot moisture ratio vs. time curves.

For the Part (2) control sheets dried on the simulator, after cockle measurement at 50% RH, expose sheets to high humidity (95%) and again measure cockle.

**Shadow Moiré Measurements:** From visual inspection pick the most cockled and flattest sheets. Prepare Moiré system for measurements (Clean dust from glass and paperholder, use 50 lines per inch glass, make sure holder is flat, make sure light source is in working condition) Set the Moiré system up to get the maximum x-y coverage and still get reliable z measurements. It would be good to make measurements on a square area of 3 to 4 inches. Also make sure your window of interest has at least 200 pixels in each direction. Once the camera is focused on the area to be measured do not change the settings until all sheets are measured. First make sure that you get good measurements for the least and most cockled sheets. Adjust as necessary. If the sheets are very flat, consider taking a second measurement using the 100 lines per inch plate. Measure all sheets with the MD direction facing the same way. Make sure that the distance between the glass and the paper is the same for each measurement (i.e., move the holder to the same starting position each time, without severely cockled sheets touching the glass) By looking at a graph of the height data make sure the image is reasonable (high frequency wrinkles or abrupt changes indicate that poor fringe patterns were obtained). Analyze the raw data so that the height is with respect to the best-fit plane (average height is zero). If the samples have curl, the low frequency response will have to be filtered using FFT. Calculate the standard deviation of the height, the average of the absolute value of the height, and the average gradient squared.

## Results of Cockle Experiments

The drying runs have been completed for nearly all of the trial conditions. The cockle analysis is in progress, but results for a portion of the trial conditions are given in Fig. 1. The “cockle standard deviation” is a measure of the sheet-average deviation of the cockled sheet surface topology from that of a flat sheet (i.e., a larger number implies greater cockle). The “leaving moisture ratio” refers to the moisture in the sample upon removal from the dryer simulator, prior to final air-drying. The data point at 1.22 g/g is a control case, in which the samples (initially at 45% solids) were entirely air-dried without restraint.



The results in Fig. 1 show several interesting features. Let us first consider the end points at high and low moisture. The cockle associated with the 1.22 g/g control is, by definition, not dependent on drying conditions. Instead, it probably reflects the effects of sheet formation and basis weight non-uniformity. The end point at lowest moisture has a very low cockle (i.e., corresponding to a flat sheet). This reflects the fact that the entire drying occurred with the sheet under restraint.

The most interesting behavior is associated with the intermediate points. The cockle is seen to be far greater in the intermediate region than at the ends, in spite of the fact that sheet was restrained for a portion of the drying process! The general trends exhibited by the peak values seem to be physically reasonable. That is, the uniform heating at higher temperature results in more cockle than uniform heating at lower temperature. This result is consistent with (but does not yet prove) the statement that high surface temperature in the first dryer section can aggravate cockle problems. The peak for non-uniform heating (e.g., representing effects of non-uniform surface deposits) is seen to further increase cockle.

The potential for shrinkage during (unrestrained) drying is a function of the moisture change. Thus, one would expect cockle severity to be associated with moisture differences (and levels) in the sheet at the beginning of the unrestrained drying period. Examples of the free shrinkage behavior of paper (vs. moisture content) are contained in Refs. 3-6. Over the range of sheet moistures occurring in the dryer section (e.g., 1.5 g/g down to about 0.05 g/g) the shrinkage function is quite non-linear, with most shrinkage occurring between 0.7 and 0.05 g/g.

The shape of the cockle vs. moisture ratio curves in Fig. 1 can, therefore, probably be explained as the competition between two phenomena:

- if the sample stays in the dryer longer (to lower moisture ratio) there is, on the average, less shrinkage potential in the subsequent unrestrained drying phase, decreasing the tendency for cockle.
- if the sample stays in the dryer longer, the local moisture deviations may be greater at the end of the restrained period, at least over part of the final moisture range, increasing the tendency for cockle.

One other observation from the experiments seems notable. The sheets tended to exhibit a small-scale “cockle” pattern matching the fabric pattern. This may be due to a fabric scale non-uniformity in the heat and mass transfer processes creating fabric scale moisture differences in the sheet.

### **Potential Next Steps**

The results to date appear to provide some new insights into the effects of drying conditions. There would seem to be merit in continuing these collaborative cockle investigations.

One direction to be considered is that of trying to more closely simulate the drying process occurring in the dryer section. A sequence of short heat input periods (in the dryer simulator), with brief periods of unrestrained or unidirectionally restrained evaporation/shrinkage in between, to simulate the open draws, could be performed.

Unfortunately, currently available laboratory drying devices are not sophisticated enough to give a truly realistic simulation of the time-varying drying and restraint conditions experienced by a sheet as it progresses through a typical dryer section. Development of a more realistic, versatile laboratory simulator for the drying process could be undertaken, if there is sufficient interest.

In any case, from the point of view of Project F021, the overall goal of future work in this area should be directed toward:

- Pinpointing the drying conditions and sources of non-uniform shrinkage in the conventional process that create the greatest degree of sheet surface non-uniformity
- Proposing and demonstrating strategies for reducing the cockle problem, that also provide an increase in drying rate.

### **REFERENCES**

1. Brecht, W., Müller, F., and H. Weiss, “Über das ‘Blasigwerden’ von Papieren”, *Das Papier* 9 (7/8): 133-142 (1955)



2. Gallay, W., "Stability of Dimensions and Form of Paper", Tappi J. 56 (12): 90-95 (1973)
3. Wahlström, T. and C. Fellers, "Biaxial Straining of Paper During Drying, Relations Between Stresses, Strains and Properties", Proceedings 1999 TAPPI Engineering Conference, pp. 705-720
4. Wahlström, T., Adolfsson, K., Östlund, S. and C. Fellers, "Numerical Modelling of the Shrinkage Profile in a Dryer Section, a First Approach", Proceedings 1999 TAPPI International Paper Physics Conference, pp. 517-531
5. Waller, M. and Singhal, A., "Development of Paper Properties During Restrained Drying of Handsheets", Proceedings 1999 TAPPI Engineering Conference, pp. 721-732
6. Wedel, G., "Drying Restraint in a Single-Tier Dryer Section", Proceedings 1989 TAPPI Annual Meeting, pp. 23-29.

#### **ACKNOWLEDGEMENTS**

Thanks to John Chabot, Warren Davis and Kerin Strange for their efforts in design, construction and debugging of the WADS, and to Georgeta Maghiari for assistance in the WADS checkout experiments.

Thanks to Paul Phelan for suggesting the use of a patterned platen to provide non-uniform heat flux for a portion of the cockle study.

Thanks to David Orloff for guidance and participation in many aspects of the reported work, and for preparation of the sections on dryer surface topology and deposits.

